METHODS FOR SPATIOTEMPORAL POWER PROFILE FROM MARINE HYDRO-KINETIC ENERGY AND WIND ENERGY FOR A PROPOSED U.S.-CARIBBEAN-SOUTH AMERICA SUPER GRID UNDER HURRICANES

by

Rodney Itiki

A dissertation submitted to the faculty of
The University of North Carolina at Charlotte
in partial fulfillment of the requirements
for the degree of Doctor of Philosophy in
Electrical Engineering

Charlotte

2023

Approved by:

_____
Dr. Madhav Manjrekar

_____
Dr. Valentina Cecchi

_____
Dr. Sukumar Kamalasadan

_____
Dr. Thomas Nicholas II

ABSTRACT

RODNEY ITIKI. Methods for Spatiotemporal Power Profile from Marine Hydro-kinetic Energy and Wind Energy for a Proposed U.S.-Caribbean-South America Super Grid under Hurricanes.

(Under the direction of DR. MADHAV MANJREKAR)

Global warming and climate change keep causing a catastrophic impact on the natural, social, economic, and political environment in many parts of the world. The urgency for the transition to a low-carbon economy through CO_2 emissions reduction calls for innovative methods to harvest renewable energy sources to displace unsustainable fossil fuel power in North America. This work presents proposed methods for marine hydrokinetic and solar renewable power generation. On another front, since addressing the causes of global warming and climate change is not timely enough, this author proposes technologies to minimize their effects, which manifest through extreme weather events. Since renewables harvesting generates variable power profiles during extreme weather events, this work investigates high voltage interconnectors to smooth the total power variability of wind power farms far distant between themselves under hurricane events. In summary, the proposed methods and high voltage enforcements address the causes and effects of climate change and global warming on the existing and future power grids. Furthermore, the proposed methods and enforcements lay the foundations for future studies on large-scale renewable multi-source super grids, with a consequential impact on reducing greenhouse gas emissions and improving power resilience in North America.

DEDICATION

This dissertation is dedicated to the scientific community working in the STEM area (Science, Technology, Engineering, and Mathematics), and more specifically, energy technologies, renewable and sustainable energy sources, mitigation of climate change, global warming, transition to a low-carbon economy, electrification, protection of natural resources, peace, and the prosperity of nations.

ACKNOWLEDGMENTS

I want to express my gratitude to my parents for providing me with a high-quality education in the early stages of my life until high school. This primary education helped me later achieve education and a career in Electrical Engineering.

I would like to thank my advisor, Dr. Madhav Manjrekar, for his words of encouragement during this COVID-19 pandemic and the academic guidance in my research, paper publications, and this proposal defense. It is my duty to extend my gratitude to the committee members Dr. Valentina Cecchi, Dr. Sukumar Kamalasadan, and Dr. Thomas Nicholas for assessing this work. I am thankful for the generous funding from EPIC (Energy Production and Infrastructure Center), the YVI Labs (Photon++ simulation software), and the Coastal Studies Institute (George Bonner, P.E.). Also, I would like to thank Prof. Dr. Chowdhury, Dr. Somasundaram Essakiappan, Fernando Libonati, and Dr. Linquan Bai for their co-authorship in the paper about wide-area controllers.

I would like to thank Dr. Silvio Giuseppe Di Santo from the University of São Paulo for advising me on the technical aspects of scientific research and paper review. I want to thank Cinthia for guiding me in my transition from a private to a research career and inspiring me to enroll in Ph.D.-level education in the United States. I also want to thank Shozo, Gabriel, Reynold, Eliane, and João Pedro, my family members. Furthermore, I was fortunate to be surrounded by extraordinary colleagues and friends: Rafael de Lin Lu, Prithwiraj, Faria Kamal, Chandra Sekhar, Olalekan, Tiancan Pang, Rakesh Belchandan, Prasanth, Robin, and Muhammad Rahman. Finally, I would like to thank all my friends from CNEC and WorleyParsons during my twenty-year career in Engineering consultancy.

TABLE OF CONTENTS

LIST OF TABLES

LIST OF FIGURES

LIST OF ABBREVIATIONS

ADCP	acoustic doppler current profiler
BOEM	Bureau of Ocean Energy Management of the United States of America
cat	hurricane category
CSI	Coast Studies Institute
DSO	distribution system operator
FEMA	U.S. Federal Emergency Management Agency
GPS	global positioning system
HF	high-frequency
HVac	high voltage alternating current
HVdc	high voltage direct current
IEEE	Institute of Electrical and Electronics Engineers
LCOE	Levelized cost of energy
MHK	marine hydrokinetic
NHC	National Hurricane Center
NOAA	National Oceanic and Atmospheric Administration
OffPS	offshore power system
OWF	offshore wind farm
PV	photovoltaic
RES	renewable energy sources
SG	super grid
SINCAL	platform for electricity network planning, simulation, and analysis
TSO	transmission system operator

CHAPTER 1: INTRODUCTION

Global warming and climate change continue to infringe catastrophic damage to the natural, social, economic, and political environment. The urgency to mitigate the impact of global warming and climate change calls for a strategy that addresses their causes and effects.

The causes of global warming are very known by the scientific community. First, greenhouse gas emissions must decrease. This necessity can be carried out by the massive expansion of renewable energy sources (RES) in the power sector and a fast transition to low-carbon energy sources, such as solar, wind, and maybe marine hydrokinetic energy.

The effects of climate change on the power sector are felt by an increase in the intensity of extreme weather events threatening the integrity of transmission, distribution, and generation assets. Extreme events such as tropical cyclones (hurricanes, typhoons, tropical storms, tropical depressions), heatwaves, wildfires, flooding, and severe drought are becoming more intense, as projected by the technical literature [1], [2], [3]. The impact of these events may cause the collapse of transmission towers, short-circuit of lines, the unexpected peak of power consumption during heatwaves, interruption of power transmission to minimize unintentional wildfires in forested parks, destruction of aerial power distribution by mudslides, an abnormal decrease in power capacity of hydropower plants due to depletion of water resources during severe seasonal drought [4]. On top of that, extreme weather events also cause severe power variability in renewable energy sources, limiting the optimum performance of the same technology (renewable power plants) that addresses the causes of global warming and climate change.

The electric grid is vulnerable to various threats such as geomagnetic storms, electromagnetic pulses (EMP), cyberattacks, and extreme weather events. In particular, wind energy variations can cause uncertain impacts on resource potential in electricity generation. High

ambient air temperatures can reduce transmission efficiency and available transmission capacity in power lines. Wildfires and storm events, including ice storms, can increase the risk of physical damage and decrease transmission capacity in transmission and distribution systems [4].

This dissertation addresses variations in wind patterns that lead to uncertain impacts on resource potential (e.g., variability caused by hurricanes).

It becomes clear that environmental systems modeling, weather forecasting included, should be taken into consideration for renewable power system studies. Since extreme weather events occur in geographical space and in a certain period, the simulation of the power system must also be sensitive to the spatiotemporal variability of renewable sources in normal and extreme weather conditions. This work covers this significant gap in the power system simulation literature, which generally circumvents the computational cost by assuming simplified equivalent models or simulations with a small number of generators. [5]

This work proposes methods to assess marine hydrokinetic, solar, and wind energy in a spatiotemporal domain to investigate the potential for large-scale expansion of renewables in North America, a region recurrently impacted by extreme weather events. The investigation of the expansion of renewables tackles the causes of global warming and climate change.

This work is organized as follows. Chapter 2, entitled “Literature Review”, presents the methods of renewable energy assessment in the technical literature. Also, it introduces the systemic representation of the North American power grid. Chapter 3, entitled “Proposed Method for MHK Energy Assessment”, presents a proposed algorithm for MHK assessment and a case study with the simulation of an MHK farm in North Carolina to demonstrate the functionalities of the proposed method. Chapter 4, entitled “Proposed Method for Wind Energy Assessment”, presents a proposed algorithm and simulation of an offshore wind farm hit by a hurricane. Chapter 5,

entitled “U.S-Caribbean Super Grid with MHK, Wind Power and extension to South America”, investigates the strategy of hybridization of marine power and offshore wind, coupled with interconnecting wind capacity outside the hurricane’s corrido to obtain lower power profile variability even on extreme weather events. Chapter 6, entitled “Discussions”, presents the implications of the proposed methods to a multitude of disciplines. It also offers a reflection on potential topics for future research derived from the proposed methods. Finally, the conclusions of this work are presented in Chapter 7.

CHAPTER 2: LITERATURE REVIEW

This chapter investigates the recent advances in renewable energy assessment methods in searching for potential gaps for further research. Starting from marine hydrokinetic energy (MHK), i.e., the energy from moving waters from oceans, this review also investigates onshore PV solar and offshore wind under extreme weather events. Finally, this review investigates architectures of large-scale interconnectivity to systemically smooth the impact of power variability of renewables before injection to the traditional power grids.

2.1 Methods for Marine Hydrokinetic Energy Assessment

Marine Hydro-Kinetic (MHK) is renewable energy in the moving waters of the oceans. However, harvesting MHK is not as technically and economically simple as other types of renewables. For this reason, MHK power generation is in the initial stage of prototype development, testing, and validation worldwide.

In 2020, Nachtane et al. investigated the MHK turbines with the highest technology readiness level in the U.S. and the U.K. [6]. Despite such development of prototypes, scaling up the turbine's aggregation into MHK farms hits the reality that the MHK resource is not equally distributed and constant everywhere in the ocean. It is thus necessary to quantify how much power, in instantaneous time, an MHK farm can potentially harvest.

In 2016, He et al. characterized the spatiotemporal variability and power density of MHK energy resources in North Carolina [7]. They measured the seawater speed off the coast of North Carolina using an Acoustic Doppler Current Profiler (ADCP), and they calculated the average mean seawater speed in the upper layers of the Gulf Stream. The annual profile of MHK power density shows high variability ranging from 0 to values in excess of 3 kW/m^2 for the same month

[7]. A mismatch of 200 W/m^2 is observed between their proposed model of the Gulf Stream and the value from the ADCP speed measurements.

The power density was calculated by the theoretical equation [7]:

$$P_{in} = \frac{1}{2}\rho S^3 \quad (1)$$

where ρ is the water density in Kg/m^3, and S is the instantaneous water speed in m/s. Using the water speed data from the ADCP and applying (1), Hu et al. derived the power density profile and calculated its annual average power density (1,016 W/m^2). According to Hu et al., some published studies suggest that around 40% of the power in the ocean current is the maximum that is reasonable to expect [7].

This research partially investigates how much power can be collected instantaneously by a pre-selected distribution of turbines located in an oceanic stream. The water speed profile, although instantaneously measured by the ADCP, is averaged for the specific location. Additionally, the calculated power based on (1) is the kinetic energy density of the water flow in front of the turbine. The kinetic energy left in the water after the blades, and losses from the shaft, gearbox, electrical generator, power converter, are not discounted in the calculation. In other words, the final and useful product of a turbine is the electrical output power. Also, Hu et al. observed an error of 17% between their proposed model and the power profile calculated from the water speed profile [7].

In 2017, Chawdhary et al. reformulated the theoretical power equation, adding more parameters to account for the turbine design specifications [8]:

$$P_{in} = \frac{1}{2}\rho A C_p S^3 \quad (2)$$

where C_p is the power coefficient of the turbine, typically around 0.35 to 0.4 [9], ρ is water density, $A = 0.25\pi D^2$ is the area intercepted by the turbine, $D$is the diameter covered by the rotational blades, and S is the incoming fluid velocity. Tested MHK turbine prototypes operate

within cut-in (minimum) and cut-out (maximum) speed range [10] [11] [12]. Equation (2) does not account for these limits.

The power generated by each MHK turbine can be more precisely estimated by considering time, each location, and the curve of speed versus output power obtained from MHK turbine testing. It should also be calculated using the measured water speed data instead of model-generated data to eliminate the propagation of modeling error into the MHK power estimation. These gaps are the focus of this work.

2.2 Methods for Wind Energy Assessment.

Modeling is applied to several issues involving hurricanes—the distribution of hurricane counts [13]; the prediction of hurricane track [14], intensity [15] and structure [16]; the prediction of landfalling hurricanes [17] and the economic damage caused by these landfalls [18].

There are also models that ponder the economic savings of waiting for improved forecasts to avoid unnecessary preparations and the higher risks of reducing the lead time to take the preparation measures for an oncoming hurricane [19].

Modeling is also used to predict hazards caused by rainfall, winds, and surge [20], as well as, to predict the rainfall itself [21], the sea-wave parameters [22], and the maximum wind speeds [23], [24], profiles [25] and fields [26]. This work, though, intends to focus on the interaction of hurricanes and electrical power. Some relevant aspects regarding electrical-energy generation structures submitted to extreme wind conditions are reviewed below.

Ahmed and Cameron (2014) present a review of the economic, social, and technical challenges to the steady growth of wind power generation. For onshore wind turbines, fauna and flora impacts, as well as visual and noise pollution, are relevant issues [27].

For offshore wind turbines, these impacts may be reduced at the expense of additional technical challenges and costs [27]. Furthermore, due to climate changes, there might be an increase in the incidence of cyclones, which corroborates the importance of the present study.

Foley and colleagues (2012) advocate the importance of wind-power forecasting. Some forecasting approaches use historical data, while others apply the outputs of a numerical weather prediction model as inputs to wind-power forecasting methods [28]. A suitable weather model depends on the definition of the geographical region to be modeled and the spatial resolution, the forecast horizon and the time resolution, and the accuracy or the time constraint for the numerical simulation [29]. In order to reduce the influence of initial conditions and systematic errors, ensemble weather forecasting may be used. This ensemble prediction could be obtained by either different initial conditions and parameter values on a single weather-prediction model or even by multiple weather prediction models [29].

Wang and collaborators (2021) proposed a parametric model to estimate wind speed in hurricanes. The model's parameters are obtained from cross-polarization synthetic aperture radar (SAR) images [30]. The model's estimates are then validated by comparison to wind-speed measurements and direct estimates from three hurricanes [30]. The relatively simpler model has shown outstanding performance in representing wind distribution asymmetries, except for the hurricane eye area [30].

Wang and colleagues (2015) proposed a sophisticated statistical technique to model and accurately estimate extreme wind speeds. These estimates were validated by the historic wind record of the 23-year interval between 1990 and 2012. They were also comparable to the results provided by other statistical methods described in the literature [31]. Nevertheless, a method used to model 10 to 22-year old data may not be adequate to forecast current extreme events. Indeed,

the modeling should be updated with recent extreme weather events since there might have been an increment in their intensity due to climate change, particularly influenced by the increasing global warming. Another limitation is that the model was based on site selection—certain hurricane-prone areas were discarded from the modeling. However, in order to design hurricane-proof turbines and explore wind energy in hurricane-prone areas, it would be important to consider these extreme-weather condition areas [32].

According to Murthy and Rahi (2017), wind characteristics determine which wind-turbine technology is suitable for a specific site. The turbine type, in turn, defines if that prospective location is economically feasible. Consequently, it is important to assess the wind-power potential. Besides a review of installed capacities, estimated potentials, and wind-turbine technologies, Murthy and Rahi also present the technologies for wind resource assessment. These encompass the mathematical modeling of conifer-tree deformation due to wind speed and the fitting of Weibull distribution to the wind-speed measurements. Data could be recorded by instruments mounted on masts and should preferably be collected over a 10-year period with a 10-minute sampling interval. Besides it, the estimation of wind energy output is also presented in that review. For the hourly, monthly, or annual estimations, several input variables could be considered, including the historic seasonal variations of wind-power availability and the frequency distribution of wind speeds [33].

Hashemi and collaborators (2021) developed a method to assess the structural integrity of the monopile jacket substructure under extreme wind and wave loads. The study was directed to Rhode Island and Massachusetts, as they were considered potential sites for future offshore wind farms. To analyze the issue of structural integrity, a computer simulation synthesized hurricane wind fields based on a parametrical model previously described in the literature [34], [35]. This

simulation provided not only wind speeds and hurricane trajectories but also the spatial distribution of wave heights. These simulated variables were then input to an open-source wind-turbine simulation software that provided the response variations of a typical turbine monopile jacket substructure. [36]. This method could be extended to other hurricanes besides the two specific ones that were modeled in the study.

In 2019, Muhs and Parvania developed a tool for the generation of hurricane events, simulation of scenarios, and analysis of the spatiotemporal impact of hurricanes on power grid resilience. The spatiotemporal hurricane-simulation module generates a wind-speed profile according to Weibull's distribution. Besides it, this module is used for a thousand hurricane paths. Each path depends on randomly selected values of normal-distributed approach angle and landfall location, as well as lognormal-distributed translation velocity, whose mean and standard deviation values are defined by historical data. The second module determines the distance of each grid component to the hurricane eye, the wind speed curve, and the correlation between wind speeds and the fragility curve to assess the impact on the specific line or pole. According to Muhs and Parvania, one possible improvement is that their method uses a straight-line trajectory for hurricane movement, and a non-linear hurricane path could be explored in the future [37].

In 2020, Watson and Etmadi proposed a hurricane-wind damage model dedicated to renewable and non-renewable power plants. The inputs of the modeling are the historical hurricane speed data from a private company (Risk Management Solutions, Inc.) for hurricanes Ike and Rita and a government agency (NOAA) for hurricane Harvey. Their method is based on ArcGis (a software that finds the intersection of a wind gust speed map with the grid elements) and Hazus (Hurricane Loss Estimation Methodology developed by FEMA, the U.S. Federal Emergency Management Agency). The output assesses damage to overhead transmission lines, poles, and

power plants based on nuclear, gas, coal, solar, and wind and restoration costs caused by hurricanes [38].

It is important to pinpoint that, in these two latest studies, hurricanes are seen as a source of damage and cost for the power infrastructure.

In contrast with these two previous works, this research considers hurricanes not exclusively as a source of damage and restoration cost but also as a source of electrical power profile variability, potential carbon abatement, and revenue for utility companies. Furthermore, the trajectory of historical hurricanes is not linear, and this work derives the equations for parabolic trajectory, which is more adherent to the historical hurricane trajectories.

Moreover, the super grid proposed in the case study of this research is built on submarine power cables. In contrast to overhead transmission lines, submarine cables by virtue of deep-water columns, naturally protect the cable against the impact of hurricanes [39].

Submarine cable has been a long-time solution for interconnectivity of the wind power farms, mostly in Europe [40] [41], but also in China [42], Japan [43], South Korea [44], Taiwan [45], Vietnam [46], and the northeastern offshore coast of the U.S. [36] [47].

However, despite being a hurricane-proof solution for interconnectivity, submarine power cables have hardly been considered along the Caribbean Sea and the Gulf of Mexico, a region well-known as the front-end of the hurricane alley of North America [32]. The Caribbean super grid built on submarine cables, as proposed in this research, is a very opportune case for investigation.

Another two critical components of the power grid resilience under a hurricane are the mechanical structure to support the wind turbine and the turbine itself. The design reinforcements on the mechanical structure supporting the wind turbine to withstand hurricanes are on the large

suction caissons, long piles for monopiles [48], or in the jackets [49] [50]. As the wind turbine by itself is a concern, the literature shows many advances to turn the turbines more resilient to hurricanes [51] [52] [53], for example, turbines with either an extended cut-out speed [54], or a soft cut-out at high speed [55].

To the best knowledge of this author, most of the literature regarding the impact of hurricanes on energy generation is concerned with either the mechanical effect of hurricanes on wind turbine substructures and overhead transmission lines or the averaged energy resource characterization. The electrical impact of hurricanes on an offshore wind farm's power profile has not been well covered by the literature [32]. This work intends to fill this research gap.

2.3 North American Power Grid

The technical literature on power system simulation of the power grid in North America assumes simplified equivalent models or a limited “n” number of buses and generators in typical IEEE n-buses systems or newly proposed ones [56] [57] [58]. FIGURE 2.1 shows an example of a newly proposed North American power grid topology presented in [58].

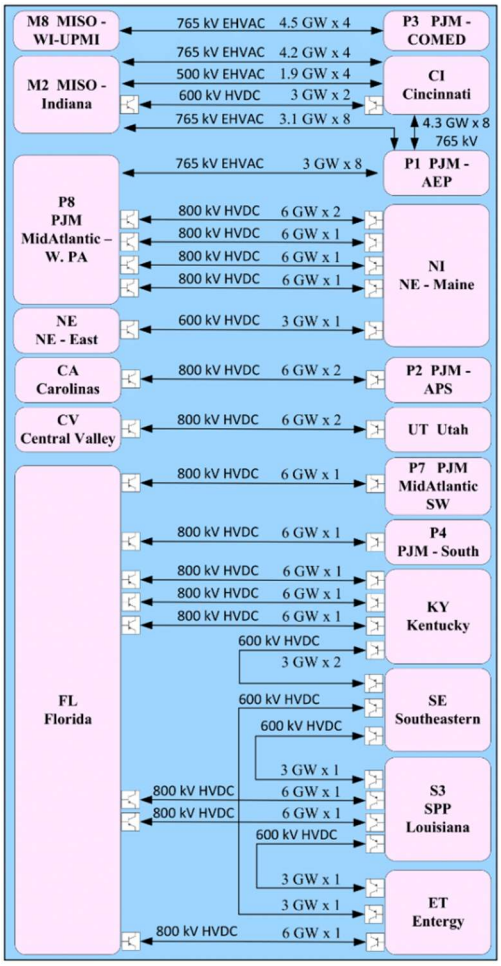

FIGURE 2.1: Topology of proposed North American SG [58] (© 2020 IEEE).

For power system simulations, a fragment of the energy sources dataset is normally collected from databases of historical measurements or just assumed to be constant in different levels of renewable penetration. Then, a proposed new control scheme of a power electronics converter is modeled, simulated, and compared against a reference benchmark [59] [60] [61] [62] [63]. This approach is computationally doable for a small number of generators and a fragment of a historical dataset of energy resource profile as input. However, scaling up the simulation with hundreds of renewable generators and associating variable energy sources to each generator demands expensive supercomputing platforms and a large dataset of historical energy resource measurements. The data acquisition may take measures from each second, minute, hour, month,

season, and year. A hybrid combination of two or more resources, e.g., offshore wind and wave energy, may complement each other from an average seasonal perspective but not instantaneously. Not rarely the location of the renewable generator is not correctly associated with any physical location (latitude and longitude). The renewable power system, in this case, is studied disconnected from the meteorologic conditions. However, in real-world conditions, the renewable energy resources intensity varies significantly for each location. This is another gap in the literature on power system simulation.

The proposed methods for renewables assessment based on environmental system modeling can generate a short-term day-ahead power flow profile. In other words, the proposed methods and tools use renewable energy forecasting, modeling, and spatial distribution to estimate renewable power generation. This work explores the temporal and spatial variability of renewable resources to generate spatiotemporal power generation profiles.

In 2019, Itiki et al., recognizing the importance of the variability of renewable resources, conceptualized a generalized architecture for offshore power systems incorporating environment subsystems onto the traditional elements of a power system [39].

In 2020, Itiki et al., during their investigation of the benefits of large-scale power interconnectivity schemes between countries, called super grids, realized the importance of the modeling of environmental systems to analyze the large-scale dynamics of power variability of super grids [64] [32]. Most of these discoveries are presented in the following sections of this dissertation. A comprehensive understanding of power system dynamics under weather events is developed in the next chapters of this dissertation.

CHAPTER 3: PROPOSED METHOD FOR MHK ENERGY ASSESSMENT

In 2021, Itiki et al. proposed a method for MHK assessment based on seawater speed data from high-frequency radar [65]. The proposed method estimates the total MHK energy harvested by turbines spatially distributed in the ocean current. The MHK energy is variable in time and space. The method represented by an algorithm is implemented in MATLAB. It reads hourly measurements of seawater speed to estimate the power profile of the generated MHK farms. In the U.S., some speed measurements from high-frequency (HF) radars in coastal areas are publicized on the internet by the National Oceanic and Atmospheric Administration (NOAA). The algorithm functionality is demonstrated in a case study with the NOAA radar measuring the seawater speed of the Gulf Stream off the coast of North Carolina. The peak value of the power profile sets a reference for the sizing of the MHK platform equipment and cabling. The algorithm is also useful for planning renewables expansion of utility companies, selection of offshore sites with high power output, techno-economic feasibility studies, and subsequent engineering steps for a proposed MHK farm project [65].

The method for MHK assessment is categorized as an intelligence system of a proposed architecture of an offshore power system with interconnection with the onshore grid. FIGURE 3.1 depicts the MHK power generation and interacting components of the architecture of the offshore power system [39].

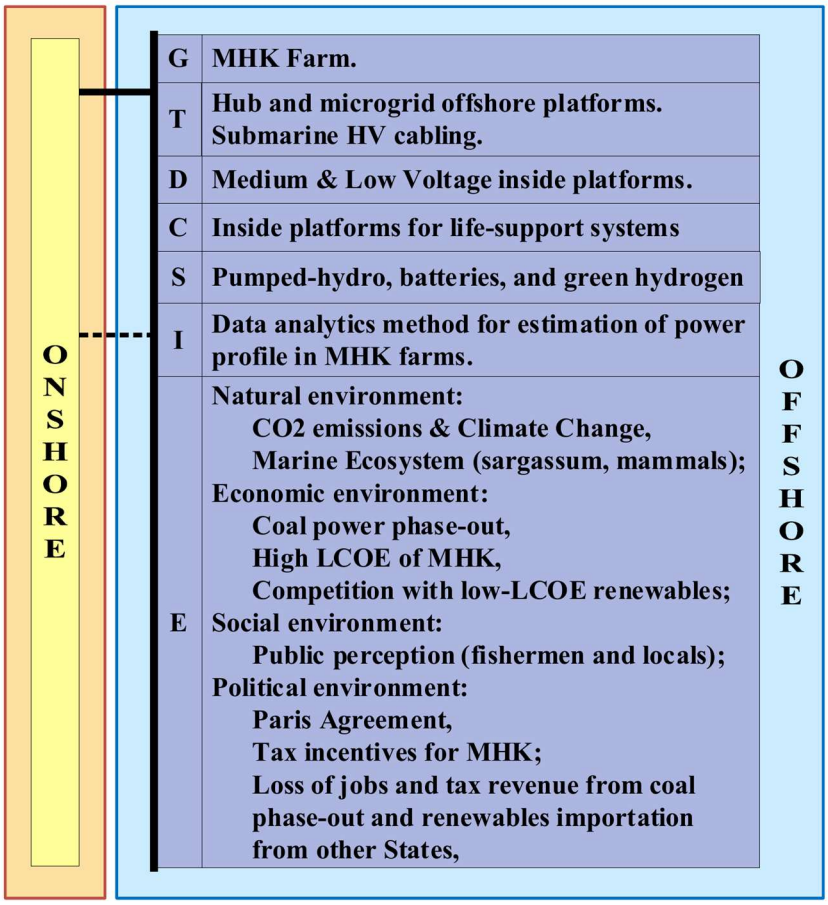

FIGURE 3.1: Architecture of Offshore Power System, adapted from [39].

3.1 Proposed algorithm for MHK assessment based on High-frequency radar.

FIGURE 3.2 shows the proposed algorithm for estimating the MHK power generation profile. The algorithm is structured in blocks: Block-1 creates the coordinates of the array of turbines of the MHK farm and the hub according to the user-defined reference coordinates. Block-2 gets the coordinates and speed data from the HF radar file, which is available online by the NOAA [66]. Block-3 interpolates the characteristic curve of power versus speed of the turbine provided by the turbine manufacturer or the technical literature [67] [10] [11] [12]. Blocks-4, 5, 6, and 7 calculate and aggregate the power-time profile of each turbine into the MHK farm hub.

Blocks-8 and 9 store the power-time profiles of turbines on the MHK farm. Block-10 plots a map with the turbine arrays created in Block-1. Block-11 plots the location of the HF radar measurements captured by Block-2. Block-12 plots the total power-time profile and the mean water speed in the MHK farm [65].

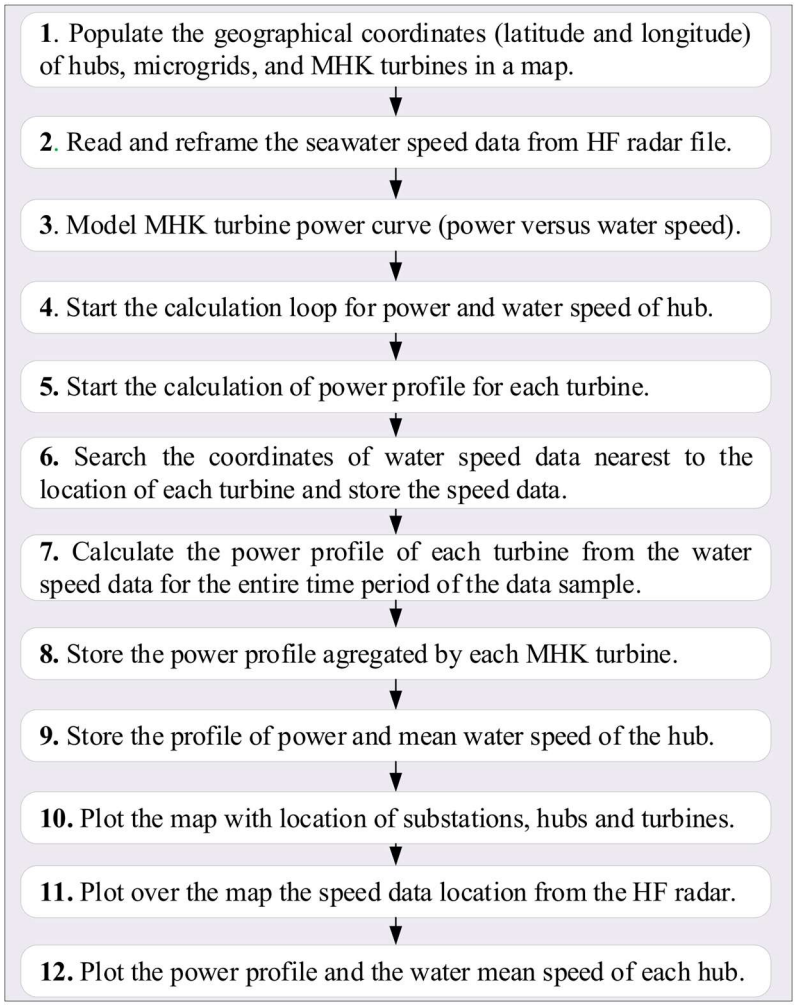

FIGURE 3.2: Proposed algorithm for MHK power profile [65]. (©2020 IEEE).

The conversion of seawater speed to power by the MHK turbines involves mechanical rotation of blades, gearbox, electric generator, and power electronic converter. For modeling and calculation purposes, such energy conversion is obtained by accessing the water speed versus power curves to generate the water speed profile of each MHK turbine. The turbines are distributed in an array of microgrids, each collecting the power of a matrix of MHK turbines populated in a parallelogram-shaped distribution over the offshore map. The proposed algorithm is mathematically represented by the following equation [65]:

$$P_{out}(t_k) = \sum_{i=1}^{m} \sum_{j=1}^{l} \sum_{r=1}^{c} P_t \left[t_k , s_d \left(T_{ijk} - S(t_k) \right) \right] \quad (3)$$

where m is the number of microgrids per hub; l is the number of lines in each microgrid; c is the number of columns in each microgrid; P_t is the power profile of each turbine, derived from the power versus water speed curve; t_k is the iteration step from 1 to 24 hours; s_d is the water speed data, measured by the NOAA HF radar at the point $S(t_k)$, which is the closest geographical coordinates to the point T_{ijk} (the MHK turbine position in the offshore map); P_{out} is the electrical output power delivered at the terminals of the turbine set.

The implementation of the algorithm in MATLAB script is detailed in APPENDIX A.

FIGURE 3.3 shows the cross-section with the components of the proposed MHK farm. The method aggregates the power profile of each turbine into the hub. The hub and the cable capacity between the hub and the onshore substation should withstand the peak value of the MHK farm power profile.

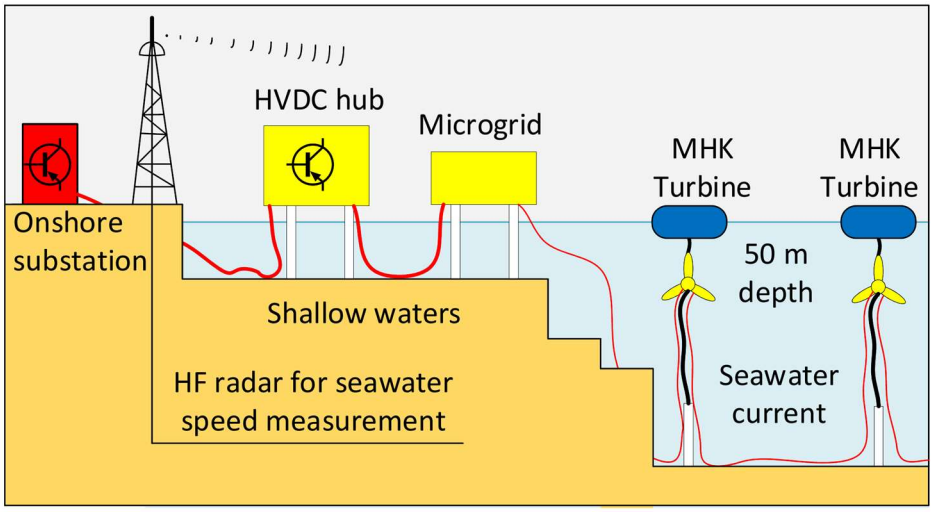

FIGURE 3.3: Cross-section of MHK power farms [65]. (© 2020 IEEE)

Following the presentation of the details of the proposed algorithm to calculate the power profile of MHK farms, this work demonstrates its functionalities by a case study.

3.2 Simulations of MHK for Gulf Stream off the coast of North Carolina.

This case study applies the method to proposed MHK farms in the Gulf Stream, off the coast of North Carolina.

FIGURE 3.4 shows the MHK turbine characteristic curve of power versus water speed for the case study. The MHK turbine curve is from the technical literature [68]. The shape of the curve depends on the design of each MHK turbine prototype. In the future, it is expected turbine manufacturers will provide this type of curve after performance tests in real and outdoor conditions. Some manufacturers have already succeeded in validating the prototype performance curve for cut-in (minimum) water speed of 0.7 m/s (IHI) [10] 1.0 m/s (Verdant Power) [12], and 1.2 m/s (Magallanes Renovables) [11]

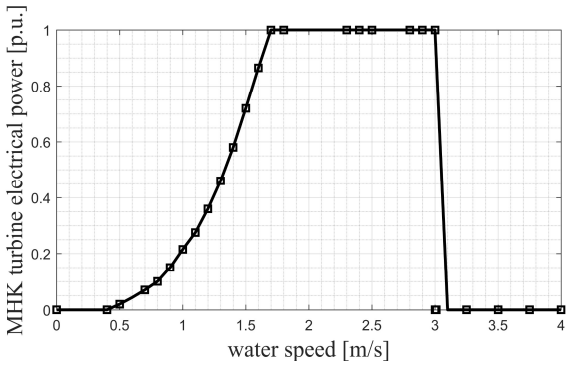

FIGURE 3.4: Curve of power versus water speed [65]. (© 2020 IEEE)

FIGURE 3.5 shows dark blue dots arranged in a parallelogram-shaped distribution, representing the MHK farms. The power of 270 turbines in the northern farm is collected by three microgrids and dispatched to hub-1. In the southern farm, six microgrids collect and dispatch the power of 540 turbines to hub-2. Each turbine capacity is 2 MW, totaling a generation capacity of 540 MW in hub-1 and 1080 MW in hub-2. The yellow dots indicate high values of water speed from the HF NOAA radar [65]. The upper 50 meters below the sea surface is an appropriate location for MHK turbines

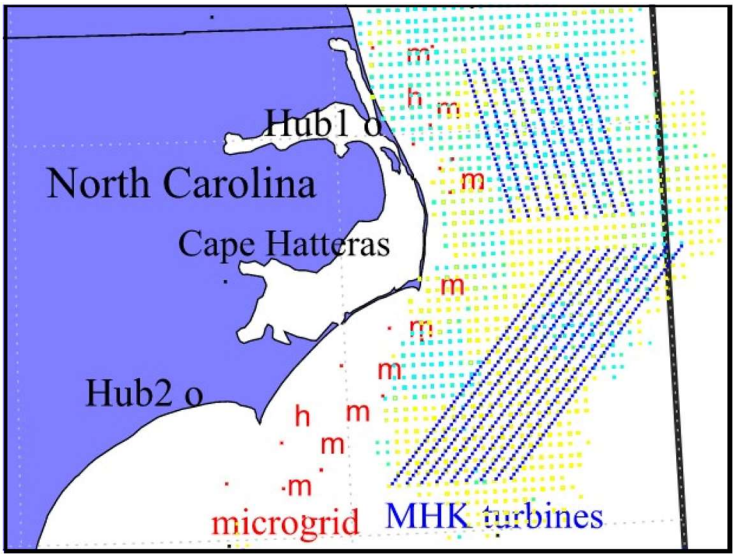

FIGURE 3.5: MHK farms off the coast of North Carolina [65]. (© 2020 IEEE)

because the kinetic energy is higher, and the water speed is similar to the superficial water speed [7].

FIGURE 3.6. shows the resulting hourly profiles of power and mean water speed in Hub-1 and 2. Hub-2 (southern MHK farm) yields 150 – 470 MW, i.e., it produces significantly more power than Hub-1 (2 – 19 MW) [65].

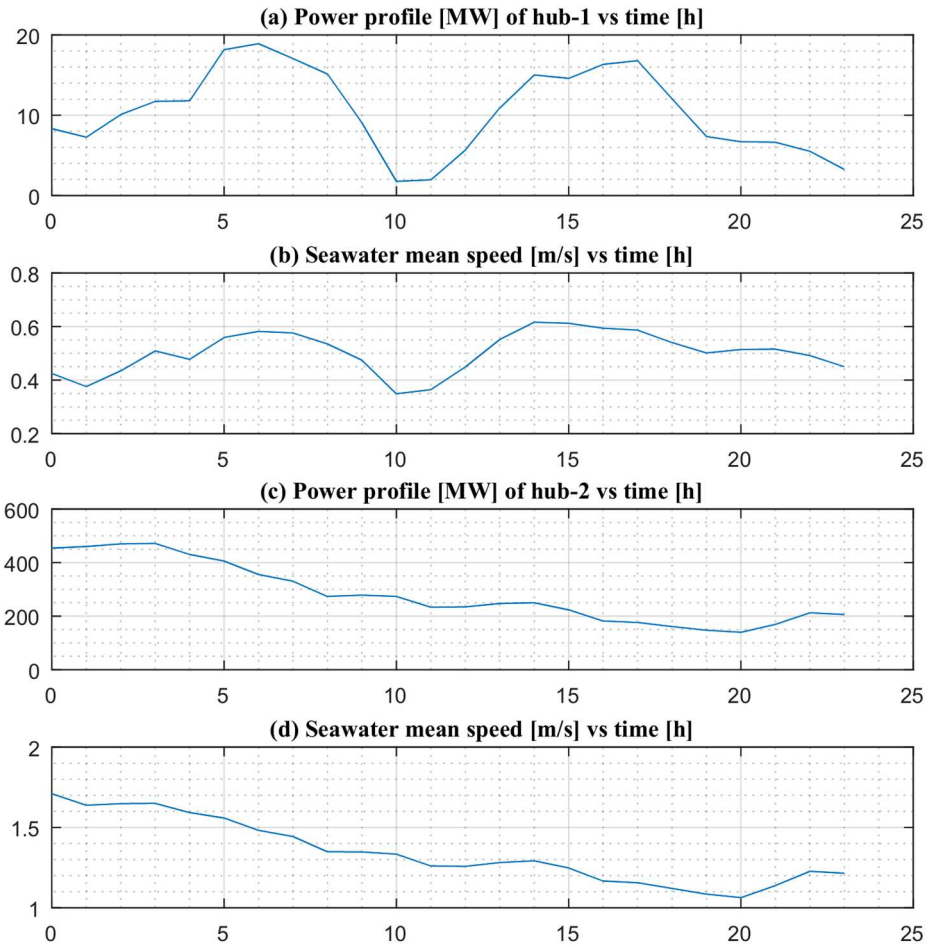

FIGURE 3.6: MHK power profile from simulations [65]. (©2020 IEEE)

The poor performance of Hub-1 in harvesting power from the northern farm can be credited to three factors. First, Hub-1was allocated with half the number of turbines of Hub-2. Second, the

northern farm, as seen in FIGURE 3.5, is located in a region with low water speed (cyan dots) as compared to the southern farm, which is over a high water speed region (yellow dots). Cyan dots represent water speed measurements below 1 m/s, whereas yellow dots represent water speed exceeding 1 m/s. Finally, as seen in FIGURE 3.4, water speed over 1 m/s generates exponentially more power than water speed below 1 m/s. Indeed, water speed below the cut-in speed of 0.5 m/s does not generate any power. FIGURE 3.6(b) confirms that the mean water speed profile, on average, rarely exceeds 0.5 m/s. Thus, the proposed northern farm is not well located in a region with higher potential MHK energy than the southern farm [65].

The 470 MW peak power shown in FIGURE 3.6(c) defines the power station capacity of the Hub-2 platform. The average capacity factor of the southern farm fluctuates around 14% and 46%. The water speed data refers to Sept-19, 2020, limiting the time range of the simulations. Nevertheless, this case study for the Gulf Stream off the coast of North Carolina demonstrates some functionalities of the proposed method for assessing the power profile for proposed MHK farms [65].

The method for estimation of MHK power profile delivers the following functionalities [65]:

- The peak value on the power profile determines the total capacity of the hub platform, the onshore substation, and the cable between them. The power capacity determines the capital expenditure (CAPEX), whereas the power profile, the revenue for the energy sale to the grid, and thus the Levelized Cost of Energy (LCOE).
- The coordinates of the MHK turbines over the map generated by the method determine the area of concern for environmental impact studies and ship navigational safety.
- The fluctuation in the power profile determines the amount of energy storage and non-critical flexible loads needed to do peak shaving and valley filling to smooth the overall power variability.

For these reasons, a comprehensive multidisciplinary and systemic discussion of the broader implications of the method and the proposed MHK power farm is relevant [65].

3.3 Comparison of proposed MHK power profile estimation method and other methods.

In 2019, Fiorentino et al. investigated methods for water speed measurements on the top 30 meters of the water column within the Gulf Stream since the literature is neither conclusive about the accuracy of capturing water speed data by bottom-mounted ADCPs nor HF radar. They proposed a submerged 300 kHz Acoustic Doppler Current Profiler (ADCP) measuring water speed to the upward position. The speed measurements buoy was installed at 40.75 km east of Cape Hatteras, North Carolina, to capture the waters of the Gulf Stream [69].

In 2021, Itiki et al. proposed a method for MHK power profile estimation using HF radar data [Itiki et al.]. The application of this method for a case study with simulations of two MHK Hubs (Hub1 and Hub2) off the coast of North Carolina was presented in the previous subsections.

In 2022, Muglia et al. proposed a method for seawater speed assessment off the coast of North Carolina based on HF radar data from NOAA [70].

FIGURE 3.7 shows the graphical differences in methods, sensors, and installations used for seawater speed measurement used in the literature. FIGURE 3.7(b) shows an ADCP facing up to the sea surface, according to the described settings of NOAA 300 kHz ADCP. [69].

FIGURE 3.7(a) shows an ADCP facing downward to the seabed, according to the described settings of the CSI 150kHz ADCP. Both have local coverage for water speed measurement. FIGURE 3.7(c) shows the wide-area coverage for water speed measurement by a NOAA HF radar, whose data were used by the Itiki in 2021 [65]. In 2022, Muglia et al. also used HF radar data for seawater speed assessment in NC [70].

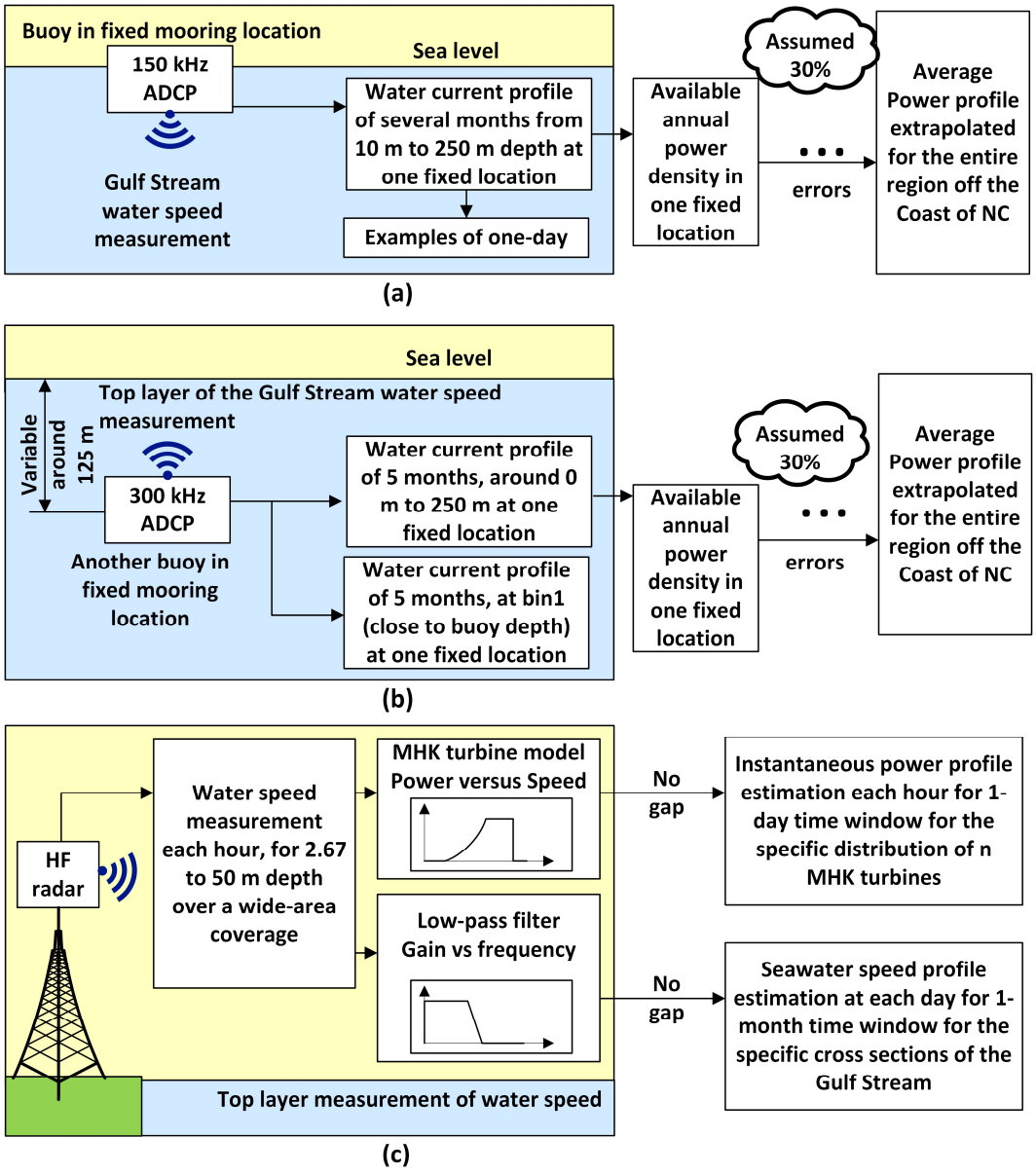

FIGURE 3.7: Methods for seawater speed measurements and estimation.

TABLE 3.1 compares four methods of water speed and power estimation utilized off the coast of North Carolina.

TABLE 3.1: Water speed measurements by ADCP and HF radar off the coast of North Carolina.

Measuring device (sensor)	NOAA 300 kHz ADCP installed in buoy off the coast of NC	CSI 150 kHz ADCP	NOAA HF radar data available on the NOAA website	NOAA 5 MHz HF radar
Area coverage of the water speed sensor	Local coverage around latitude & longitude 35.1374 N, 75.0940 W	Local coverage around 20 mi south and closer to shore (40.75 km)	Wide-area coverage of Hub2 and Hub1 off the coast of NC	Wide-area coverage of Hub2 and Hub1 off the coast of NC
Time of the measurements	May to October 2017	Starting in May 2017	One-day time period (Sept-19, 2020) in hourly resolution.	November 2014 with daily resolution (filtered).
The actual installation of the sensor device	ADCP is installed in submerged buoy target to 125 m in depth and facing up to the surface	ADCP is installed on a surface floating buoy facing down to the seabed	HF radar is installed onshore at high elevations and up in a tower.	HF radar is installed onshore at high elevations and up in a tower.
Intended measurement depth	0 - 50 m depth	0 – 250 m depth	Around 2.7 m depth	Around 2.7 m depth
Actual measurement depth	ADCP depth ranges from 65m to 125m below the sea surface, occasionally 160 m depth.	10 – 250 m depth	Around 2.7 m depth	Around 2.7 m depth
Peak current speed	As high as 3 m/s.	2.05 m/s at the surface	1.7 m/s in Hub2, 0.62 m/s in Hub1	1.217 m/s; 0.783 m/s
Normal current speed	Ranging 1.5 m/s to 2 m/s	1.54 m/s from 5 m to 100 m	1.4 m/s in Hub2; 0.48 m/s in Hub1	0.962 m/s; 0.668 m/s
Current speed at few occasions	0.5 m/s	-	1.1 m/s in Hub2; 0.35 m/s in Hub1	0.707 m/s; 0.553 m/s
Reference	Fiorentino et al, 2019 [69]	Fiorentino et al, 2019 [69]	[Itiki et al.], 2021 [65].	[Muglia et al.], 2022 [70].
Research focus	Seawater speed profile	Seawater speed profile	MHK turbine power profile	Seawater speed profile

3.4 Comparative analysis of seawater speed measurements

The comparison of methods of energy assessment takes into consideration common features of methods. For this reason, measurements from ADCP, which measures just a specific moored point in shallow waters, cannot be comprehensively compared with HF, which covers a vast area of measurements, also including deep waters.

The measurements by the method for MHK based on HF radar proposed in this dissertation by Itiki et al. in 2021 [65] are thus compared with the method proposed by Muglia et al. in 2022 [70]., which is also based on HF radars.

TABLE 3.2 shows the percent error of water speed measurement by Itiki's method over Muglia's method. The case study applying Muglia's method covers a longer period of time (30 days), which allows the indication of the speed with standard deviation to represent daily variability. Itiki's method covers measurements with 1 hour sample time over 24h period.

TABLE 3.2: Comparison of water speed based on HF radar data off the coast of North Carolina.

Location	**Method**	**Itiki et al. (Sept 19, 2020)** [65].	**Muglia et al. (Nov 2014)** [70].	**Error (%)**
Hub1 is close to the coverage of HF radar HATY 87 over edge	Peak current speed	0.62 m/s	0.783 ±0.149 m/s	-21%
	Average current speed	0.48 m/s	0.668 m/s	-28%
	Minimum current speed	0.35 m/s	0.553 ± 0.146 m/s	-37%
Hub2 is close to the coverage of HF radar CORE 72 over jet axis.	Peak current speed	1.7 m/s	1.217 ± 0.233 m/s	40%
	Average current speed	1.4 m/s	0.962 m/s	46%
	Minimum current speed	1.1 m/s	0.707 ± 0.289m/s	56%

In Hub1, the water speed daily values from Itiki's method ranges from 0.35 to 0.62 m/s, while in Muglia's sample, considering the standard deviation on the peak and minimum speed values, the overall seawater speed ranges from 0.407 to 0.932 m/s. The hourly samples excursion range used on Itiki's method is mostly within the excursion range of the measurements of Muglia's method. The average current speed of Hub1 using Itiki's method is 28% lower than using Muglia's method. Hub1 is mostly positioned over the shallow waters off the coast of NC, but not much in the direct path of the Gulf Stream as in Hub2. Both methods indicate lower water speed in Hub1 on average than in Hub2. Both methods thus show consistent average speed numbers.

In Hub2, the water speed daily values from Itiki's method ranges from 1.1 to 1.7 m/s, while in Muglia's sample, considering the standard deviation on the peak and minimum speed values, the overall seawater speed ranges from 0.418 to 1.45 m/s [65] [70]. The hourly samples excursion range used on Itiki's method is mainly within the excursion range of the measurements of Muglia's method. The average current speed of Hub2 using Itiki's method is 46% higher than using Muglia's method. Since Hub2 is located mostly over the Gulf Stream path, it is expected that the water current in September being faster than in November. MHK energy peaks in summers and slows down in winter [71]. For this reason, the water speed values estimated by Itiki's method are relatively consistent with Muglia's method and the expected seasonal variability of the Gulf Stream speed.

The error of speed estimation from Itiki's method for September 19, 2020, is compared and calculated on the basis of the average current speed values of Muglia's method, which is derived from samples of November 2014. Unfortunately, Muglia et al. in 2022 applied the method over samples of 2014, while the Itiki et al. article published in 2021 applied the method over samples of 2020. For this reason, the multi-year variability caused by the effects of global warming on the available MHK energy in the Gulf Stream is not possible to assess in this analysis. The multi-year variability of large-scale weather systems such as El Nino, La Nina, or global warming is also not captured in this analysis. In other words, this comparison assumes that the large-scale weather variability between 2014 and 2020 is negligible. Itiki's method uses speed data of a selected day, as made available by the NOAA's website [65]. In contrast, Muglia et al. analyze the Gulf Stream MHK over an entire month, with hourly variability (assumed to be speed data noise) partially eliminated by a 24h low pass filter. Despite such limitations, this comparative analysis is presented at least under the supposed similarity of area (off the coast of NC) and the same sensor technology

(HF radar, not ADCP). The resimulation using Itiki's method using NOAA's HF data of 2014 is not feasible because the time window in the NOAA's webpage is restricted to the most recent daily data.

With the characteristic curve of MHK turbines, shown in FIGURE 3.4, with the average water current speed values from Muglia's method in TABLE 3.2, it is possible to estimate the power generated by 270 turbines of Hub1 and 540 turbines of Hub2. Such estimation allows a comparison of power generation between Itiki's and Muglia's methods [65] [70].

TABLE 3.3: Comparison of power based on HF radar data off the coast of North Carolina.

Location	**Method**	**Itiki et al.** [65].	**Muglia et al.** [70].	**Variability (%)**
Hub1 is close to the coverage of HF radar HATY 87 over the edge	Peak power	20 MW	49 MW	-59%
	Average power	11 MW	32 MW	-66%
	Minimum power	2 MW	13.5 MW	-85%
Hub2 is close to the coverage of HF radar CORE 72 over the jet axis.	Peak power	475 MW	389 MW	22%
	Average power	275 MW	189 MW	46%
	Minimum power	150 MW	81 MW	85%

Muglia's method corroborates the results of Itiki's method by associating lower average current speed in Hub1 than Hub2. Considering that the cut-in speed of an MHK turbine is 0.5 m/s, the power output in Hub1 can be expected to be negligible compared to Hub2, as shown in TABLE 3.3. The average current speed by Muglia's method indicates 0.67 m/s in Hub1 and 0.96 m/s in Hub2. Only the seawater speed values that exceed the cut-in speed of 0.5 m/s produce some power on the MHK turbine.

Also, the peak power variability in TABLE 3.2 increases not linearly as compared with peak speed variability in TABLE 3.3. This is consistent with the nonlinear increment of power over current speed derived from the characteristic curve of the MHK turbine. Within the range between the cut-in and cut-out speeds of the turbine, the power curve shape increases exponentially

(cubicle 3), as expected by theoretically-derived Equation (2). In other words, the percent variability of power is higher than the percent variability of speed. This evidence leads to another conclusion on the non-appropriateness of using the average speed of Muglia's method for direct estimation of power profile.

Itiki's method estimates the daily MHK turbine power profile with an hourly resolution, while Muglia's focuses on water speed under a multi-days time window. The cut-in and cut-out speed, which represent the friction and stress of the turbine, should be applied instantaneously (or at least with hourly resolution) for estimation of the power profile under real-world turbine mechanics. In other words, the engineering limitations of the power harvesting efficiency of MHK turbines are not reflected in Muglia's method., which is more concerned with water speed estimation. Turbines do not operate with averaged filtered speed data. Turbines in the real world convert instantaneous water speed into power. Despite TABLE 3.3 showing average power estimated from the average water speed obtained from Muglia's method, power profile estimation using average speed is not conceptually exact.

Another observation of this research is that Muglia's method indicates that MHK energy is majorly located in deeper waters, e.g., in the jet axis, which coincides with the location proposed by Itiki et al., which shows higher power output for Hub2 located in deep waters than for Hub1 located in more shallow waters. In this regard, Muglia's method corroborates the findings of Itiki's method because both indicate that Hub2 has a much higher potential (around six times) for power production than Hub1. Thus, both methods indicate that location and the characteristic curve of the selected MHK turbine, including the cut-in speed, matter a lot in the productivity of an MHK farm.

Finally, Muglia's method also corroborates Itiki's findings that the average water speed in the Gulf Stream off the coast of NC (0.668 m/s in Hub1 and 0.962 m/s in Hub2) is far lower than other high-potential sites in the world, such as Scotland (over 3 m/s) [65].

The comparative analysis of the power and speed results from both methods demonstrates that the method for MHK power profile estimation proposed by Itiki in this dissertation does not show inconsistent results and numbers compared to the method proposed by Muglia et al. in 2022 [65] [70].

3.5 Validation of the method for MHK assessment.

The validation of the MHK method is carried out in two parts:

- Validation of the HF radar as an adequate sensor to estimate MHK power profile.
- Validation of speed using same dataset on Muglia's method of average speed.

The validation of the HF radar as an adequate sensor to estimate MHK power profile is executed by a literature survey.

In 2021, Itiki et al. proposed to estimate instantaneous MHK power profile with HF radar (instead of ADCP) to cover a wide area of the Gulf Stream in North Carolina [65]. The proposed method for estimation of MHK power is presented in Chapter 3. It is worth noting that Itiki et al. did not calculate average density of MHK energy, which is not useful information for power system studies. Itiki et al. calculated instantaneous (not average) power profile of a specific number of turbines (540 and 270) distributed in specific latitude and longitude off the coast of North Carolina.

In 2022, Muglia et al. corroborated the appropriateness of using HF radar data by similarly proposing to estimate MHK power with HF radar in the Gulf Stream in NC [70]. ADCP is not an appropriate sensor for MHK assessment in wide areas [69]. For this reason, the research of Muglia

et al. published in 2022, validates by corroboration the appropriateness of using HF radar sensor for MHK power assessment in the precedent research of Itiki et al, published in 2021 [65].

The second part of the validation is carried out by comparative analysis of both methods using the same input dataset. This validation of Itiki et al. method with Dr. Muglia's method is proven by application in Hub 1 (low water speed location) and Hub 2 (high water speed location).

Since Muglia et al. method does not assign a specific location and quantity of turbines off the coast of North Carolina, the estimation of power profile is obtained by assessment of the spatial average of water speed values on the proximity of the study area for each time step, estimation of averaged power density and multiplication by the same number of turbines considered on the Itiki et al. method.

FIGURE 3.8 (a) shows the water speed profile resulting from the proposed Itiki et al. method varying from 0.35 m/s to 0.61 m/s, mostly within the incursion of manually calculated power profile obtained from manual filtering of the same NOAA HF radar dataset and application of Muglia et al. method. Both profiles show short periods of water speed exceeding the turbine cut-in speed of 0.5 m/s, barely producing power. The mean average in FIGURE 3.8 (a) is 0.48 m/s and in FIGURE 3.8 (b) is 0.37 m/s, representing an error of 29%. The profile tendency of both is upward. Hub 1 (NC North) is very poor in MHK Energy.

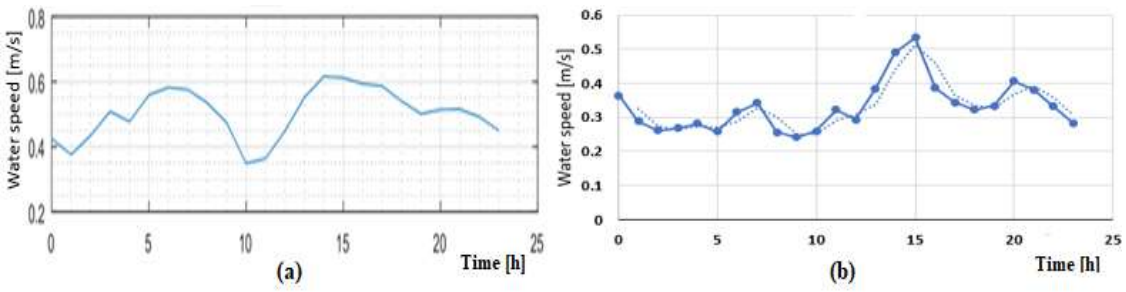

FIGURE 3.8: Hub-1 water speed by (a) Itiki and (b) Muglia method.

TABLE 3.4 shows the difference of water speed profile of Itiki et al. and Muglia et al. method for Hub 1. It should be noted that an MHK turbine does not produce any power at all for its cutout speed of 0.5 m/s. The water speed estimated by using Muglia et al method also corroborates that, as already predicted by Itiki et al. method in the Subsection 3.2, Hub 1 is not located on an area with high-density of MHK energy.

TABLE 3.4: Difference of Hub-1 water speed in Itiki and Muglia.

Time [h]	**Itiki et al.** [m/s]	**Muglia et al.** [m/s]	**Difference** [m/s]
0	0.42	0.36	0.06
5	0.55	0.26	0.29
10	0.35	0.26	0.09
15	0.61	0.54	0.07
20	0.51	0.41	0.1
23	0.45	0.28	0.17
Mean	0.48	0.35	0.13
Max	0.61	0.54	-
Min	0.35	0.26	-

FIGURE 3.9 (a) shows the water speed profile resulting from the proposed Itiki et al. method varying from 1.07 m/s to 1.70 m/s in Hub-2, mostly within the incursion of manually calculated power profile obtained from manual Excel filtering of the same NOAA HF radar dataset. Both profiles show water speed exceeding the turbine cut-in speed of 0.5 m/s, producing power for a long period of the day. Mean average in FIGURE 3.9 (a) is 1.35 m/s and in FIGURE 3.9 (b) is 1.01 m/s, representing an error of 34%. The profile tendency of both figures is downward.

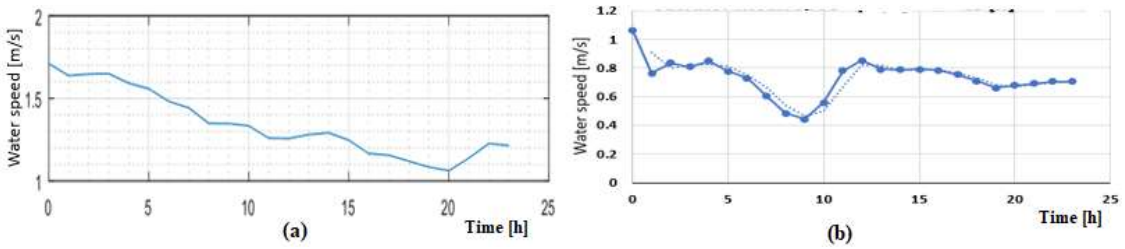

FIGURE 3.9: Hub-2 water speed by (a) Itiki and (b) Muglia method.

Hub 2 (NC South) is rich in MHK energy. Both profiles show long periods of water speed exceeding the turbine cut-in speed of 0.5 m/s.

TABLE 3.5 shows the difference of water speed profile of Itiki et al. and Muglia et al. method for Hub 2. It should be noted that an MHK turbine produces power for most of the time since the cutout speed is 0.5 m/s. The water speed estimated by using Muglia et al method also corroborates that, as already predicted by Itiki et al. method in the Subsection 3.2, Hub 2 is located on an area with high-density of MHK energy.

TABLE 3.5: Difference of Hub-2 water speed in Itiki and Muglia.

Time [h]	**Itiki et al.** [m/s]	**Muglia et al.** [m/s]	**Difference** [m/s]
0	1.7	1.05	0.65
5	1.55	0.79	0.76
10	1.33	0.56	0.77
15	1.25	0.8	0.45
20	1.07	0.68	0.39
23	1.2	0.71	0.49
Mean	1.35	0.77	0.58
Max	1.7	1.05	-
Min	1.07	0.56	-

FIGURE 3.10 shows the power profile of (a) Hub-1 on Itiki et al. method, (b) Hub-1 on Muglia et al. method, (c) Hub-2 on Itiki et al method, and (d) Hub-2 on Muglia et al method.

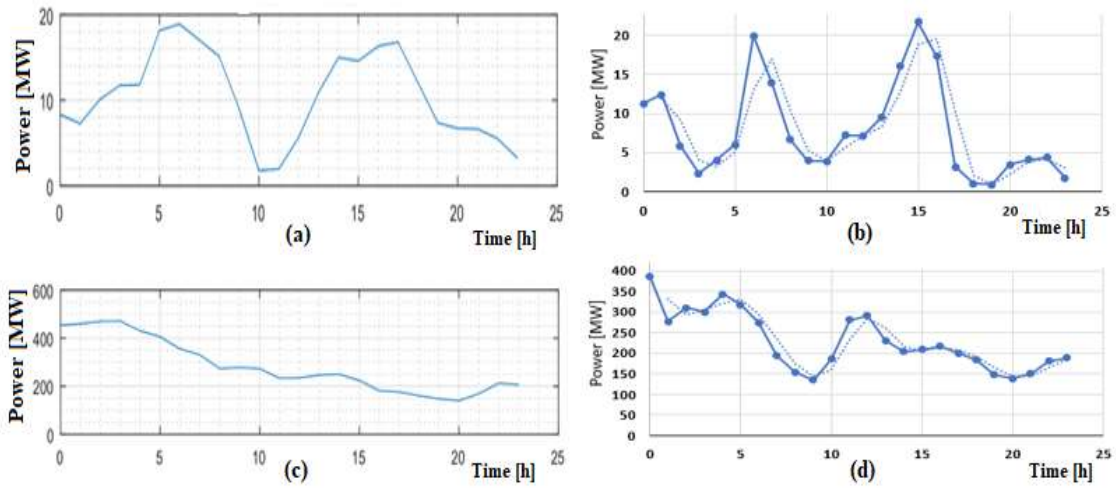

FIGURE 3.10: Hub-1 and 2 power by Itiki and Muglia methods.

Both methods show declining power profile in 24 hours in Hub-1 and 2. Muglia's method also shows that Hub-2 produces much more power (400 MW) than Hub-1 (22 MW). The curves are in the same order of magnitude.

TABLE 3.6 shows the numeric difference observed on the water speed and power estimated by Itiki et al. and Muglia et al method. A difference of water speed and average power from both methods exists and was quantified. A percentual error of only 11% was observed in the validation of results of Hub-2. In Hub-2, most of the MHK turbines operate at a water speed in excess of 0.5 m/s, resulting in lower difference in the power values obtained for both methods. In contrast, Hub-1 operates with most turbines not generating any power at all because the measured water speed is below the minimum cut-in speed of the turbine. This fact introduces a high variability of results in the power assessment by using Muglia et al. method.

TABLE 3.6: Validation points of Itiki et al. method based on Muglia et al. method.

Parameter	**Itiki et al.** [m/s]	**Muglia et al.** [m/s]	**Difference**
Input data	One-day period NOAA HF radar dataset	One-day period NOAA HF radar dataset	None
Number of turbines	Hub1: 270 turbines Hub2: 540 turbines	Hub1: 270 turbines Hub2: 540 turbines	None
Water speed [m/s]	0.48 ± 0.13 in Hub 1; 1.35 ± 0.35 in Hub2	0.35 ± 0.19 in Hub1; 0.77 ± 0.28 in Hub 2	0.13 m/s (37%) in Hub 1; 0.58 m/s (75%) in Hub 2
Power [MW]	8.7 ± 5.7 in Hub1; 283 ± 108 in Hub 2	11.5 ± 10 in Hub1; 255 ± 125 in Hub 2	-2.8 MW (-24%) in Hub 1; 28 MW (**11%**) in Hub 2

Despite the water speed dataset being the same for both methods, Itiki et al. method screens only those data near a MHK turbine, while this screening in Muglia et al method is not as precise because the data acquisition is based on collection of all data in a region surrounding the turbines, even if not the closest one. The Muglia et al. method neither assigns a fixed number of MHK turbines nor a latitude and longitude to them. The power profile in Muglia et al. method is

multiplied by the same number of turbines adopted on the case study of Itiki et al. to allow a tentative comparison and validation. To obtain the power profile in Muglia et al. method, the calculated spatial density of energy is multiplied by the number of turbines. The utilization of spatial average of water speed may not be precise because values below minimum cut-in speed do not produce any power in a MHK turbine, and for those data above cut-in speed, the power output is not linearly proportional to water speed. The simplification assumptions embedded on the Muglia et al. method introduce errors that make it questionable if Muglia et al. method is an adequate benchmark for validation of Itiki et al. method, which is based simply on direct association of the closest data to each turbine. Future alternative methods for MHK power profile estimation in wide-area coverage, possibly with other innovative sensors, such as satellite data, can open the perspective of a comprehensive cross validation of methods in the future.

The validation points obtained from this analysis are:

- In Hub-2, with high MHK energy resources, a discrepancy of 11% is observed on average power estimation using Itiki et al. method as compared to Muglia et al.
- Both methods point out that Hub-2 produces around 22 to 32 times more power than Hub1.
- Most of the range of incursion of power profile of Hub1 and Hub2 estimated using Itiki et al. method is within the range of the power profile using Dr. Muglia's method.

3.6 Conclusions about the method for MHK assessment.

The proposed method for estimating the MHK power generation profile based on HF NOAA radar was successfully implemented in MATLAB script coding. A case study in North Carolina demonstrates the algorithm's functionalities for the planning and design of MHK farms

[65]. The simulations of two proposed MHK farms show that the power profile is highly sensitive to the selected location, with significant implications for the economic feasibility. The southern MHK farm in the Gulf Stream off the coast of North Carolina shows a more robust power profile as compared to the northern MHK farm. Regarding the short time sensitivity, within the one-day time-window simulation, it is possible to conclude that the capacity factor of the MHK turbines varies significantly for one day period. More studies with a large water speed dataset are needed to evaluate the seasonal and multi-year power variability. The case study demonstrated the proposed method implemented in MATLAB script was able to simulate MHK farms with a very high number of turbines without high computational cost. The case study script processed the power profile of 540 MHK turbines in less than 5 minutes in an off-the-shelf notebook with an Intel Core i7 processor. This method fills a gap of the traditional power system algorithms, which usually circumvents the computational cost by assuming simplified equivalent models of MHK farms or simulations with just a handful of electric generators. Also, the merit of this work is the realistic approach to processing HF radar data for power system studies. In other words, the proposed data analytics method directly transforms offshore weather data into valuable power system information. The implications of the proposed method on the natural, economic, social, and political environment open the perspective of a multitude of topics for future multidisciplinary research [65].

CHAPTER 4: PROPOSED METHOD FOR WIND ENERGY ASSESSMENT AND U.S.-CARIBBEAN SG.

Kinetic energy from wind depends on the dynamics of the weather systems and, more broadly, on the environmental system. As overviewed in previous sections, the technical literature vastly covers the assessment of wind in normal conditions. This proposed method for wind energy assessment focuses instead on wind power in extreme weather events, e.g., hurricanes, which are expected to gain intensity due to most likely two degrees Celsius anthropogenic warming [72]. Since hurricanes originate in the hot waters of the oceans, this proposed wind energy assessment method can be understood within the context of an offshore power system (OffPS) architecture.

FIGURE 4.1 shows the context of the proposed method for generating wind power profiles as part of the intelligence system (I) of an OffPS. This architecture encompasses the interaction of the proposed wind assessment method with the offshore generation (G), transmission (T), distribution (D), consumption (C), and environmental (E) systems.

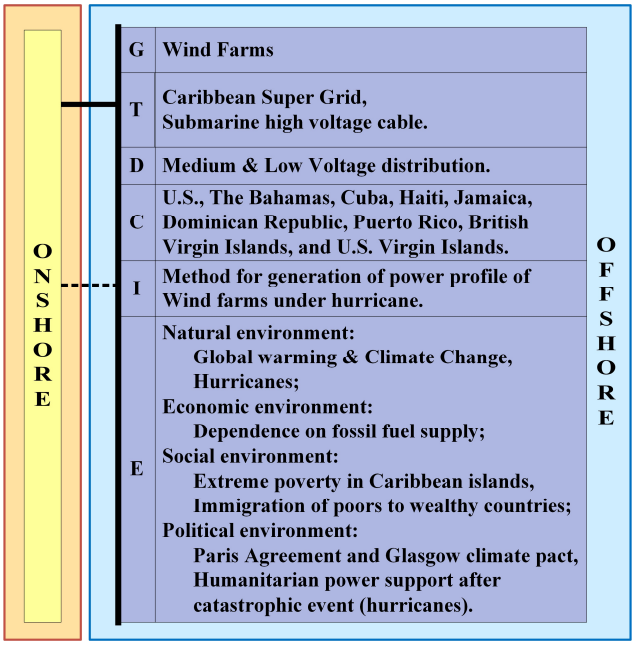

FIGURE 4.1: Architecture for offshore wind power system, adapted from [39].

In the following subsections, this work presents the details of the proposed method and a case study demonstrating its functionalities.

Under this multidisciplinary context and motivations, the method of this research was developed by successive iterations of simple elements, e.g., modeling of a characteristic curve of wind power versus speed, parametric modeling of a static hurricane by Holland's equations [73], the addition of linear movement to a hurricane model, integration of the wind turbine model hit by a moving hurricane, the generation of the power profile of a single turbine, the addition of multiple turbines by an iterative loop. Such a bottom-up approach to the development of a system led to a formal representation of the algorithm, which was necessary to control the complexities of successive incremental iterations. But the algorithm by itself was not enough for the practical objectives of this research as a tool for wind power profile generation and electrical power system studies. Given that the modeling of hurricanes by equations depends on numerous parameters and the recognition of patterns associated with the location of each turbine and the moving hurricane, the formalization of the steps of the investigation was needed to keep track of all patterns. Finally, the research aims at supporting the estimate of wind power flowing in expansions of high voltage power transmission systems, i.e., super grids. In this step, a conceptual design of a super grid was necessary to propose locations of wind turbines realistically in the Caribbeans. In summary, the method builds up into an algorithm for wind power profile calculations, a collection of patterns for modeling, and a brief conceptual design of a super grid for a realistic positioning of wind turbines and simulation. The details of each component of the method are so described in the following subsections.

4.1 A proposed algorithm for wind power under hurricanes.

The proposed algorithm for wind power under hurricanes calculates the aggregate power profile generated by a set of wind turbines spatially distributed in an offshore site in close proximity to the trajectory of a hurricane. The algorithm aims to characterize the worst-case scenario, which tends to become recurrent in times of climate change and global warming. This worst-case scenario provides the reference for the design of the components of the renewable power system [32].

In 1980, Holland and Georgio et al. formulated the classical equation of hurricanes wind speed (V_g) [73], [74]:

$$V_g(r) = \left\{\frac{B}{\rho}\left(\frac{R_{max}}{r}\right)^B (P_n - P_c) exp\left[-\left(\frac{R_{max}}{r}\right)^B\right] + \frac{1}{4}(V_{tr}\sin(\theta_{tr}) - r.f_c)^2\right\}^{0.5} + \frac{1}{2}(V_{tr}\sin(\theta_{tr}) - r.f_c) \quad (4)$$

where: V_g is the 1 min averaged gradient wind speed at a distance (r) from the eye of the hurricane; B is the Holland parameter; ρ is the air density; R_{max} is the maximum radius of the hurricane; r is the distance from the eye of the hurricane; P_n is the ambient pressure; P_c is central pressure; V_{tr} is hurricane translation speed; θ_{tr} is the angle between hurricane direction and a line connecting the center of the hurricane and a particular site; f_c is the Coriolis parameter. Typical values of parametric values are: B = 0.8 to 1.7 [75]; $\rho = 1.225\ kg/m^3$at 15^{o}C; R_{max} = 19 to 85 km (19 km for hurricane Andrew in Florida in 1992 [75], P_n = 1008 milibar (between 1,005 and 1,008 mbar) [73], and P_c= 922 milibar for hurricane Andrew [76]. R_{max}can be obtained directly from the measurements of NOAA [66] or calculated by the equation [76], [75]:

$$R_{max} = 2.63 - 0.000508(P_n - P_c)^2 + 0.0394\varphi + \epsilon_R \quad (5)$$

where: φ is the latitude of the hurricane eye and ϵ_R is an error term (km). In this present study, similar to Andrew [76], [77], $\epsilon_R = Normal(0,0.40)$ at all latitudes. B can be calculated by the equation Andrew [76], [77], [75]:

$$B = 1.38 + 0.00184(P_n - P_c) - 0.00309R_{max} \quad (6)$$

V_g can be empirically converted into the average speed $V_w(r)$ at 90m wind turbine height by the following equation [78]:

$$V_w(r) = 0.923\, V_g(r) \quad (7)$$

The average airspeed $V_w(r)$ passing through a wind turbine changes as the hurricane moves towards the turbine. The change of speed in each turbine of the wind farm is reflected in the overall power flow profile of the super grid.

Another consideration for hurricane modeling is its trajectory. The authors are assuming, by simplification, that the hurricane follows a parabolic trajectory from point A (X_A,Y_A) to Vertex (X_{vertex},Y_{vertex}), with the eye of the hurricane moving at a translational speed V_{tr}.

FIGURE 4.2 depicts the proposed algorithm that estimates the wind power profile of offshore wind farms or arrays under the approach of a hurricane. The algorithm is represented by a diagram with eight processing blocks [32].

Block-1 receives the input data of the latitude and longitude of each wind turbine, the hurricane trajectory, and the edges of the map covering the turbines and the hurricane. Also, the input data include the translational velocity, maximum radius, maximum speed, and the time of the hurricane movement.

Block-2 sets the parametric hurricane modeling based on the classical equation of hurricane speed.

Block-3 proceeds with the modeling of the wind turbine by a technique of equation fitting on the characteristic curve of the wind turbine. This technique interpolates discreet points of the power versus airspeed curve by a fitting equation to facilitate the power estimation processing. Block-4 initializes the iterative loop in which the coordinates of the eye of the hurricane moves in small steps. For each step, the distance between each turbine and the eye of the hurricane is calculated. In Block-5, with these distances, the calculation of the power harvested by each turbine is proceeded by accessing the fitting equation of the power versus airspeed curve. Block-6 proceeds the collection and storage of each calculated power value for each turbine over the entire

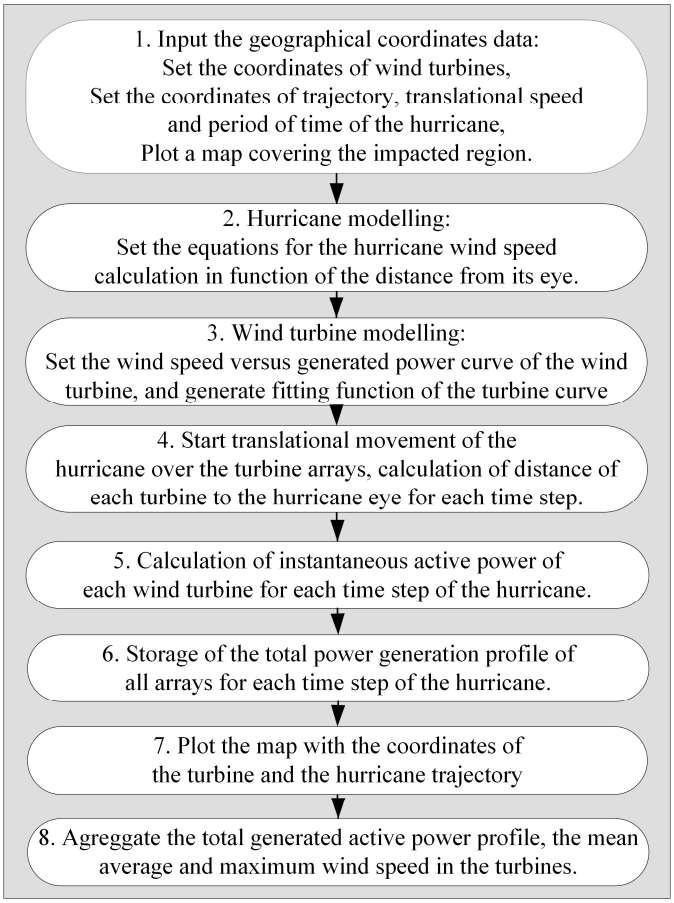

FIGURE 4.2: Algorithm for wind power profile under hurricanes [32].

extent of timesteps, i.e., the power profile of each turbine. Block-7 generates a map of the area of concern depicting the location of each turbine and the trajectory of the eye of the hurricane. Block-

8 aggregates the power profile of each turbine into the total wind power profile during the hurricane passage. It also searches the speed profile of the turbine experiencing the maximum peak of airspeed over the trajectory of the hurricane. Block-8 also calculates the total mean average airspeed profile from the airspeed profile of each turbine [32].

Block-5 and Block-6 of the proposed algorithm calculate the power profile based on the estimated wind speed hitting the turbines. This research considers two types of wind turbines: turbines with typical cutout speed, i.e., a speed above which the turbine stops generating power (typically around 25 m/s), and turbines specially designed for high cutout speed, producing power up to 40 m/s. For short, this work designates and simulates these two types as typical and special turbines, respectively [32].

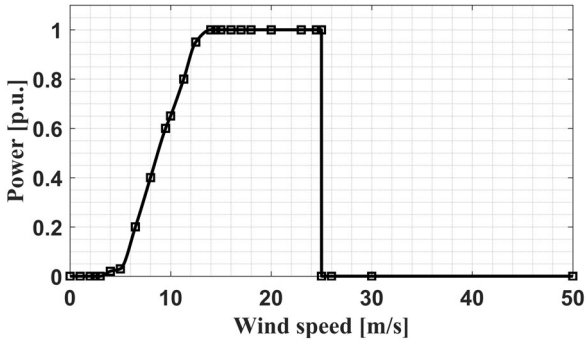

FIGURE 4.3: Curve of power versus airspeed for a 10 MW typical wind turbine [32].

FIGURE 4.3 shows the output characteristic curve of a typical turbine. In this curve, the power output saturates at a constant value if the airspeed varies from 14 m/s to 25 m/s. The turbine power output goes to zero for mechanical protection for airspeed exceeding the cutout speed of 25 m/s [32]. FIGURE 4.4 shows the power curve of a special turbine with a cutout speed of 40 m/s. This type of turbine is being tested on a 10 kW reduced scale. However, this research extrapolates this characteristic curve to a 10 MW scale to compare its performance of power profile variability during hurricanes with a typical turbine in the simulations [32]. Special turbines are commercially

available for cutout speed of 32 m/s [32]. The reason for the extrapolation is to conduct a sensitivity analysis if special wind turbine with extra-high cutout speed in hurricane-prone countries is highly beneficial in smoothing power variability [32].

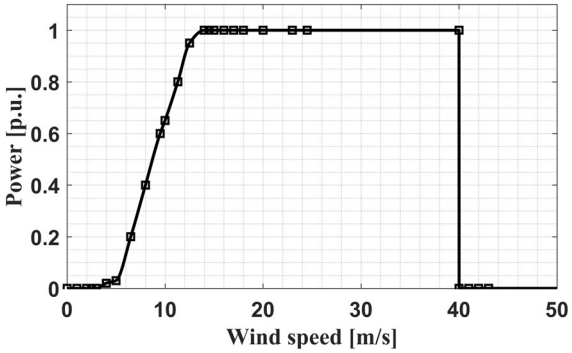

FIGURE 4.4: Curve of power versus airspeed for a 10 MW special wind turbine [32].

These two types of turbines generate two comparative scenarios of simulations.

The algorithm is implemented in MATLAB code programming to explore the practical functionalities of the proposed algorithm.

The implementation of the algorithm in MATLAB script is detailed in APPENDIX B.

A case study investigates the power profile curves of wind power under the spatiotemporal translational movement of a hurricane hitting different parts of the U.S. The case study geographically covers the contiguous U.S., offshore zones, and some countries and territories in the Caribbean region.

Before engaging in simulations, this work establishes the basis for wind power capacity estimation and projection. Later, the work investigates the patterns of hurricane trajectory to establish limited but relevant cases for simulation.

4.2 Spatial distribution of current and future wind power capacity in the U.S.

The most significant amount of wind power capacity in the U.S. territory is listed in TABLE 4.1. The values are aggregated into two macro-regions: Great Plains and West Coast. The reason for this aggregation is to facilitate the distribution of turbines over the U.S. map.

TABLE 4.1: Wind energy capacity (MW) in the top 10 Wind Energy States in U.S.

Regional Power Grids	State	Installed Capacity (MW)
Great Plains (50.7 GW).	Texas	21,450
	Iowa	6,974
	Oklahoma	6,645
	Kansas	5,110
	Illinois	4,026
	Minnesota	3,499
	Colorado	3,029
West Coast (11.6 GW)	California	5,561
	Washington	3,075
	Oregon	3,213

Source: Data of 2016, adapted from [79]

The case study realistically sets the same proportion of 50:11 turbines between the Great Plains and the West Coast. The East Coast is populated with offshore turbines to represent the future OWF sites auctioned by the BOEM (Bureau of Ocean Energy Management) [80].

TABLE 4.2 shows the distribution of wind turbines for the simulation.

TABLE 4.2: Wind turbine's spatial distribution for simulation.

Region	Installed Capacity (MW)
Great Plains	50
West Coast	11
East Coast	10
Total	71

Source: [32].

The simulations keep the proportionality of power capacity in these regions to produce meaningful results even with a reduced scale. The results for the wind power profile of the reduced

but well proportion scale can thus be extrapolated for the analysis of the full gigawatt-scale of the North American power grid.

4.3 Framing of hurricane trajectory patterns for cases study

According to the National Oceanic and Atmospheric Administration (NOAA) in its webpage "Historical Hurricane Tracks" from 1842 to 2021, only two hurricanes made landfall as category-5 in the U.S. territory from 2000 to 2021: Michael in 2018 and Maria in 2017 [66].

FIGURE 4.5 shows the trajectories of the eyes of these two category-5 hurricanes [32].

The trajectories of these two hurricanes are very peculiar. Maria passed through Puerto Rico, followed off the East coast of the Dominican Republic, and turned right to the North Atlantic. Michael hit the Western part of Florida, headed North toward Georgia, South Carolina, North Carolina, Virginia coast, and waned away in the cold waters of the North Atlantic [32].

The following patterns can be observed from the trajectories of the hurricanes making landfall as category-5 from 2000 to 2021:

FIGURE 4.5: Trajectory of category-5 hurricanes from 2000 to 2021 [66].

- One out of two hurricanes run closely parallel to the Puerto-Rico-Cuba corridor.
- The east coast of the U.S. was not directly hit by category-5 hurricanes.
- None of the two hurricanes made landfall on the West Coast (California, Oregon, and Washington State);
- There is no visual correlation between the hurricane trajectory in parallel to the Puerto Rico-Cuba corridor and the location where the hurricane hits the continent after passing the Gulf of Mexico. For example, Hurricane Maria did not pass on the Gulf of Mexico.

Also, according to the same NOAA hurricane track webpage [66], five hurricanes from 2000 to 2021 hit the U.S. coast as category-4: Laura (2020), Harvey (2017), Irma (2017), Katrina (2005), and Charley (2004).

FIGURE 4.6 shows the trajectories of hurricanes making landfall as category-4 from 2000 to 2021 [66]. Hurricanes Michael and Maria are shown as category-4 again, even classified previously as category-5 hurricanes because, in some parts of their trajectories, their speeds were

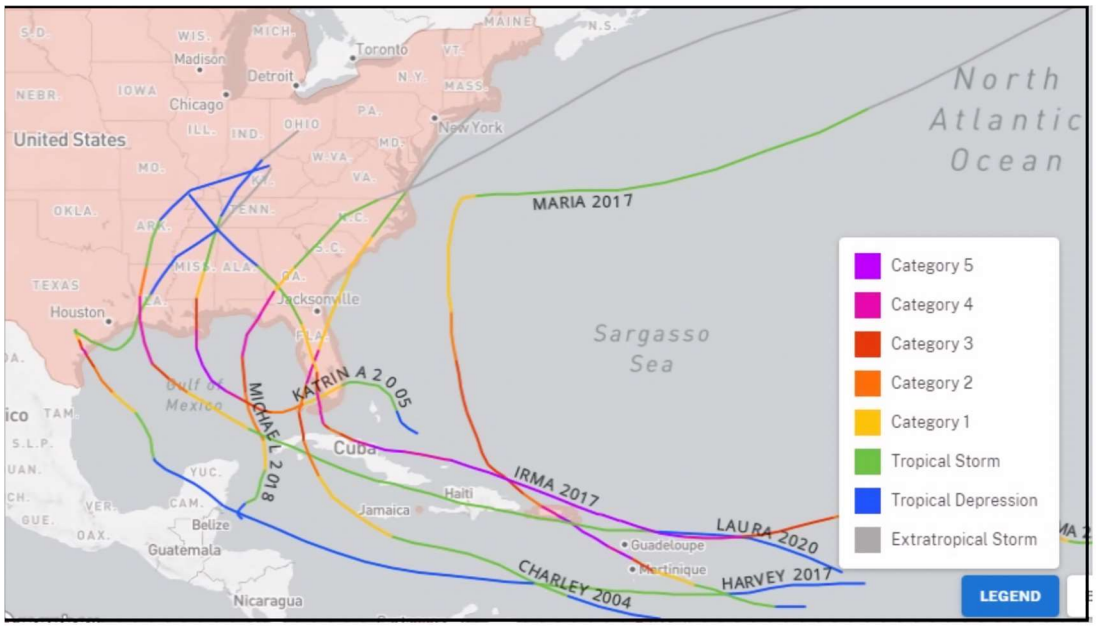

FIGURE 4.6: Trajectory of category-4 hurricanes from 2000 to 2021 [66].

of category-4.

Looking for trajectory patterns in preparation for relevant scenarios for simulation, the hurricanes tracked by NOAA present the following characteristics in common [32]:

- Four out of five category-4 hurricanes made landfall in the contiguous U.S. territory from the Gulf of Mexico and headed toward the U.S. Northeast;
- Four out of five hurricanes follow a trajectory in parallel to the corridor Puerto Rico-Cuba;
- The pattern of category-4 hurricane trajectories is not much different from the category-5 ones. Category-4 hurricanes hit the Southern States mainly by the Gulf of Mexico, e.g., Texas and Louisiana;

FIGURE 4.7 shows the trajectories of hurricanes category-3, 2, and 1, from 2000 to 2021 [66]. Hurricanes category 5 and 4 are shown as category-3, 2, 1 again because in some period along their trajectory, they slowed down to category-3, 2, and 1 speed [32].

Some hurricanes of category-3, 2, and 1 show unique trajectories [32]:

- Five hurricanes lingered over the offshore U.S. East Coast: Mathew (2016), Isaias (2020), Arthur (2014), Irene (2011), and Dorian (2019);

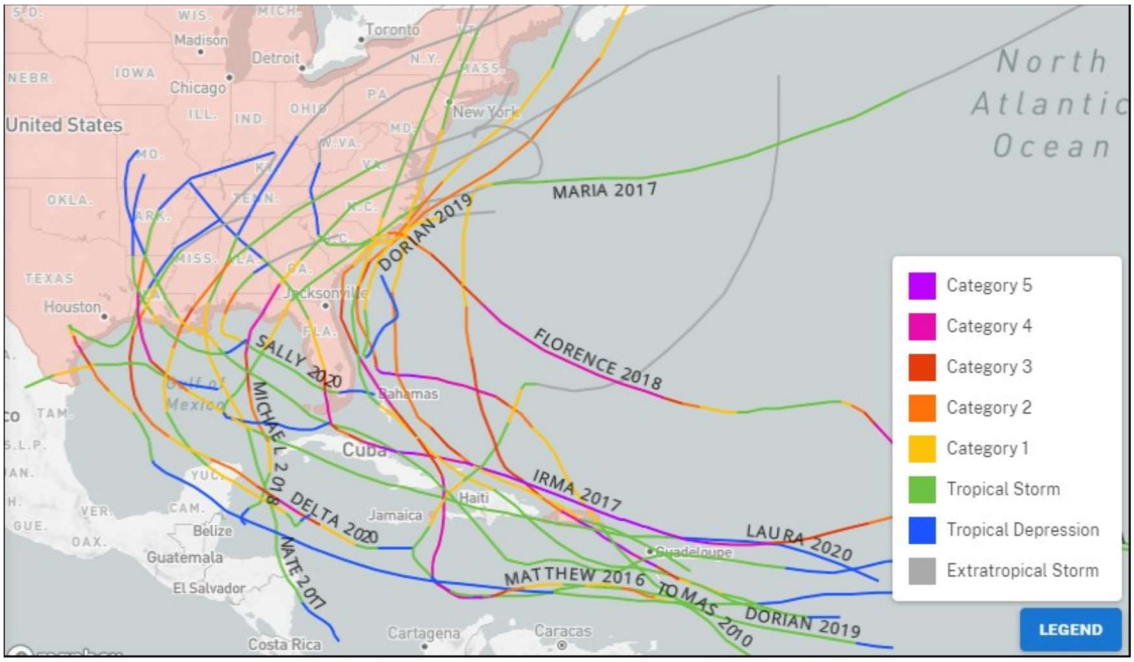

FIGURE 4.7: Trajectory of category-3, 2 and 1 hurricanes from 2000 to 2021 [66].

- A very unusual trajectory is shown on the East Coast. Hurricane Florence (2018) hits the East Coast at a perpendicular angle. However, since this event was sporadic, i.e., not a pattern, it will be neglected in this work.

Based on the recognition of patterns, the following scenarios can be framed for the simulations of wind power profile generation [32]:

- The first part of the hurricane trajectory, which runs in parallel to the Puerto Rico-Cuba corridor, is decoupled from the trajectory from the Mexico Gulf toward the U.S. Northeast. For this reason, the first part is studied apart from the second part of the hurricane trajectory;
- Category-4 and 5 hurricanes can be simulated indistinctly. In other words, a wind farm hit by a category-4 can also be hit by a category-5;
- Wind farms located in all States on the west side of New Mexico, Colorado, Missouri, Illinois, Indiana, Ohio, Pennsylvania, New York, and Vermont are not in the path of hurricanes category-4 and 5. Wind farms located off the coast of California, Oregon, and the Washington

States are not typically subjected to hurricanes, except Hawaii State and Guam island territory. The simulated trajectory of a hurricane passing over these islands is not of interest to this work because of the absence of power interconnectivity. The wind power capacity of Hawaii and Guam are not interconnected to the contiguous U.S. power grid.

Hurricanes of category-3, 2, and 1 show a unique pattern of trajectory lingering along the offshore East Coast. The U.S. East Coast presents a high potential for offshore wind power exploration [80].

FIGURE 4.5, FIGURE 4.6, and FIGURE 4.7 show a distinct pattern associated with the latitude of the hurricane trajectory. Hurricane airspeed intensity slows down from latitude 35^{o} (North of Mississippi) and depleted above latitude 45^{o} (Maine). For this reason, a linear decaying of central pressure is empirically applied in this onshore latitude range [32].

Hurricanes making landfall above latitude 35^{o}, e.g., Florence (2018), are not included in this work. These cases should investigate specific pattern considerations since their associated central pressure at landfall cannot be affected by the linear decaying adjustment before the landfall. Hurricanes making landfall above latitude 35^{o} are extremely rare, as shown in FIGURE 4.5, FIGURE 4.6, and FIGURE 4.7 [32].

The trajectory of hurricanes of category-5, 4, 3, 2, and 1 can be approximated by a pattern of the second-order polynomial equation [32]:

$$y = a.x^2 + b.x + c \tag{8}$$

where: y is the longitude of the hurricane eye, x is the latitude of the hurricane eye, and a, b, and c are constants.

The second-order polynomial equation was chosen because its first-order derivative can be analytically formulated for the trajectory of the hurricane at a constant speed.

Deriving (8) into x, then [32]:

$$\frac{dy}{dx} = 2ax + b \tag{9}$$

Assuming that the vertex point $(Lat, Long)_{vertex}$ is known, and that the derivative is null at the vertex, the parameter b is obtained as [32]:

$$b = -2a.Lat_{vertex} \tag{10}$$

By substituting (10) into (8), and assuming that a second point (Lat, Lon) in the hurricane trajectory is also known, the value of parameter a is given by [32]:

$$a = \frac{Lat - Lat_{vertex}}{(Lon - Lon_{vertex})^2} \tag{11}$$

Having calculated a, and b by (10) and (11), respectively, and knowing the second point (Lat, Lon) , c can be calculated by using (8) as [32]:

$$c = Lat - a.Lon^2 - b.Lon \tag{12}$$

Assuming that the translational speed of the eye of the hurricane is known by the hurricane forecasting, and the position of the hurricane moves at fixed angle step $\Delta step$, corresponding to a time period of one hour, then the latitude after a fixed angle step can be approximated by [32]:

$$Lat_{k+1} = Lat_k + \Delta step.\sin\theta \tag{13}$$

where: $\theta = 90 - \tan^{-1}\frac{dy}{dx}$, and $\frac{dy}{dx}$ is known by (9), and $\Delta step$ is the angle step of 1 hour on the surface of the Earth.

By knowing the values of Lat_{k+1} from (13), constant a from (11), constant b from (10), constant c from (12), and applying these values to (8), the longitude of the next time-step iteration is [32]:

$$Lon_{k+1} = a.Lat_{k+1}^2 + b.Lat_{k+1} + c \tag{14}$$

The hurricane trajectory at a fixed 1-hour step can be iteratively calculated by the simulation algorithm by (13) and (14).

Also, by visual inspection of the hurricane trajectories of FIGURE 4.5, FIGURE 4.6, and FIGURE 4.7, the parabola vertex location can be located approximately in the latitude 30º along a hurricane corridor from longitude -95.5º (Houston, TX) to longitude -79.66º (offshore coast of Jacksonville, FL). A second point of the parabola can be assumed to be located in the Caribbean Sea, in the corridor between points (10.17 º, -56.56 º) and (14.1 º, -47.79 º) [32].

TABLE 4.3 shows the second point of the parabola and the vertex point for ten simulated tracks of hurricanes [32].

TABLE 4.3: Coordinates of the parabola for hurricane trajectory modeling.

Track	Origin Latitude	Origin Longitude	Vertex Latitude	Vertex Longitude
1	8.87	-53.34	30	-95.5
2	9.45	-52.72	30	-93.74
3	10.03	-52.11	30	-91.98
4	10.61	-51.49	30	-90.22
5	11.19	-50.87	30	-88.46
6	11.78	-50.26	30	-86.7
7	12.36	-49.64	30	-84.94
8	12.94	-49.02	30	-83.18
9	13.52	-48.41	30	-81.42
10	14.10	-47.79	30	-79.66

Source: [32]

Recognizing trajectory patterns allows the modeling and framing of multiple scenarios for simulations.

FIGURE 4.8 shows the definition of some parabolic trajectories in preparation for the spatiotemporal assessment of the impact of hurricanes on wind power profile [32].

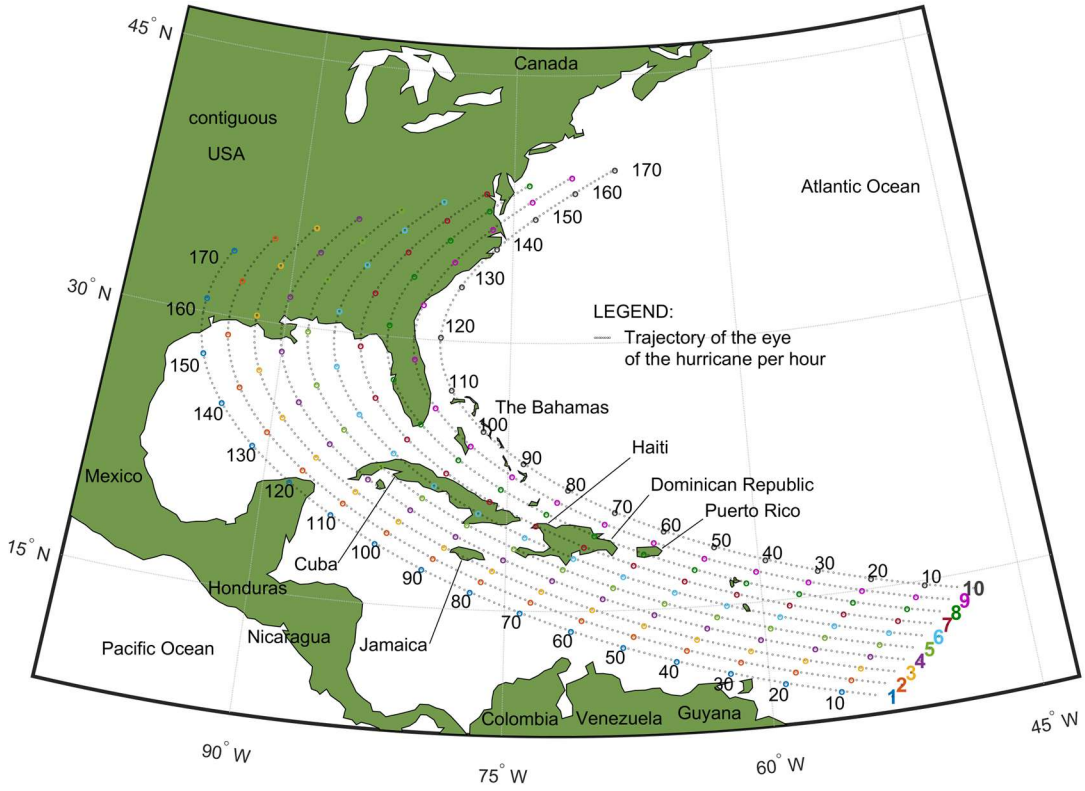

FIGURE 4.8: Scenarios of synthetic trajectories of hurricanes [32].

The synthetic trajectories in FIGURE 4.8 resemble the historical patterns of hurricanes from 2000 to 2021, shown in FIGURE 4.5, FIGURE 4.6, and FIGURE 4.7.

4.4 Patterns of hurricanes intensity

Hurricanes can be classified into five numerical categories according to the Saffir-Simpson scale [81]. TABLE 4.4 shows the association of each category with physical damage [32].

TABLE 4.4: Earlier Saffir-Simpson Hurricane Scale included hurricane damage.

Hurricane category	Winds [km/h]	Surge [m]	Damage
5	> 250	> 5.5	catastrophic
4	210- 250	4 – 5.5	extreme
3	178 - 209	3 - 4	extensive
2	154 - 177	1.8 – 2.4	moderate
1	119 - 153	1.2 – 1.5	minimal

Source: [81]

The modeling of hurricanes by the Holland equation requires previous knowledge of physical parameters as input for numerical calculation. These parameters, e.g., central pressure and the radius of maximum speed, are not in a one-to-one relationship with the classification based on categories [32].

TABLE 4.5 shows some of the parameters of hurricanes measured or estimated by the U.S. National Hurricane Center (NHC) since 2000 [32].

TABLE 4.5: Wind turbine's spatial distribution for simulation.

Hurricane	Category at landfall	Maximum speed at 10m [km/h]	Central pressure (P_C) at landfall [mBar]	Radius of maximum winds RMW (R_{MAX}) [km]	Reference
Michael (2018)	5	259.28	919	27.78	[66]
Maria (2017)	5	250.02	920	27.78	[66]
Laura (2020),	4	240.76	937	27.78	[66]
Harvey (2017)	4	212.98	937	27.78	[66]
Irma (2017),	4	212.98	931	25.928	[66]
Charley (2004)	4	240.76	941	37.04	[66]
Katrina (2005)	3	203.72	923	55.56	[66]
Wilma (2005)	3	194.46	950	55.56	[66]
Zeta (2020)	3	185.2	970	46.3	[66]
Rita (2005)	3	185.2	937	37.04	[66]
Delta (2020)	2	157.42	970	37.04	[66]
Ike (2008)	2	175.94	950	55.56	[66]
Sally (2020)	2	175.94	965	37.04	[66]

For the same category of hurricanes, it is possible to recognize some patterns for simulation. For example, category-5 hurricanes can be simulated assuming the parameters of hurricane Michael (2018), which is similar to hurricane Maria (2017). The largest radius of maximum winds of category-4 hurricanes is 37.04 km, corresponding to hurricane Charley (2005). For category-3, hurricanes Katrina (2005) and Wilma (2005) show the largest radius of maximum winds (55.56 km). However, Katrina (2005) is a very atypical category-3 hurricane with a central pressure lower than category-4 Charley (2005). Wilma (2005) is a better candidate for category-3 hurricane simulations, keeping a crescent order of central pressure between hurricane categories [32]. In summary, the parameters of hurricanes Michael (2018), Charley (2004), and Wilma (2005) present the largest radius of maximum wind in the category-5, 4, and 3, with a crescent central pressure order, respectively. The parameters of these three hurricanes are used as patterns of category-5, 4, and 3 hurricanes for the spatiotemporal wind power flow simulations [32].

The central pressure of hurricanes and the radius of maximum speed increase their magnitude after making landfall [32].

FIGURE 4.9 shows the pattern of variation of central pressure and maximum wind radius based on the location of the hurricane eye. This pattern is a simplified derivation of the original

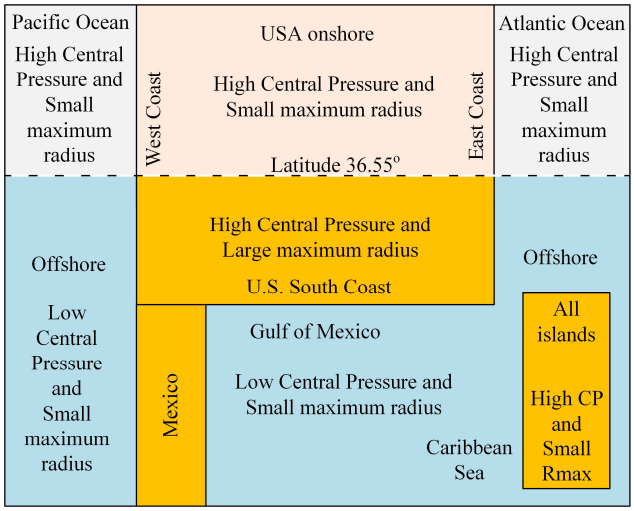

FIGURE 4.9: Patterns of central pressure and maximum radius of hurricanes [32].

curves of central pressure and maximum wind radius reported by NOAA [66]. The latitude 36.55° corresponds to the northern limit of North Carolina State. Above this latitude, the hurricanes start to wane in intensity and maximum wind radius, based on the pattern in FIGURE 4.5, FIGURE 4.6, and FIGURE 4.7 [32].

TABLE 4.6 shows the values of central pressure and the maximum radius of the three hurricanes selected for simulations. These data are obtained from the central pressure and maximum radius profiles reported by NOAA [66]. High values of hurricane wind speed are associated with low central pressure, small maximum wind radius, and offshore trajectory in low latitude (< 28.5°). These parametric values complement the patterns of the hurricane eye position shown in FIGURE 4.8 [32].

TABLE 4.6: Patterns of central pressure and maximum wind radius of hurricanes.

Hurricane name	Michael (2018)	Charley (2004)	Wilma (2005)
Hurricane category at landfall	5	4	3
Low Central Pressure [mbar]	919	941	950
Small maximum wind radius [km]	64.82	18.52	18.52
High Central Pressure after landfall [mbar]	970	975	980
Large maximum wind radius after landfall [km]	240	55.56	37.04
Translational speed at landfall [m/s]	9.722	12.5	13.333

Source: [32]

The difference between TABLE 4.5 and TABLE 4.6 is that TABLE 4.5 is valid instantaneously at landfall only, while the parameters in TABLE 4.6 are average values more appropriate for onshore and offshore trajectories [32].

The central pressure and maximum wind radius patterns are essential for the dynamic representation of the wind speed intensity and the spatiotemporal power profile simulation along

the hurricane trajectory [32]. The translational speed of the eye of hurricanes varies along the trajectory. For comparison purposes, since hurricanes are simulated along the same parabolic trajectory, the translational speed for all cases is set at the same 9.722 m/s translational speed of hurricane Michael (2018) [32].

4.5 Patterns of airspeed in wind turbines before the impact of a hurricane

Wind turbines are spread in the U.S. in regions with different average wind conditions. The average minimum airspeed is associated with each turbine based on its location. These values set the initial wind speed conditions for the power flow calculation before the impact of the approaching hurricane [32].

FIGURE 4.10 shows the airspeed in pre-hurricane conditions, based on a simplified pattern recognition of the annual average wind speed values in the United States assessed by the National Renewable Energy Laboratory [82].

Such wind speed patterns are dominant in the wind power profile simulations if the calculated hurricane speed in each turbine location does not exceed these minimum values.

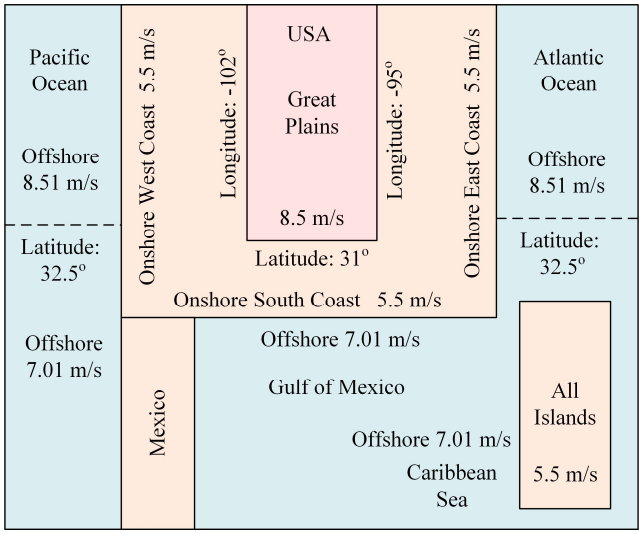

FIGURE 4.10: Patterns of airspeed in pre-hurricane conditions, simplified from [82].

4.6 Patterns of the radius of minimum wind of hurricanes

According to the National Hurricane Center, a tropical-storm-force wind can stretch as far as 300 miles (482 km) from the center of a large hurricane [83]. In other words, a hurricane's speed ranges from 17.5 to 32.7 m/s (tropical-storm speed) for a 482 km distance from its eye. However, a wind turbine operates from a cut-in speed of approximately 4 m/s up to 25 m/s for typical turbines, or 40 m/s for special turbines, as previously shown in FIGURE 4.3 and FIGURE 4.4. For power profile calculation on wind turbines under hurricanes, it is necessary to estimate the radius of minimum wind, i.e., the radius in which the airspeed starts to pick up due exclusively to its force. For simulation purposes, this minimum speed corresponds to the patterns of airspeed in pre-hurricane conditions, shown in FIGURE 4.10. For example, a hurricane in the Gulf of Mexico starts to pick up speed if the hurricane speed exceeds 7.01 m/s at 120 m height, as shown in FIGURE 4.10. In order to establish an external boundary for the simulated hurricane by a radius of minimum speed, this research applies a linear interpolation over the curve of gradient balance wind speed [m/s] versus the distance from the hurricane eye presented at [84]. For the linear interpolation, three parameters are needed: the pressure profile parameter B, pre-calculated by equation (3); the radius of maximum speed (RMW), obtained from NOAA [66]; and the pre-hurricane airspeed as shown in FIGURE 4.10.

TABLE 4.7 shows the linear interpolation results obtained from these three parameters that were applied to the curve of gradient balance wind speed versus distance according to [84]. The radius of minimum speed is calculated for offshore and onshore hurricane trajectories [32].

TABLE 4.7: Patterns of the radius of minimum wind for the selected hurricanes.

Hurricane name	Michael (2018)	Charley (2004)	Wilma (2005)
Hurricane category at landfall	5	4	3
Radius of Maximum Wind (RMW) for offshore [km] [66].	64.82	18.52	18.52
B before landfall (offshore), calculated by Equation (3)	1.34	1.45	1.43
Wind speed in offshore [m/s], according to FIGURE 4.10	7.01	7.01	7.01
Ratio of the radius of minimum wind per RMW for offshore	15.1	14.4	14.5
Radius of minimum speed [km] in offshore	981	267	269
RMW for onshore [km] [66].	74.08	55.56	37.04
B after landfall (onshore), calculated by Equation (3)	1.22	1.27	1.32
Wind speed in onshore [m/s], according to FIGURE 4.10	5.5	5.5	5.5
Ratio of the radius of minimum wind per RMW for onshore	19.0	16.7	15.8
Radius of minimum speed [km] for onshore	1408	927	585

Source: [32]

These estimates of the radius of minimum speed for offshore and onshore cases are used in the simulation to establish an external boundary for the hurricane calculated by equation (1) and the pattern for a pre-hurricane airspeed of FIGURE 4.10 [32].

4.7 Conceptual design of the Caribbean super grid

In this scenario, this research investigates the technical feasibility of a proposed submarine power interconnector between the Caribbean islands and the contiguous U.S. power grid. After the analysis of the technical feasibility of the physical trajectory, a series of simulations assess the benefits of the interconnectivity for the reduction of power variability [32].

A conceptual design of the proposed trajectory for a submarine power interconnector should meet some technical requirements. One of them is the maximum water depth for cable lying down in the seabed. According to the technical literature, 3,000 m seems to be a reference for the

maximum depth for the installation of the submarine cable [85], [86]. Another requirement is the length of the interconnector segment, which should not exceed 879 km, a circuit length feasible in existing submarine interconnector projects [87]. Lastly, the trajectory should maximize the social benefit by interconnecting islands with a high population. On the other hand, the trajectory should interconnect islands with a large fossil fuel power generation capacity to maximize the environmental benefits with the displacement of fossil fuel [32].

TABLE 4.8 shows the proposed submarine power interconnector segments. Initially, the research investigated a segment interconnecting Caicos Islands and the Dominican Republic. However, this alternative is rejected because these islands are separated by a deep trench called Western Hispaniola Trough, with an average water depth of 4,200 m [88] [89]. The Western Hispaniola Trough is 2500 m in depth at Silver Spur [89]. However, the large population of Cuba makes it more attractive than Caicos Islands as a route for the submarine cable. For this reason, the proposed Caribbean super grid interconnects Florida, the north and western islands of The Bahamas, Cuba, Haiti, Jamaica, Dominican Republic, Puerto Rico, U.S. Virgin Islands, and the British Virgin Islands [32].

TABLE 4.8: Segments of the proposed Caribbean super grid.

Segments	Distance (km)	Maximum water depth (m)	Reference
Florida (West Palm Beach) to the Bahamas (Freeport)	142	800	[90]
The Bahamas (Freeport) to Cuba	564	680	[91]
Cuba to the Haiti/Dominican Republic	639	2,000	[88]
Haiti to Jamaica (over Navassa Ridge, Formiga Bank, and Homes Bank)	537	2,500	[92]
Dominican Republic to Puerto Rico	381	1,100	[93]
Puerto Rico to the U.S. Virgin Islands (Saint Thomas)	179	79	[94]
Puerto Rico to U.S. Virgin Islands (Saint Croix)	194	2,507	[94]

Source: [32]

TABLE 4.9 shows the population of some Caribbean islands. In order to maximize the social and environmental benefit of renewable power distribution and consumption, the proposed interconnector should provide power supply services to the most highly populated Caribbean islands. Cuba, Haiti, Dominican Republic, Jamaica, and Puerto Rico have the largest populations in the Caribbean region. In the column of installed power capacity, this research assumes that only three Bahamas islands are partially supported by the interconnector since the remaining islands are separated by deep trenches, irregular seabed topography, and scarps. All islands shown in TABLE 4.9 are highly dependent on fossil fuels for power supply. The average fossil fuel dependency of these islands for the power supply was extremely high (89 %) in 2016. The installed power capacity per capita indicates a significant energy consumption gap among islands. The proposed power interconnectivity scheme between Caribbean islands can bridge this economic and social gap [32].

TABLE 4.9: Population, power capacity, and fossil fuel dependence of Caribbeans.

Country or territory	Population (*million in the year*)	Population Reference	Installed power capacity [MW] (estimated in 2016) [95]	Total installed capacity driven by fossil fuel, and estimated in 2016) [95]	Installed power capacity per capita. [MW / million people]
The Bahamas	0.4 x 22.3% = 0.089 in 2021	[96] [97]	577 x 22.3% = 129	100%	1443
Cuba	11.3 in 2021	[96]	6,998	91%	619
Haiti	11.5 in 2021	[96]	332	82%	29
Dominican Republic	11 in 2021	[96]	3,839	77%	349
Jamaica	3 in 2021	[96]	1,078	83%	359
Puerto Rico	2.8 in 2021	[96]	6,294	94%	2248
U.S. Virgin Islands (St. Thomas and St. John)	0.0557 in 2020	[98]	325 x 53% = 172	98%	3088
U.S. Virgin Islands (Saint Croix)	0.0506 in 2020	[98]	325 x 47% = 153	98%	3024
The British Virgin Islands	0.030 in 2020	[99]	45	97%	1507
Total	39.825 around 2020 and 2021	[96], [98], [99]	19,040	89%	478

TABLE 4.10 shows a comparison between the population and power capacity both in the U.S. and the Caribbean islands, which are the two regions under consideration in this research. The installed capacity driven by fossil fuel is 19% higher in the Caribbean islands than in the U.S. The relatively lower participation of fossil fuels in the U.S. can be explained mainly by the support of nuclear power (9% of total installed capacity in 2017) and hydroelectric plants (7% of total installed capacity in 2017), according to [95]. Vertical analysis of the installed capacity per capita shows that, on average, North Americans are supported by 6.8 times more power capacity than the residents of the selected Caribbean islands. This comparative analysis provides some important numbers illustrating the gap between two different worlds. This gap in the power supply availability can be shortened by the proposed interconnector between the power grids of the contiguous U.S. and the selected Caribbean islands [32].

TABLE 4.10: Population, power capacity, and fossil fuel dependence in the U.S. and some selected Caribbean islands.

Country	Population (*million in the year*)	Reference	Installed power capacity (2016 est.) [MW] [95]	Total installed capacity driven by fossil fuel, and estimated in 2016) [95]	Installed power capacity per capita [MW/million people]
United States of America	334.998398 (July 2021 est.)	[95]	1,087,000	70%	3,245
Caribbean islands, indicated in TABLE 4.9	39.825 around 2020 and 2021	[96], [98], [99]	19,040	89%	478

FIGURE 4.11 shows the proposed route of the power interconnector in the islands of the Caribbean region. Despite such opportunities for wealth distribution and humanitarian support, this research notes essential data shown in TABLE 4.10, i.e., the installed power capacity of the selected Caribbean islands of 19.04 GW. From this 19.04 GW capacity, 89% of power capacity driven by fossil fuel corresponds to 17 GW [32].

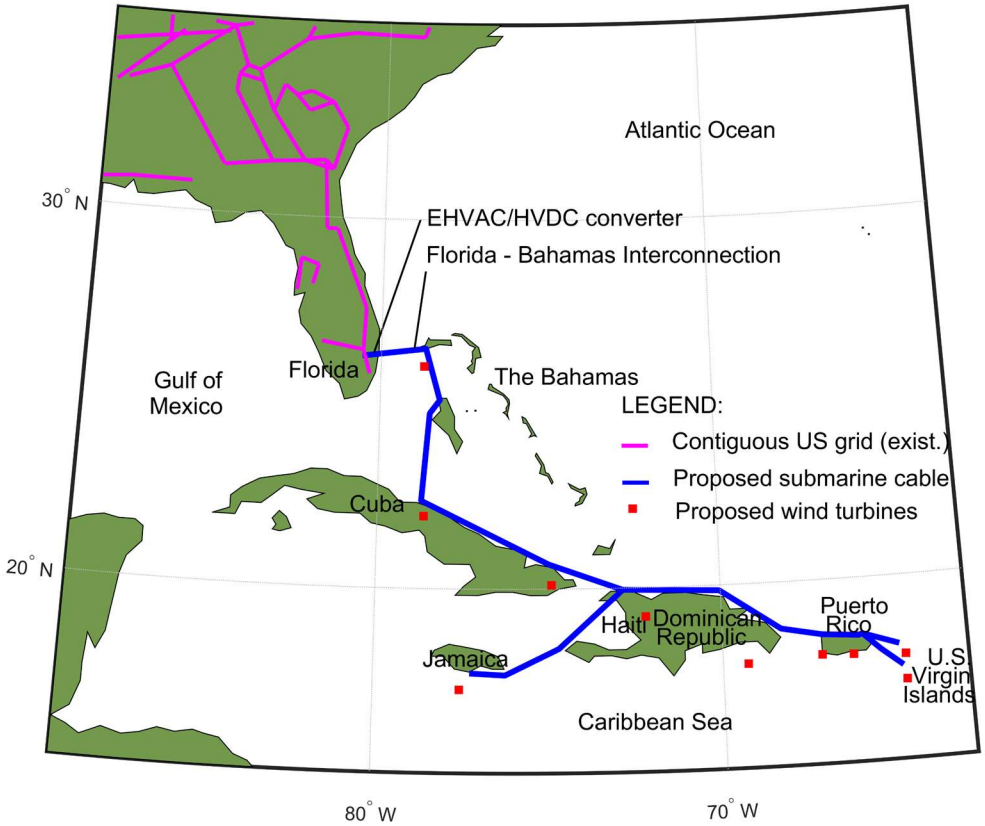

FIGURE 4.11: Proposed Caribbean SG with interconnector in Florida [32].

To structure a case study for further simulation and analysis, it is necessary to estimate the renewable power capacity.

The selected Caribbean islands have two global benchmarks for their renewable programs: Germany and the United Kingdom. According to 2017 estimates in Germany, the total installed power capacity from hydropower was 2%, from other renewable sources was 52%, and nuclear fuel was 5% [95]. The total non-carbon power capacity corresponds to 59%. Similarly, the 2017 estimates in the United Kingdom, the total installed power capacity from hydropower was 2%, from other renewable sources was 39% and from nuclear fuel was 9% [95]. The total non-carbon power capacity corresponds to 50%.

For this reason, this research makes the following assumptions [32]:

- The selected Caribbean islands would follow the highly successful examples of Germany and the U.K. and set a target of around 50% of renewables. In the case of the Caribbean islands, it is assumed that all the renewables in the selected islands would be based exclusively on wind farms, not solar power associated with battery energy storage. Under such assumptions, 50% of the total power capacity (19.040 GW) corresponds to 9.52 GW wind power capacity operating resiliently in normal weather or hurricane conditions.
- The wind turbines are hurricane-proof.
- The high voltage interconnector is mostly implemented by submarine cable and high voltage direct current (HVdc) technology with controlled bidirectional power flow. The high voltage interconnectivity scheme of these selected islands is called in this research as the Caribbean super grid.

For simulation purposes, by keeping the same proportionality of 1 GW of real wind power capacity to one simulated turbine of 10 MW, the selected Caribbean islands can be associated with ten wind power turbines of 10 MW [32].

4.8 Analysis of power profiles of offshore wind farms under hurricanes.

This work investigates ten synthetic trajectories to emulate the hurricane alley, typically stretching from the Caribbean Sea, the Gulf of Mexico, the Great Plains, and reaching the U.S. East Coast. Hurricanes can also be of five categories of intensity, and for simplification purposes, this work selected the highest ones (category-5, 4, and 3). This research also investigates the impact of an interconnection between the local Caribbean power grids and the contiguous U.S. power grid, generating two sets of simulations, i.e., with and without the Caribbean super grid. Finally, the characteristic curve of power versus airspeed of turbines [32].

TABLE 4.11 summarizes the multitude of simulation cases in different hurricane trajectories.

TABLE 4.11: Cases for simulation

The Caribbean super grid WITH interconnection to the contiguous U.S. power grid	Typical turbines (cutout speed 25 m/s)	Hurricane category-5	Trajectory #1 to 10
		Hurricane category-4	Trajectory #1 to 10
		Hurricane category-3	Trajectory #1 to 10
	Special turbines (cutout speed 40 m/s)	Hurricane category-5	Trajectory #1 to 10
		Hurricane category-4	Trajectory #1 to 10
		Hurricane category-3	Trajectory #1 to 10
The Caribbean super grid WITHOUT interconnection to the contiguous U.S. power grid	Typical turbines (cutout speed 25 m/s)	Hurricane category-5	Trajectory #1 to 10
		Hurricane category-4	Trajectory #1 to 10
		Hurricane category-3	Trajectory #1 to 10
	Special turbines (cutout speed 40 m/s)	Hurricane category-5	Trajectory #1 to 10
		Hurricane category-4	Trajectory #1 to 10
		Hurricane category-3	Trajectory #1 to 10

Source: [32]

The purpose of this multitude of cases is to investigate the positive and negative impact of hurricanes on a proposed Caribbean super grid dedicated to wind power, the benefits of wind

turbines with higher cutout speed, the differences of hurricane categories in the power system, and the influence of different trajectories in the power peak and duration of a hurricane. The collection of all simulated cases later supports a comprehensive comparative analysis of the case study [32].

4.9 US-Caribbean SG with typical turbines, category-5 and trajectory #1

The hurricane crosses the Caribbean Sea very close to Jamaica, reaches the Gulf of Mexico, makes landfall in Texas, and crosses significant portions of the Great Plains [32].

FIGURE 4.12 shows the trajectory of the hurricane model hitting the U.S. South Coast and the geospatial distribution of wind power capacity [32].

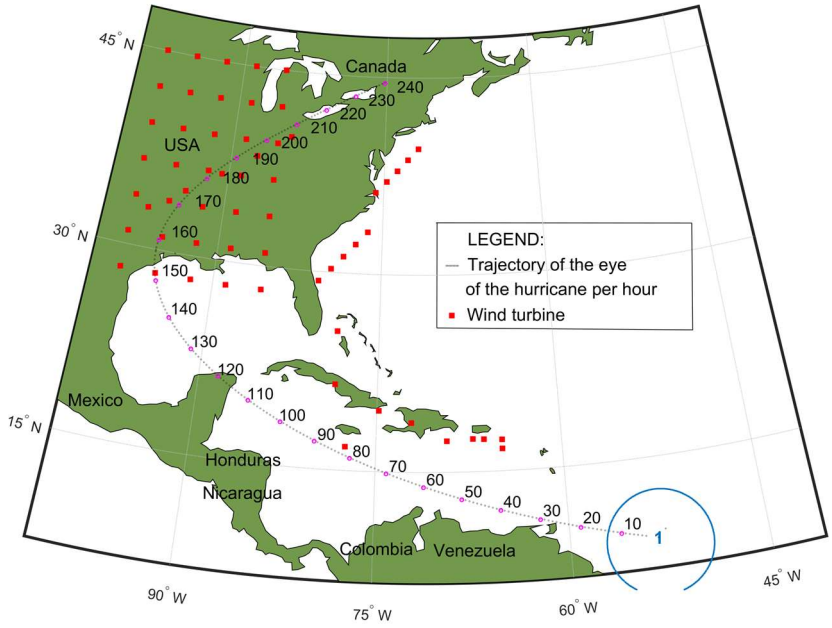

FIGURE 4.12: Map of trajectory #1 of a hurricane category-5 [32].

FIGURE 4.13 shows the total power profile generated by the hurricane's movement, the average mean airspeed experienced by all turbines, and the maximum airspeed profile experienced by a turbine with the highest airspeed peak. The power profile shows two waves. The first one corresponds to the hurricane movement in the Caribbean Sea in the period between 20 h to 110 h.

This wave is mild because the hurricane trajectory is distant from the turbines of the Caribbean super grid. The second wave, after time 155 h, is robust and corresponds to the movement of the hurricane over the Great Plains [32].

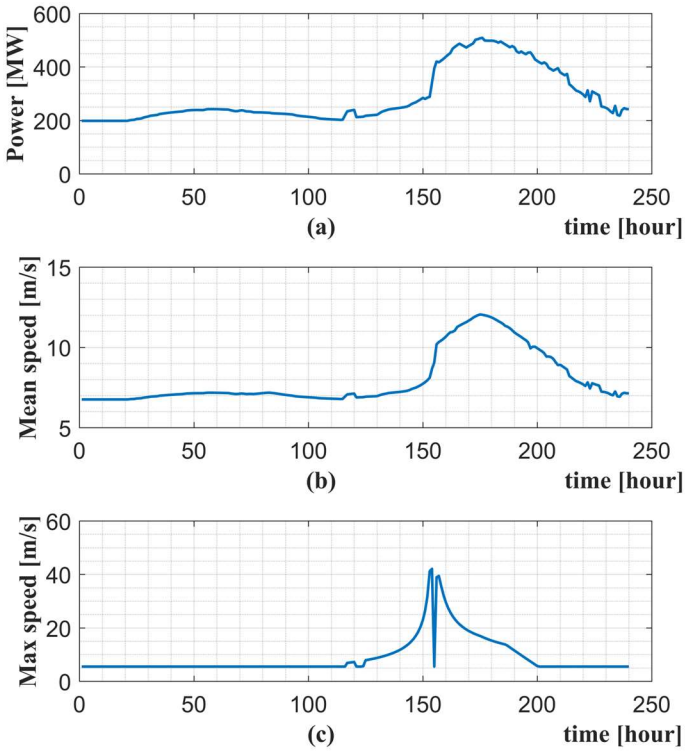

FIGURE 4.13: Profiles for category-5 hurricane in trajectory #1 [32].

4.10 US-Caribbean SG with typical turbines, category-5 and trajectory #5

FIGURE 4.14 shows hurricane trajectory #5. The hurricane crosses the Caribbean Sea on the southern coast of the U.S. Virgin Islands, Puerto Rico, Dominican Republic, Haiti, and Cuba before reaching the Gulf of Mexico. It makes landfall on the border of the Mississippi and Alabama, crosses the eastern portions of the Great Plains, and the offshore coast of Maine [32].

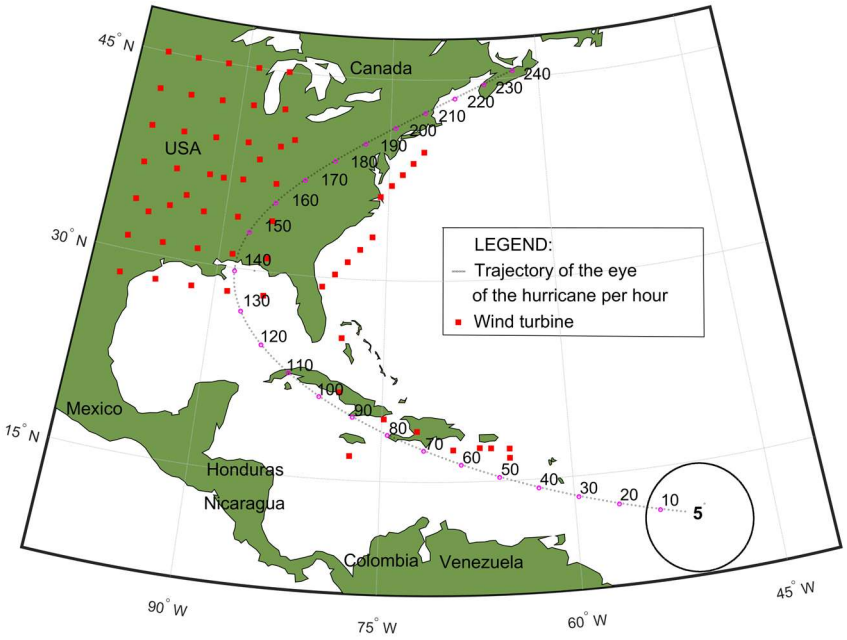

FIGURE 4.14: Map of category-5 hurricane in trajectory #5 [32].

FIGURE 4.15 shows the total power profile generated by the passage of the hurricane on trajectory #5 [32].

The first wave of hurricane wind power is very mild. Most generated power occurs on the second wave over the Great Plains. The mean airspeed faced by all turbines is higher in the inland segment because the radius of maximum speed increases significantly after running over the land [32].

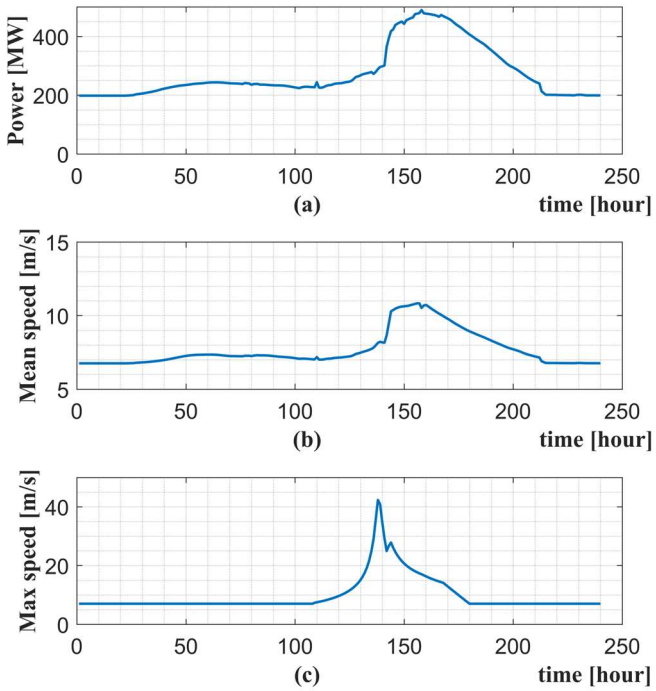

FIGURE 4.15: Power profile for category-5 hurricane in trajectory #5 [32].

4.11 US-Caribbean SG with typical turbines, category-5 and trajectory #7

FIGURE 4.16 shows a hurricane in trajectory #7 hitting the Caribbean super grid, moving toward the Gulf of Mexico, making landfall on the west coast of Florida, crossing the Southeast region, and returning to the Atlantic Ocean in New Jersey [32].

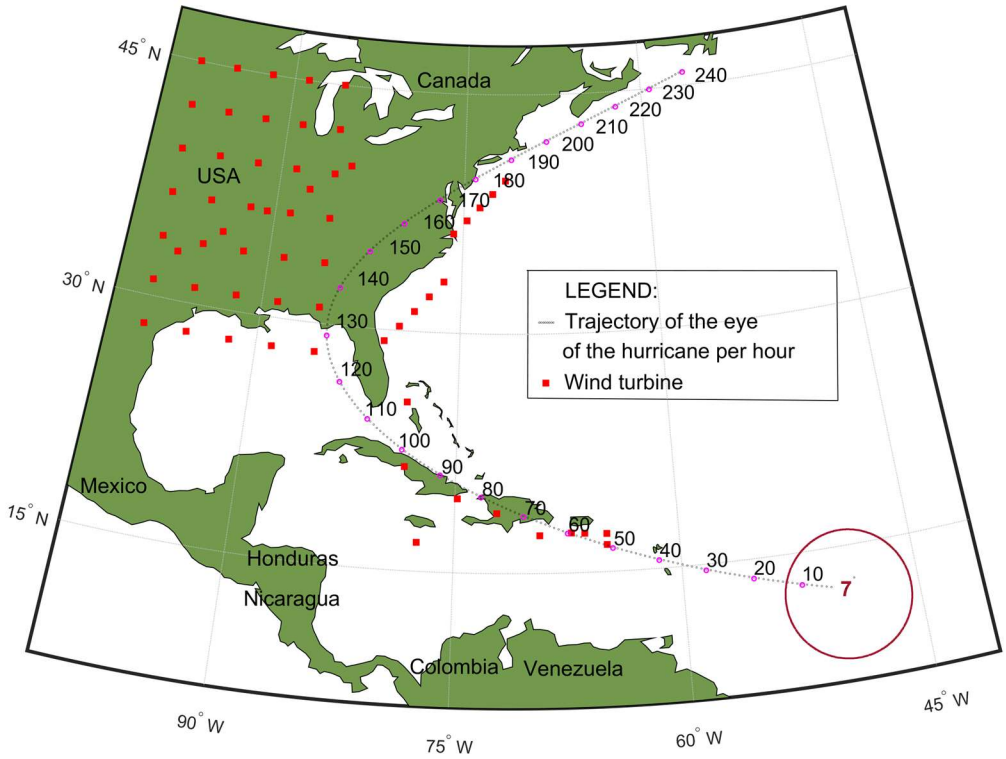

FIGURE 4.16: Map of category-5 hurricane in trajectory #7 [32].

FIGURE 4.17 shows the total power profile of the hurricane. Soon after the landfall, the hurricane radius of maximum speed increases, extending the hurricane wind coverage over some turbines of the Great Plains and the Southeast coast. After its return to the Atlantic Ocean, the hurricane loses strength, and less power is produced in the offshore Northeast coast wind farms. Also, FIGURE 4.17 shows the mean average airspeed experienced by all turbines and the maximum airspeed profile experienced by a turbine with the highest airspeed peak [32].

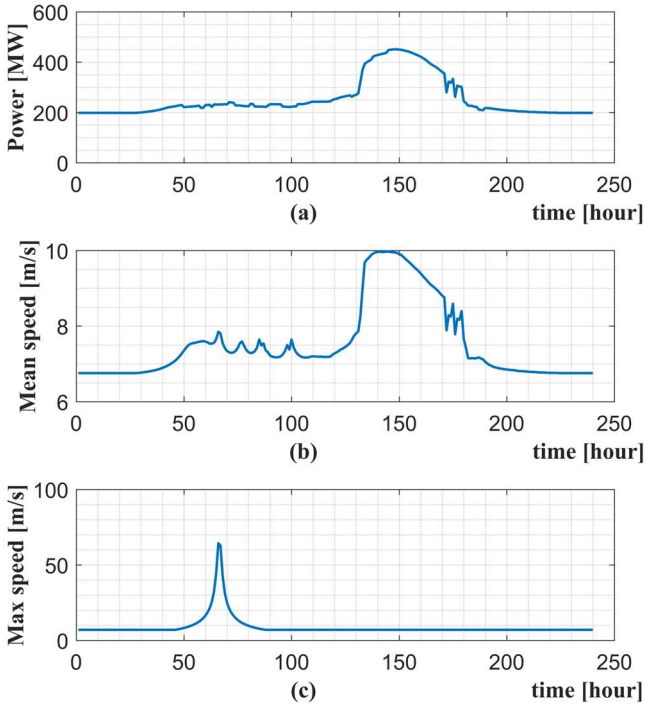

FIGURE 4.17: Power profile for category-5 hurricane in trajectory #7 [32].

4.12 US-Caribbean SG with typical turbines, category-5 and trajectory #9

FIGURE 4.18 shows hurricane trajectory #9 passing over the northern coast of Puerto Rico, Dominican Republic, Haiti, Cuba, The Bahamas, and the U.S. East Coast [32].

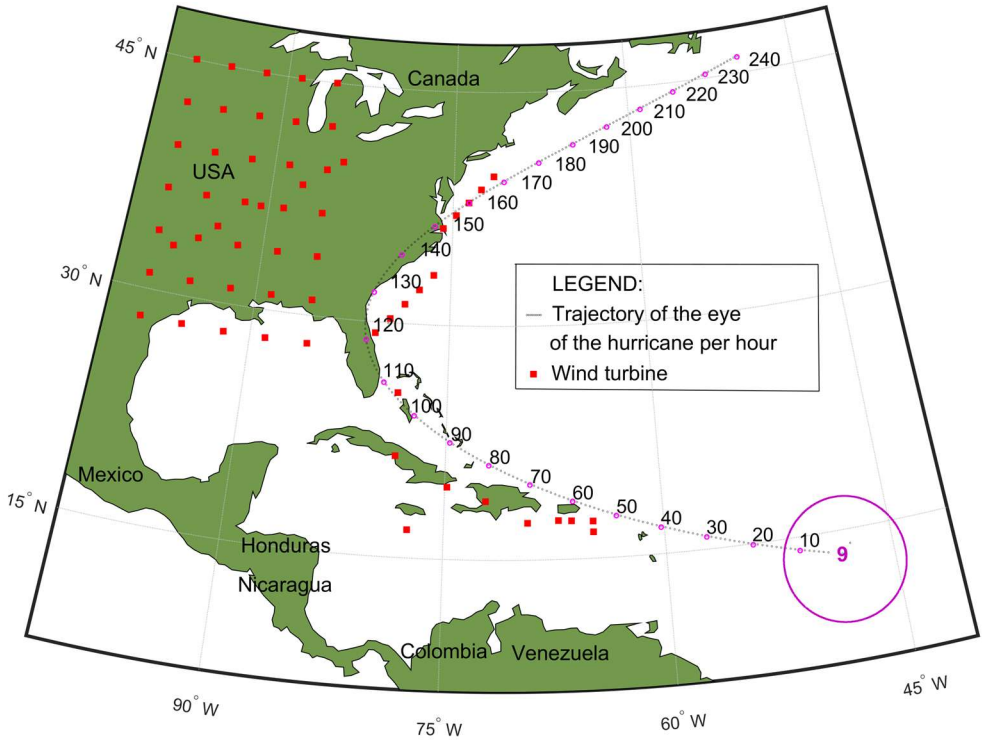

FIGURE 4.18: Map of category-5 hurricane in trajectory #9 [32].

FIGURE 4.19 shows the total power profile, the mean average airspeed experienced by all turbines, and the maximum airspeed profile experienced by a turbine with the highest airspeed peak. From time 50 h to 65 h, the hurricane approaches many turbines in Puerto Rico, which produces the first power wave in the Caribbeans. The hurricane produces a second wave from time 70 h to 150 h, which corresponds to the Southeast Coast of the U.S. The hurricane, from time 125 h to 132 h, moves back temporarily to the sea, reduces its radius of maximum speed, and limits the delivery of kinetic energy to distant turbines. As soon as the hurricane reentries the land after time 135 h, the power profile increases [32].

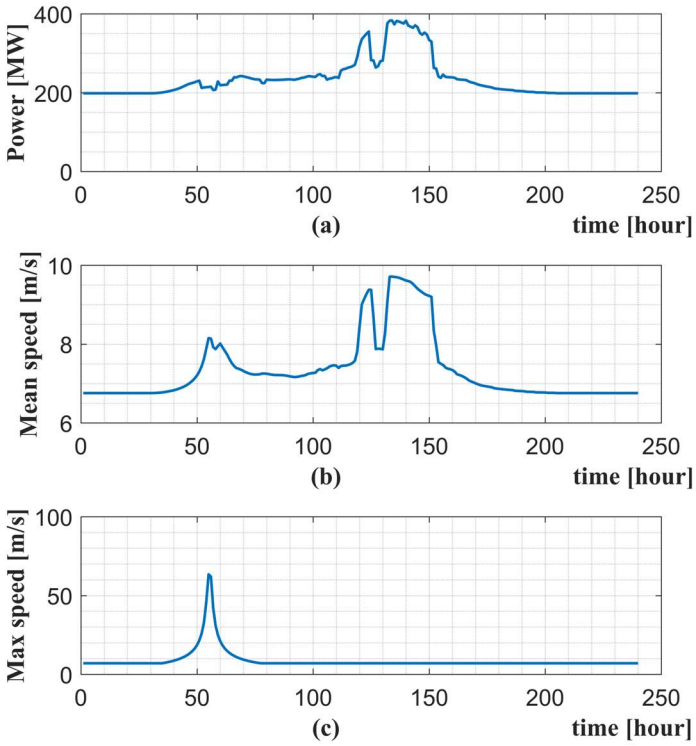

FIGURE 4.19: Power profile for category-5 hurricane in trajectory #9 [32].

The combinations of all possible cases would result in 120 individual cases for simulations. The compression and grouping of scenarios are necessary to facilitate the analysis [32]. The grouping of scenarios is presented in four cases. These four cases correspond to the simulation framing shown in columns 1 and 2 of TABLE 4.11.

4.13 US-Caribbean super grid with typical turbines, category-5, 4, and 3 over synthetic trajectories #1 to 10

The interconnection of the Caribbean super grid with the contiguous U.S. power grid by a submarine power cable between the Bahamas and Florida grid aims at balancing the peak of locally produced wind power boosted by a hurricane with distant centers of baseload stable wind power generation. Such centers are located on the U.S. West Coast and the western areas of the Great Plains. These areas are not normally hit by hurricanes [32].

Also, even in areas along the hurricane corridor, because of the long extent of the corridor in comparison to the diameter of the hurricane, the first impact of the hurricane in one end of the corridor can be absorbed by steady wind power production in the other end. So, the submarine interconnector in Florida Strait distributes the peak impact of a hurricane in a vast wide spatiotemporal base of steady wind power production [32].

FIGURE 4.20 shows the power profiles of the selected category-5 hurricane hitting the integrated Caribbean super grid and the contiguous U.S. power grid [32].

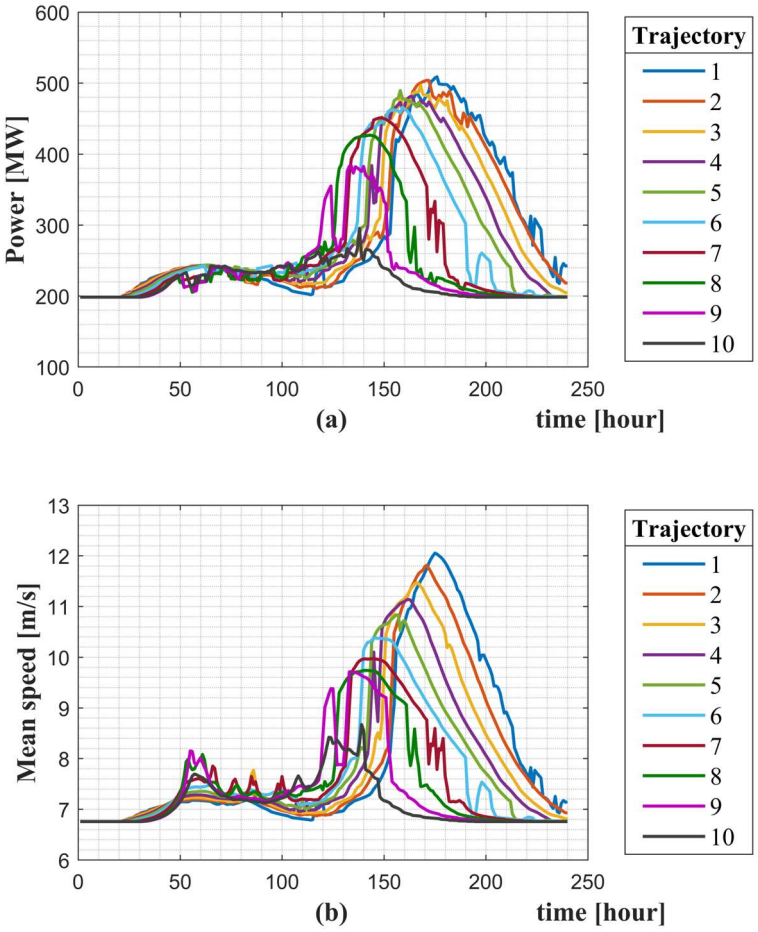

FIGURE 4.20: Profiles of US-Caribbean SG for category-5 [32].

FIGURE 4.21 shows the power profiles of the selected category-4 hurricane hitting the integrated Caribbean super grid and the contiguous U.S. power grid [32].

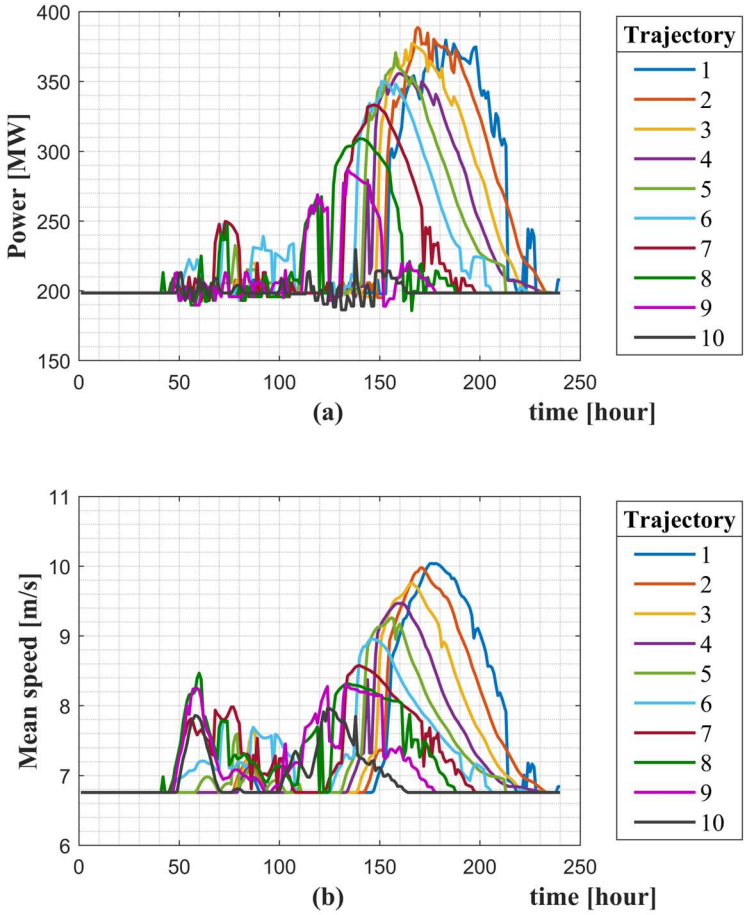

FIGURE 4.21: Profiles of US-Caribbean SG for category-4 [32].

FIGURE 4.22 shows the power profiles of the selected category-3 hurricane hitting the integrated Caribbean super grid and the contiguous U.S. power grid. FIGURE 4.22(a) and (b) show increased variability of power and mean wind speed profile in the turbines under the selected category-3 hurricane. Due to a smaller radius of maximum and minimum speed, a category-3 hurricane has less capability of delivering kinetic energy to a large pool of distant wind turbines

along its trajectory. This shortage of residual power reflects the power variability of low-category hurricanes [32].

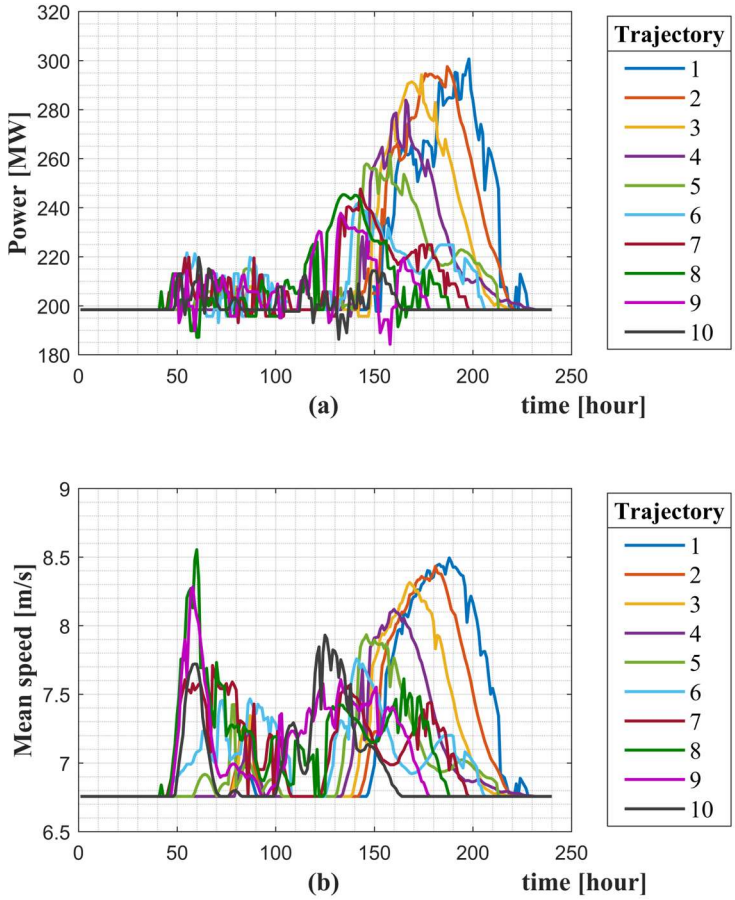

FIGURE 4.22: Profiles of US-Caribbean SG for category-3 [32].

The interconnector between the Caribbean super grid and the contiguous U.S. grid shows a percental power variability for the selected category-5, 4, and 3 hurricanes. In the sequence, the effect of not installing the submarine power interconnector is investigated [32].

4.14 US-Caribbean super grid with special turbines, cat-5, 4, and 3 over synthetic trajectories #1 to 10

This scenario is similar to the last one but with a wind turbine with an expanded cutout speed of 40 m/s, i.e., much higher than the cutout speed of a typical turbine (25 m/s). A speed above these cutout limits forces an intended shutdown of the turbine power for mechanical structural protection [32].

FIGURE 4.23 shows the power profile for the selected category-5 hurricane in ten trajectories over the interconnected Caribbean super grid with special turbines [32].

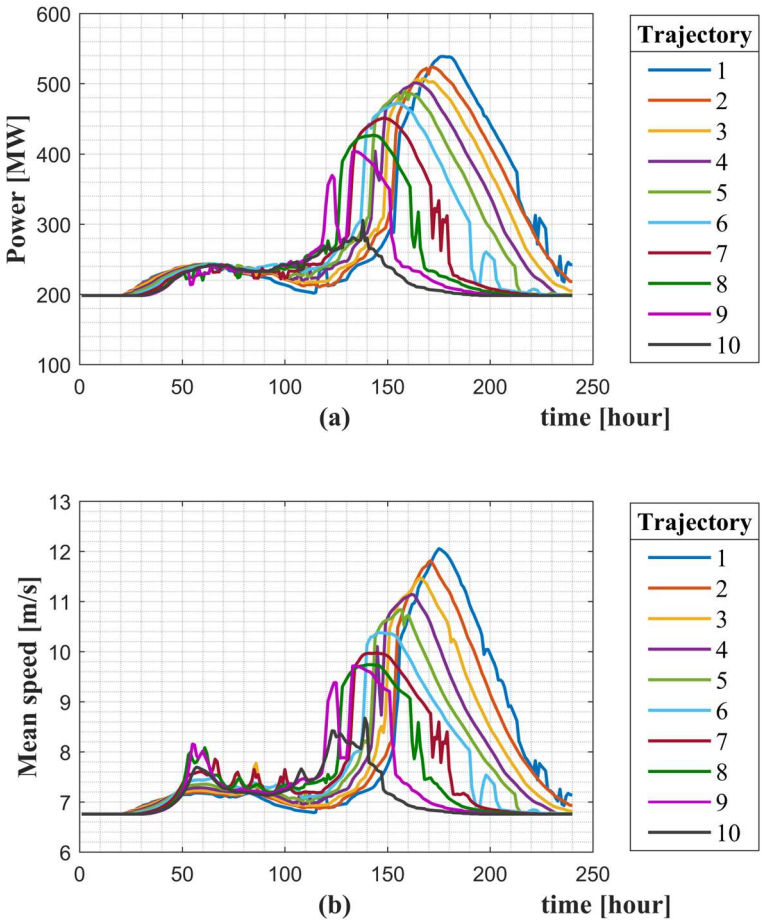

FIGURE 4.23: Profiles of US-Caribbean SG with special turbines for cat-5 [32].

FIGURE 4.24 shows the power profile for the selected category-4 hurricane in ten trajectories over the non-interconnected Caribbean super grid with special turbines. FIGURE 4.24(b) shows that a hurricane in trajectories #8, 9, and 10 spatially moves over the Caribbean super grid and causes a robust increment of the mean speed from 40 h to 80 h, compared to trajectories #5 and 6. However, this increment of kinetic energy is not fully converted into power due to the turbine characteristic curve due to the power cap and cutout speed [32].

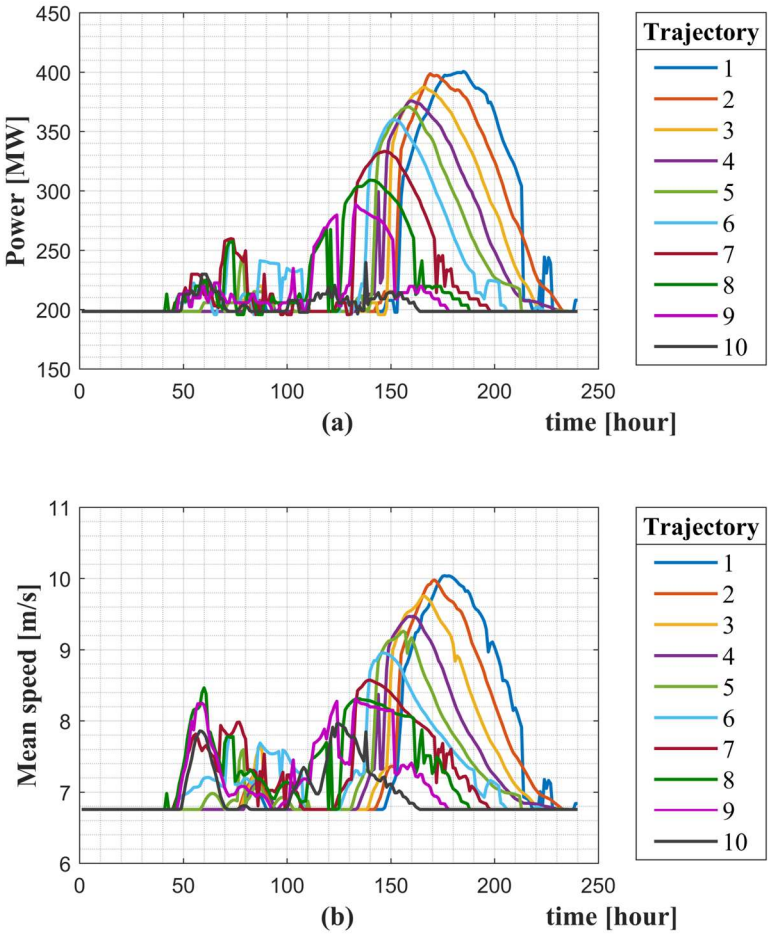

FIGURE 4.24: Profiles of US-Caribbean SG with special turbines for cat-4 [32].

FIGURE 4.25 shows the power profile for the selected category-3 hurricane in ten trajectories over the interconnected Caribbean super grid with special turbines. The power variability around 40 h to 100 h, i.e., over the Caribbean super grid, is strongly dependent on the hurricane geometry (with a small radius of maximum and minimum speed), the high spatial density of wind turbines in small islands, and frequent entries of the category-3 hurricane eye in the islands, which changes its geometry and central pressure. Over the Great Plains, from 100 h to 210 h, the power profile of the selected category-3 hurricane on trajectories #1 to 5 is smoother than the trajectories #7, 8, and 9 over the Caribbean super grid [32].

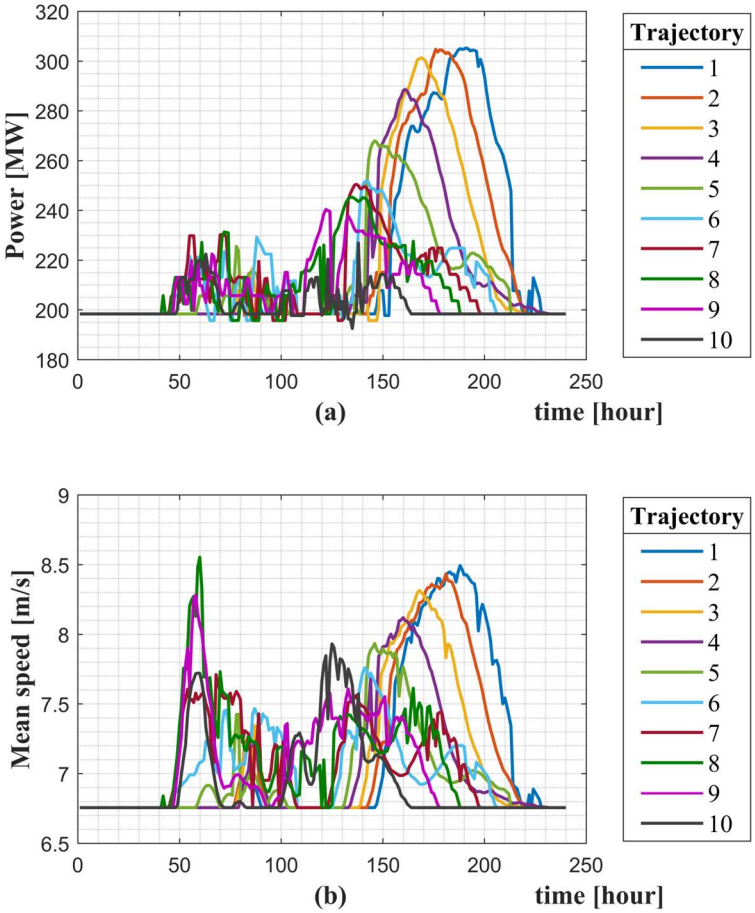

FIGURE 4.25: Profiles of US-Caribbean SG with special turbines for cat-3 [32].

4.15 Standalone Caribbean super grid with typical turbines, cat-5, 4, and 3 over synthetic trajectories #1 to 10

In this scenario, this research investigates the Caribbean super grid but disconnected with the contiguous U.S. power grid. The interconnector between the Bahamas and Florida grid is not present in this scenario. From the perspective of the Caribbean power system, even with integration between local islands, the purpose is to analyze how the local wind power capacity would absorb the impact of hurricanes. In other words, this scenario assesses the power variability without interconnection in comparison with the previous scenario with interconnection. This comparison evaluates the magnitude of the technical benefits of anchoring a relatively small local wind capacity, even in a local super grid, in a large wind capacity of the contiguous U.S. power grid [32].

The local Caribbean super grid is tested by the simulated impact of category-5, 4, and 3 hurricanes in ten trajectories. The shape of the trajectories is the same parabolas as previous ones.

FIGURE 4.26 shows the wind power profile and the mean average speed in the wind turbines exclusively located in the Caribbean super grid under the impact of a category-5 hurricane in ten trajectories [32].

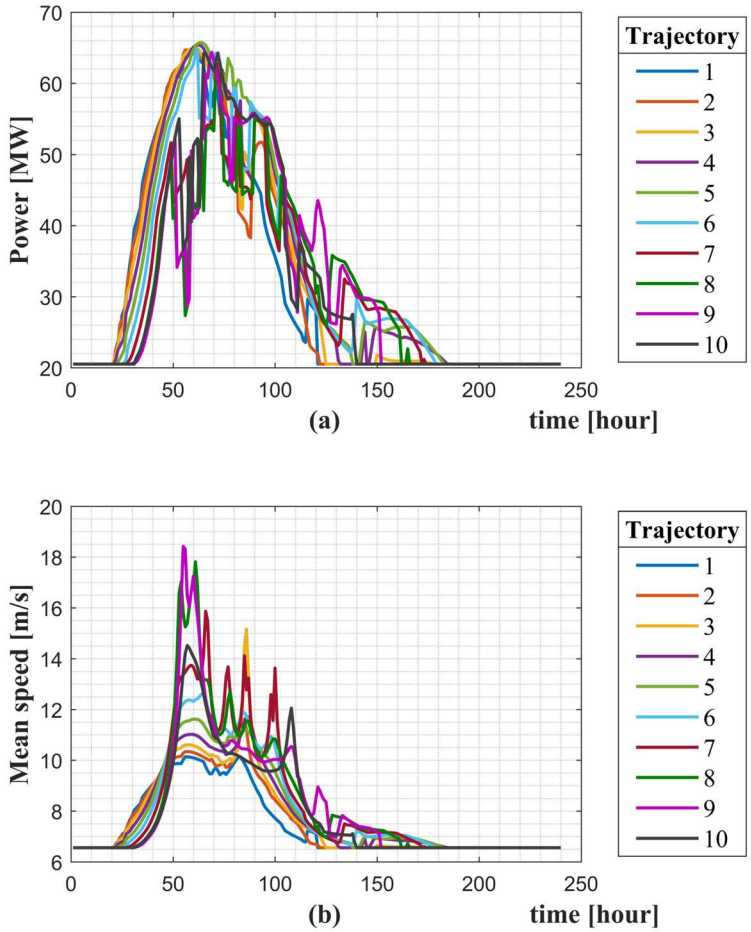

FIGURE 4.26: Profiles of standalone Caribbean SG for category-5 [32].

The eye of the hurricane passes close to Puerto Rico around time 40 hours and physically leaves the Bahamas and Cuba around time 100 hours. A significant share of kinetic energy from winds between time 50 to 70 hours, observed in the average mean speed profile, does not convert into electrical power due to the speed of power cap (14 m/s) and cutout speed (25 m/s). But two aspects are relevant for the final analysis of the results. Firstly, the initial pre-hurricane power level is just 20 MW. In this scenario, the wind power from the contiguous U.S. is not computed because they are not interconnected. Secondly, the hurricanes come as a wave with an initial steep power ramp, reaching its peak at 66 MW, i.e., three times the initial power, and wanes down more slowly,

recapturing part of the energy coming even after the landfall in the continent due to the enlargement of the radius of maximum speed (RMW) in the inland segment. Despite some power fluctuations caused by the several entries of the eye of the hurricane over the islands of the Caribbean, there is some rationale for the shape of the curves [32].

FIGURE 4.27 shows the wind power profile and the mean average speed in the same wind turbines under the impact of a category-4 hurricane in the same ten trajectories [32].

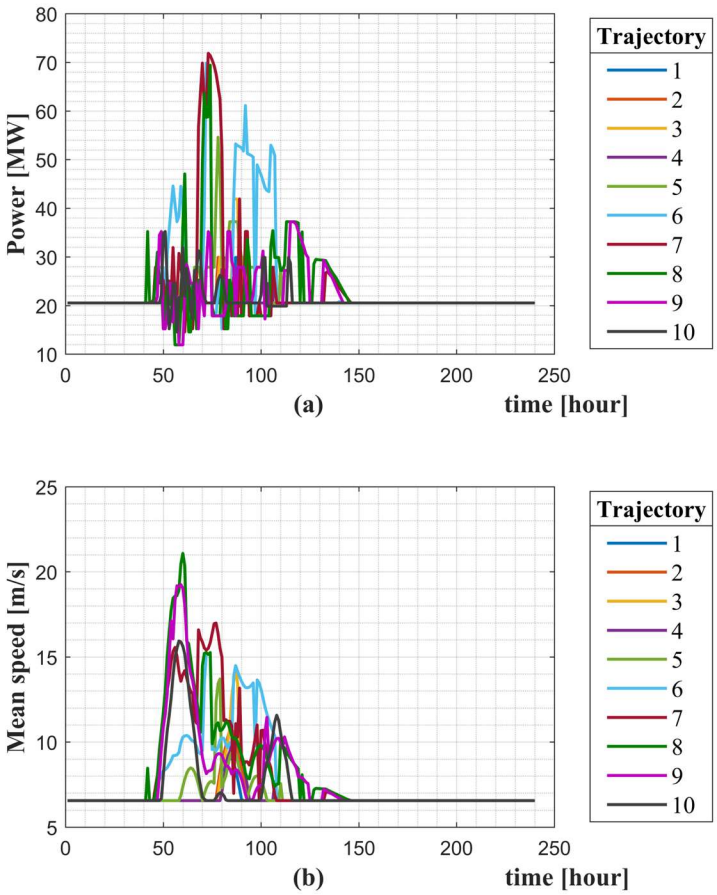

FIGURE 4.27: Profiles of standalone Caribbean SG for category-4 [32].

FIGURE 4.27, compared to FIGURE 4.26, shows much more power variability, lower energy harvesting between 50 to 100 hours, and a power tailgate ending at time 145 hours, shorter than the 185 hours of FIGURE 4.20. In this case, the power variability is exclusively caused solely

by the characteristics of the category-4 hurricane since the trajectories are the same as the previous one. The selected category-4 hurricane has a smaller radius of minimum speed offshore (267 km) compared to a category-5 hurricane (981 km), which partially explains why category-4 is less generous in distributing kinetic energy to the wind turbines reflecting eventually in a lower power profile. Also, as indicated in TABLE 4.7, the radius of the minimum speed onshore is much extended for the selected category-5 (1,408 km) than for the category-4 (927 km), which explains the larger tailgate of category-5 blowing minimum winds from the continent to the northern part of the Caribbeans even exceeding time 145 hours. Soon after the landfall, the increase of the onshore radius of hurricane minimum speed boosts distant wind power generation, even crossing some offshore zones. Just the outer band of minimum wind speed, i.e., not exceeding 25 m/s in the selected wind turbine model of this simulation, produces any power. The larger the radius of minimum speed is, the more extensive the zone of contact of this outer band with wind power turbines [32].

FIGURE 4.28 shows the wind power profile and the mean average speed in the same wind turbines under the impact of a category-3 hurricane [32].

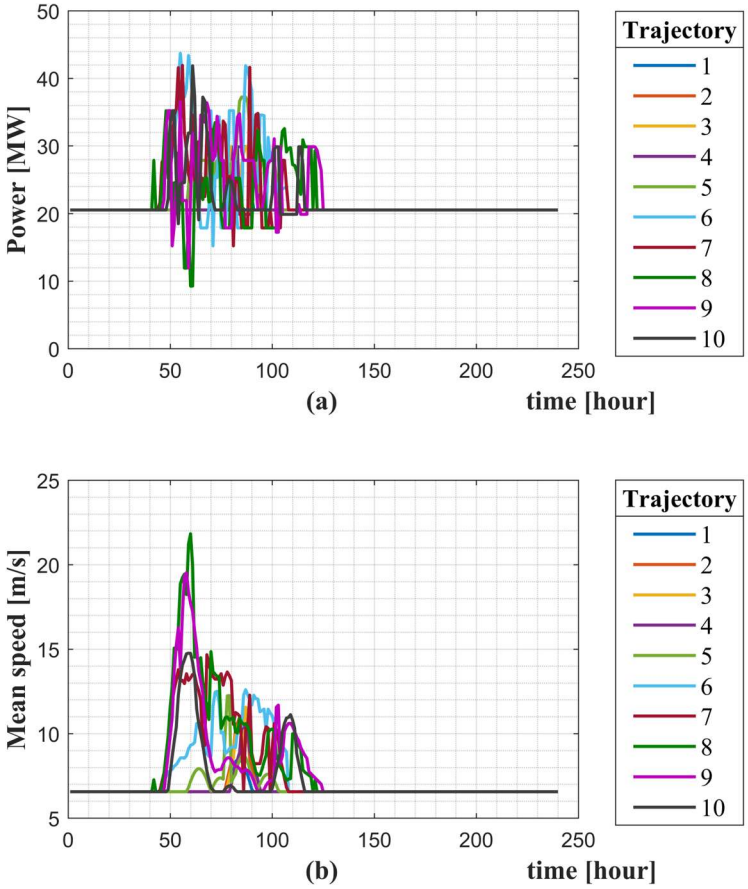

FIGURE 4.28:. Profiles of standalone Caribbean SG for category-3 [32].

The power profile of this category-3 hurricane is even more modest, both in peak magnitude and duration. Although the offshore radius of minimum category-3 hurricane speed is modestly larger than the category-4, the onshore radius (858 km) is significantly lower than of the category-4 (927 km), diminishing the extension of the tailgate by post-landfall power recovery. As indicated in TABLE 4.7, the central pressure (980 mbar) of the category-3 hurricane is more robust than the selected category-4 hurricane (975 mbar), producing lower delta pressure, reducing the hurricane strength, and leading to low power profile magnitude. The power peak of the selected category-3 hurricane (44 MW) is smaller than category-4 (70 MW), as shown in FIGURE 4.21 and FIGURE 4.22 [32].

Over the pre-hurricane wind speed conditions, the power peak variability is 65 MW peak over 20 MW, 70 MW peak over 20 MW, and 44 MW peak over 20 MW, i.e., an increment of 225%, 250%, and 120%, for category-5, 4, and 3, respectively. The instantaneous power variability is relatively low in category-5 and increases substantially in hurricanes category-4 and 3 [32].

These numbers of power variability are very high without the power interconnection of the Caribbean super grid with the contiguous U.S. power grid through a Florida submarine interconnector. A future power interconnector is highly beneficial to draining the local excessive peak and fluctuations of wind power generation in the Caribbean region under hurricanes to the massive power consumption of the North American power grid. Stand-alone or locally integrated wind power generation does not cope with the seasonal impact of hurricanes [32].

4.16 Standalone Caribbean super grid with special turbines, cat-5, 4, and 3 over synthetic trajectories #1 to 10.

This scenario is similar to the last one but with a wind turbine with an expanded cutout speed of 40 m/s. For comparison, a typical turbine cutout speed is around 25 m/s. A speed level above these cutout limits forces an intended shutdown of the turbine power for mechanical structural protection [32].

FIGURE 4.29 shows the power profile for the selected category-5 hurricane in ten trajectories over the non-interconnected Caribbean super grid with special turbines [32].

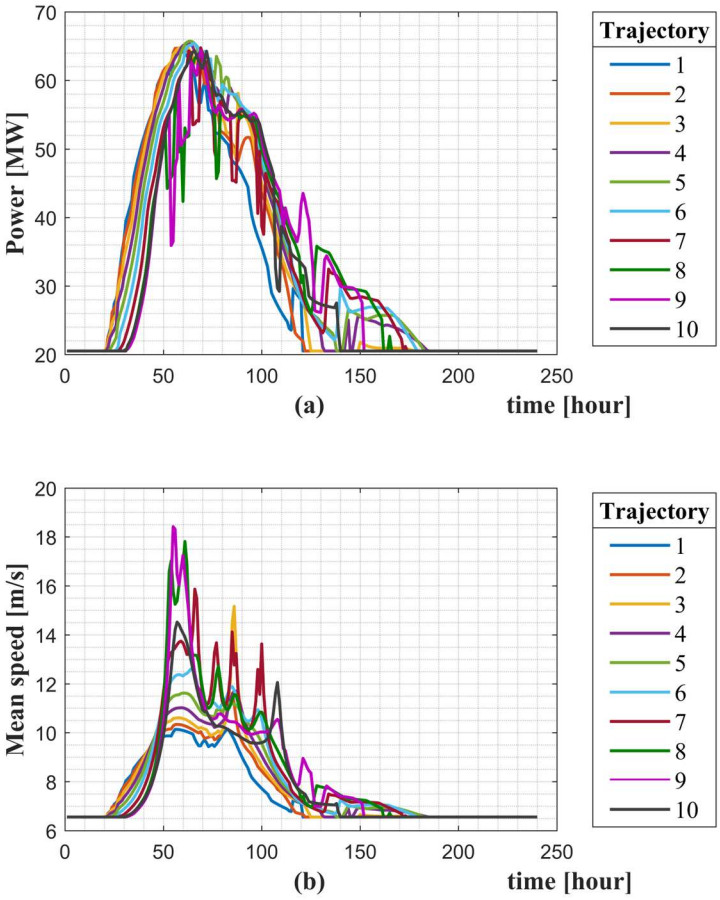

FIGURE 4.29: Profiles of standalone Caribbean SG in cat-5 with special turbines [32].

FIGURE 4.30 shows the power profile for the selected category-4 hurricane in ten trajectories over the non-interconnected Caribbean super grid with special turbines. This selected category-4 hurricane produces more wind variability, causing high variability in the generating power profile than the selected category-5 hurricane [32].

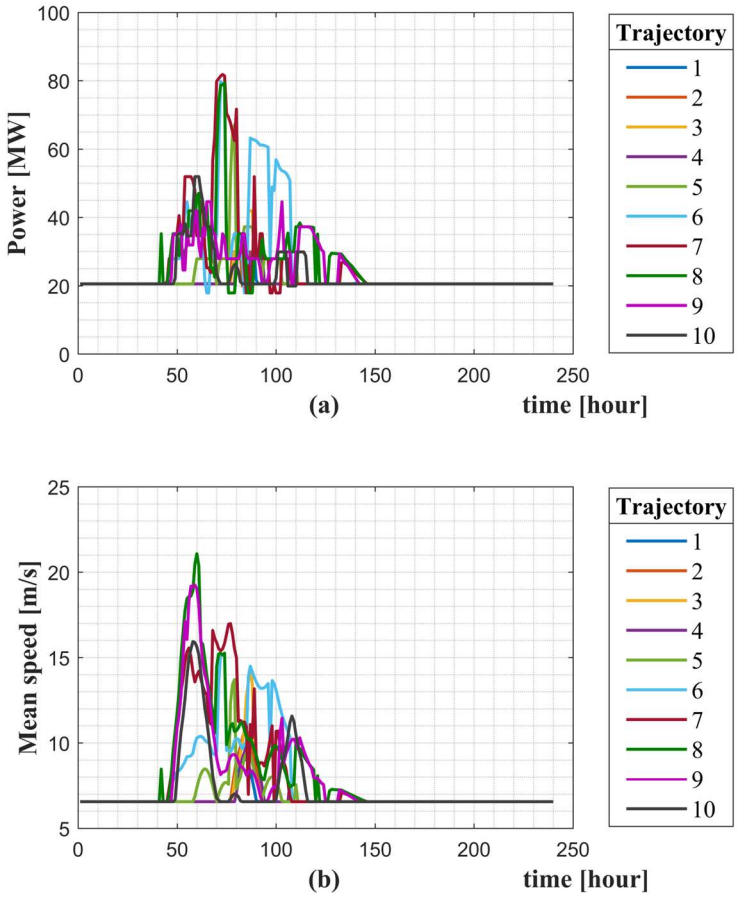

FIGURE 4.30: Profiles of standalone Caribbean SG in cat-4 with special turbines [32].

FIGURE 4.31 shows the power profile for the selected category-3 hurricane in ten trajectories over the non-interconnected Caribbean super grid with special turbines. Compared to category-5 and 4, the selected category-3 produces even more wind variability, causing extremely high variability of power profile in a disconnected Caribbean super grid [32].

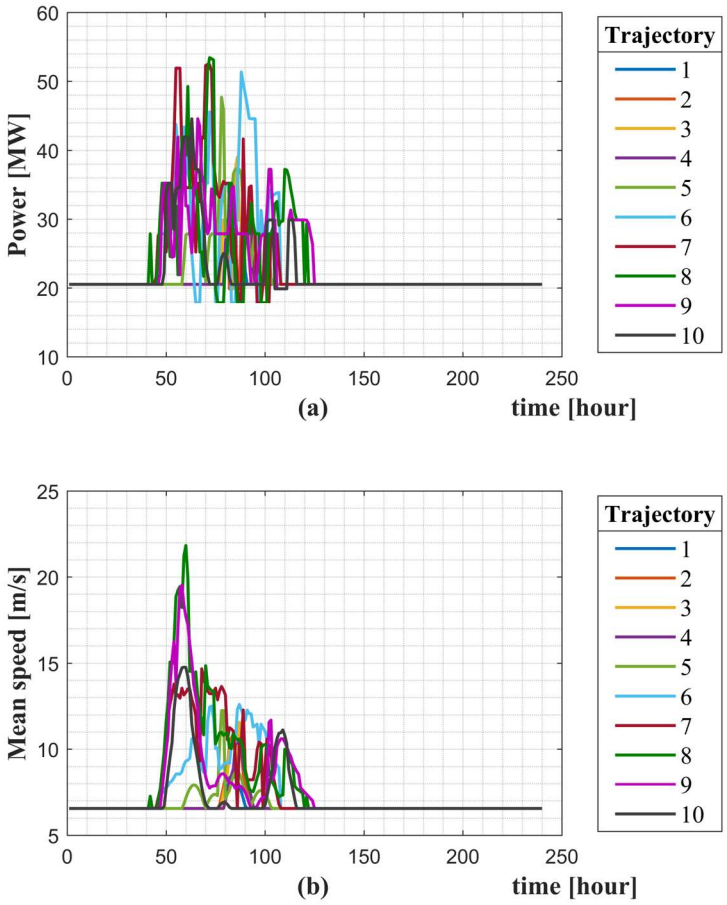

FIGURE 4.31: Profiles of standalone Caribbean SG in cat-3 with special turbines [32].

4.17 General comparative analysis

This section presents a comparative analysis of the simulation results. The first analysis compares the difference in the performance of typical and special turbines in a Caribbean super grid interconnected to the contiguous U.S. grid. The second analysis compares typical and special turbines in a disconnected Caribbean super grid. The last analysis investigates the power variability with interconnection and disconnection of the Caribbean super grid. The purpose of these comparisons is to investigate the advantages of special turbines over typical ones and the benefits

of the Caribbean super grid interconnection to the contiguous U.S. power grid in reducing the power variability under hurricanes.

4.18 Comparison of special and typical wind turbines on the US-Caribbean SG.

Hurricanes hitting the Caribbean super grid interconnected to the contiguous U.S. power grid generate a power profile with two waves. The first wave has a modest power peak because it aggregates the power from the Caribbean super grid with ten turbines, and the second wave is more robust due to a large number of turbines in the Great Plains and the U.S. East Coast. Moreover, in the onshore segment of the trajectory, the hurricane radius increases compared to the offshore segment, covering an even larger area of the U.S. continent during its movement [32].

This work investigates the differences in the power profile if the turbines are changed from typical to special ones. As previously characterized in FIGURE 4.4, this research assumes a special turbine that can generate power even for high airspeed from 25 m/s to 40 m/s. TABLE 4.12 summarizes the comparison of the power profiles with typical and special turbines [32].

TABLE 4.12: Analysis of power variability in the U.S.-Caribbean super grid with different types of turbines.

Interconnection	U.S.-Caribbean Super Grid Interconnected	U.S.-Caribbean Super Grid Interconnected
Turbine type	Typical turbine with cutout speed of 25 m/s.	Special turbine with cutout speed of 40 m/s.
Category-5 hurricane	FIGURE 4.20: The peak power from the Caribbean turbines is the same (245 MW). The peak power from the Great Plains with typical turbines is lower (510 MW) than with special turbines, as shown in the next column. From 56 to 58 h, the power drops to 205 MW (severe power drop), but it is still above the pre-hurricane level of 200 MW. Trajectory #1 shows a power drop to 202 MW from 110 and 115 h, but it is still above the pre-hurricane level of 200 MW.	FIGURE 4.23: The peak power from the Caribbean turbines is the same (245 MW) The peak power from the Great Plains with special turbines is higher (540 MW) than typical turbines, as shown in the previous column. From 53 to 56 h, the power drops to 210 MW (minor power drop), but it is still above the pre-hurricane level of 200 MW. Trajectory #1 shows a power drop to 202 MW from 110 and 115 h, but it is still above the pre-hurricane level of 200 MW.
Category-4 hurricane	FIGURE 4.21: The peak power from the Caribbean turbines is low (250 MW). The peak power from the Great Plains is low (390 MW). From 49 to 53 h, the power drops to 195 MW; from 53 to 70 hours, 190 MW; from 75 to 105 h, 195 MW; from 121 to 135 h, 185 MW; from 135 to 157 h, 187 MW; from 162 to 167 h, 185 MW, totaling 92 h of power drop, i.e., the profile shows a severe and long-lasting power drop in relation to the pre-hurricane power level of 200 MW.	FIGURE 4.24: The peak power from the Caribbean turbines is high (260 MW). The peak power from the Great Plains is higher (400 MW). From 64 to 66 hours, from 75 to 78 h, from 83 to 88 h, from 97 to 102 h, from 129 to 134 h, and from 142 to 145h, the power drops to 195 MW for 23 hours total in relation to the pre-hurricane power level of 200 MW, i.e., the profile shows a moderate and short-time power drop in relation to the pre-hurricane power level of 200 MW.
Category-3 hurricane	FIGURE 4.22: The peak power wave from the Caribbean turbines is the same (222 MW). The peak power wave from the Great Plains is small (300 MW). The power drop ranges from 183 MW to 195 for 60 hours, i.e., the profile shows a severe and long-lasting power drop in relation to the pre-hurricane power level of 200 MW.	FIGURE 4.25: The peak power wave from the Caribbean turbines is the same (232 MW). The peak power wave from the Great Plains is small (305 MW). The power drop stays 196 MW for a total 29 hours, and from 133 to 137 h, it reaches 192 MW, i.e., the profile shows a moderate and short-time power drop in relation to the pre-hurricane power level of 200 MW.

Source: [32].

In most categories (3 and 4), a special turbine with a cutout speed of 40 m/s increases the peak power production during the hurricane [32].

Special turbines cause a less severe and shorter time of power drop in relation to the pre-hurricane level because they produce power even at high speeds (> 25 m/s and < 40 m/s).

The turbine type is not the primary cause of power variability. However, a turbine with high cutout speed minimizes the severity and time duration of the power drop by producing power even at high airspeed. The specific hurricane radius of maximum and minimum speed, and the numerous inland entries and offshore departure of the hurricane eye alter the parameters of the hurricane, causing significant power variability in the profile. The power profile ripple of the Great Plains is lower than the Caribbeans because the turbines are well equidistantly distributed over a larger area than the Caribbeans [32].

4.19 Comparison of special and typical turbines on standalone Caribbean SG

TABLE 4.13 compares wind power variability of typical and special turbines in the proposed Caribbean super grid without interconnection with the contiguous U.S. power grid [32].

TABLE 4.13: Analysis of power variability in the Caribbean super grid without interconnection.

Interconnection	U.S.-Caribbean Super Grid **Not** Interconnected	U.S.-Caribbean Super Grid **Not** Interconnected
Turbine type	Typical turbine with cutout speed of 25 m/s.	Special turbine with cutout speed of 40 m/s.
Category-5 hurricane	FIGURE 4.26: The peak power is the same 65 MW. The power tailgate ranges from the same period (130 to 185 hours). Between 50 to 70 hours, the power drops to 28 MW (a very severe drop).	FIGURE 4.29: The peak power is the same 65 MW. The power tailgate ranges from the same period (130 to 185 hours). Between 50 to 70 hours, the power drops to 38 MW (less severe drop).
Category-4 hurricane	FIGURE 4.27: The peak power is low (72 MW). The power tailgate is indistinguishable, and the total power profile variability ranges from the same period (35 to 145 hours). Between 50 to 70 hours, power drops to 12 MW (very severe 40% power drop from pre-hurricane level).	FIGURE 4.30: The peak power is high (81 MW). The power tailgate is indistinguishable, and the total power profile variability ranges from the same period (35 to 145 hours). Between 50 to 70 hours, power drops to 17 MW (less severe 15% power drop from pre-hurricane level).
Category-3 hurricane	FIGURE 4.28: The peak power is low (44 MW). The power tailgate is indistinguishable, and the total power profile variability ranges from the same period (35 to 130 hours). Between 65 to 105 hours, power drops to 9 MW (very severe 55% power drop from pre-hurricane level).	FIGURE 4.31: The peak power is high (54 MW). The power tailgate is indistinguishable, and the total power profile variability ranges from the same period (35 to 130 hours). Between 65 to 105 hours, power drops to 18 MW (less severe 10% power drop from pre-hurricane level).

Source: [32].

In most categories, a special turbine with a cutout speed of 40 m/s increases the peak power production during a hurricane [32].

Special turbines cause a less severe drop in power profile from the pre-hurricane level because they keep capturing power even at high speeds (> 25 m/s and < 40 m/s).

The type of turbine is not the major cause of power variability, although a turbine with high cutout speed minimizes power drop by pushing power even at high airspeed. The specific hurricane radius of maximum and minimum speed, and the numerous inland entries and offshore departure

of the hurricane eye alter the parameters of the hurricane, causing significant power variability in the profile [32].

4.20 Comparison of power variability of Standalone Caribbean SG and US-Caribbean SG

This comparison analyses the power variability in two scenarios: with and without the submarine interconnector between Florida and The Bahamas [32].

Some indicators are proposed to facilitate the comparison. The power variability between the maximum and minimum values can be calculated by [32]:

$$\Delta_{max} = \frac{P_{max} - P_{min}}{P_{max}} \quad (15)$$

where: P_{max} and P_{min} are the maximum and minimum values in the power profile curve.

The power minimum variability over pre-hurricane conditions can be calculated by [32]:

$$\Delta_{min} = \frac{P_o - P_{min}}{P_o} \quad (16)$$

where: P_o and P_{min} are the pre-hurricane and minimum power values in the power profile curve.

TABLE 4.14 shows the wind power variability caused by a hurricane hitting the proposed Caribbean super grid with and without interconnection with the contiguous U.S. power grid [32].

TABLE 4.14: Analysis of power variability with and without Caribbean super grid interconnection.

Caribbean super grid with interconnection with the contiguous U.S. power grid	Interconnected	Not interconnected
Turbine type	Typical (cutout speed of 25 m/s)	Typical (cutout speed of 25 m/s)
Total number of turbines	81 interconnected	10 turbines in the Caribbeans isolated from 71 in the contiguous U.S.
Power profiles	FIGURE 4.20, FIGURE 4.21, and FIGURE 4.22	FIGURE 4.26, FIGURE 4.27, and FIGURE 4.28
Pmax (Peak power in the Caribbean side) [MW] for category-5, 4, and 3	245 / 250 / 222	65 / 72 / 44
Pmin (Minimum power) [MW] for category-5, 4, and 3	205 / 185 / 183	28 / 12 / 9
Po (Pre-hurricane power) [MW] for category-5, 4, and 3	200 / 200 / 200	20.5 / 20.5 / 20.5
Δ_{max} **(Maximum power variability) for category-5, 4, and 3**	16.3% / 26% / 62.6%	132% / 500% / 388%
Δ_{min} **(Minimum power variability) for category-5, 4, and 3**	-2.5% / 7.5% / 8.5%	-36.6% / 41.4% / 56.1%

Source: [32].

The power variability in the Caribbean is significantly reduced if the Caribbean super grid is interconnected to the contiguous U.S. power grid [32].

4.21 Validation of the proposed method and existing literature.

The validation of the spatiotemporal method is conducted in 3-parts:

- Validation of the hurricane wind speed as predicted by the model.
- Validation of the algorithm to compute the mechanical-electrical power conversion of a single turbine.

- Validation of the aggregation of power profiles of all turbines into total power profile of the Caribbean grid.

In 2016, Kim et al. investigated hurricane Ike (2008), making landfall in Texas. Before landfall, the wind speed was estimated at two points over the waters of the Gulf of Mexico. Points A and B were located 60 km on the right and left sides of the hurricane trajectory, respectively. Both points were perpendicular to the hurricane trajectory [100].

The trajectory of Ike approaching close to Texas from the Gulf of Mexico is similar to the synthetic trajectory 1, simulated in this dissertation. FIGURE 4.32 shows the comparison of wind profiles in the Kim et al. studies and the profile of the maximum speed in a turbine generated for the method proposed in this dissertation. The profile of trajectory 1 refers to a turbine located in Texas. A hurricane, after landfall, changes its characteristics of maximum speed and size due to changes in its parameters, such as central pressure, maximum radius, and maximum wind speed. Such changes can be observed by the offshore profile shown in green color (trajectory 7) and blue color (trajectory 1). In addition, the peak speed in the hurricane eye border reduces significantly after landfall.

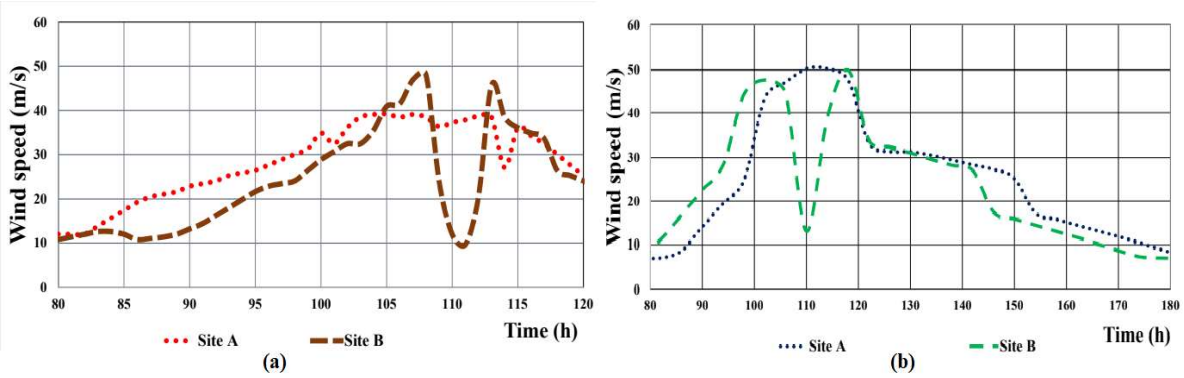

FIGURE 4.32: Comparison of Kim et al. [100] and spatiotemporal methods.

FIGURE 4.32(a) is adjusted by a factor of 1.203 to estimate the wind speed at 90m height since the original data refers to 10 m height. FIGURE 4.32(a) and (b) peaks 48m/s, validating the

proposed method by Itiki et al with existing literature of Kim et al. The profile does not have a steep drop in speed at time 111 h because the onshore turbine is not close enough to capture the low-speed zone within the hurricane eye.

The wind speed profile of the turbine receiving the impact of the hurricane over trajectory 1 (in blue color) captures the low-speed eye zone at time 111 h because of the turbine's proximity to the hurricane trajectory. This onshore turbine absorbs a hurricane originally coming as category-5 from the sea but slows down soon after landfall. The dark blue wind speed profile is consistent with the patterns of hurricanes after landfall.

This comparative analysis demonstrates the consistency of the wind speed profiles generated by the spatiotemporal method based on parametric hurricane modeling proposed in this dissertation. Furthermore, this analysis corroborates the applicability of the parametric hurricane modeling based on Holland and Georgio's equations, already validated by numerous existing technical literature in the scope of weather science [73] [74].

The second part is the validation is the algorithm to compute mechanical-electrical power conversion of a single turbine. In this part, the focus is on the correct calculation of instantaneous power of one turbine based on the estimated wind speed profile from hurricane. The reference basis for this is FIGURE 4.33, the characteristic curve of turbine provided by manufacturers or obtained from the technical literature.

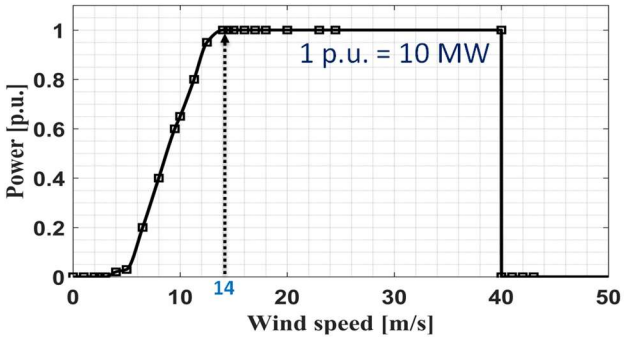

FIGURE 4.33: Characteristic curve of a wind turbine

For wind speed between 14m/s to 40 m/s, the output power is capped in 10 MW, as shown in FIGURE 4.33. And for wind speed exceeding 40 m/s in special turbines, the power drops to zero, as also shown in FIGURE 4.33.

FIGURE 4.34 shows the conversion of wind profile (b) into power profile (a). Like the characteristic curve of the turbine, for wind speed between 14m/s to 40 m/s, the output power profile is capped in 10 MW and for wind speed exceeding 40 m/s, the power drops to zero.

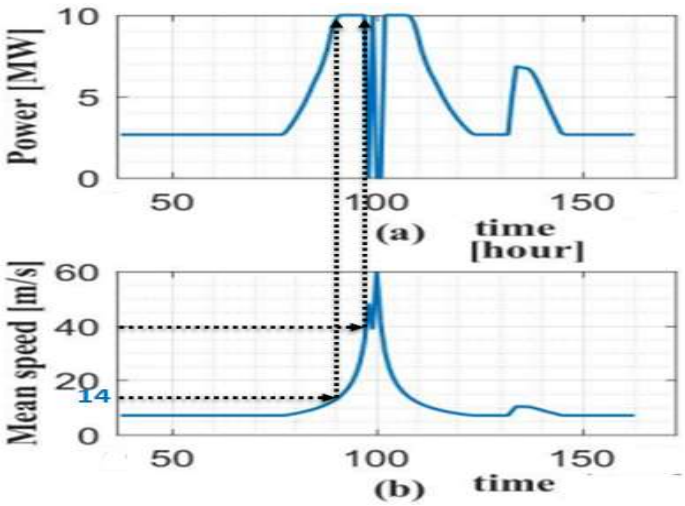

FIGURE 4.34: Power profile (a) obtained from wind profile estimation (b).

These checking points validate the correctness of the algorithm for conversion of wind speed into power in a single turbine.

The third part of the validation aims at certifying that the power profiles of each turbine are correctly aggregated into the overall power profile of the super grid.

FIGURE 4.35 shows the aggregated power profile of standalone Caribbean super grid hit by category-5 hurricane over trajectory #7. This profile was obtained by the spatiotemporal method proposed in this research.

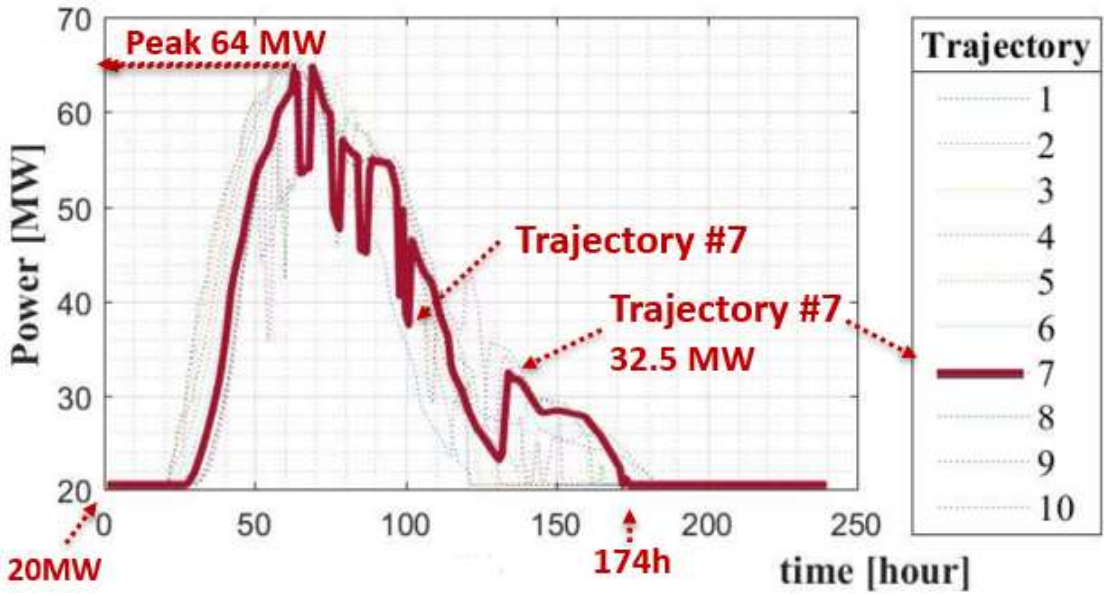

FIGURE 4.35: Power profile of standalone Caribbean super grid.

Standalone Caribbean super grid is proposed with ten turbines. By running the spatiotemporal algorithm for each turbine, it is possible to obtain the individual power profile of ten turbines in text format file. Using a time-series power flow software, such as Sincal, it is possible to model the standalone Caribbean super grid with ten buses, and inject in each bus the profile generated by the proposed spatiotemporal method. For simplification purposes, the modeling of the standalone Caribbean super grid can be carried out by high voltage alternating current, and isolated cables to emulate the submarine interconnectors of the super grid. After power flow simulation, it is possible to obtain the time-series power flow from Bahamas to Florida, by considering the contiguous US power grid as a infinite bus consuming all power from the Caribbeans, and verify the consolidation of the aggregation of power generated by the standalone Caribbean super grid. These possibilities are explored in this research in order to validate the aggregation algorithm developed in MATLAB coding.

FIGURE 4.36 shows the single line diagram of the US-Caribbean super grid which is modeled and simulated in Sincal. The U.S. Grid is modeled as a swing bus and consumer of all power generated by wind turbines on the Caribbean super grid. On each bus of the Caribbean super grid the synchronous generator capacity has the same power of the load, letting all power generated by wind turbines on the Caribbean super grid to be drained to the U.S. Grid.

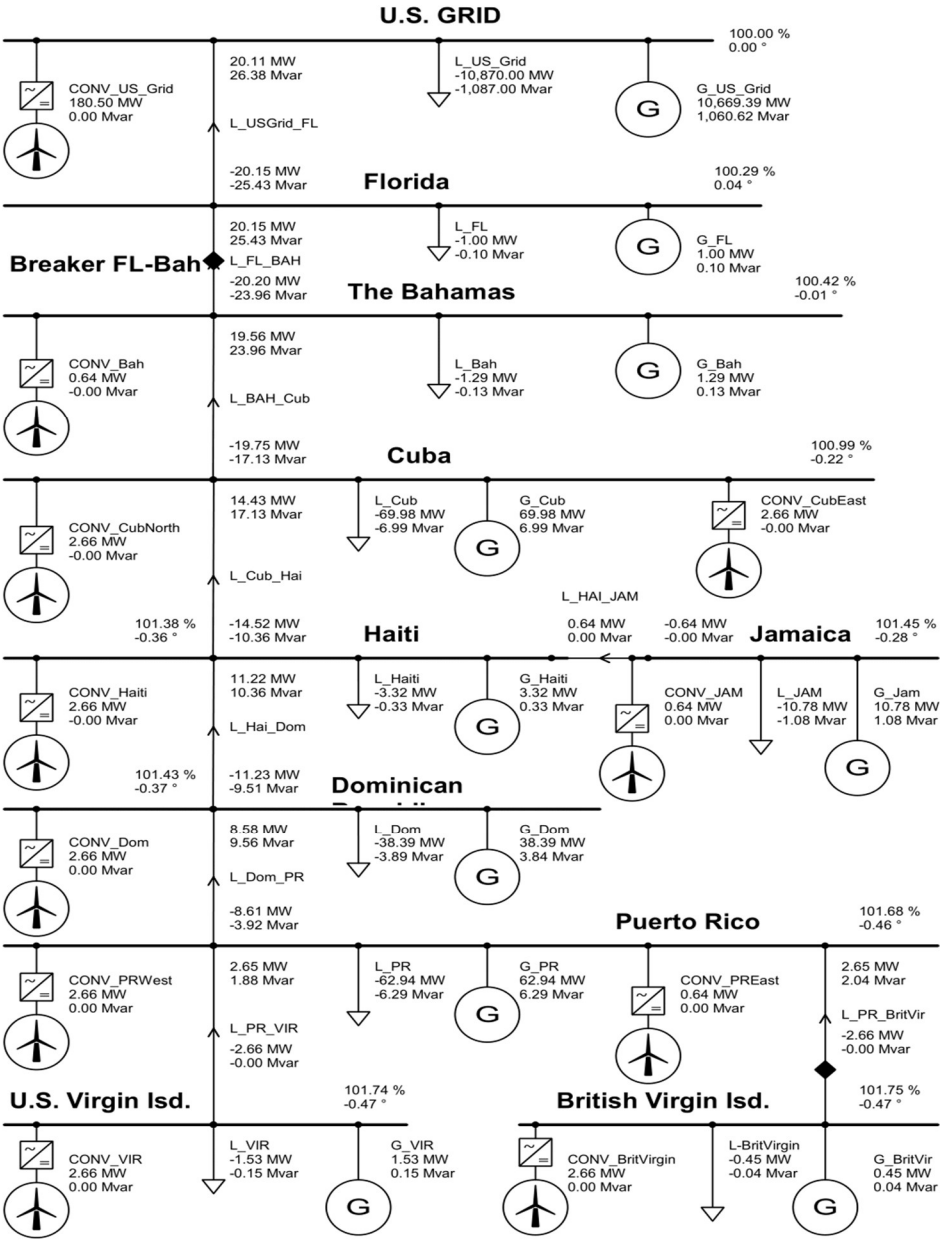

FIGURE 4.36: Single line diagram of US-Caribbean super grid.

FIGURE 4.37 shows the simulation results with the injection of power profile by each wind turbine on the super grid.

FIGURE 4.37: Power profile using time-series simulator Sincal.

Comparing FIGURE 4.35 and 4.37, the shape is similar, and the peak power in 4.37 is a slightly lower than FIGURE 4.35 because Sincal accounts line losses, resulting in lower power flow in the Bahamas-Florida interconnector.

TABLE 4.15 shows the percentual power error between the proposed spatiotemporal method, shown on FIGURE 4.35, and the time-series power flow using Sincal, shown in FIGURE 4.37. The percentual error does not exceed 5% and can be credited to transmission losses in the interconnectors of the Caribbean super grid. The spatiotemporal method consolidates the power profile of each wind turbine. Sincal simulation presents the time-series power flow profile in the interconnector between the Bahamas and Florida, indicated as “Breaker FL-Bah” on FIGURE 4.36. The input data for the Sincal simulation is the power profile of each wind turbine, obtained

from the spatiotemporal method. The low percentual values of error between the methods demonstrates that with the same input, the output value in both methods is very similar. Thus, the loop of MATLAB coding of the spatiotemporal method carrying out the aggregation of power profile of each turbine is validated by the power flow simulation in Sincal.

TABLE 4.15: Error between spatiotemporal and load flow methods.

Time [hours / date]	Spatiotemporal [MW]	Sincal [MW]	Error [%]
30 h / Sept 16 plus 6 h	20.5	20	2.5%
50h / Sept 17 plus 2 hours	52	50	4%
62 / Sept 17 plus 14 hours	64	62	3.2%
79h / Sept 18 plus 7h	57.5	56	2.7%
89h / Sept 18 plus 17h	55	53.5	2.8%
100 h / Set 19 plus 4h	46.5	45	3.3%
130 / Sept 20 plus 10h	23	22.5	2.2%
133 / Sept 20 plus 13h	32.5	32	1.6%
150 h / Sept 21 plus 6h	28	27.6	1.4%
174 h / Sept 22 plus 6h	20.5	20	2.5%

This proposed method of spatiotemporal wind speed and power profile estimation does not propose to compete with weather science. In other words, this proposed spatiotemporal method neither pursues an improvement of fitness of the Holland and Georgio's equations with datasets from weather measuring stations nor tries to compete with high-performance supercomputing machines for weather forecasting, which is undoubtedly the traditional scope of weather science.

From a systemic perspective, this proposed method for spatiotemporal wind speed and power profile estimation aims to bridge the gap between weather and power systems, which are apparently disconnected in the existing literature. By proposing to cover a research gap characterized by a vacuum of scientific knowledge in an interdisciplinary space, the single-part validation of the proposed bridging method by comparison with existing methods is not quite

feasible because of the shortage of literature on the gap and because the power profile is dependent on a specific spatial distribution of wind turbines in the Caribbean. Alternatively, this 3-parts validation shows evidence that the proposed method for spatiotemporal wind speed profile estimation produces results consistent with some existing weather science or mechanical engineering literature covering hurricane speed estimation, such as Kim et al. [100], and aggregation loops of the coding do not generate results inconsistent with load flow method.

The existing literature about the impact of hurricanes on power systems focuses on assessing damage and reconstruction costs instead of wind power generation profiles.

TABLE 4.16 gives more details on the differences and similarities of spatiotemporal methods to evaluate the impact of hurricanes on power grids. The method proposed in this research covers all the extent of the hurricane translational movement, i.e., from the Caribbeans to the U.S Midwest, being thus more adequate for estimation of power generation profile of wind capacity supported by wide-area transmission systems such as super grids.

TABLE 4.16: Comparison of methods for estimating the impact of hurricanes on the power systems.

Method description	Spatiotemporal linear trajectory with parametric hurricane modeling and probabilistic parameters.	Spatiotemporal multi-segments trajectory with hurricane modeling by historical geospatial speed data from NHC GISlibrary.	Spatiotemporal parabolic trajectory with parametric hurricane modeling and fixed onshore and offshore parameters
Authors	John W. Muhs and Masood Parvania	E. B. Watson and A. H. Etemadi.	R. Itiki, et al.
Reference, year	[37], 2019	[38], 2020	[32], 2022
Purpose	Estimation of damage to distribution lines.	Estimation of damage to transmission, substations, coal, gas, nuclear, solar plants, and non-hurricane-proof wind turbines	Estimation of power profile generated by hurricane-proof wind turbines for power simulations
Hurricane category	Historical probabilistic distribution	Category 4 only (Harvey)	Categories 5, 4 and 3
Radius of maximum speed	Rmax is estimated by an empirical equation.	Non-applicable.	Average Rmax is measured by NOAA NHC.
Earth curvature	Neglected	Possibly considered.	Considered
Scenarios	1,000 trajectories hitting one point	Years 2017; 2050 with 50% renewables; and 2050 with 80% renewables	10 trajectories offshore and onshore, with/without interconnection of US-Caribbean super grid.
Impacted area	Point of impact: Houston	The state of Texas.	Caribbeans, Gulf of Mexico, and North America
Impacted component	Overhead distribution line with fragility curve	Typical 2 MW wind turbines, solar, coal, gas, and nuclear plants, and overhead transmission.	81 units of 10 MW hurricane-proof wind turbines, with and without high cutout speed.
Impacted system	Local distribution system	Local transmission and generation.	Wide area transmission and generation
Simulation time	24 h (1 day)	< 12 h	240 h (10 days)
Software Platform	Not informed.	ArcGIS, and HAZUS (developed by FEMA)	MATLAB 2017 only.

Source: [32].

4.22 Discussions

The development of the method for generating wind power profiles under hurricanes and the proposed Caribbean super grid addresses practical problems of electrical power system engineering. This section discusses how the comparison of power profiles provides valuable information for power system analysis and stakeholders [32].

4.23 The importance of the method for power system stakeholders

The proposed method is a tool for planning and preliminary design of the expansion, duplication, and reinforcement of the high voltage power grid, including interconnected super grids, such as the proposed Caribbean super grid. For instance, the value of peak power generated in the Caribbean super grid is a parameter for designing a series of electrical equipment and materials. The proposed cable that interconnects Florida to the Bahamas should be sized to transmit the worst-case scenario of the power profile. The peak power of the Caribbean super grid sets the reference for the engineering decision on the maximum level of allowable curtailment of wind power generation in hurricanes event, which ultimately leads to the final parameter of ampacity for the cable sizing and its installation. In other words, a submarine cable sized for average conditions of wind speed and power of the Caribbean super grid, i.e., the pre-hurricane power of 20 MW in this research, will undoubtedly not withstand the peak power of the worst-case trajectory of a hurricane, i.e., 63 MW according to the simulations. It is important to point out that the simulations are conducted on a reduced scale, where 20 MW and 63 MW correspond to 2 GW and 6.3 GW in full scale. Also, on both ends of a power interconnector, costly equipment requires sizing, specification, acquisition, and installation. Such assets are typically switchyards, high voltage circuit breakers, power transformers, and high voltage direct current (HVdc) converters. In the initial phases of engineering, the proper sizing of equipment and cabling defines the capital expenditure, which, in this case, is highly dependent on the peak power profile [32].

During the detailed engineering phase, a professional engineer should stamp technical responsibility for the proper cable and equipment sizing and specification, no matter if the hurricane is stochastic and complex to mensurate, forecast, model, and simulate. Based on

simplified patterns and with the perspective of further evolution, this method fills and raises awareness in the science of a significant gap between meteorology science and power engineering.

From the perspective of the high voltage power grid operator, the second power profile wave shown in FIGURE 4.20 to FIGURE 4.25 represents an opportunity for temporarily decreasing the dispatch of fossil fuel power generation while surfing in the clean wave of the hurricane. The reduction of dispatch of fossil fuel plants is not just because the wind power delivers clean energy, but because an excessive injection of power generation in the grid without balance with the demand can potentially cause oscillation in the grid frequency and overvoltage. Moreover, the simulations show different power profiles for each synthetic trajectory and hurricane category. Supposing a fully operational Caribbean super grid, the power grid operator in charge of the power transmission to Florida would require a set of specific operational procedures and training for each forecasted synthetic trajectory and category of hurricanes. The existing power system must accommodate the injection of different power profiles according to the hurricane trajectory and category. The development of a tool for wind power profile forecasting under hurricanes thus again proves necessary for power system operation [32].

From the perspective of wind power plant owners, investors, and wind turbine manufacturers, this research shows that wind turbines with high cutout speed, although not commercially available on MW-rating scale yet, have a positive effect on reducing the power variability. The comparative analysis of the power profile with typical and special turbines provides the quantification of the value added by extra-power obtained by high cutout turbines. The mathematical integration of the extra-power profile over the period (145 hours in the simulation with special turbines) results in an amount of energy exclusively brought by high cutout speed characteristics in special wind turbines. This energy from the hurricanes can be associated

with carbon emissions abatement and revenue for companies. However, the assessment of return over investment on 40 m/s cutout speed characteristics is yet to be seen since the MW-rating scale turbines with such features are not commercially available [32].

For energy policymaking and transmission system planning, the simulation shows that islands are relatively more impacted by high instantaneous fluctuations of power during hurricanes than vast extensions of land such as the contiguous U.S. territory. A hurricane radius of minimum speed can easily cover an island and cause severe disturbance to weather-dependent wind power generation. The wind power capacity in the West Coast and the western part of the Great Plains, located outside the hurricane alley, minimizes the overall power variability by injecting more stable wind power flow into the aggregate power supply. This physical reality faced by islanded countries is a strong point for policymakers to expand the interconnectivity schemes between islands and large countries for cross-border power-sharing. The interconnectivity facilitates adding the wind power capacity in the face of systemic risks of hurricane-induced power variability. It opens the door for peak power transmission to remote areas of the grid with a more stable power profile. The comparative analysis in TABLE 4.14 shows that a Caribbean super grid has lower power variability (16.3%, 26%, and 62.6% for hurricane category-5, 4, and 3, respectively) while interconnected to the contiguous U.S. power grid than isolated (132%, 500%, and 388% for hurricane category-5, 4, and 3, respectively) [32].

From the perspective of power system analysis, systemic risks caused by hurricanes need future assessment. To the author's knowledge, it is unknown if the low-frequency harmonics within the wind power profile during hurricanes may potentially induce wide-area or inter-area low-frequency oscillations in the power grid. These oscillations, without proper damping, may lead to the risks of future grid collapse of the contiguous U.S. power grid after low-frequency power

injection of wind power in the existing power grid. A modal analysis in the frequency domain of the power grid under hurricanes is a prolific topic for future research [32].

From the perspective of power system protection, the high variability of operational power profile from 20 MW in pre-hurricane conditions to 63 MW after hurricane landfall suggests that the overload protection (relay ANSI 51) should be adjusted in two different groups of settings to protect the cable against abnormal overloading. The ramp of electrical current up to three times from the pre-hurricane condition during a hurricane becomes a second temporary new normal reference for protection. An interconnector scheme for overload protection should not mistakenly detect an increment of current reference due to a hurricane by an overloading event caused by a fault. The hurricane became a new temporary normal for operation and protection schemes, and this normal power profile should be known [32].

Finally, from the perspective of the weather sciences, the practical necessities of information from wind power system engineering are detailed, motivating the continuous improvement of parametric modeling of hurricanes [32].

The proposed methods up to this chapter capture the expected power variability of MHK, and wind energy under hurricanes, supporting the planning, design, and operation of power systems with high penetration of renewables. However, climate change and global warming potentialize extreme variability of power profile beyond normality. An extension of the U.S.-Caribbean super grid to South America integrating wind power capacity of areas outside the hurricane corridor of the Caribbeans and Gulf of Mexico is a potential proposition to smooth power variability in areas prone to hurricanes. This hypothesis is investigated in the following chapter.

CHAPTER 5: U.S.-CARIBBEAN SUPER GRID FOR MHK, WIND POWER AND EXTENSION TO SOUTH AMERICA

In the previous chapters, two methods for spatiotemporal power profile estimation were proposed and implemented in MATLAB: one dedicated to assessing MHK power based on superficial water speed data measured by a HF radar and another for wind power estimation during hurricanes by parametric modeling. The simulations in both chapters generated individual maps and estimated MHK profile of turbines off the coast of North Carolina (Gulf Stream) and wind power profiles under hurricanes in the Caribbeans.

Despite the algorithms for MHK and wind power profile estimation being segregated, this Chapter 5 elaborates a procedure to integrate the results of MHK power profile into the U.S.-Caribbean super grid, thus making possible to investigate the performance of the super grid in smoothing the power variability of both MHK and wind power under hurricanes. Such integration is possible by exporting the MHK power profile estimation from MATLAB matrix to a text file (*.txt) framed in comma-separated values (csv format). Then, using MATLAB, it is possible to incorporate some additional commands on the algorithm that estimates wind power profile to read the file containing the MHK power profile in txt format.

FIGURE 5.1 shows the flowchart on the integration of these algorithms with the generation of text files for data exchange. The MHK estimation code should be run first to disclose the power profile data in text file format for further reading and aggregation into the wind power profile estimation. The same functionalities are kept the same, with options to run the Caribbean super grid standalone, with interconnection with the contiguous U.S. and with the extension to South America. Also, the wind power estimation can be conducted assuming category-3, 4, and 5, in ten different trajectories. The quantity and allocation of wind turbines is also selectable by the user.

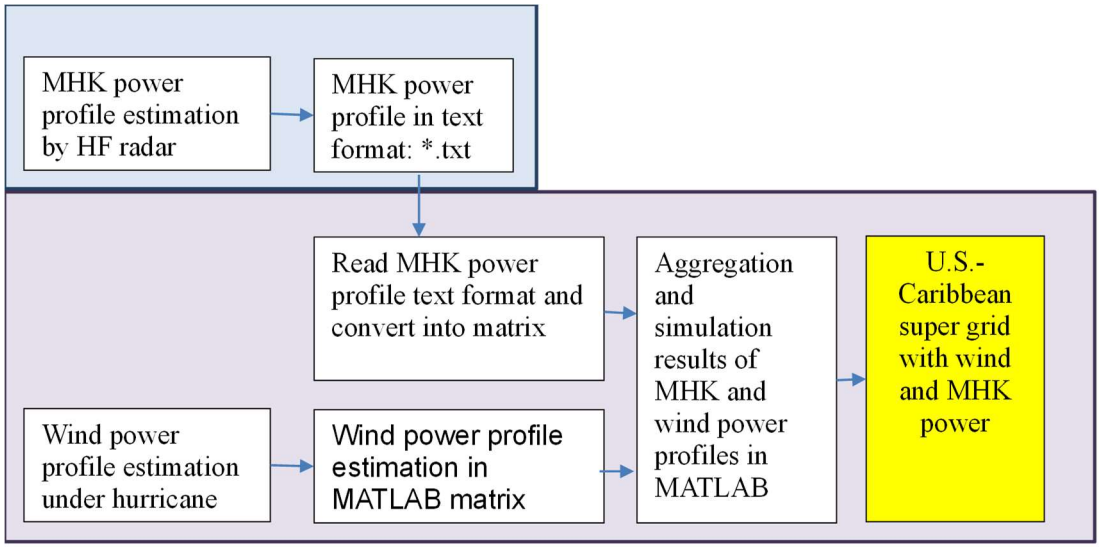

FIGURE 5.1: Integration of algorithms for MHK and wind power assessment.

With the implementation of MATLAB coding of such integration of a MHK data-driven algorithm with a parametric wind power algorithm, the next subsections investigate the multitude of scenarios of hybridization of these two renewable energy sources.

FIGURE 5.2 illustrates the type of hybridization and simulation scenario this research is focused on. The power generation profile derived from both renewable energy resources is merged

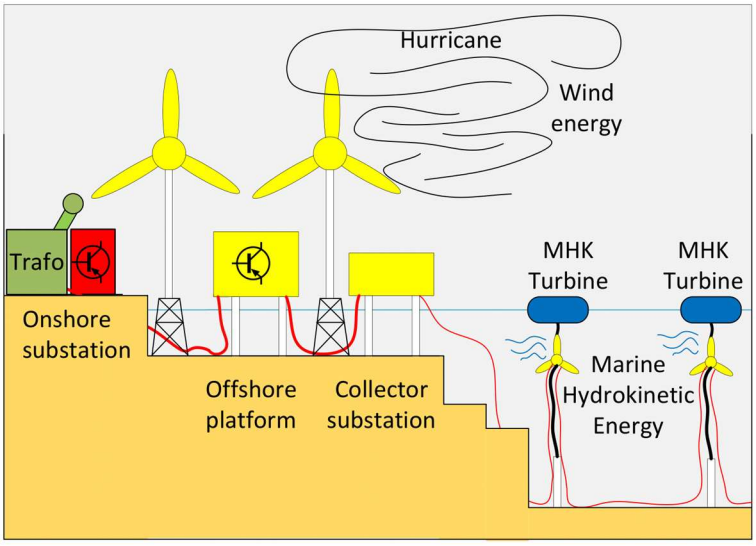

FIGURE 5.2: Hybridization of MHK and wind power.

to investigate the combined power variability of the US-Caribbean super grid.

5.1 Standalone Caribbean SG with MHK and wind power.

The hurricane will be simulated in trajectories 1 and 7.

Trajectory 1 was selected because it is the most impactful trajectory for the wind turbines located in the US Midwest and it is the closest to the wind power turbines in South Caribbean and South America. Despite not being accounted on the power aggregation of the standalone Caribbean super grid, it is relevant as a base reference for a comparative analysis in future scenarios with U.S. interconnection.

Trajectory 7 is of interest because it is the most impactful for most wind turbines allocated off the coast of the Caribbean islands.

FIGURE 5.3 shows the simulation results from the algorithm integrating MHK and wind power profiles from hurricane on trajectory 1. MHK introduces ripple in the power profile due to spatiotemporal water speed variability during the same day. The MHK power profile is estimated from water speed measured by high-frequency radar data made available by NOAA. The MHK algorithm executes electromechanical conversion of water speed into power as studied in Chapter 3, sections 3.2, and the profile extended to a hurricane period of 14 days to allow the analysis of MHK and hurricane in a same time base. The top water layers of the ocean streams do not deliver constant kinetic energy resources, causing such power ripples. The wind power profile (in red) is for standalone Caribbean super grid (with 10 wind turbines only), where standalone means without interconnectivity neither with the contiguous U.S. nor the South America power grid.

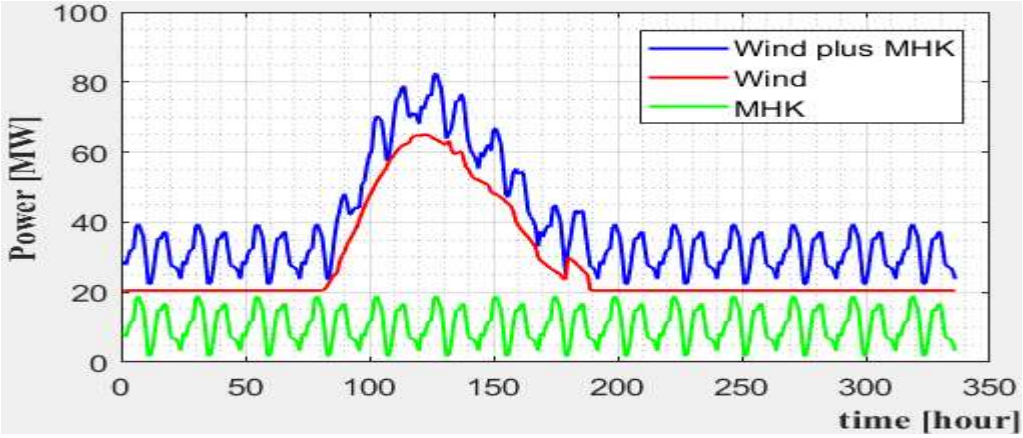

FIGURE 5.3: Profile of MHK plus wind under hurricane trajectory 1 over standalone Caribbean SG.

FIGURE 5.4 shows the simulation results from the algorithm integrating MHK and wind power profiles. In this scenario, the hurricane moves on a synthetic parabolic trajectory 7, impacting the Caribbeans for a long period (from 70 h to 225 h) as compared to the trajectory 1, (from 70 h to 180 h). The reason for this long period is that the hurricane is passing through a large population of wind turbines allocated along the coast of most of the Caribbean islands.

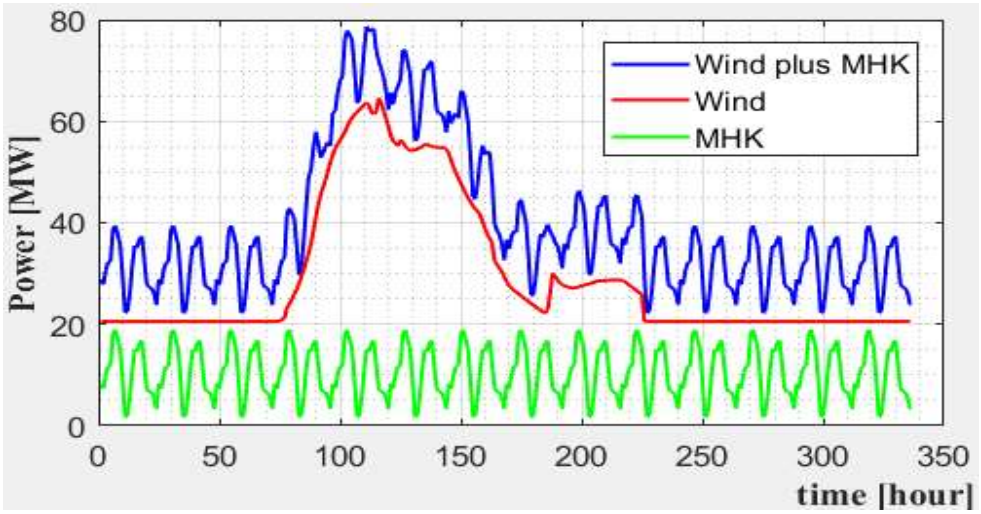

FIGURE 5.4: Profile of MHK plus wind under hurricane trajectory 7 over standalone Caribbean SG.

5.2 U.S.- Caribbean SG with MHK and wind power.

A category-5 hurricane is simulated moving on trajectories 1 and 7. With the interconnection of Caribbean Super Grid with the contiguous U.S. power grid, the power profile presents two humps: one in the Caribbeans, and another in the U.S. contiguous states.

FIGURE 5.5 shows MHK adding ripple in the power profile, but its effect is relatively minor as compared to the profile with standalone Caribbean super grid shown in FIGURE 5.3 and FIGURE 5.4. The overall number of turbines in the super grid increased from 10 turbines in standalone Caribbean Super Grid to 85 turbines with interconnection to the contiguous U.S. power grid, creating a high pre-hurricane power level that turns MHK ripple comparatively negligible.

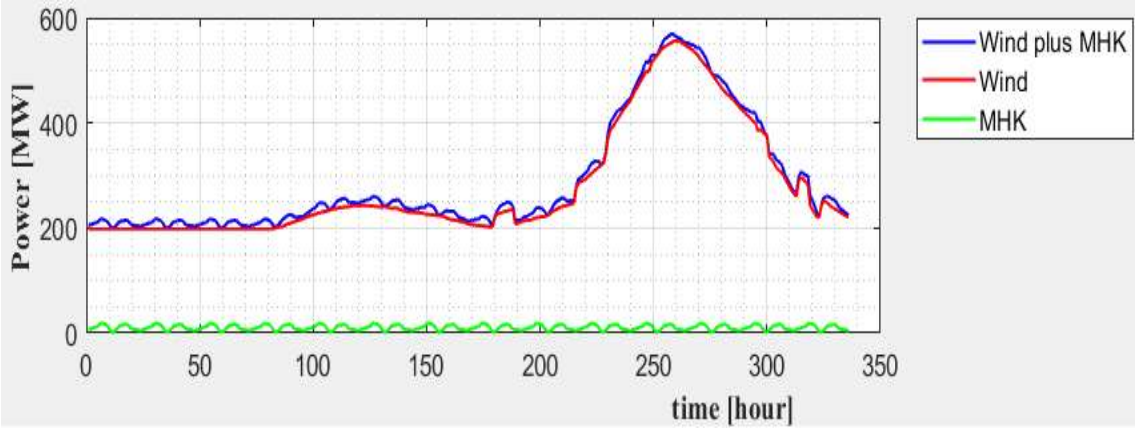

FIGURE 5.5: Profile of MHK plus wind under hurricane trajectory 1 over U.S.-Caribbean SG.

FIGURE 5.6 shows MHK power adding ripple in the overall profile, but its effect is relatively minor. From time 120 h to 170h, trajectory 7 produces more sustained power in the Caribbeans than trajectory 1 because the hurricane passes closer to most of the Caribbean islands before reaching Florida. Trajectory 1 crosses a void of turbines in the center of the Gulf of Mexico

making the power profile to drop sharply even with high hurricane winds. The turbines are allocated offshore but close to the shallow waters along the coastal areas. In contrast, trajectory 7 generates lower peak power in the US Southeast (480 MW) than in the US Midwest (560 MW) because of the lower spatial density of turbines in Southeast area as compared to the US Midwest.

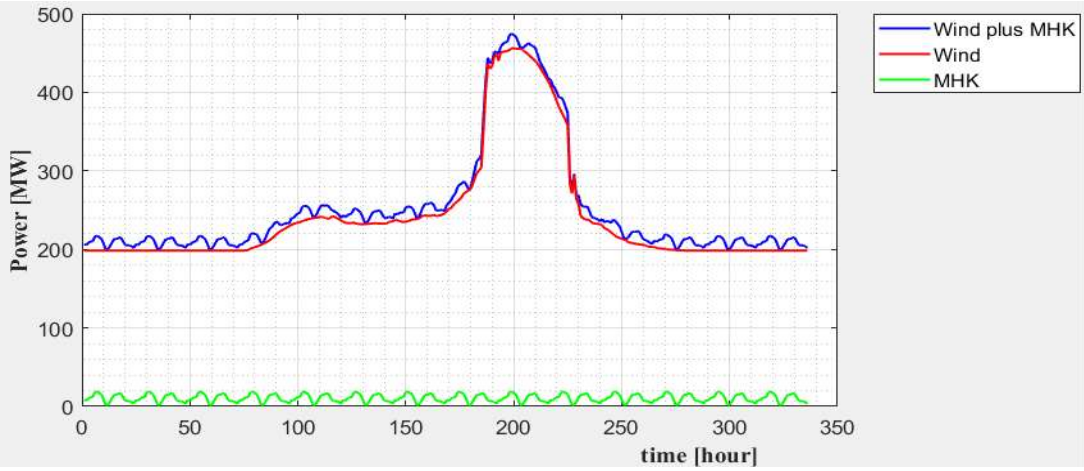

FIGURE 5.6: Profile of MHK plus wind under hurricane trajectory 7 over U.S.-Caribbean SG.

5.3 U.S.- Caribbean-South America SG with MHK and wind power.

The category-5 hurricane is simulated in trajectories 1 and 7. With the interconnection with both the contiguous U.S. power grid and South America, the power profile presents two humps: one in the Caribbeans, and another in the U.S. Midwest or U.S. Southeast. The hurricane corridor does not pass over South America. For this reason, a high level of pre-hurricane power is expected, making the power variability even more accommodated.

FIGURE 5.7 shows MHK power adding ripple in the overall power profile, but its effect is relatively negligible as compared to the standalone Caribbean super grid. The overall number of turbines in the doubled-interconnected U.S-Caribbean-South America super grid increased from

10 in standalone to 113 turbines with extension to Brazil, creating a strong pre-hurricane quasi-baseload level, particularly from wind turbines located in Brazil, outside the hurricane's corridor, and not generating any power humps.

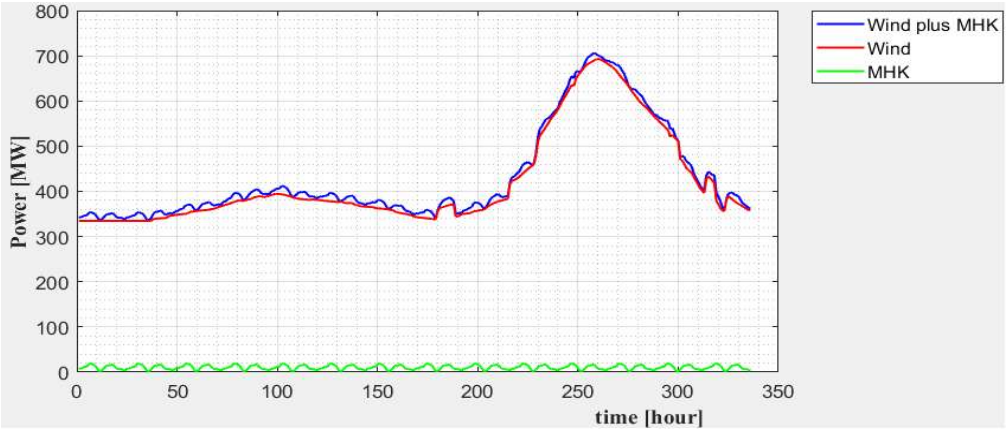

FIGURE 5.7: Profile of MHK plus wind under hurricane trajectory 1 over U.S.-Caribbean-South America SG.

FIGURE 5.8 shows MHK power adding ripple in the overall power profile, but its effect is also relatively minor as compared to standalone Caribbean super grid. Trajectory 7 produces more sustained power in the Caribbeans (400 MW from time 120 h to 170 h) than trajectory 1, which shows a power drop between time 120 h to 170 h. The peak power in the US Southeast (600 MW at time 200 h) in FIGURE 5.8 is lower than in the US Midwest (700 MW in time 260 h) in FIGURE 5.7.

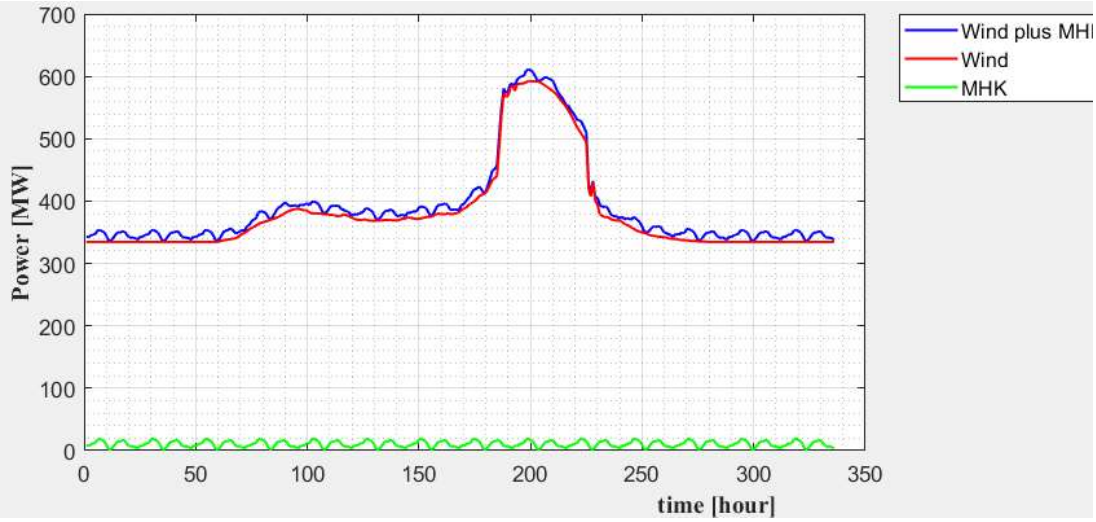

FIGURE 5.8: Profile of MHK plus wind under hurricane trajectory 7 over U.S.-Caribbean-South America SG.

To understand the differences of peak power on the second hump of FIGURE 5.7 and FIGURE 5.8, it is necessary to analyze the spatial allocation of turbines in the hurricane's corridor. The super grid interconnectivity of local power grids improves smoothness of the overall power profile, but other factors also play an important role in power variability. Keeping constant spatial distribution of the wind turbines in the trajectory of the hurricanes results in lower power profile variability.

5.4 Comparison of power variability in Caribbean SG with MHK plus wind.

In this Chapter 5, the simulations cover scenarios of standalone Caribbean super grid, U.S.-Caribbean super grid, and U.S.-Caribbean-South America super grid.

FIGURE 5.9 shows the wind turbines allocation, the impacted countries, and the submarine cable route in the Caribbeans and South America.

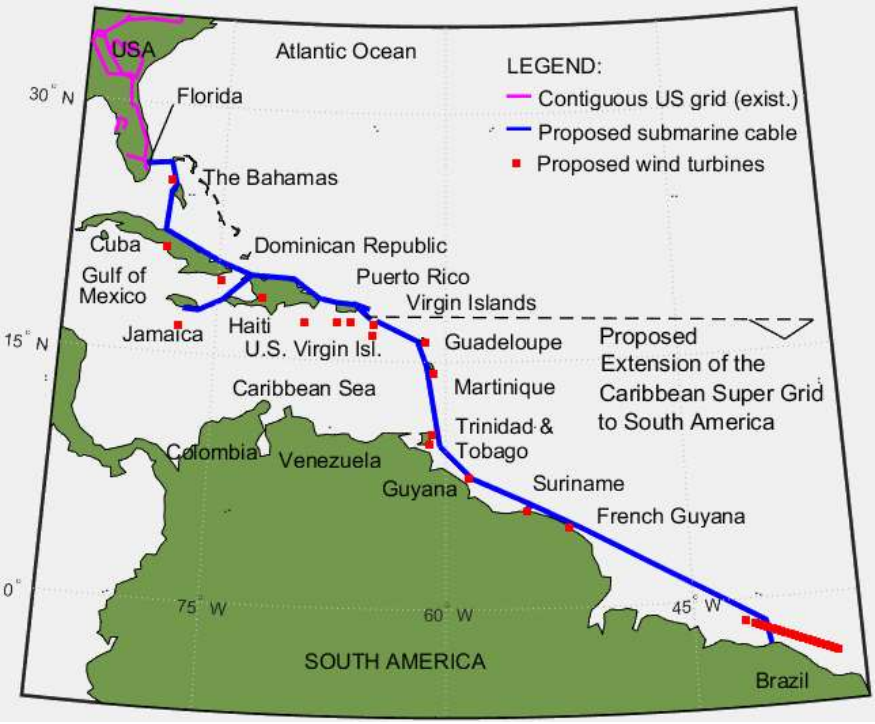

FIGURE 5.10: Proposed U.S.-Caribbean-South America SG [115] (©2023 IEEE).

FIGURE 5.10 shows trajectory 7 of the hurricane. Each trajectory makes the hurricane hit the wind turbines from different distances, generating different shapes of power profiles, and, consequently, different values of power variability.

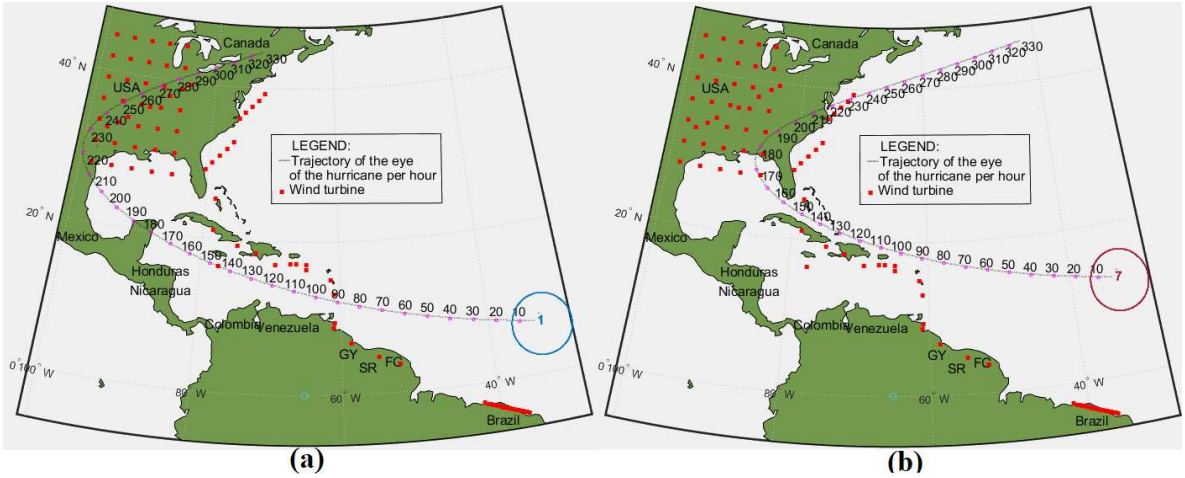

FIGURE 5.9: Hurricane over trajectory 1 and 7 [115] (© 2023 IEEE).

TABLE 5.1 summarizes important performance indicators for the analysis of power variability.

TABLE 5.1: Comparison of power variability in the proposed super grid.

Super grid	**Standalone Caribbean**	**U.S.-Caribbean**	**U.S.-Caribbean-South America**
Number of turbines	10 (North Caribbean)	75 (U.S.), and 10 (North Caribbean)	75 (U.S.), 10 (North Caribbean), 4 (South Caribbean), and 24 (South America)
Power profiles	Fig. 5.3 and 5.4 (trajectory 1 and 7)	Fig. 5.5 and 5.6 (trajectory 1 and 7)	Fig. 5.7 and 5.8 (trajectory 1 and 7)
Location of peak:	Caribbeans	Caribbeans	Caribbeans
Pmax [MW]	82 and 79	240 and 245	400 and 370
Pmin [MW]	21 and 21	198 and 198	335 and 335
Δ_{max}	74.39% and 73.42%	17.50% and 19.18%	16.25% and 9.46%
Location of peak:	-	U.S. Midwest or Southeastern states	U.S. Midwest or Southeastern states
Pmax [MW]	-	557 and 456	693 and 590
Pmin [MW]	-	198 and 198	335 and 335
Δ_{max}	-	64.45% and 56.58%	51.66% and 43.22%

The numbers presented in TABLE 5.1 supports the following analytical conclusions:

- Power variability reduction: The interconnection of the Caribbean Super Grid with the United States and South America leads to a notable reduction in power variability. This means that with this interconnection, the fluctuations in power generation are minimized, resulting in a more stable and reliable energy supply.
- Benefits of extending the super grid: The extension of the U.S.-Caribbean super grid to South America offers substantial benefits, particularly for the Caribbeans. In trajectory 7, which represents a worst-case scenario where the Caribbeans are directly hit by a hurricane, the power variability sharply decreases from 19.18% to 9.46%. This reduction in variability signifies a more consistent and stable power supply for the Caribbeans. Additionally, the U.S. Midwest and Southeastern states would also experience benefits from this extension, although to a lesser extent, with power variability decreasing from 64.45% to 51.66% in trajectory 7.
- Impact of turbine concentration: The analysis reveals that regions with a higher concentration of turbines experience an increase in peak power production when a hurricane strikes. Specifically, the U.S. Midwest and Southeastern states generate more peak power compared to the Caribbeans. This is attributed to the significantly larger number of turbines in these regions (85 turbines in the contiguous U.S.) compared to the Caribbeans (10 turbines). Concentration of many turbines in just one place is not recommended.
- MHK power variability is diluted with the increasing number of wind turbines.

In summary, the analysis derived from the numbers presented in TABLE 5.1 highlights the positive effects of interconnecting the Caribbean Super Grid with the United States and South America. It emphasizes the role of turbine concentration in peak power production during hurricanes and underscores the significant benefits of extending the super grid to South America for the Caribbeans, as well as the U.S. Midwest and Southeastern states.

CHAPTER 6: DISCUSSIONS

This chapter elaborates on the merits of the proposed methods of renewables assessment and high voltage enforcements for the transition of the current North American power grid to a low-carbon renewable future. The future of the North American power grid lies not exclusively on the causes of global warming, i.e., GHG emissions, but on enforcing the power grid for the new future with frequent extreme weather events. Such endeavor is constrained by many challenges and conflicting interests in the environmental system. This chapter also discusses these challenges in a systematic approach.

Firstly, it is important to understand the context of the proposed methods for weather-driven energy sources in the North American power grid.

FIGURE 6.1 gives a comprehensive integration of the partial architectures developed in previous chapters into the North American power grid architecture. The methods encompass all parts of the North American power grid, thus laying the foundation for a comprehensive spatiotemporal perspective of the impact of climate change and global warming on the power system operations.

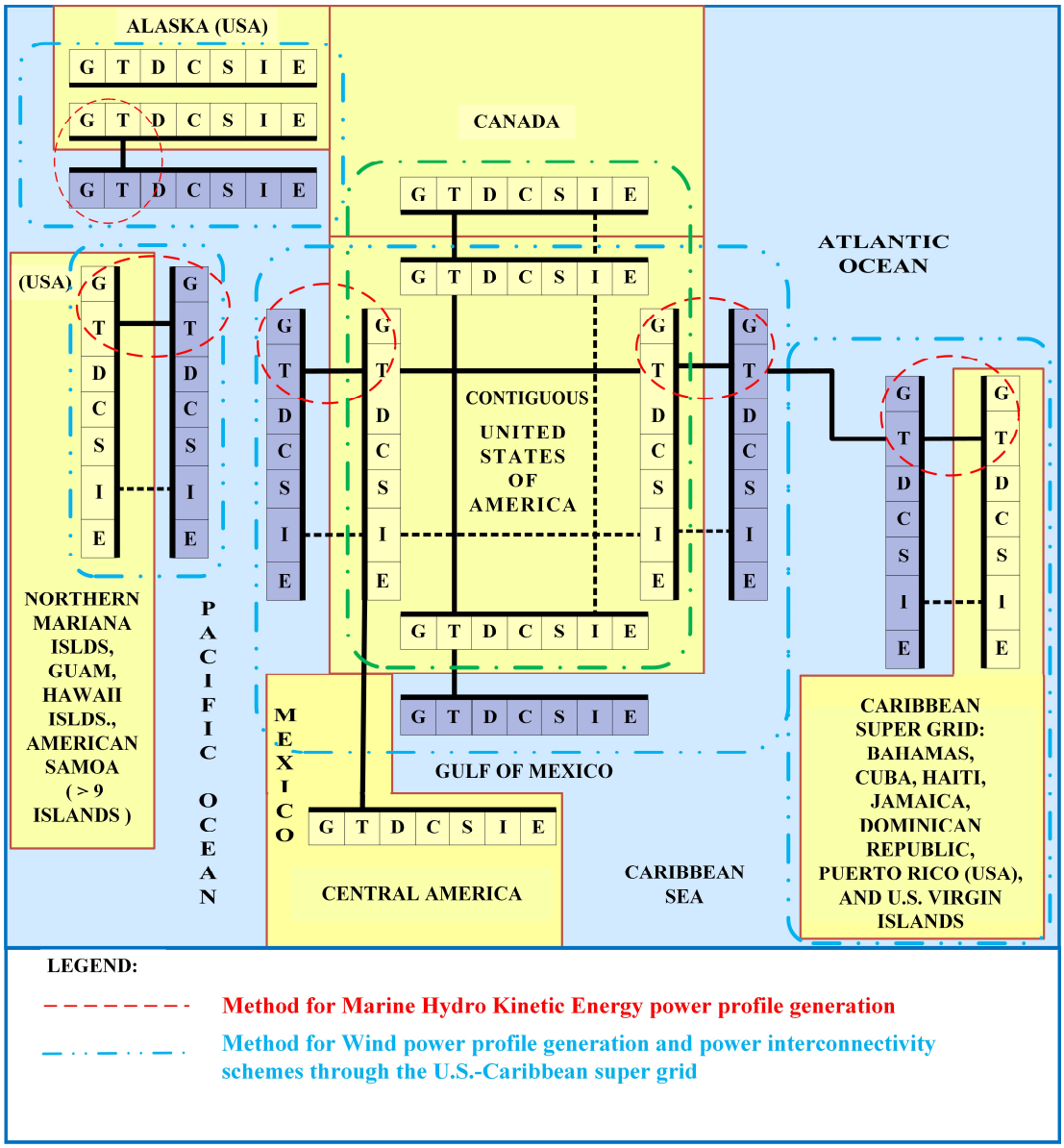

FIGURE 6.1: Architecture of North American Power Grid integrated with U.S.-Caribbean SG, adapted from [39] and [32].

The methods for the assessment of weather-driven energy sources have a multitude of applications and create other multidisciplinary implications, which are discussed in the following subsections.

6.1 Method and tool for spatiotemporal MHK power profile generation

The proposed method for estimating the MHK power generation profile based on HF NOAA radar was successfully implemented in MATLAB script coding [65]. A case study in North Carolina demonstrates the algorithm's functionalities for the planning and design of MHK farms. The simulations of two proposed MHK farms show that the power profile is highly sensitive to the selected location, with significant implications for the economic feasibility. The southern MHK farm in the Gulf Stream off the coast of North Carolina shows a more robust power profile as compared to the northern MHK farm. Regarding the short time sensitivity, within the one-day time-window simulation, it is possible to conclude that the capacity factor of the MHK turbines varies significantly for one day period. More studies with a large water speed dataset are needed to evaluate the seasonal and multi-year power variability case study demonstrated the proposed method implemented in MATLAB script was able to simulate MHK farms with a very high number of turbines without high computational cost. The case study script processed the power profile of 540 MHK turbines in less than 5 minutes in an off-the-shelf notebook with an Intel Core i7 processor. This method fills a gap in the traditional power system algorithms, which usually circumvents the computational cost by assuming simplified equivalent models of MHK farms or simulations with just a handful of electric generators. Also, the merit of this work is the realistic approach to processing HF radar data for power system studies. In other words, the proposed data analytics method directly transforms offshore weather data into valuable power system information [65]. The implications of the proposed method on the natural, economic, social, and political environment open the perspective of a multitude of topics for future multidisciplinary research. In this work, the implications of the method for the environment system classify into four categories: natural, economic, social, and political [39] [65].

6.1.1 Natural Environment

The planning and design of large-scale MHK farms must consider the risk of impact on the local marine ecosystem [101]. The typical effects of submarine cabling and offshore fixed platforms are well known from the environmental impact assessments carried out on the offshore wind industry in Europe [102] [103] [104]. The major risk of ocean energy comes from the sound and electromagnetic fields from MHK devices that can disturb the marine biota [101] [105] [106]. However, the same renewables that jeopardize marine biota also positively impact the environmental system. Ocean energy produces far less CO_2 than power from coal or natural gas [101]. TABLE 6.1 shows the comparison of ocean energy with other sources of energy [65].

TABLE 6.1: CO_2 Emissions by Sources.

Unit	**Energy sources** [101]		
	Coal	***Natural Gas***	***Ocean Energy***
g CO_2eq/kWh	1,689	930	23

Source: [65] (© 2020 IEEE)

A mechanism for reconciling trade-offs between ocean renewables and the protection of marine biota is needed. In 2021, Booth et al. proposed compensatory conservation schemes [106].

6.1.2 Economic Environment

Despite promising environmental performance in CO_2 emissions mitigation, MHK power competes with other well-mature renewable technologies [65]. TABLE 6.2 shows the projection of the Levelized Cost Of Electricity (LCOE) of variable renewables to 2030 [107] [68]. MHK power generated from ocean current turbines, e.g., MHK turbines, is not cost-competitive as other renewable technologies, and a breakthrough performance innovation is needed to reverse this trend. The LCOE of the ocean current turbine indicated in TABLE 6.2 refers to the cost for MHK in the Gulf Stream off the coast of Florida, which has a water speed higher than in North Carolina [68] [108]. The MHK LCOE in North Carolina is expected to be higher than the value indicated

in TABLE 6.2. Photovoltaic (PV) solar, e.g., has low LCOE and is not susceptible to the high seasonal variability of renewable sources such as MHK power. The PV's low variability can also be adequately smoothed by battery or power management [109] [110]. MHK power competes with other renewables in North Carolina [65].

TABLE 6.2: LCOE of Renewables.

Unit	**Renewable sources**				
	Wind Onshore in 2030 [107]	***Offshore Wind in 2030*** [107]	***Solar in 2030*** [107]	***Tidal Stream in 2030*** [107]	***Ocean Current Turbine*** [68]**.**
$/kWh	0.089–0.146	0.178–0.229	0.093–0.128	0.351–0.756	0.150 – 0.200 for 100 units

Source: [65] (© 2020 IEEE)

North Carolina nuclear and coal power plants are aging, considering future decommissioning and local economic losses. On the other hand, delays in the local expansion of renewable power capacity open the door for the importation of the abundant and more affordable Midwest onshore wind power through the high voltage transmission lines, potentially resulting in economic losses to North Carolina. With LCOE lower than MHK power, offshore wind is a competing alternative for North Carolina to minimize overdependence on renewables importation by keeping some local power generation and revenue [65].

6.1.3 Social Environment

Even in the early stages of a proposal for an MHK farm, the potential social impact is resultant from environmental protection, locals' reluctance to renewables close to their properties, and economic interests [65]. A proposal for MHK farm has a social impact on stakeholders (e.g., fishermen, local community, scientists, and investors). In 2018, Chamorro et al. investigated the impact of MHK on the human dimension and focused on public perceptions, social acceptability, public conflicts, and stakeholder participation [111]. The public perception of the potential positive

or negative social impact of the MHK farm on stakeholders reverberates into the political environment [65].

6.1.4 Political Environment

The incentives for the expansion of renewables depend on political decisions. The Paris Agreement, which institutionalizes the global commitment to mitigate global warming and GHG emissions, is an example of the role of the political system [64]. In addition, renewables tax incentives and subsidies passed by local lawmakers impact the LCOE of renewables [112] [113] [114].

FIGURE 6.2 summarizes the implications and the interactions of the method for estimation of MHK power with the multisystemic environment. For this reason, it creates a multitude of new topics for multidisciplinary research in the renewable energy domain [65].

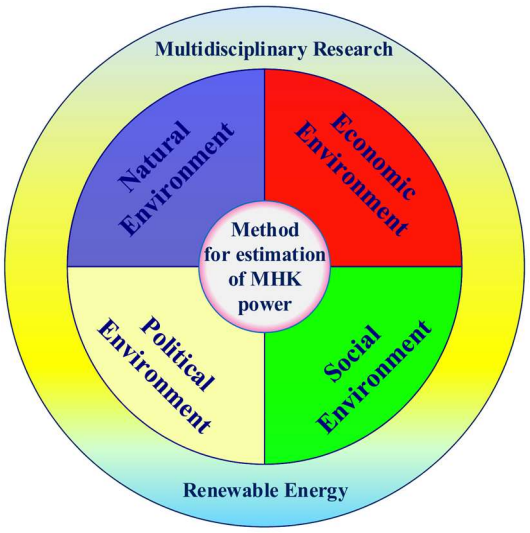

FIGURE 6.2: The proposed MHK method and the multidisciplinary research on renewable energy [65] (© 2020 IEEE).

6.2 Method for spatiotemporal wind power profile under hurricanes

The research on wind power generation under hurricanes delivers a multitude of practical engineering and scientific results [32]. First, it proposes a spatiotemporal method for the generation of power profile curves of wind farms during hurricane events. In this work, the parametric modeling of hurricanes has been applied iteratively over space and time for power system applications. The trajectories are parabolic, more adherent to the historical hurricane trajectories. The traditional techniques of power systems simulate the grid under electrical disturbances, e,g., short-circuit, harmonics, and disconnection of transmission lines. This novel approach complements the traditional power system simulations with extreme weather-driven disturbances, such as hurricanes. For this reason, this research is important in the analysis of the impact of climate change and global warming on the future site selection of turbines forming an electrical power grid. The choice for modeling hurricanes using equations proved to be computationally efficient. The method was adequate for purposes of power system simulation and implemented in MATLAB script, not demanding expensive resources of supercomputing [32].

Besides it, this research proposes a super grid of the Caribbean islands and interconnection to the contiguous U.S. power grid. The proposed scheme is investigated regarding its technical feasibility. The segments of submarine power cable between islands do not exceed the maximum length and installation depth limits known from existing projects reported in the technical literature [32].

Furthermore, implementing the proposed method for generating power profiles in MATLAB and carrying the simulations on the proposed Caribbean super grid shows that the interconnectivity with the contiguous U.S. power grid is beneficial for reducing the variability of wind power in the Caribbean islands during hurricane seasons. Large-scale power

interconnectivity eliminates the restrictions on the expansion of wind power capacity in the Caribbean region, making transitioning the region to a low-carbon economy easier. This would result in lower dependence on fossil fuels [32].

6.3 Extension of the U.S.-Caribbean Super Grid to South America

The proposed extension of the U.S.-Caribbean Super Grid to South America was investigated in Chapter 5 from the electrical perspective. It was demonstrated that super grid causes smoothness effect on the wind power variability when the peak surplus power in the Caribbeans is drained to the super grid interconnections. The scope of this 6.3 subsection is to discuss the implications of the wind power smoothness effect on the economic and natural environment. In other words, the focus of this subsection is on the opportunities for cost reduction and positive outcome on reducing GHG emissions.

6.3.1 Economic Environment

In 2023, Itiki et al formulated the procedure to evaluate the opportunity cost of temporarily reducing the dispatch of natural gas power plants in open cycle and exploring the peak power surplus generated by wind power on the U.S.-Caribbean Super Grid [115]. The simulations generated wind power profile estimations with and without the extension to South America. Natural gas, a fossil fuel resource, was selected as a cost reference because open cycle power plants have fast response in load-following mode and is typically used by utility companies to supply extra power during peak demand. Based on the surplus peak wind power from hurricane forces, it is possible to assess the total energy harvested by the wind turbines during hurricane by [115] :

$$E_h = \int_{t=1}^{nt} \left(P_t - P_{ph}\right) dt \tag{17}$$

where, P_{ph} is the power in pre-hurricane conditions excluded from the assessment, P_t is the estimation of aggregated power profile of the U.S.-Caribbean-South America Super Grid, and nt is total hours. The generated energy accounted for the hurricane excludes the energy that would otherwise be harvested if there were no hurricane, i.e., in pre-hurricane conditions. This peak energy harvested from the hurricane can substitute the dispatch of fossil-fire generation. Assuming that the power profile is estimated in time steps of 1 hour, equation (17) can be simplified to:

$$E_h = \sum_{t=1}^{nt}\left(P_t - P_{ph}\right) \tag{18}$$

where P_t is the power profile values in [MW] estimated and P_{ph} is the minimum value of the power profile, corresponding to the pre-hurricane power level.

The energy harvested from the hurricane reduces the fossil fuel cost can be calculated by [115]:

$$C_h = E_h \times LCOE \tag{19}$$

where: E_h is the energy harvested by wind turbines during the hurricane in [MWh] and LCOE is the levelized cost of energy with reduction of dispatchable fossil-fired generation. For instance, the LCOE of an open cycle power plant was typically $175 per megawatt-hour in 2019 [116].

6.3.2 Natural Environment

In 2023, Itiki et al also formulated the procedure to assess the potential reduction of carbon emissions if the dispatch of gas power plants was decreased during the surplus peak power generated by the hurricane [115]. The total mass of carbon dioxide is estimated by [115] :

$$M_{CO2} = E_h \times CO2 \tag{20}$$

where: E_h is the energy harvested by wind turbines during the hurricane and $CO2$ is the carbon dioxide emissions rate with a dispatchable fossil-fired generation. For instance, on average, an open cycle power plant using natural gas emits approximately 0.8335 Tons of carbon dioxide per MWh of electricity generated [117].

The implementation of the equations for assessment of economic and natural environment impact of wind power production in the U.S. and Caribbean region under hurricanes is carried out by processing the power profile estimated in MATLAB as input data. The result of such simulation is presented on TABLE 6.3.

TABLE 6.3: Economic opportunities and CO_2 emissions during Hurricanes.

U.S.-Caribbean super grid	**Standalone**	**Without extension to South America**	**With extension to South America**
Number of 2 MW MHK turbines in reduced scale	270	270	270
Number of 10 MW wind turbines in reduced scale	10	85	113
Trajectory	#1 and 7	#1 and 7	#1 and 7
MHK plus wind Energy in full scale [GWh]	262 and 295	2,696 and 1,460	2,892 and 1,538
Natural gas savings in full scale [$ millions]	46 and 52	472 and 255	506 and 269
CO_2 reduction in full scale [tons]	218,030 and 246,090	2,247,000 and 1,216,900	2,410,690 and 1,282,100

The simulations were conducted on a reduced scale where each 10 MW turbine corresponds to 1 GW wind power capacity. In full scale, the energy, cost, and tons shown in TABLE 6.3 is multiplied by 100 times scale. Despite the scientific merit of quantifying the economic and environmental opportunities and impact of a hurricanes on hurricane-proof wind turbines, the proposed U.S.-Caribbean-South America super grid in conjunction with a large-scale expansion

of wind power capacity in these regions, is conceived to operate in non-extreme weather conditions. The impact of the proposed super grid was motivated by reduction of GHG emissions in a region with abysmal dependence on fossil fuel. TABLE 6.4 gives a detailed understanding of the challenges faced by South Caribbean islands and South American countries to transition to low carbon energy.

TABLE 6.4: Population and Energy in South Caribbean and South America.

Country or territory	**Population**	**Installed capacity [MW]**	**Installed capacity driven by fossil fuel**
Anguilla	19,079	26	96.2%
Montserrat	5,440	5	91%
Guadeloupe	411,507	551.2	68.9%
Dominica	74,629	42	74.8%
Martinique	361,225	438.1	85.1%
St Lucia	167,122	92	99.1%
St Vincent and the Grenadines	100,969	49	73.5%
Grenada	113,949	55	98.3%
Trinidad & Tobago	1,405,646	2,123	99.9%
Guyana	789,683	380	97.4%
Suriname	632,638	542	40.5%
French Guyana	327,000	281.2	45.3%
Brazil	217,240,060	199,037	11.8%
Total	221,648,947	203,621	13.4%

Note: Population and power data from [115]. (© 2023 IEEE)

TABLE 6.4 indicates that the islands in the South Caribbean, including Trinidad & Tobago, are strongly dependent on fossil power, whereas South American countries, except Guyana, are much more independent. The interconnection of Caribbean islands to the U.S. and South America is not just an opportunistic technological proposition to smooth power variability during hurricanes, but also an important opportunity to fast-speed and facilitate the expansion of renewable power in the Caribbeans. The expansion of renewable power for either normal or

extreme weather conditions is imperative in the global strategy to address global warming and climate change. From one side, hurricanes cannot be used as an excuse by local governments for not expanding renewable wind power in the Caribbeans. On the other side, the large-scale contiguous US and South America power grids have a major opportunity to facilitate the carbon transition to renewables in the Caribbeans by absorbing sporadic surplus peak power generated by hurricanes.

CHAPTER 7: CONCLUSIONS

This dissertation is motivated by the causes and effects of global warming and climate change on renewable power generation. FIGURE 7.1 summarizes the rationale behind the development of this research, showing the interactions of effects, necessities, proposed methods, tools, and systems to support the expansion and diversification of renewable energy in North America, the Caribbean, and South America. Some effects of global warming and climate change are characterized by extreme weather events. Hurricanes are expected to become more intense with global warming, impacting wind power generation on a spatiotemporal dimension. This research concludes that the proposed U.S.-Caribbean super grid and its extension to South America is a possible solution to smooth the power variability caused by hurricanes since it allows for a geospatial diversification of wind power capacity. The expansion of weather-dependent renewables also calls for a diversification of types of energy resources to capture the temporal complementarity of variable energy resources. Marine hydrokinetic is a non-traditional renewable energy source and a strong candidate for energy diversification. This research developed a method and tool for forecasting the MHK power profile with HF radar data. This method was later integrated to the algorithm for wind power profile estimation to obtain the overall power profile forecast with hybridization of MHK and wind power in the same proposed super grid.

The main conclusions of this dissertation can be categorized into four subtopics of research achievements.

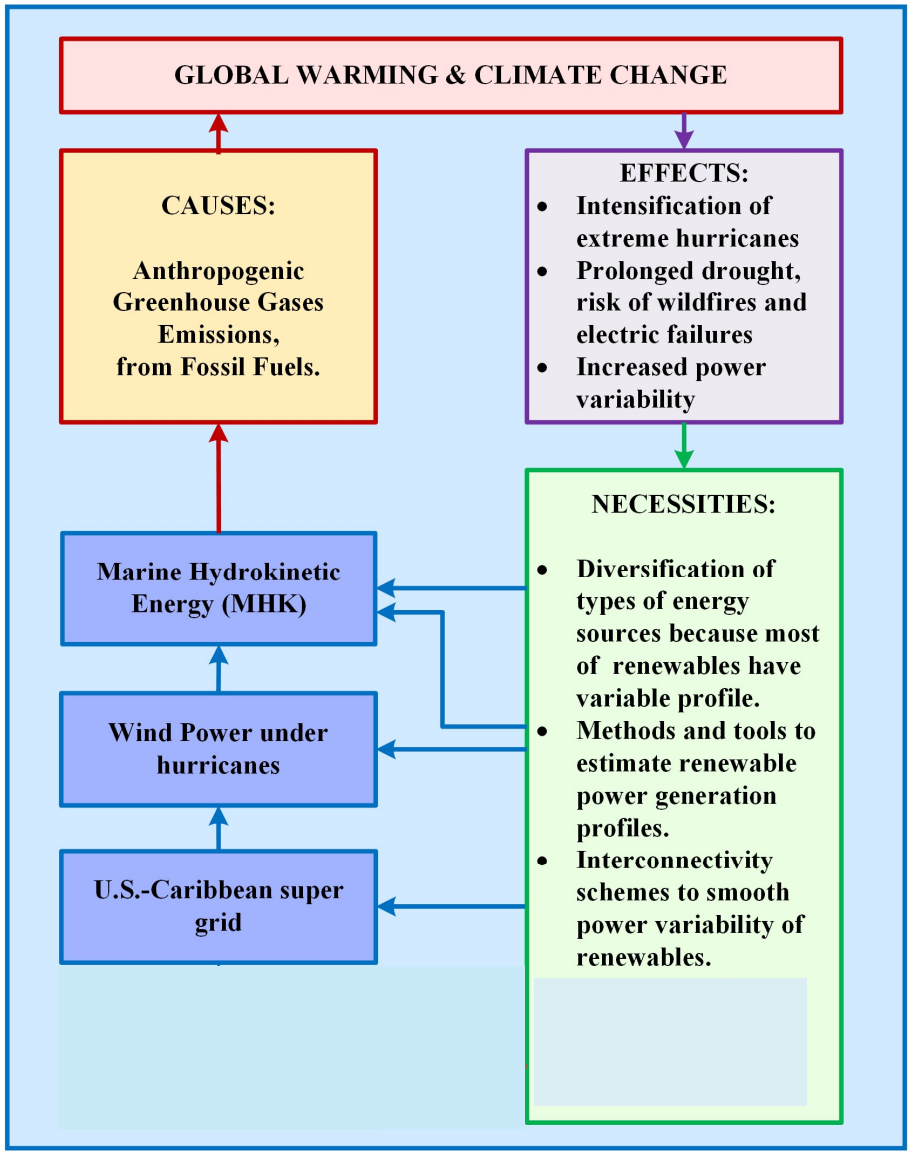

FIGURE 7.1: Context and merits of the proposed methods and Caribbean SG to the expansion of renewables in the Americas.

From the perspective of the proposed method for MHK power profile, the implementation of the algorithm for profile estimation shows that it is perfectly possible to estimate the MHK power profile of a proposed MHK farm with around 400 turbines distributed over the surface off the coast of North Carolina, if water speed data are made available by the NOAA´s webpage. The application of the proposed estimation tool for MHK power profile is also possible since the HF radar network of NOAA covers other vast portions of the U.S. in the West Coast, East Coast and

Puerto Rico. Specifically, in North Carolina, the conclusion is that the simulation results show high power variability on the estimated power profile from a proposed MHK farm. This suggests that hybridization of renewable sources and energy storage in North Carolina are needed to minimize the power peaks and valleys brought by the fast and variable speed waters of the Gulf Stream and ultimately maintain high levels of reliable power supply service to customers. More broadly, the proposed MHK assessment method developed into a MATLAB-based tool is useful for the planning and design of reinforcements to existing power infrastructure in consideration for the future expansion of MHK farms in North America and the world.

From the perspective of wind power simulations under hurricanes, the conclusions are that special turbines withstanding high-speed operation, e.g., up to 40 m/s, minimize the severity and time-duration of power drop under hurricane conditions. However, despite the benefits of special turbines, the simulation shows that the primary cause of extreme power variability is the hurricane's spatiotemporal variability, not the type of turbines. Under the proposition of a U.S.-Caribbean super grid, the simulations show that the percentual wind power variability in the Caribbean is reduced more than five times with the interconnection of the Caribbean super grid with the contiguous U.S. power grid. Later proposition and simulation of the extension of the US-Caribbean super grid to South America shows that power variability can be reduced even more. With the super grid extension to South America, the power variability can be reduced 19.18% to 9.46% in the Caribbeans, and from 64.45% to 51.66% in the US Midwest and Southeastern states.

The methods, tools, simulations, and analysis of these research topics address some key necessities originating from the effects of global warming and climate change. Renewable energy sources are even more variable on a spatiotemporal basis, which reflects the dynamics of the renewable power generation profile. The massive expansion of renewables in North America to

support the transitioning of the power sector from dispatchable fossil fuel to weather-dependent energy sources creates the need for power grids capable of spatiotemporally, actively, and intelligently controlling the power variability. To do that in real-world conditions, the electrical power grid, which is traditionally studied in its components of generation, transmission, distribution, consumption, and intelligence (i.e., automation, protection, and control), should also incorporate modeling of environmental system. The research topics of MHK and wind power under hurricanes encompass some methods and tools for environmental modeling for power system analysis in realistic conditions.

The specific contributions of this research on MHK and wind to power system area can be summarized in three main aspects: input for load flow simulation, power variability, and computational efficiency for simulation with high number of turbines.

The first contribution is that the two methods generate input data for power system studies in realistic conditions. This input data is the power profile of MHK turbines or hubs, wind turbines and super grids under hurricanes. These data are critical to simulations of time-series power flow tools, such as Sincal, in realistic conditions. It should be noted that the power profile generated by the MHK algorithm is valid for any assumed quantity of MHK turbines (e.g., 270 or 540 units as studied), in any offshore location under coverage of the HF radar network of NOAA. As for the wind turbines, the method generates power profile of wind turbines in any location along the hurricane corridor of the Caribbeans, Gulf of Mexico, U.S. Southern States, and the U.S. East Coast. The profile can also be estimated for any combination of three categories of hurricanes (cat-5, 4, and 3), in typical or high cutout special turbines, in any of the ten-trajectories band. This results 60 available options for the user to select the type of hurricane and turbine scenario it

intends to generate. Such flexibility and availability of options is a handful tool for power system research intending to simulate power systems in realistic conditions.

Another contribution is the power variability assessment. The proposed spatiotemporal methods are tools for studies on the reduction of power variability on large-scale systems such as super grids. Differently from load flow tools, which is based on temporal algorithm, the proposed spatiotemporal method is capable to address power variability concerns related to the planning of physical distribution (latitude and longitude) of future MHK and wind power capacity. For example, in Chapter 3, the MHK method allowed the identification that Hub-2 is a better place to install MHK turbines than Hub-1 off the coast of North Carolina, and quantify the magnitude of power variability. Power variability assessment is needed to determine the amount of curtailment or energy storage capacity necessary to smooth the power profile by peak shaving and valley filling. Another example, in Chapter 4, the spatiotemporal wind power estimation method supported the identification of an interconnectivity scheme that reduces power variability. It was concluded on Chapter 4 that the standalone Caribbean super grid produces lower power variability if connected to the U.S. power grid. On Chapter 5, the method supported the conclusion that extending the U.S-Caribbean super grid to South America reduces even more the power variability because the location of turbines in South America outside the hurricane corridor increases the pre-hurricane power level without generating an additional power hump in the super grid power profile. Spatiotemporal methods support some power allocation planning (latitude and longitude of turbines) that temporal methods, such as load flow, do not.

The third contribution of the research is the efficiency of the proposed algorithms in processing weather data for simulation of high number of turbines. For example, in Chapter 4, it was simulated 540 individual MHK turbines. On Chapter 5, the simulation involved 81 wind

turbines. In Chapter 6, the simulation was carried out on 270 MHK turbines in hybridization with 113 hurricane-proof turbines. The proposed spatiotemporal methods are iterative but do not involve convergence of results. This makes a huge difference as compared to load flow methods, because the proposed spatiotemporal method may take more processing time with additional turbines to reach to the result (the map and the power profile curve), but they do not stop running in a state of non-convergence of results, as possible on some load flow algorithms. For this reason, the spatiotemporal methods are appropriate for studies of large-scale power systems, such as super grids.

Despite the significant contributions of this research to the power system area, a myriad of new challenges was discovered during the scientific investigation on the macro theme of the effects of global warming and climate change on the power grid. Such new challenges are registered herein for future works.

7.1 Future works

The effects of global warming and climate change lead to a multitude of necessities not entirely covered by this research.

A hurricane, for example, wraps a massive volume of humid air and sustains a gigantic opaque disk of clouds around its eye. The capacity of PV generation would be temporarily unable under the shading of the cloud disk induced by the hurricane during daytime.

Also, the atmosphere is under extreme wind forces during a hurricane, which, on average, boosts the wind power profile. The power variability of wind power under hurricanes is highly variable. However, the same cannot be said about the underwater currents, which are protected by a dense seawater column under a hurricane. If the power profile of an MHK farm under hurricane conditions would deliver a steadier power supply for critical loads, e.g., hospitals, communication,

and water treatment facilities in the Caribbean, it is yet to be investigated in future studies. However, it should be noted that the water speed measurements of NOAA HF radars do not cover a major part of the Caribbeans, including Puerto Rico and the U.S. Virgin Islands. The other countries of the Caribbean also do not have online HF radar seawater speed measurements available to feed into a comprehensive study of the MHK resources to plan a proposed U.S.-Caribbean super grid. Future studies involving the installation of HF radars in these areas would result in valuable information about the real MHK resource assessment of the Caribbeans.

REFERENCES

[1] T. R. Knutson, M. V. Chung, G. Vecchi, J. Sun, T.-L. Hsieh and A. J. P. & Smith, "Climate change is probably increasing the intensity of tropical cyclones," ScienceBrief Review, Eds: Corinne Le Quéré, Peter Liss, Piers, 2021.

[2] G. J. Van Oldenborgh, S. Philip, S. Kew, M. van Weele, P. Uhe, F. Otto, R. Singh, I. Pai, H. Cullen and K. and AchutaRao, "Extreme heat in India and anthropogenic climate change," *Nat. Hazards Earth Syst. Sci.,* vol. 18, p. 365–381, 2018.

[3] S. Huang, G. Leng and Q. e. a. Huang, "The asymmetric impact of global warming on US drought types and distributions in a large ensemble of 97 hydro-climatic simulations.," *Sci Rep 7, 5891,* 2017.

[4] M. Dumas, B. Kc and and C. I. Cunliff, "Extreme Weather and Climate Vulnerabilities of the Electric Grid: A Summary of Environmental Sensitivity Quantification Methods," Oak Ridge National Lab. (ORNL), TN, Aug. 2019.

[5] M. L. Ourari, L. .. -A. Dessaint and and Van-Que Do, "Dynamic equivalent modeling of large power systems using structure preservation technique," *IEEE Transactions on Power Systems, vol. 21, no. 3,* pp. 1284-1295, Aug. 2006.

[6] M. Nachtane, M. Tarfaoui, I. Goda and M. Rouway, "A review on the technologies, design considerations and numerical models of tidal current turbines," *Renewable Energy, vol. 157,,* pp. 1274-1288, 2020.

[7] R. He, J. Bane, M. Muglia, S. Haines, C. Lowcher, Y. Gong and P. Taylor, "Gulf stream marine hydrokinetic energy resource characterization off Cape Hatteras, North Carolina USA," in *OCEANS 2016*, Shanghai, 2016.

[8] S. Chawdhary, C. Hill, X. Yang, M. Guala, D. Corren, J. Colby and Fotis Sotiropoulos, "Wake characteristics of a TriFrame of axial-flow hydrokinetic turbines," *Renewable Energy, vol. 109,* pp. 332-345, 2017.

[9] G. I. A. Vazquez, "LCOE (levelised cost of energy) mapping: A new geospatial tool for tidal stream energy," *Energy, vol. 91,,* pp. 192-201, 2015.

[10] T. Ueno, S. Nagaya, M. Shimizu, H. Saito, S. Murata and a. N. Handa, "Development and Demonstration Test for Floating Type Ocean Current Turbine System Conducted in Kuroshio Current," in *2018 OCEANS - MTS/IEEE Kobe Techno-Oceans (OTO)*, Kobe, 2018.

[11] E. Díaz-Dorado, C. Carrillo, J. Cidras, D. Román and J. Grande, "Performance evaluation and modelling of the Atir marine current turbine.," *IET Renew Power Gener. , 15,,* p. 821– 838, 2021.

[12] B. Gunawan, V. S. Neary and J. Colby, "Tidal energy site resource assessment in the East River tidal strait, near Roosevelt Island, New York," *Renewable Energy, vol 71,,* pp. 509-517, 2014.

[13] T. H. J. a. J. B. Elsner, "A Consensus Model for Seasonal Hurricane Prediction," *Journal of Climate, Vol. 23, No. 22,* pp. 6090-6099, November 2010.

[14] S. D. Aberson and a. M. D. , "Verification of a Nested Barotropic Hurricane Track Forecast Model (VICBAR)," *Monthly Weather Review, 122.12,* pp. 2804-2815, 1994.

[15] J. Persing and a. M. T. Montgomery, "Hurricane Superintensity," *Journal of the Atmospheric Sciences 60.19,* pp. 2349-2371, 2003.

[16] J. P. Kossin and a. M. Sitkowski, "An Objective Model for Identifying Secondary Eyewall Formation in Hurricanes," *Monthly Weather Review 137.3,* pp. 876-892, 2009.

[17] C. Davis, W. Wang, S. S. Chen, Y. Chen, K. Corbosiero, M. DeMaria, J. Dudhia, G. Holland, J. Klemp, J. Michalakes, H. Reeves, R. Rotunno, C. Snyder and a. Q. Xiao., "Prediction of Landfalling Hurricanes with the Advanced Hurricane WRF Model," *Monthly Weather Review 136.6,* pp. 1990-2005, 2008.

[18] R. W. Katz, "Stochastic Modeling of Hurricane Damage," *Journal of Applied Meteorology 41.7,* pp. 754-762, 2002.

[19] E. Regnier and a. P. A. Harr, "A Dynamic Decision Model Applied to Hurricane Landfall," *Weather and Forecasting 21.5,* pp. 764-780, 2006.

[20] N. Lin, J. A. Smith, G. Villarini, T. P. Marchok and a. M. L. Baeck, "Modeling Extreme Rainfall, Winds, and Surge from Hurricane Isabel (2003)," *Weather and Forecasting 25.5,* pp. 1342-1361, 2010.

[21] M. Lonfat, R. Rogers, T. Marchok and J. and Frank D. Marks, "A Parametric Model for Predicting Hurricane Rainfall," *Monthly Weather Review 135.9,* pp. 3086-3097, 2007.

[22] Y. Y. Chao and a. H. L. Tolman, "Performance of NCEP Regional Wave Models in Predicting Peak Sea States during the 2005 North Atlantic Hurricane Season," *Weather and Forecasting 25.5,* pp. 1543-1567, 2010.

[23] T. H. Jagger and a. J. B. Elsner, "Climatology Models for Extreme Hurricane Winds near the United States," *Journal of Climate 19.13,* pp. 3220-3236, 2006.

[24] G. Holland, "A Revised Hurricane Pressure–Wind Model," *Monthly Weather Review 136.9,* pp. 3432-3445, 2008.

[25] G. J. Holland, J. I. Belanger and a. A. Fritz., "A Revised Model for Radial Profiles of Hurricane Winds," *Monthly Weather Review 138.12,* pp. 4393-4401, 2010.

[26] D. Chang, S. Amin and a. K. Emanuel., "Modeling and Parameter Estimation of Hurricane Wind Fields with Asymmetry," *Journal of Applied Meteorology and Climatology 59.4,* pp. 687-705, 2020.

[27] N. A. Ahmed and Michael Cameron, "The challenges and possible solutions of horizontal axis wind turbines as a clean energy solution for the future," *Renewable and Sustainable Energy Reviews, vol 38,* pp. 439-460, 2014.

[28] C. Wei, "Forecasting surface wind speeds over offshore islands near Taiwan during tropical cyclones: Comparisons of data-driven algorithms and parametric wind representations," *J. Geophys. Res. Atmos., 120,* p. 1826– 1847, 2015.

[29] A. M. Foley, P. G. Leahy, A. Marvuglia and Eamon J. McKeogh, "Current methods and advances in forecasting of wind power generation," *Renewable Energy,,* vol. 37, no. 1, pp. 1-8, 2012.

[30] S. Wang, X. Yang, H. Li, K. Ren, X. Yin, D. Hu and Y. Du, "An Improved Asymmetric Hurricane Parametric Model Based on Cross-Polarization SAR Observations," *IEEE Journal of Selected Topics in Applied Earth Observations and Remote Sensing, vol. 14,* pp. 1411-1422, 2021.

[31] J. Wang, S. Qin, S. Jin and Jie Wu, "Estimation methods review and analysis of offshore extreme wind speeds and wind energy resources," *Renewable and Sustainable Energy Reviews, vol. 42,,* pp. 26-42, 2015.

[32] R. Itiki, M. Manjrekar, S. G. D. Santo and C. Itiki, "Method for spatiotemporal wind power generation profile under hurricanes: U.S.-Caribbean super grid proposition," *Renewable and Sustainable Energy Reviews,* vol. 173, no. 113082, pp. 1-25, March 2023.

[33] K. Murthy and O.P. Rahi, "A comprehensive review of wind resource assessment," *Renewable and Sustainable Energy Reviews, vol. 72,,* pp. 1320-1342, 2017.

[34] I.-J. Moon, I. Ginis, T. Hara, H. L. Tolman, C. W. Wright and a. E. J. Walsh, "Numerical Simulation of Sea Surface Directional Wave Spectra under Hurricane Wind Forcing," *Journal of Physical Oceanography 33.8,* pp. 1680-1706, 2003.

[35] C. Bender, J. M. Smith, A. Kennedy and R. Jensen, "STWAVE simulation of Hurricane Ike: Model results and comparison to data," *Coastal Engineering, vol 73,* pp. 58-70, 2013.

[36] M. Hashemi, B. Kresning, J. Hashemi and I. Ginis, "Assessment of hurricane generated loads on offshore wind farms; a closer look at most extreme historical hurricanes in New England," *Renewable Energy, vol. 175,,* pp. 593-609, 2021.

[37] J. W. Muhs and M. Parvania, "Stochastic Spatio-Temporal Hurricane Impact Analysis for Power Grid Resilience Studies," in *2019 IEEE Power & Energy Society Innovative Smart Grid Technologies Conference (ISGT)*, Washington, DC, 2019.

[38] E. B. Watson and A. H. Etemadi, "Modeling Electrical Grid Resilience Under Hurricane Wind Conditions With Increased Solar and Wind Power Generation," *IEEE Transactions on Power Systems,* vol. 35, pp. 929-937, March 2020.

[39] R. Itiki, S. G. D. Santo, C. Itiki, M. Manjrekar and B. H. Chowdhury, "A comprehensive review and proposed architecture for offshore power system," *International Journal of Electrical Power & Energy Systems,* vol. 111, pp. 79-92, 10 April 2019.

[40] I. Arrambide, I. Zubia and A. Madariaga, "Critical review of offshore wind turbine energy production and site potential assessment," *Electric Power Systems Research,* vol. 167, pp. 39-47, 31 October 2018.

[41] R. Itiki, M. Manjrekar e S. G. D. Santo, “Comparative Evaluation of Super Grid Topologies proposed for Europe and Latin America,” em *2019 North American Power Symposium (NAPS)*, Wichita, KS, 2019.

[42] B. Bağcı, "Towards a Zero Energy Island," *Renewable Energy,* vol. 34, no. 3, pp. 784-789, March 2009.

[43] Y. Bae, M. Kim and H. Kim, "Performance changes of a floating offshore wind turbine with broken mooring line,," *Renewable Energy,,* vol. 101, pp. 364-375, February 2017.

[44] T. Kim, J.-I. Park e J. Maeng, “Offshore wind farm site selection study around Jeju Island, South Korea,” *Renewable Energy,* vol. 94, pp. 619-628,, August 2016.

[45] A. M.-Z. Gao, C.-H. Huang, J.-C. Lin e W.-N. Su, “Review of recent offshore wind power strategy in Taiwan: Onshore wind power comparison,” *Energy Strategy Reviews,* Vols. %1 de %2Volume 38,, nº 100747, November 2021.

[46] N. D. Luong, “A critical review on potential and current status of wind energy in Vietnam,” *Renewable and Sustainable Energy Reviews,* vol. 43, pp. 440-448,, March 2015.

[47] I. C. Gil-García, A. Ramos-Escudero, M. García-Cascales, H. Dagher e A. Molina-García, “Fuzzy GIS-based MCDM solution for the optimal offshore wind site selection: The Gulf of Maine case,” *Renewable Energy,* vol. 183, pp. 130-147, January 2022.

[48] H. Díaz e C. G. Soares, “Review of the current status, technology and future trends of offshore wind farms,” *Ocean Engineering,* vol. 209, nº 107381, 1 August 2020.

[49] D. Willis, C. Niezrecki, D. Kuchma, E. Hines, S. Arwade, R. Barthelmie, M. DiPaola, P. Drane, C. Hansen, M. Inalpolat, J. Mack, A. Myers e M. Rotea, “Wind energy research: State-of-the-art and future research directions,” *Renewable Energy,* vol. 125, pp. 133-154, September 2018.

[50] K. Wei, S. Arwade, A. Myers, S. Hallowell, J. Hajjar, E. Hines e W. Pang, “Toward performance-based evaluation for offshore wind turbine jacket support structures,,” *Renewable Energy,,* vol. 97, pp. 709-721, November 2016.

[51] A. A. Raina, K. T. Lee e K. Wetzel, “Optimization and Design of a 105m Blade for a 10MW Hurricane-Resilient Wind Turbine,” em *AIAA 2015-1206. 33rd Wind Energy Symposium*, Kissimmee, Florida, January 2015.

[52] E. Loth, L. Fingersh, D. Griffith, M. Kaminski and C. Qin, "Gravo-Aeroelastically Scaling for Extreme-Scale Wind Turbines," in *35th AIAA Applied Aerodynamics Conference*, June 2017.

[53] M. Kaminski, C. Noyes, E. Loth, R. Damiani, S. Hughes, C. Bay, M. Chetan, D. T. Griffith, K. Johnson e D. Martin, “Gravo-aeroelastic scaling of a 13-MW downwind rotor for 20% scale blades,” *Wind Energy,* vol. 24, p. 229– 245, 2021.

[54] Challenergy, "Specifications," Challenergy, Japan, 2022 [accessed Feb 01, 2022].

[55] V. Petrović and C. L. Bottasso, "Wind turbine envelope protection control over the full wind speed range," *Renewable Energy,* vol. 111, pp. 836-848, October 2017.

[56] F. Bellizio, J. L. Cremer e G. Strbac, “Machine-learned security assessment for changing system topologies,” *International Journal of Electrical Power & Energy Systems,* vol. 134, pp. 1-10, Jan 2022.

[57] S. Mutlu and E. Şenyiğit, "Literature review of transmission expansion planning problem test systems: detailed analysis of IEEE-24," *Electric Power Systems Research,* vol. 201, pp. 1-14, Dec 2021.

[58] R. Itiki, M. Manjrekar, S. G. D. Santo and L. F. M. Machado, "Topology Design Method for Super Grids based on experiences in China and North America," in *2020 IEEE Power & Energy Society Innovative Smart Grid Technologies Conference (ISGT)*, Washington, DC, 2020.

[59] Y.-K. Wu, G.-Y. Han and C.-Y. Lee, "Planning 10 onshore wind farms with corresponding interconnection network and power system analysis for low-carbon-island development on Penghu Island, Taiwan," *Renewable and Sustainable Energy Reviews,* vol. 19, pp. 531-540, March 2013.

[60] N. Chintapalli, M. K. Sharma and J. Bhattacharya, "Linking spectral, thermal and weather effects to predict location-specific deviation from the rated power of a PV panel," *Solar Energy,* vol. 208, pp. 115-123, 15 Sept 2020.

[61] P. R. Chowdhury, E. Soubaki and M. Manjrekar, "Comparison of Power Control Methods for Renewable Energy Resources Operating in a Weak Grid," in *2020 52nd North American Power Symposium (NAPS)*, Tempe, AZ, 2021.

[62] P. R. Chowdhury, S. Essakiappan, M. Manjrekar, K. Schneider and S. Laval, "Optimized Dispatch of Distributed Energy Resources for Resiliency and Power Quality Improvements at the Grid-Edge," in *2021 IEEE Kansas Power and Energy Conference (KPEC)*, Manhattan, KS, 2021.

[63] P. Gayen, P. R. Chowdhury and P. Dhara, "An improved dynamic performance of bidirectional SEPIC-Zeta converter based battery energy storage system using adaptive sliding mode control technique," *Electric Power Systems Research,* vol. 160, pp. 348-361, Jul 2018.

[64] R. Itiki, M. Manjrekar, S. G. D. Santo and L. F. M. Machado, "Technical feasibility of Japan-Taiwan-Philippines HVdc interconnector to the Asia Pacific Super Grid," *Renewable and Sustainable Energy Reviews,* vol. 133, no. 110161, pp. 1-14, November 2020.

[65] R. Itiki, P. R. Chowdhury, F. Kamal, M. Manjrekar, B. Chowdhury and G. G. Bonner, "Method for Estimation of Marine Hydro-Kinetic Power based on High-frequency Radar Data," *OCEANS 2021: San Diego – Porto,* pp. 1-7, 20-23 September 2021.

[66] National Oceanic and Atmospheric Administration (NOAA), "Historical Hurricane Tracks," Washington, DC, 2021. Available: https://coast.noaa.gov/hurricanes/#map=2.32/18.83/-50.31&search=eyJzZWFyY2hTdHJpbmciOiJFc3RhZG9zIFVuaWRvcyBkYSBBbcOpcmljYSIsInNlYXJjaFR5cGUiOiJnZW9jb2RlZCIsIm9zbUlEIjoiMTQ4ODM4IiwiY2F0ZWdvcmllcyI6WyJINSIsIkg0Il0sInllYXJzIjpbXSwibW9u.

[67] K. Haas, "Assessment of Energy Production Potential from Ocean Currents along the United States Coastline," GeorgiaTech Research Corporation., 2013, Available: https://www.osti.gov/servlets/purl/1093367/ [accessed Feb 27, 2022].

[68] V. S. Neary, M. Previsic, R. A. Jepsen, M. J. Lawson, Y.-H. Yu, A. E. Copping, A. A. Fontaine, K. C. Hallett and D. K. Murray, "Methodology for Design and Economic Analysis of Marine Energy Conversion (MEC) Technologies," Sandia National Laboratories, Albuquerque, New Mexico, March 2014.

[69] L. A. Fiorentino, R. Heitsenrether, C.-C. Teng and M. Muglia, "Field Test Results from Ellipsoid ADCP Buoy Moored at the Edge of the Gulf Stream," *2019 IEEE/OES Twelfth Current, Waves and Turbulence Measurement (CWTM),* pp. 1-8, March 2019.

[70] M. Muglia, H. Seim and P. Taylor, "Gulf Stream Position, Width, and Orientation Estimated from HF Radar Radial Velocity Maps off Cape Hatteras, North Carolina," *Journal of Atmospheric and Oceanic Technology,* vol. 39, no. 5, pp. 689-705, 23 May 2022.

[71] D. Kang, E. N. Curchitser and A. Rosati, "Seasonal Variability of the Gulf Stream Kinetic Energy," *Journal of Physical Oceanography,* vol. 46, no. 4, pp. 1189-1207, 01 April 2016.

[72] T. Knutson, S. J. Camargo, J. C. L. Chan, K. Emanuel, C.-H. Ho, J. Kossin, M. Mohapatra, M. Satoh, M. Sugi, K. Walsh and L. Wu, "Tropical Cyclones and Climate Change Assessment: Part II: Projected Response to Anthropogenic Warming," *Bulletin of the American Meteorological Society,* vol. 101.3, pp. E303-E322, 2020.

[73] G. J. Holland, "An Analytic Model of the Wind and Pressure Profiles in Hurricanes," *Monthly Weather Review 108.8,* pp. 1212-1218, 1980.

[74] P. Georgiou, A. Davenport and B. Vickery, "Design wind speeds in regions dominated by tropical cyclones," *Journal of Wind Engineering and Industrial Aerodynamics,* vol. 13, no. 1–3, pp. 139-152, December 1983.

[75] P. J. Vickery, P. F. Skerlj, A. C. Steckley and L. A. Twisdale, "Hurricane Wind Field Model for Use in Hurricane Simulations," *Journal of Structural Engineering,* vol. 126, no. 10, October 2000.

[76] W. Cui e L. Caracoglia, “Exploring hurricane wind speed along US Atlantic coast in warming climate and effects on predictions of structural damage and intervention costs,” *Engineering Structures,* vol. 122, nº 1, pp. 209-225, September 2016.

[77] K. H. Lee and D. V. Rosowsky, "Synthetic Hurricane Wind Speed Records: Development of a Database for Hazard Analyses and Risk Studies," *Natural Hazards Review,* vol. 8, no. 2, 01 May 2007.

[78] K. Wei, S. R. Arwade, A. T. Myers, V. Valamanesh and W. Pang, "Effect of wind and wave directionality on the structural performance of non-operational offshore wind turbines supported by jackets during hurricanes," *Wind Energy,* vol. 20, no. 2, pp. 289-303, February 2017.

[79] F. Faturay, V. S. G. Vunnava, M. Lenzen and S. Singh, "Using a new USA multi-region input output (MRIO) model for assessing economic and energy impacts of wind energy expansion in USA," *Applied Energy,* vol. 261, no. 114141, 1 March 2020.

[80] A. Russell, S. Bingaman and H.-M. Garcia, "Threading a moving needle: The spatial dimensions characterizing US offshore wind policy drivers," *Energy Policy,* vol. 157, no. 112516, pp. 1-13, October 2021,.

[81] J. Camelo e T. Mayo, “The lasting impacts of the Saffir-Simpson Hurricane Wind Scale on storm surge risk communication: The need for multidisciplinary research in addressing a multidisciplinary challenge,” *Weather and Climate Extremes,* vol. 33, nº 100335, September 2021.

[82] National Renewable Energy Laboratory, “Wind Resource of the United States - Annual Average Wind Speed at 120 Meters above Surface Level. Available: https://www.nrel.gov/gis/assets/images/wtk-120m-2017-01.jpg. [accessed Feb 27, 2022],” NREL, Denver, Colorado, 2017.

[83] (U.S.), Tropical Prediction Center/National Hurricane Center, "Hurricane basics," National Hurricane Center, Miami, 2005.

[84] P. J. Vickery and D. Wadhera, "Statistical Models of Holland Pressure Profile Parameter and Radius to Maximum Winds of Hurricanes from Flight-Level Pressure and H*Wind Data," *Journal of Applied Meteorology and Climatology,* vol. 47, no. 10, pp. 2497-2517, 2008.

[85] A. Purvins, L. Sereno, M. Ardelean, C.-F. Covrig, T. Efthimiadis e P. Minnebo, “Submarine power cable between Europe and North America: A techno-economic analysis,” *Journal of Cleaner Production,* vol. 186, pp. 131-145, 10 June 2018.

[86] M. Brinkerink, B. Ó. Gallachóir and P. Deane, "A comprehensive review on the benefits and challenges of global power grids and intercontinental interconnectors," *Renewable and Sustainable Energy Reviews,* vol. 107, pp. 274-287, June 2019.

[87] A. M. Papadopoulos, “Renewable energies and storage in small insular systems: Potential, perspectives and a case study,” *Renewable Energy,* vol. 149, pp. 103-114, April 2020.

[88] S. Leroy and e. al., "Segmentation and kinematics of the North America-Caribbean plate boundary offshore Hispaniola," *Terra Nova,* vol. 27, pp. 467-478, 01 October 2015.

[89] A. Rodríguez-Zurrunero, J. Granja-Bruña, A. Muñoz-Martín, S. Leroy, U. t. Brink, J. Gorosabel-Araus, L. G. d. l. Peña, M. Druet e A. Carbó-Gorosabel, “Along-strike segmentation in the northern Caribbean plate boundary zone (Hispaniola sector): Tectonic implications,” *Tectonophysics,* vol. 776, nº 228322, pp. 1-35, 5 February 2020.

[90] J. Zhang, M. Baringer, C. Fischer and e. al, "An estimate of diapycnal nutrient fluxes to the euphotic zone in the Florida Straits," *Sci Rep,* vol. 7, pp. 1-8, 23 November 2017.

[91] A. Jo, G. P. Eberli and M. Grasmueck, "Margin collapse and slope failure along southwestern Great Bahama Bank," *Sedimentary Geology,* vol. 317, pp. 43-52, 15 March 2015.

[92] J. Corbeau, F. Rolandone, S. Leroy, B. M. d. Lépinay, B. Meyer, N. Ellouz-Zimmermann and R. Momplaisir, "The northern Caribbean plate boundary in the Jamaica Passage: Structure and seismic stratigraphy," *Tectonophysics,* vol. 675, pp. 209-226, 22 April 2016.

[93] J. D. Chaytor and U. S. t. Brink, "Extension in Mona Passage, Northeast Caribbean," *Tectonophysics,* vol. 493, pp. 74-92, 8 October 2010.

[94] W. J. Pringle, J. Gonzalez-Lopez, B. R. Joyce, J. J. Westerink and A. J. v. d. Westhuysen, "Baroclinic Coupling Improves Depth-Integrated Modeling of Coastal Sea Level Variations Around Puerto Rico and the U.S. Virgin Islands," *Journal of Geophysical Research: Oceans,* vol. 124, p. 2196– 2217, 13 February 2019.

[95] Central Intelligence Agency, "The World Factbook - CIA," CIA, Langley, VA, 2022 [accessed Mar 01, 2022].

[96] United Nations, "World Population Dashboard 2021," United Nations Population Fund, NY, USA, 2022, Available: https://www.unfpa.org/data/world-population-dashboard [accessed Mar 01, 2022].

[97] The Government of The Bahamas, "Census of Population and Housing 2010," Department of Statistics - The Commonwealth of The Bahamas, Nassau, 2017.

[98] United States Census 2020, “Understanding the Population of the U.S. Virgin Islands,” U.S. Virgin Islands, St. Thomas and St. John, 2020.

[99] The World Bank, "Population, total - British Virgin Islands," The World Bank, Washington, D.C., 2019 [accessed Mar 01, 2022].

[100] E. Kim, L. Manuel, M. Curcic, S. S. Chen, C. Phillips and P. Veers, "On the Use of Coupled Wind, Wave, and Current Fields in the Simulation of Loads on Bottom-

Supported Offshore Wind Turbines during Hurricanes - March 2012 — September 2015," National Renewable Energy Laboratory, Golden, Colorado, June 2016.

[101] L. Dubbs, A. G. Keeler and T. O'Meara, "Permitting, Risk and Marine Hydrokinetic Energy Development," *The Electricity Journal,* Vols. 26, , no. 10, pp. 64-74, December 2013.

[102] B. Taormina, J. Bald, A. Want, G. Thouzeau, M. Lejart, N. Desroy and A. Carlier, "A review of potential impacts of submarine power cables on the marine environment: Knowledge gaps, recommendations and future directions," *Renewable and Sustainable Energy Reviews,* vol. 96, pp. 380-391, November 2018.

[103] B. Taormina, C. D. Poi, A.-L. Agnalt, A. Carlier, N. Desroy, R. H. Escobar-Lux, J.-F. D'eu, F. Freytet and C. M. Durif, "Impact of magnetic fields generated by AC/DC submarine power cables on the behavior of juvenile European lobster (Homarus gammarus)," *Aquatic Toxicology,* vol. 220, no. 105401, pp. 1-8, March 2020.

[104] A. M. Fowler, A.-M. Jørgensen, J. C. Svendsen, P. I. Macreadie, D. O. Jones, A. R. Boon, D. J. Booth, R. Brabant, E. Callahan, J. T. Claisse, T. G. Dahlgren, S. Degraer, Q. R. Dokken, A. B. Gill and e. al, "Environmental benefits of leaving offshore infrastructure in the ocean," *Front Ecol Environ,* vol. 16, no. 10, p. 571– 578, 2018.

[105] L. L. Dubbs, M. Piehler and J. Colby, "An examination of pelagic Sargassum community primary productivity and nutrient cycling in the face of Gulf Stream based energy," in *OCEANS 2015 - MTS/IEEE*, Washington, 2015.

[106] H. Booth, W. N. S. Arlidge, D. Squires and E. J. Milner-Gulland, "Bycatch levies could reconcile trade-offs between blue growth and biodiversity conservation," *Nature Ecology & Evolution,* p. 715–725, 10 May 2021.

[107] W. Shen, X. Chen, J. Qiu, J. A. Hayward, S. Sayeef, P. Osman, K. Meng and Z. Y. Dong, "A comprehensive review of variable renewable energy levelized cost of electricity," *Renewable and Sustainable Energy Reviews,* vol. 133, no. 110301, pp. 1-14, November 2020.

[108] A. K. Sleiti, "Tidal power technology review with potential applications in Gulf Stream," *Renewable and Sustainable Energy Reviews,* vol. 69, pp. 435-441, March 2017.

[109] A. J. Swart and P. E. Hertzog, "Varying percentages of full uniform shading of a PV module in a controlled environment yields linear power reduction," *Journal of Energy in Southern Africa,* vol. 27, no. 3, p. 28–38, 23 09 2016.

[110] P. R. Chowdhury, P. K. Sahu, S. Essakiappan, M. Manjrekar, K. Schneider e S. Laval, "Power Quality and Stability in a Cluster of Microgrids with Coordinated Power and Energy Management," em *2020 IEEE Industry Applications Society Annual Meeting*, 2020.

[111] C. Ruano-Chamorro, J. C. Castilla and S. Gelcich, "Human dimensions of marine hydrokinetic energies: Current knowledge and research gaps," *Renewable and Sustainable Energy Reviews,* vol. 82, no. 3, pp. 1979-1989, February 2018.

[112] T. T. Tran and A. D. Smith, "fEvaluation of renewable energy technologies and their potential for technical integration and cost-effective use within the U.S. energy sector," *Renewable and Sustainable Energy Reviews,* vol. 80, pp. 1372-1388, December 2017.

[113] J. G. Vining and A. Muetze, "Economic Factors and Incentives for Ocean Wave Energy Conversion," *IEEE Transactions on Industry Applications,* vol. 45, no. 2, pp. 547-554, March-April 2009.

[114] S. Golroodbari, D. Vaartjes, J. Meit, A. v. Hoeken, M. Eberveld, H. Jonker e W. v. Sark, "Pooling the cable: A techno-economic feasibility study of integrating offshore floating photovoltaic solar technology within an offshore wind park," *Solar Energy,* vol. 219, pp. 65-74, 1 May 2021.

[115] R. Itiki, M. Manjrekar e S. G. Di Santo, "Proposed Extension of the U.S.-Caribbean Super Grid to South America for Resilience during Hurricanes," *IEEE Transactions on Sustainable Energy,* pp. 1-10, 2023 (in review).

[116] M. Shafiullah, S. D. Ahmed and F. A. Al-Sulaiman, "Grid Integration Challenges and Solution Strategies for Solar PV Systems: A Review," *IEEE Access,* vol. 10, pp. 52233-52257, 2022.

[117] S. Kaloti, F. Kamal, A. A. Mamun e B. Chowdhury, ""Is Achieving Net-Zero Carbon Emissions Possible for Electric Utilities with Current Technology?,"," em *2021 North American Power Symposium (NAPS)*, College Station, TX, USA. , 2021.

APPENDIX A: MATLAB SCRIPT OF MHK ALGORITHM

```
% MHK Power assessment
% https://hfradar.ndbc.noaa.gov/tab.php?from=2020-09-18+11%3A00%3A00&to=2020-09-18+12%3A00%3A00&uom=cms&p=1&lat=34.01069740217323&lng=-77.59897611733172&lat2=36.69829665135132&lng2=-73.2044448673329
clear all
dirpath=['C:\Users\Rodney\Desktop\PhD Dissertation\MatPower\matpower7.0\'];
T = readtable('hfradar-20200919040246.txt','Format','%f %f %f %f %s %d %s')
% Mostra=T(1,:)  % not necessary to delete first row
% T(1,:) = [];   % not necessary to delete first row
% MatLab is smart enough to not readtable the following description as numerical data:
% lat long speed angle year month day hour%
% summary(T);

%% 1. POPULATE MICROGRIDS IN A MAP
% Populate Array of offshore hubs and microgrids
gis1=[]; % substation: number, location;
    % hub = number, location;
    % microgrid = number, location;
    % turbines = number, location;

%%%%% gis1 stores in column 4, 5 and 6 the number of hubs and location
gis1 = [1  36.066694 -75.7006   1 36.191795 -75.438944;
    2  34.748318 -76.803354 2 34.622449 -76.207997   ];
%      3  34.225444 -77.828277 3 34.191408 -76.543872; eliminating NewBern
%       3  33.959798 -78.010995 3 33.539845, -77.955730]; % no speed data
%%%%% gis2 stores in column 1, 2 and 3 the number of hubs and location
%%%%% and in columns 4, 5 and 6 the number of microgrids and location
gis2 = [1  36.066694 -75.7006   1 36.408817 -75.385789;
    1  36.066694 -75.7006   2 36.129606 -75.215667;
    1  36.066694 -75.7006   3 35.770395 -75.085544;
    2  34.748318 -76.803354 1 35.248312   -75.242194;
    2  34.748318 -76.803354 2 35.04426     -75.446246;
    2  34.748318 -76.803354 3 34.840208   -75.650298;
    2  34.748318 -76.803354 4 34.636156   -75.85435;
    2  34.748318 -76.803354 5 34.479531   -76.016005;
    2  34.748318 -76.803354 6 34.275479   -76.225204];


% hub microgrid turbines
%%%%%%%%%%%%%%%%%%%%%%%%%%%%%%%%%%%%%%%%%%%%%%%%%%%%%%%%%%%%%%%%%%% hub = 1
gis_Lat = [];
gis_Lon = [];
%%%%%%%%%%%%%%%%%%%%%%%%%%%%%%%%%%%%%%%%%%%%%%%%%%%%%%%%%%%%%%%%%%
% Hub 1  has 3 microgrids
Lat_1m1=36.488817 -0.1;
Lon_1m1=-75.345789 + 0.2;   % shifting 0.1 degrees
Lat_1m5=35.770395 -0.1;
Lon_1m5=-75.085544 + 0.2;   % shifting 0.1 degrees
Lat_m=[];
Lon_m=[];
```

```
spacing = 0.09;         % in longitude spacing between turbines ( = 1 km )
spacingLat=(Lat_1m1 - Lat_1m5)/(9*3);  % hub1: 3 micrgrids within latitude range
spacingLon=(Lon_1m1 - Lon_1m5)/(10*3);
for lin=1:10*3              % in latitude (3 micrgrids within range)
   for col=1:9              % in longitude (9 turbines in same latitude)
      gis_Lat(lin,col+2) = Lat_1m1 - spacingLat*(lin-1);
      gis_Lon(lin,col+2) = Lon_1m1 + spacing*(col-1) - spacingLon*(lin-1) ;
   end
gis_Lat(lin,1)=1;
gis_Lon(lin,1)=1;
if (lin < 11)
   gis_Lat(lin,2)=1;
   gis_Lon(lin,2)=1;
end
if (lin >= 10)&(lin<20)
   gis_Lat(lin,2)=2;
   gis_Lon(lin,2)=2;
end
if (lin >= 20)&(lin<31)
   gis_Lat(lin,2)=3;
   gis_Lon(lin,2)=3;
end
end
gis_Lat;
gis_Lon
[m1,n1]=size(gis_Lat)
%%%%%%%%%%%%%%%%%%%%%%%%%%%%%%%%%%%%%%%%%%%%%%%%%%%%%%%%%%%%%%%%%%%%%%%%%%%%%%%%%%%%%%%%%%%%%%%%%%%%%%%%
%%%%%%%%%%%%%%%%%%%%%%%%%%%% hub = 2
% Hub 2  has 6 micrgrids
gis_2Lat = [];
gis_2Lon = [];
Lat_2m1=35.023462 + 0.2 + 0.2;
Lon_2m1=-75.493303 + 0.2 + 0.2 + 0.2 + 0.2 + 0.1;   % shifting 0.1 degrees
Lat_2m5=34.005069 + 0.2 + 0.2;
Lon_2m5=-76.629577 + 0.2 + 0.2 + 0.2 + 0.2 + 0.1;   % shifting 0.1 degrees

Lat_m=[];
Lon_m=[];
spacing = 0.09;         % in longitude spacing between turbines ( = 1 km )
spacingLat=(Lat_2m1 - Lat_2m5)/(9*6);  % hub2: 6 micrgrids within latitude range
spacingLon=(Lon_2m1 - Lon_2m5)/(10*6);
for lin=1:10*6              % in latitude (6 micrgrids within range)
   for col=1:9              % in longitude (9 turbines in same latitude)
      %gis_2Lat(lin,col+2) = Lat_2m1 - spacingLat*(lin-1);
      %gis_2Lon(lin,col+2) = Lon_2m1 + spacing*(col-1) - spacingLon*(lin-1) ;
      gis_2Lat(lin,col+2) = Lat_2m1 - spacingLat*(lin-1);
      gis_2Lon(lin,col+2) = Lon_2m1 + spacing*(col-1) - spacingLon*(lin-1) ;


   end
gis_Lat(lin,1)=1;
gis_Lon(lin,1)=1;
if (lin < 11)
   gis_2Lat(lin,2)=1;
   gis_2Lon(lin,2)=1;
end
```

```
if (lin >= 10)&(lin<20)
   gis_2Lat(lin,2)=2;
   gis_2Lon(lin,2)=2;
end
if (lin >= 20)&(lin<31)
   gis_2Lat(lin,2)=3;
   gis_2Lon(lin,2)=3;
end
if (lin >= 30)&(lin<41)
   gis_2Lat(lin,2)=4;
   gis_2Lon(lin,2)=4;
end
if (lin >= 40)&(lin<51)
   gis_2Lat(lin,2)=5;
   gis_2Lon(lin,2)=5;
end
if (lin >= 50)&(lin<61)
   gis_2Lat(lin,2)=6;
   gis_2Lon(lin,2)=6;
end
end
gis_2Lat
gis_2Lon
[m2,n2]=size(gis_2Lat)
%%%%%%%%%%%%%%%%%%%%%%%%%%%%%%%%%%%%%%%%%%%%%%%%%%%%%%%
%%%%%%%%%%%%%%%% hub = 3
%gis_3Lat = [];
%gis_3Lon = [];
% Hub 3  has 3 micrograms
%Lat_3m1=33.456317 + 0.2;
%Lon_3m1=-77.722631 + 0.2 + 0.2;   % shifting 0.1 degrees
%Lat_3m5=33.269779;
%Lon_3m5=-77.889654 + 0.2;   % shifting 0.1 degrees
%Lat_3m=[];
%Lon_3m=[];
%spacing = 0.09;         % in longitude spacing between turbines ( = 1 km )
%spacingLat=(Lat_3m1 - Lat_3m5)/(9*3);  % hub1: 3 microgrids within latitude range
%spacingLon=(Lon_3m1 - Lon_3m5)/(10*3);
%for lin=1:10*3               % in latitude (3 microgrids within range)
%    for col=1:9              % in longitude (9 turbines in same latitude)
%        gis_3Lat(lin,col+2) = Lat_3m1 - spacingLat*(lin-1);
%        gis_3Lon(lin,col+2) = Lon_3m1 + spacing*(col-1) - spacingLon*(lin-1) ;
%    end
%gis_3Lat(lin,1)=1;
%gis_3Lon(lin,1)=1;
%if (lin < 11)                % assignment of microgrid number
%    gis_3Lat(lin,2)=1;
%    gis_3Lon(lin,2)=1;
%end
%if (lin >= 10)&(lin<20)
%    gis_3Lat(lin,2)=2;
%    gis_3Lon(lin,2)=2;
%end
%if (lin >= 20)&(lin<31)
%    gis_3Lat(lin,2)=3;
%    gis_3Lon(lin,2)=3;
```

```
%end
%end
%gis_3Lat
%gis_3Lon
%[m3,n3]=size(gis_3Lat)

%% 2. OPEN, UPLOAD AND MANIPULATE DATA FROM RF RADAR  %%%%%%%%%%
T(:,6:7)=[];  % delete column 6 and 7 not need in the algorithm, to freed memory.
C1=T(:,1:4);
C1to4 = table2array(C1);
clear C1;
C1to4(:,3) = 0.01 *C1to4(:,3);  % to convert 1 cm to meters/s
C5=T(:,5);
C5table=C5;
C5= table2array(C5);

C5arraysplited=split(C5);
S=size(C5arraysplited);
C5arraysplited=erase(C5arraysplited,"");
ano=(year(C5arraysplited(:,1)));
mes=(month(C5arraysplited(:,1)));
dia=(day(C5arraysplited(:,1)));
hora=(hour(C5arraysplited(:,2)))
Cadd = [ano mes dia hora];
Ctotal = [C1to4 Cadd];  %% Ctotal contains the wind speeds by lat and long
clear T;
clear C1to4;
clear Cadd;
clear ano; clear mes; clear dia; clear hora;

%%%%%%%%%%%%%%%%%%%%%%%%%%%%%%%%%%%%%%%%%%%%%%%%%%%%%
%%%%%%%%%%%%%%%%%%%%%%%%
%%%% 6.2. MODELING OF MHK TURBINE (Power versus tidal speed)
  clear x;
  clear y;
  x = [0, 0.4, 0.5, 0.7, 0.8, 0.9, 1.0, 1.1, 1.2, 1.3, 1.4, 1.5, 1.6,  1.7,  1.8,  2.3,  2.4,  2.5,  2.8,  2.9,  3.0,
3.001,3.002, 3.01,3.25, 3.5, 3.75, 4];
  y = [0,   0,  20,  70, 100, 150, 215, 275, 360, 460, 580, 720, 865, 1000, 1000, 1000, 1000, 1000, 1000,
1000, 1000,   0, 0,    0,   0,   0,   0, 0];
  y = y/1000;    % in [MW]
  %[ref] Vincent S. Neary, Mirko Previsic, Richard A. Jepsen,
  %     Michael J. Lawson, Yi-Hsiang Yu, Andrea E. Copping,
  %     Arnold A. Fontaine, Kathleen C. Hallett, Dianne K. Murray.
  %     SANDIA REPORT, SAND2014-9040, 2014,
  %     Methodology for Design and Economic
  %     Analysis of Marine Energy Conversion
  %     (MEC) Technologies,
  %     Ps.: (originally 2 rotors of 2 MW in each point coordinate)
  cs = pchip(x,y);

 Anok = 2020;
 Mesk = 09;
 Diak = 18;
 Horak = 22;
 ano=2017; mes=0; dia=0; hora=0;
 [m,n]=size(Ctotal);%% Ctotal contains the wind speeds by lat and long
```

```
%%%%%%%%%%%%%%%%%%%%%%%%%%%%%%%%%%%%%%%%%%%%%%%%%%%%%%%%%%%%
%%%%%%%%%%%%%%%%%%%%%%%%
% ITERATIONS START BE HERE

%%% 3. Start loop for calculation of sum of power profile of all hubs into the offshore backbone.
   Ctotal(:, 9)=0;
for hub=1:3
   if (hub == 1)    % track hub 1 only
      nmicro=3;
      for i=1:m1   % track all longitude of turbines of hub 1
         for j=3:n1    % track all latitude of turbines of hub 1
            % it start with 3 because 1 and 2 are index numbers for hub and microgrid
            LakMHKT = gis_Lat(i,j);
            LokMHKT = gis_Lon(i,j);
            %%% 6. Start loop for calculation of power profile of each MHK turbine
            %%%  6.1 FINDING THE SPEED (24h) FOR TURBINES (LakMHKT and LokMHKT)
            for ii=1:m           % m = total elements of Ctotal (all speed measurements)
               dist=sqrt((LakMHKT-Ctotal(ii,1))*(LakMHKT-Ctotal(ii,1))+(LokMHKT-
Ctotal(ii,2))*(LokMHKT-Ctotal(ii,2)));
               Ctotal(ii, 9)=dist;      %%% colum 9 store distance to turbine
            end
            c=min(Ctotal(:,9))          % c is the minimum distance
            [cvalue,cindex]= min(Ctotal(:,9));
            cindex=cindex
            Ctotal=sortrows(Ctotal,[7 8]);    %** hour ascending sort
            kk=0; % Time hour loop
            for iii=1:m     % m is the total rows of Ctotal
              if (Ctotal(iii,9)==c  &  Ctotal(iii,5)==Anok & Ctotal(iii,6)==Mesk & Ctotal(iii,7)==Diak &
Ctotal(iii,8)==kk);
                 kk=kk+1;
                 %c=min(Ctotal(:,9))          % c is the minimum distance
                 Cpoint(kk,:) = Ctotal(iii,:);  % Cpoint is the speed (24h) for minimum distance to turbine
                 Sp_kMHKT(i,j,kk)=Ctotal(iii,3);  % Matrix column 3 is speed [m/s]  *                    *
                 Power_kMHKT(i,j,kk)= ppval(cs,Sp_kMHKT(i,j,kk)); % Power of each MHKTurbine *
                 Time_kMHKT(i,j,kk)=Ctotal(iii,8);  % hour time for shortest distance c  *
                 Ctotal(iii,9)=99999;
              end
            end


            c=min(Ctotal(:,9))          % c is the minimum distance
            [cvalue,cindex]= min(Ctotal(:,9));
            cindex=cindex
            Ctotal=sortrows(Ctotal,[7 8]);    %** hour ascending sort
            kk=0; % Time hour loop
            for iii=1:m     % m is the total rows of Ctotal
              if (Ctotal(iii,9)==c  &  Ctotal(iii,5)==Anok & Ctotal(iii,6)==Mesk & Ctotal(iii,7)==Diak &
Ctotal(iii,8)==kk);
                 kk=kk+1;
                 if Sp_kMHKT(i,j,kk)==0
                    %c=min(Ctotal(:,9))          % c is the minimum distance
                    Cpoint(kk,:) = Ctotal(iii,:);  % Cpoint is the speed (24h) for minimum distance to turbine
```

```
                    Sp_kMHKT(i,j,kk)=Ctotal(iii,3);  % Matrix column 3 is speed [m/s]  *                    *
                    Power_kMHKT(i,j,kk)= ppval(cs,Sp_kMHKT(i,j,kk)); % Power of each MHKTurbine *
                    Time_kMHKT(i,j,kk)=Ctotal(iii,8);  % hour time for shortest distance c  *
                  end
                end
              end

              Cpoint=sortrows(Cpoint,8) %Cpoint is the speed (24h) for minimum distance to turbine  *
              [mm,nn]=size(Cpoint);
              %MLong=mode(Cpoint(:,1))
              %MLat=mode(Cpoint(:,2))

              %if mm ~= 24
              %   h = msgbox('24 hours NOT ok')
              %end

              %%% 6.3. FINDING THE POWER PROFILE FOR A TURBINE IN(LakMHKT and LokMHKT)
              %%%      BASED ON THE SPEED PROFILE Cpoint(:,3)    (24h period)
              power=ppval(cs,Cpoint(:,3));    %[p.u. value]
              Power = [];
              Power = power  %*Tpower;  % [MW], each turbine 2 MW
              %%% gis_Power is for Kity Hawk
              gis_Power(i,j,:)=Power;  % columns 1 and 2 are zeroed (j from 3 ...)
              gis_Time(i,j,:)=Cpoint(:,8);
              gis_Speed(i,j,:)=Cpoint(:,3);

            end % j loop of latitude of each turbine of hub1
          end % i loop of longitude of each turbine of hub1

        % filling missing measurements in space and time
            for i=1:m1   % track all longitude of turbines of hub 1
              for j=3:n1    % track all latitude of turbines of hub 1
                for kk=1:24
                  if Sp_kMHKT(i,j,kk)==0
                    Sp_kMHKT(i,j,kk)=mean2(nonzeros(Sp_kMHKT(:,:,kk)));   % Matrix column 3 is speed
[m/s]  *                  *
                    Power_kMHKT(i,j,kk)= ppval(cs,Sp_kMHKT(i,j,kk)); % Power of each MHKTurbine *
                    Time_kMHKT(i,j,kk) = mean2(nonzeros(Time_kMHKT(:,:,kk)));
                  end
                end
              end
            end
        Sp_kMHKT(i,j,kk)=Sp_kMHKT(i,j,kk)

        end % loop of hub1 only

          Ctotal(:, 9)=0;
          if (hub == 2)     % track hub 2 only
            nmicro=6;
            for i=1:m2   % track all turbines of hub 2
              for j=3:n2    % it start with 3 because 1 and 2 are index numbers for hub and microgrid
                LakMHKT = gis_2Lat(i,j);
                LokMHKT = gis_2Lon(i,j);
                %%% 6. Start loop for calculation of power profile of each MHK turbine
                %%%  6.1 FINDING THE SPEED (24h) FOR TURBINES (LakMHKT and LokMHKT)
                for ii=1:m
```

```
                    dist=sqrt((LakMHKT-Ctotal(ii,1))*(LakMHKT-Ctotal(ii,1))+(LokMHKT-
Ctotal(ii,2))*(LokMHKT-Ctotal(ii,2)));
                    Ctotal(ii, 9)=dist;      %%% colum 9 store distance to turbine
                  end
                  c=min(Ctotal(:,9))
                  kk=0
                  for iii=1:m
                    if (Ctotal(iii,9)==c   &   Ctotal(iii,5)==Anok & Ctotal(iii,6)==Mesk & Ctotal(iii,7)==Diak &
Ctotal(iii,8)==kk);
                    kk=kk+1;
                    Cpoint(kk,:) = Ctotal(iii,:);  % Cpoint is the speed (24h) for minimum distance to turbine
                    Sp_2kMHKT(i,j,kk)=Ctotal(iii,3);  % Matrix column 3 is speed [m/s]  *
                    Power_2kMHKT(i,j,kk)= ppval(cs,Sp_2kMHKT(i,j,kk)); % Power of each MHKTurbine *
                    Time_2kMHKT(i,j,kk)=Ctotal(iii,8);  % hour time for shortest distance c  *
                    Ctotal(iii,9)=99999;
                    end
                  end
                  c=min(Ctotal(:,9))
                  kk=0
                  for iii=1:m
                    if (Ctotal(iii,9)==c   &   Ctotal(iii,5)==Anok & Ctotal(iii,6)==Mesk & Ctotal(iii,7)==Diak &
Ctotal(iii,8)==kk);
                    kk=kk+1;
                     if Sp_2kMHKT(i,j,kk)==0
                      Cpoint(kk,:) = Ctotal(iii,:);  % Cpoint is the speed (24h) for minimum distance to turbine
                      Sp_2kMHKT(i,j,kk)=Ctotal(iii,3);  % Matrix column 3 is speed [m/s]  *
                      Power_2kMHKT(i,j,kk)= ppval(cs,Sp_2kMHKT(i,j,kk)); % Power of each MHKTurbine *
                      Time_2kMHKT(i,j,kk)=Ctotal(iii,8);  % hour time for shortest distance c  *
                     end
                    end
                  end
                  Cpoint=sortrows(Cpoint,8) %Cpoint is the speed (24h) for minimum distance to turbine
                  [mm,nn]=size(Cpoint);
                  %%% 6.3. FINDING THE POWER PROFILE FOR A TURBINE IN(LakMHKT and LokMHKT)
                  %%%     BASED ON THE SPEED PROFILE Cpoint(:,3)    (24h period)
                  power=ppval(cs,Cpoint(:,3));    %[p.u. value]
                  Power = [];
                  Power = power  %*Tpower;  % [MW], each turbine 2 MW
                  %%% gis_Power is for Morehead
                  gis_2Power(i,j,:)=Power;  % columns 1 and 2 are zeroed (j from 3 ...)
                  gis_2Time(i,j,:)=Cpoint(:,8);
                  %gis_2Speed(i,j,:)=Cpoint(:,3);
                end % loop of latitude of each turbine of hub2
              end % loop of longitude of each turbine of hub2

            % filling missing measurements in space and time
              for i=1:m2   % track all longitude of turbines of hub 1
                for j=3:n2    % track all latitude of turbines of hub 1
                  for kk=1:24
                    if Sp_2kMHKT(i,j,kk)==0
                      Sp_2kMHKT(i,j,kk)=mean2(nonzeros(Sp_2kMHKT(:,:,kk)));  % Matrix column 3 is speed
[m/s]  *                 *
                      Power_2kMHKT(i,j,kk)= ppval(cs,Sp_2kMHKT(i,j,kk)); % Power of each MHKTurbine *
                      Time_2kMHKT(i,j,kk) = mean2(nonzeros(Time_2kMHKT(:,:,kk)));
                    end
                  end
```

```
            end
          end
          Sp_2kMHKT(i,j,kk)=Sp_2kMHKT(i,j,kk)
          Power_2kMHKT(i,j,kk)= Power_2kMHKT(i,j,kk)
      end % loop of hub2 only
          Ctotal(:, 9)=0;
%     if (hub == 3)
%       nmicro=3;
%       for i=1:m3   % hub 3 = Brunswick (Duke)
%           for j=3:n3    % it start with 3 because 1 and 2 are index numbers for hub and microgrid
%           LakMHKT = gis_3Lat(i,j);
%           LokMHKT = gis_3Lon(i,j);
            %%% 6. Start loop for calculation of power profile of each MHK turbine
            %%%  6.1 FINDING THE SPEED (24h) FOR TURBINES (LakMHKT and LokMHKT)
%           for ii=1:m    %Não seria LakMHT(i,j)?
%                                   dist=sqrt((LakMHKT-Ctotal(ii,1))*(LakMHKT-Ctotal(ii,1))+(LokMHKT-
Ctotal(ii,2))*(LokMHKT-Ctotal(ii,2)));
%             Ctotal(ii, 9)=dist;      %%% colum 9 store distance to turbine
%           end
%           c=min(Ctotal(:,9))
%           kk=0
%           for iii=1:m
%             if (Ctotal(iii,9)==c  &  Ctotal(iii,5)==Anok & Ctotal(iii,6)==Mesk & Ctotal(iii,7)==Diak);
%             kk=kk+1;
%             Cpoint(kk,:) = Ctotal(iii,:);  % Cpoint is the speed (24h) for minimum distance to turbine
%             Sp_3kMHKT(i,j,kk)=Ctotal(iii,3);  % Matrix column 3 is speed [m/s]  *                    *
%             Power_3kMHKT(i,j,kk)= ppval(cs,Sp_3kMHKT(i,j,kk)); % Power of each MHKTurbine *
%             Time_3kMHKT(i,j,kk)=Ctotal(iii,8);  % hour time for shortest distance c  *
%             end
%           end
%           Cpoint=sortrows(Cpoint,8) %Cpoint is the speed (24h) for minimum distance to turbine
%           [mm,nn]=size(Cpoint);
%           %%% 6.3. FINDING THE POWER PROFILE FOR A TURBINE IN(LakMHKT and LokMHKT)
%             %%%     BASED ON THE SPEED PROFILE Cpoint(:,3)    (24h period)
%           power=ppval(cs,Cpoint(:,3));    %[p.u. value]
%           Power = [];
%           Power = power  %*Tpower;  % [MW], each turbine 2 MW
            %%% gis_Power is for Brunswick (Duke)
%           gis_3Power(i,j,:)=Power;  % columns 1 and 2 are zeroed (j from 3 ...)

%         end % loop of latitude of each turbine of hub3
%       end % loop of longitude of each turbine of hub3
%   end % loop of hub3 only

end;
%%%  4. Start loop for calculation of power profile of microgrids agregated by each hub

%%%     for micro=1:nmicro

%%%    5. Start loop for calculation of power profile of MHK turbines agregated for each microgrid
%%%      for turbine=1:10*9   % each micro with 10 rows and 9 columns of MHK



  %%% 7. Calculate and store the power profile of MHK turbines agregated for each microgrid
```

```
 %%% 8. Calculate and store the power profile of microgrids agregated by each hub
 %%% end % of for
%gis_Power(:,:,:);   %%% 3D=[longitude rows, latitude columns, time]


%%% 9. Calculate and store the sum of power profile of all hubs into the offshore backbone.
%%% end % of for



%%%%%%%%%%%%%%%%%%%%%%%%%%%%%%%%%%%%%%%%%%%%%%%%%%%%%%%%%%%%%%%%%%%%%%%%%%%%%%%%%%%%%%%%%%%%%%%%%%%%%%%
%%%% 10.1 PLOT MHK TURBINE CURVE (Power versus tidal speed)
figure();
[m,n]=size(y);
%%% Ploting the curve of MHK turbine (speed [m/s] versus Power [MW])
clear xq1;
clear power;
Tpower=2;   % 2 [MW] according to
xq1 = 0:0.1:4; %mm;
plot(x,y,'ks',xq1,ppval(cs,xq1),'-k','linewidth',2);   % plot once outside iteration in black (k)
xlabel(''water speed [m/s]'','fontname','times','linewidth',2,'FontSize', 16);
ylabel(''MHK turbine electrical power [p.u.]'','fontname','times','linewidth',2,'FontSize', 16);
grid on
grid minor

%%%%%%%%%%%%%%%%%%%%%%%%%%%%%%%%%%%%%%%%%%%%%%%%%%%%%%%%%%%%%%%%%%%%%%%%%%%%%%%%%%%%%%%%%%%%%%%%%%%%%%%

%%%%%%%%%%%%%%%%%%%%%%%%%%%%%%%%%%%%%%%%%%%%%%%%%%%%%%%%%%%%%%%%%%%%%%%%%%%%%%%%%%%%%%%%%%%%%%%%%%%%%%%%%%%%%%%%
%%%% 10.2 Plot over the map of North Carolina Coast, the location of
%%%%    substations, hubs, microgrids, and MHK turbines
%%%%    Map of USA East Coast - Cape Hatteras - North Carolina
  figure
  title('USA East Coast, North Carolina - Cape Hatteras')
  %ax = usamap({'NC','RI'});
  %ax = usamap({'NC','VA'});
  ax = usamap({'NC'});
  set(ax, 'Visible', 'off')
  latlim = getm(ax, 'MapLatLimit');
  lonlim = getm(ax, 'MapLonLimit');
  %lonlim = [-80 -70]
  states = shaperead('usastatehi',...
        'UseGeoCoords', true, 'BoundingBox', [lonlim', latlim']);
  geoshow(ax, states, 'FaceColor', [0.5 0.5 1])

  lat = [states.LabelLat];
  lon = [states.LabelLon];
  tf = ingeoquad(lat, lon, latlim, lonlim);
  textm(35.825853, -77.8,'North Carolina','fontname','times','FontSize', 14)
  textm(35.5,-77,'Cape Hatteras','fontname','times','FontSize', 12)
  %textm(34.1,    -76.225204,'microgrid','fontname','times','FontSize', 12);
```

```
textm(34.1,       -76.85,'microgrid','fontname','times','FontSize', 12,'Color', 'r');
textm(34.1,       -75.8,'MHK turbines','fontname','times','FontSize', 12,'Color', 'b');
% textm(LakMHKT,LokMHKT,'x MHK','HorizontalAlignment','left','VerticalAlignment','middle','Color',
'r')


% Plot hub platforms in the map
for i=1:2 % 3         % no speed data in hub 3
   textm(gis1(i,5),gis1(i,6),'h','HorizontalAlignment','right','VerticalAlignment','middle','Color', 'r')
end

% Plot microgrid platforms in the map
for i=1:9 % 12         % no speed data in hub 3
   textm(gis2(i,5),gis2(i,6),'m','HorizontalAlignment','right','VerticalAlignment','middle','Color', 'r')
end

% Plot RF radar speed measurement points in the map
[n,m]=size(Ctotal);
 for ii=1:n
    if Ctotal(ii,3)>0.4
       textm(Ctotal(ii,1),                                                                    Ctotal(ii,2),
'.','HorizontalAlignment','center','VerticalAlignment','middle','Color','y');
    end
    if  Ctotal(ii,3)<=0.4
       textm(Ctotal(ii,1),                                                                    Ctotal(ii,2),
'.','HorizontalAlignment','center','VerticalAlignment','middle','Color','c');
    end
 end


% Plot substations and areas of shallow waters in the map
%Kitty Hawk (PJM)
LatSub=36.066694;
LonSub=-75.7006;
textm(LatSub,LonSub,'Hub1          o','HorizontalAlignment','right','VerticalAlignment','middle','Color',
'k','fontname','times','FontSize', 13);
LatCluster=36.495252;
LonCluster=-75.717171;
textm(LatCluster,LonCluster,'.','HorizontalAlignment','right','VerticalAlignment','middle','Color', 'r')
LatCluster=36.488817;
LonCluster=-75.345789;
textm(LatCluster,LonCluster,'.','HorizontalAlignment','right','VerticalAlignment','middle','Color', 'r')
LatCluster=35.770395;
LonCluster=-75.085544;
textm(LatCluster,LonCluster,'.','HorizontalAlignment','right','VerticalAlignment','middle','Color', 'r')
LatCluster=35.754636;
LonCluster=-75.277815;
textm(LatCluster,LonCluster,'.','HorizontalAlignment','right','VerticalAlignment','middle','Color', 'r')
LatCluster=35.877476;
LonCluster=-75.334136;
textm(LatCluster,LonCluster,'.','HorizontalAlignment','right','VerticalAlignment','middle','Color', 'r')
LatCluster=35.921332;
LonCluster=-75.252759;
textm(LatCluster,LonCluster,'.','HorizontalAlignment','right','VerticalAlignment','middle','Color', 'r')
LatCluster=36.095911;
LonCluster=-75.380747;
```

```
textm(LatCluster,LonCluster,'.','HorizontalAlignment','right','VerticalAlignment','middle','Color', 'r')
LatCluster=36.004839;
LonCluster=-75.491449;
textm(LatCluster,LonCluster,'.','HorizontalAlignment','right','VerticalAlignment','middle','Color', 'r')

% Plot the MHK turbines in the map
for i=1:m1
   for j=3:n1    % it start with 3 because 1 and 2 are index numbers for hub and microgrid
      textm(gis_Lat(i,j),gis_Lon(i,j),'.','HorizontalAlignment','right','VerticalAlignment','middle','Color',
'b')
   end
end

%New Bern (Duke)
%LatSub=35.1413;
%LonSub=-77.1235;
%textm(LatSub,LonSub,'s2 (< 5GW) o','HorizontalAlignment','right','VerticalAlignment','middle','Color',
'r')

LatCluster=35.088664;
LonCluster=-75.688311;
textm(LatCluster,LonCluster,'.','HorizontalAlignment','right','VerticalAlignment','middle','Color', 'r')
LatCluster=35.023462;
LonCluster=-75.493303;
textm(LatCluster,LonCluster,'.','HorizontalAlignment','right','VerticalAlignment','middle','Color', 'r')
LatCluster=34.751881;
LonCluster=-75.746240;
textm(LatCluster,LonCluster,'.','HorizontalAlignment','right','VerticalAlignment','middle','Color', 'r')
LatCluster=34.911128;
LonCluster=-75.991056;
textm(LatCluster,LonCluster,'.','HorizontalAlignment','right','VerticalAlignment','middle','Color', 'r')

%Morehead (Duke)
LatSub=34.748318;
LonSub=-76.803354;
%LatSub= 35.1467;
%LonSub=-76.8397;
textm(LatSub,LonSub,'Hub2       o       ','HorizontalAlignment','right','VerticalAlignment','middle','Color',
'k','fontname','times','FontSize', 13)


LatCluster=34.393527;
LonCluster=-76.138750;
textm(LatCluster,LonCluster,'.','HorizontalAlignment','right','VerticalAlignment','middle','Color', 'r')
textm(LatCluster,LonCluster,'.','HorizontalAlignment','right','VerticalAlignment','middle','Color', 'r')
LatCluster=34.536190;
LonCluster=-76.372210;
textm(LatCluster,LonCluster,'.','HorizontalAlignment','right','VerticalAlignment','middle','Color', 'r')


LatCluster=34.307040;
LonCluster=-76.370903;
textm(LatCluster,LonCluster,'.','HorizontalAlignment','right','VerticalAlignment','middle','Color', 'r')
LatCluster=34.163834;
LonCluster=-76.255423;
textm(LatCluster,LonCluster,'.','HorizontalAlignment','right','VerticalAlignment','middle','Color', 'r')
```

```
            LatCluster=34.005069;
            LonCluster=-76.629577;
            textm(LatCluster,LonCluster,'.','HorizontalAlignment','right','VerticalAlignment','middle','Color', 'r')
            LatCluster=34.341373;
            LonCluster=-76.715032 ;
            textm(LatCluster,LonCluster,'.','HorizontalAlignment','right','VerticalAlignment','middle','Color', 'r')    ,
            for i=1:m2            % Plot the MHK turbines in the map
               for j=3:n2
                  textm(gis_2Lat(i,j),gis_2Lon(i,j),'.','HorizontalAlignment','right','VerticalAlignment','middle','Color',
'b')
               end
            end


          %textm(Lat_2m1,Lon_2m1,'2m1','HorizontalAlignment','right','VerticalAlignment','middle','Color', 'r')
          %textm(Lat_2m5,Lon_2m5,'2m5','HorizontalAlignment','right','VerticalAlignment','middle','Color', 'r')


            %Wrightsville (Duke)
            %LatSub=34.225444;
            %LonSub=-77.828277;
            %textm(LatSub,LonSub,'s3 o','HorizontalAlignment','right','VerticalAlignment','middle','Color', 'r')

            %Brunswick (Duke)
            LatSub=33.959798;
            LonSub=-78.010995;
            textm(LatSub,LonSub,'Hub3              o','HorizontalAlignment','right','VerticalAlignment','middle','Color',
'k','fontname','times','FontSize', 13)

            LatCluster= 33.663471;
            LonCluster=-77.967339;
            textm(LatCluster,LonCluster,'.','HorizontalAlignment','right','VerticalAlignment','middle','Color', 'r')
            LatCluster= 33.456317;
            LonCluster=-77.722631;
            textm(LatCluster,LonCluster,'.','HorizontalAlignment','right','VerticalAlignment','middle','Color', 'r')
            LatCluster= 33.269779;
            LonCluster=-77.889654;
            textm(LatCluster,LonCluster,'.','HorizontalAlignment','right','VerticalAlignment','middle','Color', 'r')
            LatCluster= 33.453076;
            LonCluster=-78.085809;
            textm(LatCluster,LonCluster,'.','HorizontalAlignment','right','VerticalAlignment','middle','Color', 'r')

            % Plot the MHK turbines in the map
          %  for i=1:m3
          %     for j=3:n3
          %       textm(gis_3Lat(i,j),gis_3Lon(i,j),'.','HorizontalAlignment','right','VerticalAlignment','middle','Color',
'b')
          %     end
          %  end

          % 11. Plot the rectangle of the maximum lat and long of measurements
            LaMax=max(Ctotal(:,1)); % to draw rectangle limits of measurements
            LaMin=min(Ctotal(:,1));
            LoMax=max(Ctotal(:,2));
            LoMin=min(Ctotal(:,2));
            delta = 0.001;
```

```
textm(LaMax, LoMax, '.','HorizontalAlignment','center','VerticalAlignment','middle');
textm(((LaMax+LaMin)/2), LoMax, '.');
textm(LaMin, LoMax, '.','HorizontalAlignment','center','VerticalAlignment','middle');
textm(LaMax, ((LoMax+LoMin)/2),'.');
textm(LaMax, LoMin, '.','HorizontalAlignment','center','VerticalAlignment','middle');
textm(((LaMax+LaMin)/2), LoMin, '.');
textm(LaMin, LoMin, '.','HorizontalAlignment','center','VerticalAlignment','middle');
textm(LaMin, ((LoMax+LoMin)/2),'.');

%%%%%%%%%%%%%%%%%%%%%%%%%%%%%%%%%%%%%%%%%%%%%%%%%%%%%%%%%%%%%%%%%%%%%%%%%%%%%%%%%%%%%%%%%%%%%%%%%%%%%%%%%
%%% 12. Plot the power profile of MHK turbines
  % for ti=Cpoint(:,8)                  % 1:mm  (hour time)
  %       Cpoint(:,9)=Tpower*ppval(cs,ti); % column 9 is power [MW]
  % end
  % Cpoint;

hub=1;
  %%% Agregate power profile by hub
 if hub==1
   [m,n,p]=size(Sp_kMHKT)

   Sp_kMHKT=Sp_kMHKT;
   Power_kMHKT=Power_kMHKT;
   Time_kMHKT= Time_kMHKT;
   for kk=1:p   % p = 24 hours
     meanSp(kk)=mean2(nonzeros(Sp_kMHKT(:,:,kk)));   % mean speed profile in hub1=  *
     sumPower_kMHKT(kk)=sum(sum((Power_kMHKT(:,:,kk))));   % sum of power profile in hub1 *
     %sumPower_kMHKT(kk)=sum(Power_kMHKT(:,:,kk));
     %time_kMHKT(kk)=mean2(nonzeros(Time_kMHKT(:,:,kk))); % hour time for shortest distance c
     if kk==1
        time_kMHKT(kk)=mode(mode(Time_kMHKT(:,:,kk))); % hour time for shortest distance c
     else
        time_kMHKT(kk)=mode(mode(nonzeros(Time_kMHKT(:,:,kk)))); % hour time for shortest distance
c
     end
   end


   %hub1_result=[meanSp sumPower_kMHKT time_kMHKT];
   %hub1_result=sortrows(hub1_result,3);
   %meanSp(:,1) = hub1_result(:,1);
   %sumPower_kMHKT(:,1) = hub1_result(:,2);
   %time_kMHKT(:,1)= hub1_result(:,3);

  [im,jm,km]=size(gis_Power)
  Paux=gis_Power;         %% gis_Power is for Kitty Hawk
                  %%% Paux is 3D matrix
  %%% [MHK rows in hub, 9 turbines in same latitude, 24h time]
  aux=sum(Paux,2);        %% group power by row
                  %%% 2D [MHK rows in hub, 24h time]
  aux=sum(aux,1);  %% [sum power of all rows (hub), time]= Power profile
  [s,t]=size(aux);
  Power=aux(:);
```

```
            %Power = gis_Power(:,10,:);   %%% sum of all microgrid in hub 1
            GEN_power=Power;
            GEN_time=Cpoint(:,8) % gis_Time(i,j,:)? valid only for same day!!! different day does not work!

           [mt,nt]=size(GEN_power)
           Anokstr = num2str(Anok);
           Meskstr = num2str(Mesk);
           Diakstr = num2str(Diak);
           %fig_Title=strcat('MHK power assessment in',{' '},Diakstr,'/',Meskstr,'/',Anokstr);
           figure();
           subplot(4,1,1)
           %subplot(2,1,1)
           %plot(GEN_time,GEN_power);
           plot(time_kMHKT(:),sumPower_kMHKT(:));       %* hub1 Power profile
           grid on
           set(gca,'FontSize',8)
           axh=gca;
           set (axh, 'GridLineStyle','-');
           grid minor;
           title('(a) Power profile [MW] of hub-1 vs time [h]','FontName', 'Times','fontsize',9)
           %xlabel('time [hour]')

           subplot(4,1,2)
           %subplot(2,1,2)
           %plot(GEN_time,Cpoint(:,3));
           plot(time_kMHKT(:),meanSp(:));               %* hub1 Speed profile
           grid on
           set(gca,'FontSize',8)
           axh=gca;
           set (axh, 'GridLineStyle','-');
           grid minor;
           title('(b) Seawater mean speed [m/s] vs time [h]','FontName', 'Times','fontsize',9)
           %xlabel('time [hour]')

           %suptitle(fig_Title);
         end

         hub=2;
         if hub==2
            [m,n,p]=size(Sp_2kMHKT)
            for kk=1:p
              mean2Sp(kk)=mean2(nonzeros(Sp_2kMHKT(:,:,kk)));   % mean speed profile in hub1  *
              %sumPower_2kMHKT(kk)=sum(sum((Power_2kMHKT(:,:,kk))));   % mean power profile in hub1 *
              sumPower_2kMHKT(kk)=sum(sum(Power_2kMHKT(:,:,kk)));   % mean power profile in hub1 *

              %if Time_2kMHKT(:,:,kk)==0
              %    Time_2kMHKT(:,:,kk)=0.0000000001;
              %end
              %time_2kMHKT(kk)=mean2(nonzeros(Time_2kMHKT(:,:,kk))); % hour time for shortest distance c
              if kk==1
                 time_2kMHKT(kk)=mode(mode(Time_2kMHKT(:,:,kk))); % hour time for shortest distance c
              else
                 time_2kMHKT(kk)=mode(mode(nonzeros(Time_2kMHKT(:,:,kk))));  % hour time for shortest
distance c
              end
            end
```

```
 %hub2_result=[mean2Sp sumPower_2kMHKT time_2kMHKT];
 %hub2_result=sortrows(hub2_result,3);
 %mean2Sp(:,1) = hub2_result(:,1);
 %sumPower_2kMHKT(:,1) = hub2_result(:,2);
 %time_2kMHKT(:,1)= hub2_result(:,3);

 [im,jm,km]=size(gis_2Power)
Paux=gis_2Power;          %% gis_Power is for Morehead
                    %%% Paux is 3D matrix
%%% [MHK rows in hub, 9 turbines in same latitude, 24h time]
aux=sum(Paux,2);         %% group power by row
                     %%% 2D [MHK rows in hub, 24h time]
aux=sum(aux,1);  %% [sum power of all rows (hub), time]= Power profile
[s,t]=size(aux);
Power=aux(:)


 %Power = gis_Power(:,10,:);   %%% sum of all microgrid in hub 1
 GEN_power=Power;
 GEN_time=Cpoint(:,8) % gis_Time(i,j,:)? valid only for same day!!! different day does not work!

[mt,nt]=size(GEN_power)
Anokstr = num2str(Anok);
Meskstr = num2str(Mesk);
Diakstr = num2str(Diak);
%fig_Title=strcat('MHK power assessment in',{' '},Diakstr,'/',Meskstr,'/',Anokstr);

subplot(4,1,3)
%figure();
%subplot(2,1,1)
%plot(GEN_time,GEN_power);
plot(time_2kMHKT(:),sumPower_2kMHKT(:));       %* hub2 Power profile
grid on
set(gca,'FontSize',8)
axh=gca;
set (axh, 'GridLineStyle','-');
grid minor;
title('(c) Power profile [MW] of hub-2 vs time [h]','FontName', 'Times','fontsize',9)
%xlabel('time [hour]')

subplot(4,1,4)
%subplot(2,1,2)
%plot(GEN_time,Cpoint(:,3));
plot(time_2kMHKT(:),mean2Sp(:));                %* hub2 Speed profile
grid on
set(gca,'FontSize',8)
axh=gca;
set (axh, 'GridLineStyle','-');
grid minor;
title('(d) Seawater mean speed [m/s] vs time [h]','FontName', 'Times','fontsize',9)
%xlabel('time [hour]')

 %suptitle(fig_Title);
end

%hub=3;
```

```
%if hub==3
%    [m,n,p]=size(Sp_3kMHKT);
%    for kk=1:p
%      mean3Sp(kk)=mean2((Sp_3kMHKT(:,:,kk)));   % mean speed profile in hub1  *
%      sumPower_3kMHKT(kk)=sum(sum((Power_3kMHKT(:,:,kk))));   % mean power profile in hub1 *
     %if Time_3kMHKT(:,:,kk)==0
     %    Time_3kMHKT(:,:,kk)=0.0000000001;
     %end
%      time_3kMHKT(kk)=mean2(nonzeros(Time_3kMHKT(:,:,kk))); % hour time for shortest distance c
%    end
%    hub3_result=[mean3Sp sumPower_3kMHKT time_3kMHKT];
%    hub3_result=sortrows(hub3_result,3);
%    mean3Sp(:,1) = hub3_result(:,1);
%     sumPower_3kMHKT(:,1) = hub3_result(:,2);
%     time_3kMHKT(:,1)= hub3_result(:,3);

%     [im,jm,km]=size(gis_3Power)
%    Paux=gis_3Power          %% gis_3Power is for Brinckewich
                        %%% Paux is 3D matrix
   %%% [MHK rows in hub, 9 turbines in same latitude, 24h time]
%    aux=sum(Paux,2);         %% group power by row
                         %%% 2D [MHK rows in hub, 24h time]
%    aux=sum(aux,1);  %% [sum power of all rows (hub), time]= Power profile
%    [s,t]=size(aux);
%    Power=aux(:)


    %Power = gis_Power(:,10,:);   %%% sum of all microgrid in hub 1
%     GEN_power=Power;
%     GEN_time=Cpoint(:,8) % gis_Time(i,j,:)? valid only for same day!!! different day does not work!

%    [mt,nt]=size(GEN_power)
%    Anokstr = num2str(Anok);
%    Meskstr = num2str(Mesk);
%    Diakstr = num2str(Diak);
%    fig_Title=strcat('MHK power assessment in',{' '},Diakstr,'/',Meskstr,'/',Anokstr);
%    figure();

%    subplot(2,1,1)
   %plot(GEN_time,GEN_power);
%    plot(time_3kMHKT(:),sumPower_3kMHKT(:));       %* hub3 Power profile
%    grid on
%    axh=gca;
%    set (axh, 'GridLineStyle','-');
%    grid minor;
%    title('(a) Total MHK turbine power profile [MW] of hub-3')
%    xlabel('time [hour]')

%    subplot(2,1,2)
   %plot(GEN_time,Cpoint(:,3));
%    plot(time_3kMHKT(:),mean3Sp(:));               %* hub3 Speed profile
%    grid on
%    axh=gca;
%    set (axh, 'GridLineStyle','-');
%    grid minor;
%    title('(b) NOAA HF radar measurement of Gulf Stream surface water speed [m/s]')
```

```
%    xlabel('time [hour]')

%    suptitle(fig_Title);
% end

[m,n]=size(Ctotal);
```

APPENDIX B: MATLAB SCRIPT OF THE US-CARIBBEAN SG

```
%%%%%%%%%%%%%%%%%%%%%%%%%%%%%%%%%%%%%%%%%%%%%%%%%%%%%%%%%%%%%%%%%%%%%%%%%%%
%%%%%%%%%%%%%
%                                                    %
%    Rodney Itiki - PhD Dissertation Research Project (2023)       %
%    Hurricane modeling and U.S.-Caribbean Super Grid proposition    %
%%%%%%%%%%%%%%%%%%%%%%%%%%%%%%%%%%%%%%%%%%%%%%%%%%%%%%%%%%%%%%%%%%%%%%%%%%%
%%%%%%%%%%%%%
clc;
clear all;
close all;
feature('accel','on')
r= 6371008.8;   %[meters]
verbose = 1;
region = "USA"
%region = "Japan"
%alternative = 1;  % Hurricane/Typhoon modeling by fitting
alternative = 0;  % Hurricane/Typhoon modeling by Holland
%trajectoryType = "Straight";
trajectoryType = "Parabole";
if trajectoryType == "Parabole"
   alternative = 0;
   %set(0,"DefaultFigureVisible","off");  % Figuras invisíveis pois lento
end

    hurricaneCategory = 3;   %4 or 3;
    PR=[5 4 3;    % Michael (2018)      Charley (2004)       Wilma (2005)
        919 941 950;
        18.52 37.04 55.56;
        970 975 980;
        55.56 55.56 57.412];
    jp = 10;   % select the trajectory of hurricane from 1 to 10

turbineType = 'typical'; % select typical for cutout 25 m/s or 'special', 40 m/s

caso = 21;  % case 1  is Taiwan landfall,
         % case 2  is in Kyushu,
         % case 3  in Philippines,
         % case 4  interconnector and hitting TWN
         % case 5  interconnector and hitting JPN
         % case 6  interconnector and hitting PHP
         % case 7  spare
         % case 8  spare
         % case 9  spare
         % case 10 spare
         % case 20 is USA WITH interconnection to Caribbean Supergrid
         % case 21 is USA WITHOUT interconnection to Caribbean Supergrid
co = [   0,    0.4470,    0.7410;
   0.8500,    0.3250,    0.0980;
   0.9290,    0.6940,    0.1250;
   0.4940,    0.1840,    0.5560;
   0.0000,    0.0000,    0.0000;
   0.3010,    0.7450,    0.9330;
   0.6350,    0.0780,    0.1840;
        0,    0.5000,         0;
   0.7500,         0,    0.7500;
   0.2500,    0.2500,    0.2500];
   trajectColor=co(jp,:)
```

```
%%%%%%%%%%%%%%%%%%%%%%%%%%%%%%%%%%%%%%%%%%%%%%%%%%%%%%%%%%%%%%%%%%%%%
%%%%%%%%%%%%%
%                POPULATE TURBINES IN A MAP                  %
%  Populate Array of offshore wind turbines                  %
if region == "USA"
  % Coordinates in front of Cappe Hateras [35.159081, -75.359408]
  % Coordinates in from of Jacksonvile FL [30.303634, -80.710187]
  LaC=35.159081;
  LoC=-75.359408;
  LaD=30.303634;
  LoD=-80.710187;

                   % Array 2
  LaE= 41.439191;       % Rodhe Island
  LoE= -70.674311;
  LaF= 37.222078;       % Virginia
  LoF= -75.805868;

                  % Array 3
  LaG= 47.755556;       % Washington - (North)
  LoG= -124.680542;
  LaH= 34.611117;       % California - Morro Bay (South)
  LoH= -120.647408;

                  % Array 4
  LaI= 32.290339;       % Texas - North
  LoI= -100.417739;
  LaJ= 41.000219;       % Amami City Omaha - Amami Oshima island
  LoJ= -84.492314;

  %LaK=;   % Caribbean
  %LoK=;
  %LaL=;
  %LoL=;
%   n = 5;        % number of turbines in array in NC (ok)
%   n2= 15;        % Rodhe Island
%   n3= 11;        % California - Morro Bay (North)
%   n4= 5;        % Texas - North

end

if region == "Japan"   % Coordinates C:  Array
  if (caso == 1)     % Taiwan hit
  %LaC= 30.9958661; % Kyushu
  %LoC= 130.6457063;
  %LaD= 24.4656195; %Hatoma Island - Japan (close to Ishigaki Island)
  %LoD= 123.8001116;
                   % Array 1
  %LaC=  28.3316642;      % Kikajima JPN (Amani island)
  %LoC=   129.9210169;
  %LaD= 24.451915;        % Western point of JPN
  %LoD= 122.9320186;
  LaC=  28.3316642;      % Kikajima JPN (Amani island)(Joker)
  LoC=   129.9210169;
  LaD= 24.451915;        % Western point of JPN
  LoD= 122.9320186;

                   % Array 2 (Joker - just 1 turbine)
  LaE= 22.4284448;       % Green Island - South Taiwan
  LoE= 120.9759741;
  LaF= 9.467899;         % Palanan - Philippines
```

```
LoF= 126.533833;

                    % Array 3
LaG= 34.6062689;        % Iki Island SouthWest JPN  (Joker)
LoG= 129.701097;
LaH= 45.0316192;        % Hishiri Island Hokkaido JPN
LoH= 141.0141986;
                  % Array 4
LaI= 34.2781138;        % Tsushima JPN South West Island (Joker)
LoI= 129.3639537;
LaJ= 28.433371;        % Amami City Omaha - Amami Oshima island
LoJ= 129.456680;


n = 1;         % number of turbines in array
n2= 1;
n3= 1;
n4= 1;

end

if (caso == 2)    % Array
%LaC= 33.5768705;  % Wakayama - Honshu JPN
%LoC= 135.0501018;
%LaD= 24.4656195;
%LoD= 123.8001116;
                  % Array 1
LaC=  28.3316642;       % Kikajima JPN (Amani island)
LoC=   129.9210169;
LaD= 24.451915;         % Western point of JPN
LoD= 122.9320186;

                    % Array 2 (Joker - just 1 turbine)
LaE= 22.4284448;        % Green Island - South Taiwan
LoE= 120.9759741;
LaF= 9.467899;          % Palanan - Philippines
LoF= 126.533833;

                    % Array 3
LaG= 34.6062689;        % Iki Island SouthWest JPN
LoG= 129.701097;
LaH= 45.0316192;        % Hishiri Island Hokkaido JPN
LoH= 141.0141986;
                  % Array 4
LaI= 34.2781138;        % Tsushima JPN South West Island
LoI= 129.3639537;
LaJ= 28.433371;        % Amami City Omaha - Amami Oshima island
LoJ= 129.456680;


n = 14;         % number of turbines in array
n2= 1;
n3= 30;
n4= 14;


end

if (caso == 3)     % Array
%LaC= 10.9183955;   % Luzon - Philippines
%LoC= 122.6521798;
%LaD= 16.9969 ;       % Palanan - Philippines
```

```
%LoD= 122.4014;

%LaC= 22.4284448;        % Green Island - South Taiwan
%LoC= 120.9759741;
%LaD= 9.467899;          % Palanan - Philippines
%LoD= 126.533833;
                    % Array 1 (Joker - not turbine)
LaC=  28.3316642;       % Kikajima JPN (Amani island)
LoC=   129.9210169;
LaD= 24.451915;         % Western point of JPN
LoD= 122.9320186;

                    % Array 2
LaE= 22.4284448;        % Green Island - South Taiwan
LoE= 120.9759741;
LaF= 9.467899;          % Palanan - Philippines
LoF= 126.533833;

                  % Array 3 (Joker)
LaG= 34.6062689;        % Iki Island SouthWest JPN
LoG= 129.701097;
LaH= 45.0316192;        % Hishiri Island Hokkaido JPN
LoH= 141.0141986;
                  % Array 4  (Joker)
LaI= 34.2781138;        % Tsushima JPN South West Island
LoI= 129.3639537;
LaJ= 28.433371;         % Amami City Omaha - Amami Oshima island
LoJ= 129.456680;


n = 1;          % number of turbines in array
n2= 21;
n3= 1;
n4= 1;

end

if (caso == 4)      % Three Arrays
                  % Array 1
LaC=  28.3316642;       % Kikajima JPN (Amani island)
LoC=   129.9210169;
LaD= 24.451915;         % Western point of JPN
LoD= 122.9320186;
%LaC= 26.2070433;        % Okinawa JPN
%LoC=127.6426332;
%LaD= 8.2235979;         % Bislig - Philippines
%LoD= 126.1165143;       % 17.0208965,122.202
%LaD= 16.9969 ;          % Palanan - Philippines
%LoD= 122.4014;

                  % Array 2
LaE= 22.4284448;        % Green Island - South Taiwan
LoE= 120.9759741;
LaF= 9.467899;          % Palanan - Philippines
LoF= 126.533833;
                  % Array 3
LaG= 34.6062689;        % Iki Island SouthWest JPN
LoG= 129.701097;
LaH= 45.0316192;        % Hishiri Island Hokkaido JPN
LoH= 141.0141986;
                  % Array 4
LaI= 34.2781138;        % Tsushima JPN South West Island
```

```
  LoI= 129.3639537;
  LaJ= 28.433371;        % Amami City Omaha - Amami Oshima island
  LoJ= 129.456680;

  end
end

if region=="Japan"
  %n = 30;        % number of turbines in array

  if (caso == 4)     % Array
  n = 14;        % number of turbines in array
  n2= 21;
  n3= 30;
  n4= 14;
  end

end

if region=="USA"   % USA has just one case, n should be fixed %%%
%n = 10;        % number of turbines in array
    n = 5;        % number of turbines in array in NC
    n2= 5;        % Rodhe Island
    n3= 11;         % California - Morro Bay (North)
    n4= 5;         % Texas - North
    n5= 11;        % Caribbean Islands
end

%%%%%% Array 1 %%%%%%%%%%%%%%%%%%%%%%%%%%%%%%%%%%%%%%%%%%%%%
Tpower=10;   % each turbine array is 10 MW
% Angle between point C and D
deltaAngle = (distance(LaC,LoC,LaD,LoD));   %angle in [degree]
% Distribution of n turbines array between point C and D.
deltadeltaAngle = deltaAngle/n;
Turb_array=zeros(n, 3);
for k=1:n
deltaLa_k = k*(LaD-LaC)/n;  % [delta Latitude degree]
deltaLo_k = k*(LoD-LoC)/n;  % [delta Longitude degree]
LakT=LaC+deltaLa_k;    %Latitude of turbine
LokT=LoC+deltaLo_k;    %Longitude of turbine
Turb_array(k,1:3)=[LakT LokT Tpower];
labelLat = LakT;
labelLon = LokT;
end
Turb_array;     %OWF_table = [Lat Lon turbinePower]

%%%%%% Array 2 %%%%%%%%%%%%%%%%%%%%%%%%%%%%%%%%%%%%%%%%%%%%%
Tpower=10;   % each turbine array is 10 MW
% Angle between point E and F
deltaAngle = (distance(LaE,LoE,LaF,LoF)) ;  %angle in [degree]
% Distribution of n turbines array between point C and D.
deltadeltaAngle = deltaAngle/n2;
Turb_array2=zeros(n2, 3);
for k=1:n2
deltaLa_k = k*(LaF-LaE)/n2;  % [delta Latitude degree]
deltaLo_k = k*(LoF-LoE)/n2;  % [delta Longitude degree]
LakT=LaE+deltaLa_k;    %Latitude of turbine
LokT=LoE+deltaLo_k;    %Longitude of turbine
Turb_array2(k,1:3)=[LakT LokT Tpower];
labelLat = LakT;
labelLon = LokT;
end
```

```
Turb_array2;     %OWF_table = [Lat Lon turbinePower]

%%%%%% Array 3 %%%%%%%%%%%%%%%%%%%%%%%%%%%%%%%%%%%%%%%%%%%%%%%%
Tpower=10;    % each turbine array is 10 MW
% Angle between point E and F
deltaAngle = (distance(LaG,LoG,LaH,LoH))   %angle in [degree]
% Distribution of n turbines array between point C and D.
deltadeltaAngle = deltaAngle/n3;
Turb_array3=zeros(n3, 3);
for k=1:n3
deltaLa_k = k*(LaH-LaG)/n3;  % [delta Latitude degree]
deltaLo_k = k*(LoH-LoG)/n3;  % [delta Longitude degree]
LakT=LaG+deltaLa_k;    %Latitude of turbine
LokT=LoG+deltaLo_k;    %Longitude of turbine
Turb_array3(k,1:3)=[LakT LokT Tpower];
labelLat = LakT;
labelLon = LokT;
end
Turb_array3;     %OWF_table = [Lat Lon turbinePower]


%%%%%% Array 4 %%%%%%%%%%%%%%%%%%%%%%%%%%%%%%%%%%%%%%%%%%%%%%%%
Tpower=10;    % each turbine array is 10 MW
% Angle between point E and F
deltaAngle = (distance(LaI,LoI,LaJ,LoJ))   %angle in [degree]
% Distribution of n turbines array between point C and D.
deltadeltaAngle = deltaAngle/n4;
Turb_array4=zeros(n4, 3);
for k=1:n4
deltaLa_k = k*(LaJ-LaI)/n4;  % [delta Latitude degree]
deltaLo_k = k*(LoJ-LoI)/n4;  % [delta Longitude degree]
LakT=LaI+deltaLa_k;    %Latitude of turbine
LokT=LoI+deltaLo_k;    %Longitude of turbine
Turb_array4(k,1:3)=[LakT LokT Tpower];
labelLat = LakT;
labelLon = LokT;
end
Turb_array4;     %OWF_table = [Lat Lon turbinePower]

%%%%%% Array 5 %%%%%%%%%%%%%%%%%%%%%%%%%%%%%%%%%%%%%%%%%%%%%%%%
Tpower=10;    % each turbine array is 10 MW
Turb_array5(1,1:3)=[26.565417 -78.702523 Tpower];  %Bahamas
Turb_array5(2,1:3)=[22.511881 -78.638524 Tpower];  % Cuba North
Turb_array5(3,1:3)=[20.651904 -74.875190 Tpower];   % Cuba East
Turb_array5(4,1:3)=[19.759219 -72.158172 Tpower];  % Haiti
Turb_array5(5,1:3)=[18.369845 -69.254780 Tpower];  % Dominican Republic
Turb_array5(6,1:3)=[17.813980 -77.537822 Tpower];  % Jamaica
Turb_array5(7,1:3)=[18.467404 -66.231590 Tpower];  % Puerto Rico northeast
Turb_array5(8,1:3)=[18.509169 -67.128103 Tpower];   % Puerto Rico northwest
Turb_array5(9,1:3)=[18.385191 -64.745133 Tpower];  % British Virgin Island
Turb_array5(10,1:3)=[17.695063 -64.760318 Tpower]; % U.S. Virgin (Saint Croix)
Turb_array5;     %OWF_table = [Lat Lon turbinePower]



% Populate coordinates of Rectangle OWF.
if region == "USA"
  % Block Island close to Rhode Island [41.1894261,-71.6487164]
  %LaOWF=41.1894261;
  %LoOWF=-71.6487164;

  % Charleston, West Virginia
```

```
  LaOWF=38.3433652;          % origin of the rectangle
  LoOWF=-81.7839763;

  LaOWF_D = 30.888958;       % angular direction AJUSTAR PARA USA
  LoOWF_D = -100.963295;

  Dir_D= sqrt((LoOWF-LoOWF_D)*(LoOWF-LoOWF_D)+(LaOWF-LaOWF_D)*(LaOWF-LaOWF_D));

end

if region == "Japan"     % OWF.
  if caso == 1
  %LaOWF = 23.398352;    % Pengu Island, Taiwan
  %LoOWF= 119.680246;

  LaOWF =   23.078255;       % Pengu Island TWN
  LoOWF =   119.455503;
  LaOWF_D = 25.533403;       % angular direction
  LoOWF_D = 120.076722;
  Dir_D= sqrt((LoOWF-LoOWF_D)*(LoOWF-LoOWF_D)+(LaOWF-LaOWF_D)*(LaOWF-LaOWF_D));
  end
  if caso == 2
  LaOWF = 32.4278423;   % Goto island - Japan
  LoOWF = 128.4827148;  % close to Nagasaki
  end
  if caso == 3
  LaOWF = 20.2519165;    % Basco island - Phillipines
  LoOWF = 121.8214398;   % close to Luzon strait
  end
  if caso == 4
  LaOWF =   23.078255;       % Pengu Island TWN
  LoOWF =   119.455503;
  LaOWF_D = 25.533403;       % angular direction
  LoOWF_D = 120.076722;

  %LaOWF = 34.2781138;        %%Tsushima JPN West Island
  %LoOWF = 129.3639537;
  %LaOWF_D = 28.433371;       %% Amami City Omaha - Amami Oshima island
  %LoOWF_D = 129.456680;      %% angular direction
  Dir_D= sqrt((LoOWF-LoOWF_D)*(LoOWF-LoOWF_D)+(LaOWF-LaOWF_D)*(LaOWF-LaOWF_D));
  end
end

if region=="USA"
lines = 10;          % Turbo_rect (Midwest)
columns = 5;
end

if region=="Japan"
lines = 15;
columns = 1;
  if caso == 4 | caso == 1   % interconnector
  lines = 15;    % Pengu island - TW
  columns = 1;
  end
end

spacing = 500; % [m], linear spacing between turbines
Lo_delta=0;  % if not interconnector
La_delta=0;
spacing_angle = (360/(2*pi()*r))*spacing;
  if caso == 4  | caso == 1  % interconnector
```

```
    spacing = 0;
    Lo_delta=(LoOWF-LoOWF_D)/lines;
    La_delta=(LaOWF-LaOWF_D)/lines;
  end

if region=="USA"
spacing = 10;
    Lo_delta=(LoOWF-LoOWF_D)/columns;  %lines, not columns
    La_delta=(LaOWF-LaOWF_D)/lines;
end

LaT0=LaOWF;
LoT0=LoOWF;
Turb_rect =[0 0 Tpower];
for li=1 : lines
  for col=1:columns
  LaTi = LaT0 - li*spacing_angle-li*La_delta;
  LoTi = LoT0 - col*spacing_angle-li*Lo_delta;
  k=k+1;
  aux = [LaTi LoTi Tpower];
  Turb_rect=[Turb_rect; aux];
  end
end

if region=="USA"
   clear Turb_rect;
   %Turb_rect =[0 0 Tpower];
   LaT0=46;
   LoT0=-105;
   k=0;
   lincolum=6;
  for lin=0:lincolum
    for colu=0:lincolum
    LaTi = LaT0 - lin*2.8;
    LoTi = LoT0 + colu*3.2;
    auxUSA = [LaTi LoTi Tpower];
    k=k+1;
    %Turb_rect = [Turb_rect; auxUSA];
    Turb_rect(k,:)=auxUSA;
    end
  end
end

%       Group all turbines in an single matrix of size mt x nt            %
if region=="Japan"
  if caso == 1
    TurbTotal = [Turb_rect];
  end
  if caso == 2
    TurbTotal = [Turb_array; Turb_array3; Turb_array4];
  end
  if caso == 3
    TurbTotal = [Turb_array2];
  end
  if caso == 4 | caso == 5 | caso == 6
    TurbTotal = [Turb_array; Turb_array2; Turb_array3; Turb_array4;  Turb_rect];
  end
end

TurbTotal = [Turb_array5];
if region=="USA"
   if (caso == 20)  % WITH Caribbean Supergrid
```

```
    TurbTotal = [Turb_array; Turb_array2; Turb_array3; Turb_array4; Turb_array5; Turb_rect];
  end
  if (caso == 21)  % WITHOUT Caribbean Supergrid
    TurbTotal = [Turb_array5];
  end
  %if caso ~= 20 | caso ~= 21 % WITHOUT Caribbean Supergrid
  %   TurbTotal = [Turb_array; Turb_array2; Turb_array3; Turb_array4; Turb_array5; Turb_rect];
  %end
end

  [mtArray,ntArray]=size(Turb_array); % turbines in array are first
  [mtRect,ntRect]=size(Turb_rect); % turbines of OWF are in the end
  [mt,nt]=size(TurbTotal);          % TurbTotal has 3 columns
  mt_global=mt;
  clear Turb_array;
  clear Turb_array2;
  clear Turb_array3;
  clear Turb_array4;
  clear Turb_array5;
%               End of Turbine population                        %
%%%%%%%%%%%%%%%%%%%%%%%%%%%%%%%%%%%%%%%%%%%%%%%%%%%%%%%%%%%%%%%%%%%%%%%%
%%%%%%%%%%%%

%for jp=1:10

%%%%%%%%%%%%%%%%%%%%%%%%%%%%%%%%%%%%%%%%%%%%%%%%%%%%%%%%%%%%%%%%%%%%%%%%
%%%%%%%%%%%%
%          Minimum airspeed before hurricane landfall                 %
%                                                      %
for k=1:mt
     LakT = TurbTotal(k,1);
     LokT = TurbTotal(k,2);
     coast = load('coast.mat');
     TurbineIsInOnshore = inpolygon(LakT,LokT,coast.lat,coast.long);
       if (TurbineIsInOnshore ==1) & (region == "USA")  % USA
             VminOnshore = 5.5;           % assumption: minimum speed onshore
             TurbTotal(k,4)=VminOnshore;
       else
             VminOffshore = 8.51;
             TurbTotal(k,4)=VminOffshore;
       end
       if (LokT > -102) & (LokT < -95) && (LakT > 31)& (region == "USA")& (TurbineIsInOnshore ==1)  % USA
             VminOnshore = 8.5;
             TurbTotal(k,4)=VminOnshore;
       end
       if (region == "USA")& (TurbineIsInOnshore ==0) & (LakT > 32.5) %~= 1)
             VminOffshore = 8.51;  % 7;     % National Renewable Energy Lab
             TurbTotal(k,4)=VminOffshore;
       end
       if (region == "USA")& (TurbineIsInOnshore ==0) & (LakT < 32.51) %~= 1)
             VminOffshore = 7.01;  % 7;     % National Renewable Energy Lab
             TurbTotal(k,4)=VminOffshore;
       end
       if (region == "Japan")& (TurbineIsInOnshore ==1)  % Japan Onshore
             % Hsin-Fa Fang, Wind energy potential assessment for the
             % offshore areas of Taiwan west coast and Penghu Archipelago,
             % Renewable Energy, Volume 67, 2014,
             VminOnshore = 3.5;
             TurbTotal(k,4)=VminOffshore;
       end
       if (region == "Japan")& (TurbineIsInOnshore ==0)  % Japan Offshore
             VminOffshore = 9.5;   % Strait Taiwan/
```

```
            TurbTotal(k,4)=VminOffshore;
        end
end
  TurbTotal(:,4)=TurbTotal(:,4)
%           End of minimum airspeed before hurricane landfall        %
%%%%%%%%%%%%%%%%%%%%%%%%%%%%%%%%%%%%%%%%%%%%%%%%%%%%%%%%%%%%%%%%%%%
%%%%%%%%%%%%


%%%%%%%%%%%%%%%%%%%%%%%%%%%%%%%%%%%%%%%%%%%%%%%%%%%%%%%%%%%%%%%%%%%
%%%%%%%%%%%%
%%%%%%%%%%%%%%%%%%%%%%%%%%%%%%%%%%%%%%%%%%%%%%%%%%%%%%%%%%%%%%%%%%%
%%%%%%%%%%%%
%         Input of Hurricane trajectoryType: Straight or Parabole       %
%                                                           %
Vtr = 9.722; %8 m/s [28.8 km/h] - 9 m/s [32.4 km/h] 20m/s [72 km/h] = translational speed of hurricane eye
% 8 m/s Andrew , Vtr from 20 to 28 m/s over water of North Atlantic [49],
% 9.722 m/s Michael2018, 9.722 m/s Charley2004, 13.333m/s Wilma2005landfall
w = Vtr*360/(2*pi()*r)   %[degree/second] = angular speed of hurricane eye

if region == "USA" & trajectoryType == "Straight"
   % fprintf("Wait 5 minutes to calculate")
   % trajectoryType : Straight (points A and B on Earth)
   % Hurricane trajectory 1
   % LaA =  24.232543;    %Gulf of Mexico
   % LoA =  -90.082728;
   % LaB =   47.955969;    %Lake superior
   % LoB =  -88.399579;

   % Hurricane trajectory 2
   %   LaA =   21.802322;  %Cuba (Carebean)
   %   LoA =   -85.239624;
   %   LaB =   43.435968;  %Gulf of Maine
   %   LoB =   -66.781393;

   % Hurricane trajectory 3
   %  LaA =  29.869451;   %EastCoast
   %  LoA =  -72.461012;
   %  LaB =  36.667736;
   %  LoB =  -80.040129;

   % Hurricane trajectory 4
   %   LaA = 25;   % Point A: Puerto Rico/San Juan @18.5746314,-66.669562,8.67z
   %   LoA = -70;
      LaA =  13.679202;   % Hiting Puerto Rico
      LoA =  -60.495106;
      LaB =  38.678683;    %reaching Wichita KS
      LoB =  -100.100049;
   %   LaB = 41.8333908;  % Chicago
   %   LoB = -88.012854;
end

if region == "USA" & trajectoryType == "Parabole"
    Lat1=[8.87         9.451111111         10.03222222         10.61333333         11.19444444         11.77555556
            12.35666667          12.93777778          13.51888889          14.1];
    Long1 = [-53.34  -52.72333333         -52.10666667         -51.49     -50.87333333         -50.25666667         -49.64     -
49.02333333          -48.40666667         -47.79];
    Latmin=  [30          30  30   30          30           30           30           30           30           30  ];
    Longmin= [-95.5  -93.74    -91.98      -90.22      -88.46      -86.7       -84.94      -83.18      -81.42     -79.66 ];

    LaACircle=Lat1(jp);
    LoACircle=Long1(jp);
```

```
    LaA =  13.679202;   % Hiting Puerto Rico % just to bypass bug
    LoA =  -60.495106;
    LaB =  38.678683;    %reaching Wichita KS % just to bypass bug
    LoB =  -100.100049;
end

if region == "Japan"       % typhoon trajectory is assumed always Straight
  fprintf("Do not select any country, please.")
  fprintf("Just press CANCEL button in the Figure 1, and wait 5 minutes ...")
  if caso == 1
    LaA = 23; % Point A: Pacific Ocean
    LoA = 140;
    LaB = 25;  %Point B: Taiwan Strait (close to China Mainland)
    LoB = 120;
  end
  if caso == 2          % typhoon trajectory
    %LaA = 29.511689;   % Philippine Sea
    %LoA = 122.8939938;
    LaA = 15;
    LoA = 130;
    LaB =34.5442569;   % South Korea coast
    LoB = 127.4683968;
  end
  if caso == 3          % typhoon trajectory
    LaA = 5;           % Philippine Sea
    LoA = 135;
    LaB = 23.4801656;  % Pengu island - Taiwan
    LoB = 118.9587459;
  end
  if caso == 4          % typhoon trajectory
    LaA = 23; % Point A: Pacific Ocean
    LoA = 140;
    LaB = 25;  %Point B: Taiwan Strait (close to China Mainland)
    LoB = 120;
  end
end
%     End of input of Hurricane trajectoryType: Straight or Parabole    %
%%%%%%%%%%%%%%%%%%%%%%%%%%%%%%%%%%%%%%%%%%%%%%%%%%%%%%%%%%%%%%%%%%%%%%%
%%%%%%%%%%%

%%%%%%%%%%%%%%%%%%%%%%%%%%%%%%%%%%%%%%%%%%%%%%%%%%%%%%%%%%%%%%%%%%%%%%%
%%%%%%%%%%%
%     Just opening the Map of USA Straight, USA parabole and Japan      %
%                                                                       %
  deltaAngle = distance(LaB,LoB,LaA,LoA);  % distance command is in [degree]
  % Assuming w angular speed of hurricane, then:
  deltaTime=deltaAngle/w   ;                      % [s]
  % Distance between points in the Earth surface:
  arclen = (distance(LaB,LoB,LaA,LoA)); % distance command is in [degree]
  delta_d=deg2km(arclen)*1000;                     % distance [m]

if region == "USA" & trajectoryType == "Straight"
  % Map of USA East Coast
  figure(1)
  latlim= [6.54 46];   %[19.54 49.2];
  lonlim= [-126.28 -56.87];  % [-126.28 -66.87];
  ax = worldmap(latlim,lonlim);

  load coastlines
  geoshow(ax, coastlat, coastlon,...
  'DisplayType', 'polygon', 'FaceColor', [.45 .60 .30])
  textm(38.94, -101.67,'United States of America','HorizontalAlignment','center','VerticalAlignment','middle');
```

```
  textm(27.7264, -105.08,'Mexico','HorizontalAlignment','center','VerticalAlignment','middle');
  textm(25.804782, -78.564135,'Bahamas','HorizontalAlignment','center','VerticalAlignment','middle');
  textm(21.64, -78.51,'Cuba','HorizontalAlignment','center','VerticalAlignment','middle');
  textm(18.144674, -77.515694,'Jamaica','HorizontalAlignment','center','VerticalAlignment','middle');
  textm(47.109121, -79.504786,'Canada','HorizontalAlignment','center','VerticalAlignment','middle');
  textm(19.3, -71.605227,'Haiti','HorizontalAlignment','center','VerticalAlignment','middle');
  textm(18.0, -72.305227,'Dominican','HorizontalAlignment','center','VerticalAlignment','middle');
  textm(16.8, -72.305227,'Republic','HorizontalAlignment','center','VerticalAlignment','middle');
  textm(17.260834, -66.163626,'Puerto Rico','HorizontalAlignment','center','VerticalAlignment','middle');
  textm(16.060834, -65.163626,'Virgin Islds','HorizontalAlignment','center','VerticalAlignment','middle');
end

if (region == "USA") & (trajectoryType == "Parabole")
  figure(1)

  latlim= [6.54 48];
  lonlim= [-101 -41];
  ax = worldmap(latlim,lonlim);

  load coastlines
  geoshow(ax, coastlat, coastlon,...
  'DisplayType', 'polygon', 'FaceColor', [.45 .60 .30])
  textm(38.24, -95,'USA','HorizontalAlignment','center','VerticalAlignment','middle','FontSize',12);
  textm(45.785316, -79.476563,'Canada','HorizontalAlignment','left','VerticalAlignment','middle','FontSize',12);
  %textm(27.7264, -105.08,'Mexico','HorizontalAlignment','center','VerticalAlignment','middle');
  textm(17.9, -98,'Mexico','HorizontalAlignment','center','VerticalAlignment','middle','FontSize',12);
  %textm(25.804782, -78.564135,'Bahamas','HorizontalAlignment','center','VerticalAlignment','middle');
  %textm(21.64, -78.51,'Cuba','HorizontalAlignment','center','VerticalAlignment','middle');
  %textm(18.144674, -77.515694,'Jamaica','HorizontalAlignment','center','VerticalAlignment','middle');
  %textm(47.109121, -79.504786,'Canada','HorizontalAlignment','center','VerticalAlignment','middle');
  %textm(19.3, -71.605227,'Haiti','HorizontalAlignment','center','VerticalAlignment','middle');
  %textm(18.0, -72.305227,'Dominican','HorizontalAlignment','center','VerticalAlignment','middle');
  %textm(16.8, -72.305227,'Republic','HorizontalAlignment','center','VerticalAlignment','middle');
  %textm(17.260834, -66.163626,'Puerto Rico','HorizontalAlignment','center','VerticalAlignment','middle');
  %textm(16.060834, -65.163626,'Virgin Islds','HorizontalAlignment','center','VerticalAlignment','middle');
  textm(15.247465, -85.5,'Honduras','HorizontalAlignment','center','VerticalAlignment','middle','FontSize',12);
  textm(12.738486, -85.265994,'Nicaragua','HorizontalAlignment','center','VerticalAlignment','middle','FontSize',12);
  textm(9.209673, -74.704474,'Colombia','HorizontalAlignment','center','VerticalAlignment','middle','FontSize',12);
  textm(9.088066, -67.285904,'Venezuela','HorizontalAlignment','center','VerticalAlignment','middle','FontSize',12);
end

if region == "Japan"      % Drawing a Map of Japan-Taiwan-Philippines
  figure(1)
  title('Japan-Taiwan-Philippines  ')
  latlim= [5 50];
  lonlim= [115 150];
  ax = worldmap(latlim,lonlim);

  load coastlines
  geoshow(ax, coastlat, coastlon,...
  'DisplayType', 'polygon', 'FaceColor', [.45 .60 .30])
  textm(36.102910, 138.310039,'JPN','HorizontalAlignment','center','VerticalAlignment','middle');
  textm(21.6604142,120.1699955,'TWN','HorizontalAlignment','center','VerticalAlignment','middle');
  textm(9.043888, 120.814447,'PHL','HorizontalAlignment','center','VerticalAlignment','middle');
end

for k=1:mt     % Plot ALL turbines over the USA or Japan map
       if region == "Japan" | (region=="USA"  & trajectoryType == "Straight")
         labelLat = TurbTotal(k,1);
         labelLon = TurbTotal(k,2);
         textm(labelLat,
labelLon,'.','HorizontalAlignment','center','VerticalAlignment','middle','FontWeight','bold','FontSize',28,'Color', 'r');
```

```
        end
        if region == "USA"  & (trajectoryType == "Parabole")
           if  TurbTotal(k,2)> -100
               labelLat = TurbTotal(k,1);
               labelLon = TurbTotal(k,2);
               textm(labelLat,
labelLon,'.','HorizontalAlignment','center','VerticalAlignment','middle','FontWeight','bold','FontSize',28,'Color', 'r');
           end
        end
end
%                                                   %
%   End of opening the Map of USA Straight, USA parabole and Japan        %
%%%%%%%%%%%%%%%%%%%%%%%%%%%%%%%%%%%%%%%%%%%%%%%%%%%%%%%%%%%%%%%%%%%%%%%%%%%%
%%%%%%%%%%%%%


%%%%%%%%%%%%%%%%%%%%%%%%%%%%%%%%%%%%%%%%%%%%%%%%%%%%%%%%%%%%%%%%%%%%%%%%%%%%
%%%%%%%%%%%%%
%  Modeling the characteristic curve of the wind turbine (power vc speed) %
%  by fitting cs using interpolator function pchip                        %
%
   clear x;
   clear y;  % x = wind_speed [m/s];  y = wind_power [pu]

   if turbineType=="special"   %cutout 40 m/s
       x = [0, 1, 2, 2.5, 3,    4,    5, 6.5,   8, 9.5,   10, 11.3, 12.5, 14, 14.5, 15, 16, 17, 18, 20, 23, 24.5, 40, 40.001,  40.002, 40.003,
41, 42, 43, 100, 101];
       y = [0, 0, 0, 0,   0, 0.02, 0.03, 0.2, 0.4, 0.6, 0.65,  0.8, 0.95,  1,    1,  1,  1,  1,  1,  1,  1,    1,  1,      0,       0,      0,  0,  0,  0,   0,
0];
   else    %typical cutout speed 25 m/s
       x = [0, 1, 2, 2.5, 3,    4,    5, 6.5,   8, 9.5,   10, 11.3, 12.5, 14, 14.5, 15, 16, 17, 18, 20, 23, 24.5, 25, 25.001,  25.002, 25.003,
26, 30, 50, 100, 101];
       y = [0, 0, 0, 0,   0, 0.02, 0.03, 0.2, 0.4, 0.6, 0.65,  0.8, 0.95,  1,    1,  1,  1,  1,  1,  1,  1,    1,  1,      0,       0,      0,  0,  0,  0,   0,
0];
   end

   cs = pchip(x,y);
   x_global=x;
   y_global=y;
%  End of modeling characteristic curve of wind turbine (power vc speed)  %
%%%%%%%%%%%%%%%%%%%%%%%%%%%%%%%%%%%%%%%%%%%%%%%%%%%%%%%%%%%%%%%%%%%%%%%%%%%%
%%%%%%%%%%%%%

%%%%%%%%%%%%%%%%%%%%%%%%%%%%%%%%%%%%%%%%%%%%%%%%%%%%%%%%%%%%%%%%%%%%%%%%%%%%
%%%%%%%%%%%%%
%  Modeling the characteristic curve of the hurricane for alternative 1   %
%  for USA or Japan
   if (alternative==1) & (region=="USA")   % fitting csH of the hurricane speed [m/s] versus radius [km]
      distant = [0, 15, 20, 30, 35, 40, 50, 55, 60, 70,  100, 135, 140, 148,  150, 160, 180, 200, 300, 400, 500, 5000];
      Vg =[0, 10, 15, 25, 38, 39, 42, 43, 38, 37,   32,  26,  28,  28, 24.5,  24,  20,  20,  15,  10,   5,    3];
      csH = pchip(distant,Vg);
   end
%  Fitting csH of the Marakot typhoon speed [m/s] versus radius [km]
%  [ ] Chung-Chieh WANG et al., A Modeling Study on the Impacts of Typhoon Morakot's (2009) Vortex Structure
%  on Rainfall in Taiwan Using Piecewise Potential Vorticity Inversion
   if (alternative==1) & (region=="Japan")
      distant = [0, 75, 100, 150,  200, 250, 300, 350, 400,  450, 500, 550,  600, 650, 700,  750, 2000];
      Vg      =[0, 20,  25,  32, 31.5,  31,  32,  30,  27, 23.5,  20,  18, 16.5,  16,  15, 14.5,    0];
      csH = pchip(distant,Vg);
   end
% End of modeling the characteristic curve of the hurricane alternative 1 %
```

```
%%%%%%%%%%%%%%%%%%%%%%%%%%%%%%%%%%%%%%%%%%%%%%%%%%%%%%%%%%%%%%%%%%%%%%%%%%%%%%%%%%%%
%%%%%%%%%%%%%

%%%%%%%%%%%%%%%%%%%%%%%%%%%%%%%%%%%%%%%%%%%%%%%%%%%%%%%%%%%%%%%%%%%%%%%%%%%%%%%%%%%%
%%%%%%%%%%%%%
%                                              %
%         setting of hurricane simulation time                %
if (region == "USA" & trajectoryType == "Straight")
   hurricane_time = 24*1; %5;   % aprox 120 hours = 5 days
   textm(LaA, LoA, 'o','HorizontalAlignment','center','VerticalAlignment','middle');  % origin of eye trajectory
textm(LaB, LoB, 'o','HorizontalAlignment','center','VerticalAlignment','middle','FontSize',4);  % destine of eye trajectory
end
if (region == "USA") & (trajectoryType == "Parabole")
   hurricane_time = 24*10;   % 9 days=216h; 240 hours = 10 days
end
if (region == "Japan")
   hurricane_time = 24*1; %5;  %*5, not divided by 60;   % aprox 1 days
   textm(LaA, LoA, 'o','HorizontalAlignment','center','VerticalAlignment','middle');  % origin of eye trajectory
   textm(LaB, LoB, 'o','HorizontalAlignment','center','VerticalAlignment','middle','FontSize',4);  % destine of eye trajectory
end
%         End of setting of hurricane simulation time             %
%%%%%%%%%%%%%%%%%%%%%%%%%%%%%%%%%%%%%%%%%%%%%%%%%%%%%%%%%%%%%%%%%%%%%%%%%%%%%%%%%%%%
%%%%%%%%%%%%%


%%%%%%%%%%%%%%%%%%%%%%%%%%%%%%%%%%%%%%%%%%%%%%%%%%%%%%%%%%%%%%%%%%%%%%%%%%%%%%%%%%%%
%%%%%%%%%%%%%
%                                              %
%           Plot hurricane trajectory &                    %
%           Calculation of power profile                   %
%                                              %
if region == "Japan" | (region == "USA"  & trajectoryType == "Straight")
aux=0;
Rmaxmax=0;

landfallTime=0;    % [hours] , i is also in [hours].            % **
coast = load('coast.mat');                                   % **
for i=1:hurricane_time        % PARA CADA PASSO DE TEMPO DE FURACAO

  ti = i*3600; %3600;    % originally 3600;       % hours = 3600[s] = 60 [min]
  deltaLa_i=ti*w*(LaB-LaA)/deltaAngle;  % [delta Latitude degree]   STEPSIZE 2s
  deltaLo_i=ti*w*(LoB-LoA)/deltaAngle;  % [delta Longitude degree]   STEPSIZE 2s
  Lai=LaA+deltaLa_i;    %Latitude of hurricane after time ti
  Loi=LoA+deltaLo_i ;  %Longitude of hurricane after time ti

  textm(Lai, Loi, 'o','HorizontalAlignment','center','VerticalAlignment','middle','FontSize',4);
  if (mod(i,10)==0)
  iString = num2str(i);
  textm((Lai+1), Loi, iString,'FontSize',12)
  end

  for k=1:mt                % COMPUTE A POTENCIA DE TODAS AS TURBINAS
    LakT=TurbTotal(k,1);
    LokT=TurbTotal(k,2);
    IsInOnshore = inpolygon(Lai,Loi,coast.lat,coast.long);

  if (alternative == 0) & (region == "USA")
    % Calc of Hurricane speed in each turbine given the instantaneous distance
    hurricane_Model = 'Holland_and_Georgio';  % Holland and Georgio model

        if hurricaneCategory == 5
           catCol=1;
```

```
      end;
      if hurricaneCategory == 4
         catCol=2;
      end;
      if hurricaneCategory == 3
         catCol=3;
      end;

if  Lai > 41.09 & Lai < 50.35 & Loi <-75.65 & Loi > -93.36 % Great Lakes
   IsInOnshore =1;
end
if IsInOnshore == 1  & Lai > 28.5      % if onshore
   Rmax = PR(5, catCol);
   Pc =  PR(4, catCol);
end
if IsInOnshore == 1  & Lai < 28.501    % if onshore but small islands does not change Pc and Rmax
   Rmax = PR(3, catCol);
   Pc =  PR(2, catCol);
end
if IsInOnshore ==0                     % if offshore and Lai < 36.55
   Rmax = PR(3, catCol);
   Pc =  PR(2, catCol);
end
if Lai > 36.55  &  IsInOnshore ==0           % if offshore and Lai > 36.55
   Rmax = PR(3, catCol);
   Pc =  PR(4, catCol);
end
Pn=1008;   % Between 1000 and 1015 %944;    % Pn = 944 milibar for Andrew [44],

%%%%%%% Linear decaying above North Mississipi to Cleveland %%%%%%%%%%
if  Lai > 35 & Lai < 41  % & IsInOnshore == 1; % Decaying from North Mississipi to Cleveland
   Pc = Pc + (Pn-Pc)*(Lai - 35)/(41-35);
end

if  Lai > 39.9999 % & IsInOnshore == 1;              % Above Cleveland, no hurricane.
   Pc = Pn;
end
%%%%%%% Linear decaying above North Mississipi to Cleveland %%%%%%%%%%

 phi = Lai;    % Phi = Lai, latitude of hurricane eye or turbine ?
 phi2=phi*2*pi()/360;
% Rmax = exp(2.636 - 0.00005086*(Pn - Pc)^2 + 0.0394899*phi2);  %[km]
 if  Rmaxmax < Rmax
   Rmaxmax = Rmax;
 end

B = 1.38 + 0.00184*(Pn - Pc) - 0.00309*Rmax;
% B = 1.34 + 0.00328*(Pn - Pc)- 0.00522*Rmax
% B = 1.6; % for Andrew [48]
% Calc of f = coriolis paramenter if function of latitude [1/s]
Omega = 2*pi()/(24*60*60); % [rad/s] - OK, Omega value is right.
% Omega is angular velocity of the Earth (7.292 X 10E-5 [1/s]

 phi = Lai;  % supposing latitude 40 degree [degree]
 f = 2*Omega*sin((phi*2*pi())/360); % where
 % f = 7.2722e-05 calculated value seems in right magnitude.
 % In Oklahoma f = 10 x 10E-5 [1/s]

%%%   Calculation of alpha based on the eye trajectory
%https://stackoverflow.com/questions/1560492/how-to-tell-whether-a-point-is-to-the-right-or-left-side-of-a-line
% wind speed is calculated on the turbine coordinates
LakT;       %=LaC+deltaLa_k;    %Latitude of turbine
```

```
LokT;      %=LoC+deltaLo_k;    %Longitude of turbine
Lai;       %=LaA+deltaLa_i;    %Latitude of hurricane after time ti
Loi;       %=LoA+deltaLo_i;    %Longitude of hurricane after time ti
LaB;       % Latitude of hurricane at destination
LoB;       % Longitude of hurricane at destination


LaBs=LaB-Lai;
LoBs=LoB-Loi;
LakTs=LakT-Lai;
LokTs=LokT-Loi;
Lais=0;
Lois=0;
LokTs=LokTs-LoBs;
LoBs=0;
if LokTs == Lois
   LokTs = LokTs - 0.0000001
end
if (LakTs > 0)&(LokTs > 0)
   quadrant = 1;
end
if (LakTs > 0)&(LokTs < 0)
   quadrant = 4;
end
if (LakTs < 0)&(LokTs > 0)
   quadrant = 2;
end
if (LakTs < 0) & (LokTs < 0)
   quadrant = 3;
end
a = (distance(LakT, LokT, Lai, Loi));  % [deg]
b = (distance(LaB, LoB, Lai, Loi));    % [deg]
c = (distance(LakT, LokT, LaB, LoB));  % [deg]
a = deg2km(a);     %[km]
b = deg2km(b);     %[km]
if b==0
   b=0.00000001;
end
c = deg2km(c);     %[km]
angleUpto180 = acos((c*c - a*a - b*b)/(-2*a*b));
if (quadrant==1) | (quadrant==2)
   alpha = angleUpto180;
end
if (quadrant==3) | (quadrant==4)
  alpha = 2*pi() - angleUpto180; % [radians]
end

alphaM(k,i)= alpha;
alphadegree = 0;
alphadegree = alpha*360/(2* pi());
deltaP = (Pn - Pc);
rho = 1.225;   % [kg/m^3]  density of dry air at 20oC
rho = 1.096;   % [kg/m^3]  density of humid air and hot air
% at 70 °F and 14.696 psi, dry air has a density of 0.074887 lb/ft³.
%%% Georgio´s Hurricane speed equation (Vg)
a=a;     % instantaneous distance between eye and turbine kT [km]
Vg1 = 0.5*(Vtr*sin(alpha) - f*a);
Vg2 = 0.25*(Vtr*sin(alpha) - f*a)^2 + (100*B*deltaP/rho)*((Rmax/a)^B)*exp(-(Rmax/a)^B);
% Obs: Cui´s equation is right! [] (It is 100*B*deltaP/rho, not B*delta/rho);
Vg = Vg1 + sqrt(Vg2);
  %%% where: f = Coriolis parameter; r = radial distance from storm center
  %%% alpha = angle, clockwise positive from translation direction
```

```
      %%% delta p = delta of pressure at distance r
      %%% rho = air density
      %%% VT = storm translation speed
      %%% p = pressure, at distance r
      %%% Vgb = mean gradient balance wind speed at (r, alpha).
      %%% Rmax = radius of maximum winds,
      %%% B = pressure profile exponent
      %%% delta p = central pressure difference,
      % Vw at 10m is 0,71*Vg [Valamanesh et al]
    Vw = 0.923*Vg;  % Speed Vw at 90m wind turbine height
    Vwm(k,i)=Vw;
  end

   if (alternative == 0) & (region == "Japan")
    % Calc of Hurricane speed in each turbine given the instantaneous distance
    hurricane_Model = 'Holland_and_Georgio modified for Typhoon Marakot';
    % Holland H10 model at Typhoon Marakot hitting Taiwan
     Pcs=990; %850;     % [hPa] Marakot typhoon. Generically, 990 hPa Marakot,
     Vms = 3.45*((1010-Pcs)^0.644);           % simplified equation
     bethaS= 0.3327 ;                        % Marakot (0.1320 for Wipha)
     Rmax=196;                % [km] Marakot (10 times more than Andrew!)
     Rn = distance(22, 118, 25, 120);        % [degree]
     Rn = deg2km(Rn);                        % [km]
     aux=((Rmax/Rn)^bethaS)*exp(1-(Rmax/Rn)^bethaS);
     Vrsn=21.5;                              % [m/s]
     Xn= (log(Vrsn/Vms))/log(aux);
     a = (distance(LakT, LokT, Lai, Loi));  % [deg]
     a = abs(deg2km(a));                     % [km]
     if a<Rmax
        X = 0.5;
     else X = 0.5+(a-Rn)*(Xn-0.5)/(Rn-Rmax);
     end
     X=0.5;
     Vrs = ((Rmax/a)^bethaS)*exp(1-(Rmax/a)^bethaS);
     Vrs = Vrs^X;
     Vrs = Vms*Vrs;
     Vg = Vrs;
     Vw = 0.923*Vg;  % Speed Vw at 90m wind turbine height
     Vwm(k,i)=Vw;
   end

if alternative==0 & (region == "Japan") % Holland Decaying for Japan only)
    landfallTime=0;    % [hours] , i is also in [hours].              % **
    if IsInOnshore                                                    % **
      % decaying model R, alphaTime and Vb
      % Southern R=0.90  alphaTime = 0.095 [1/hour]  Vb = 26.7 [kt]
      % above 37 degree latitude is northern of northern hemisphere
      % Northern R=0.90  alphaTime = 0.187 [1/hour]  Vb = 29.6 [kt]
      % V(t)= Vb +(RV0-Vb)* exp(-alphaTime*t)[Kaplan and DeMaria, 2000]
      % reduction factor = 0.9, according to [Kaplan and DeMaria, 2000]
      if abs(Lai) > 37         % northern of northern hemisphere     % **
         alphaTime = 0.187;                                           % **
      else alphaTime = 0.095;   % southern of northern hemisphere     % **
      end                                                           % **
      decaymentWindSpeedFactor=0.3+(0.9*1-0.3)*exp(-alphaTime*landfallTime);
      landfallTime = landfallTime + 1; %[hours] deltaTimeTrajectory=1 hour
    else decaymentWindSpeedFactor=1;                                  % **
    end                                                             % **
    Vw=decaymentWindSpeedFactor*Vw;    %[m/s]
    Vwm(k,i)=Vw;
  end
```

```
  if alternative==1  % direct fitting of Hurricane speed [m/s] versus radius from eye [km]
    xq1 = 0: 1: 5000;
    plot(distant,Vg,'o',xq1,ppval(csH,xq1),'-');
    a = (distance(LakT, LokT, Lai, Loi));  % [deg]
    a = deg2km(a);           %[km]

    coast = load('coast.mat');                                  % **
    IsInOnshore = inpolygon(Lai,Loi,coast.lat,coast.long);            % **
    if IsInOnshore                                          % **
      % decaying model R, alphaTime and Vb
      % Southern R=0.90  alphaTime = 0.095 [1/hour]  Vb = 26.7 [kt]
      % above 37 degree latitude is northern of northern hemisphere
      % Northern R=0.90  alphaTime = 0.187 [1/hour]  Vb = 29.6 [kt]
      % V(t)= Vb +(RV0-Vb)* exp(-alphaTime*t)[Kaplan and DeMaria, 2000]
      % reduction factor = 0.9, according to [Kaplan and DeMaria, 2000]
      if abs(Lai) > 37         % northern of northern hemisphere     % **
         alphaTime = 0.187;                                  % **
      else alphaTime = 0.095;   % southern of northern hemisphere     % **
      end                                                 % **
      decaymentWindSpeedFactor=0.3+(0.9*1-0.3)*exp(-alphaTime*landfallTime);
      landfallTime = landfallTime + 1; %[hours] deltaTimeTrajectory=1 hour
    else decaymentWindSpeedFactor=1;                            % **
        landfallTime=0;
    end                                                   % **
    Vw=decaymentWindSpeedFactor*0.923*ppval(csH,a);    %[m/s]

      if (Vw < TurbTotal(k,4)) %VminOffshore)
         Vw = TurbTotal(k,4);  %VminOffshore;
      end
    Vwm(k,i)=Vw;
  end

    %% Calculation of turbine wind power based on wind speed
    clear xq1;
    clear power;
    xq1 = 0:.01:101;
    plot(x,y,'o',xq1,ppval(cs,xq1),'-');
    power=ppval(cs,Vw);    %[p.u. value]
    Power = power*Tpower;  % [MW], each turbine 10 MW
    power_Profile(k,i) = Power;  % where i = hurricane time step and k = number of turbines
    ik=size(power_Profile);

  end  % end of iteration on number of turbines
 end  % end of iteration of hurricane trajectory time
end  % Japan or USA Straight
%                                                         %
%      End of power profile calculation for USA Straight and Japan        %
%%%%%%%%%%%%%%%%%%%%%%%%%%%%%%%%%%%%%%%%%%%%%%%%%%%%%%%%%%%%%%%%%%%%%%%%%%%%
%%%%%%%%%%%%%%%%%%%%%%%%%%%%%%%%%%%%%%%%%%%%%%%%%%%%%%%%%%%%%%%%%%%%%%%%%%%%
%                                                         %
%          Plot hurricane trajectory for USA Parabole                  %
%                                                         %
%                                                         %
if region == "USA"  & (trajectoryType == "Parabole")
      if  jp==10 % for time indication just for hurricane trajectory #10
```

```
        Lat1(11)=Lat1(10)+Lat1(10)-Lat1(9);
        Long1(11) =Long1(10)+Long1(10)-Long1(9);
        Latmin(11)=Latmin(10)+Latmin(10)-Latmin(9);
        Longmin(11)=Longmin(10)+Longmin(10)-Longmin(9);
    end
  for j=jp:jp+1
    ap = (Long1(j) - Longmin(j))/((Lat1(j)*Lat1(j)-Latmin(j)*Latmin(j))-2*Latmin(j)*(Lat1(j)-Latmin(j)));
    bp = -2*ap*Latmin(j);
    cp = Long1(j) - ap*Lat1(j)*Lat1(j) + 2*ap*Latmin(j)*Lat1(j);
    Lati(1)=Lat1(j);
    Long(1)=Long1(j);

    for i=1:hurricane_time
        ti = i*3600;    %3600;              % hours = 3600[s] = 60 [min]
        if i==round(1)
            LatiPreced = (Lati(i));
            LotiPreced = (Long(i));
            Lati(i)= Lat1(j);
            Long(i)= Long1(j);
            LaA=Lati(i);
            LoA=Long(i);
        else
            Vtr=9.722; %8m/s % 9.722 m/s Michael2018, 9.722 m/s Charley2004, 13.333m/s Wilma2005landfall
            wKmpH=Vtr*(1/1000)/(1/3600); %km/h
            stepAngle=km2deg((wKmpH)*1); %time step is 1h, assuming Earth Great Circle
            teta = (90-atand((2*ap*LatiPreced+bp)));
            Lati(i)= LatiPreced+stepAngle*sind(teta); %step Angle for 8m/s in 1h = 28.8km
            Long(i)=ap*Lati(i)*Lati(i)+bp*Lati(i)+cp;
            LaB=Lati(i);
            LoB=Long(i);
            LaA=Lati(i-1);
            LoA=Long(i-1);
        end
            LatiPreced = Lati(i);
            LongPreced = Long(i);
        if (i > 3)    & (j==jp)
            textm(Lati(i), Long(i), 'o','HorizontalAlignment','center','VerticalAlignment','middle','FontSize',2,'color', 'k');
            %textm(Lati(i), Long(i), 'o','HorizontalAlignment','center','VerticalAlignment','middle','FontSize',8, 'color', 'm');
        end
        if (mod(i,10)==0) & (j==jp)   %+1)
            iString = num2str(i);
            textm(Lati(i), Long(i), 'o','HorizontalAlignment','center','VerticalAlignment','middle','fontweight','bold','FontSize',6,
'color','m');
        end

        auxLa(i)=Lati(i);
        auxLo(i)=Long(i);
        if (mod(i,10)==0) & (j==jp+1)
            iString = num2str(i);
            deltaLati=Lati(i)-auxLa(i);
            deltaLong=Long(i)-auxLo(i);
            textm(0.2+(0.983)*Lati(i), 0.99*Long(i)-0.027*Lati(i),
iString,'HorizontalAlignment','center','VerticalAlignment','middle', 'FontSize',11)
        end

        if i==1 & (j==jp)
            %deltaLati=Lati(i)-auxLa(i);
            %deltaLong=Long(i)-auxLo(i);
            textm(Lati(i), Long(i),
num2str(j),'HorizontalAlignment','center','VerticalAlignment','middle','fontweight','bold','FontSize',12, 'Color',trajectColor); %'r');
            %Lai(i)=Lati(i);  % transfering to Lai, Loi for power calculation (next section)
            %Loi(i)=Long(i);
```

```
            end
             if (j==jp)
                Lai(i)=Lati(i);  % transfering to Lai, Loi for power calculation (next section)
                Loi(i)=Long(i);
             end

      end   % hurricane time

   textm(Lat1(j),Long1(j),'o','HorizontalAlignment','center','VerticalAlignment','middle','FontSize',2);
   textm(Latmin(j), Longmin(j), 'o','HorizontalAlignment','center','VerticalAlignment','middle','FontSize',2);
   %hold off
   end
end
%          End of Plot hurricane trajectory for USA Parabole            %
%%%%%%%%%%%%%%%%%%%%%%%%%%%%%%%%%%%%%%%%%%%%%%%%%%%%%%%%%%%%%%%%%%
%%%%%%%%%%%%%




%%%%%%%%%%%%%%%%%%%%%%%%%%%%%%%%%%%%%%%%%%%%%%%%%%%%%%%%%%%%%%%%%%
%%%%%%%%%%%%%%
%                                                          %
%             Calculation of power profile for USA Parabole              %
%                                                          %
if region == "USA"  & (trajectoryType == "Parabole")
   aux=0;
   Rmaxmax=0;
   Rmaxmin=10000000000;

   coast = load('coast.mat');   % **
   Vwm=zeros(mt, hurricane_time);
   RmWarray(1:hurricane_time)=500;
   RmaxArray(1:hurricane_time)=500;
   IsInOnshoreArray(1:hurricane_time)=0;
   PcArray(1:hurricane_time)=1000;
    for i=1:hurricane_time        % PARA CADA PASSO DE TEMPO DE FURACAO

     ti = i*3600; %3600;    % originally 3600;       % hours = 3600[s] = 60 [min
     IsInOnshore = inpolygon(Lai(i),Loi(i),coast.lat,coast.long);
     IsInOnshoreArray(i)=IsInOnshore;

%%%%%%%%%%%%%%%%%%%%%%%%%%%%%%%%%%%%%%%%%%%%%%%%%%%%%%%%%%%%%%%%%%
%%%%%%%%%%%%
     %    Radius of minimum winds for Map of USA parabole                  %
     %                                                      %
     if hurricaneCategory == 5 & IsInOnshore==1    % Radius of minimum Wind speed
        RmW = 1408*1.1;
     end
     if hurricaneCategory == 4 & IsInOnshore==1    % Radius of minimum Wind speed
        RmW = 927*1.1;
     end
     if hurricaneCategory == 3  & IsInOnshore==1   % Radius of minimum Wind speed
        RmW = 585*1.1;
     end
     if hurricaneCategory == 5 & IsInOnshore==0    % Offshore Radius of minimum Wind speed
        RmW = 981*1.1;
     end
     if hurricaneCategory == 4 & IsInOnshore==0    % Offshore Radius of minimum Wind speed
        RmW = 267*1.1;
```

```
    end
    if hurricaneCategory == 3  & IsInOnshore==0   % Offshore Radius of minimum Wind speed
       RmW = 269*1.1;
    end
    RmWarray(i)= RmW;     % Array of Radius of minimum Wind speed
    %     End of Radius of minimum winds for Map of USA parabole            %

%%%%%%%%%%%%%%%%%%%%%%%%%%%%%%%%%%%%%%%%%%%%%%%%%%%%%%%%%%%%%%%%%%%
%%%%%%%%%%%
   if (alternative ==0) & (region == "USA") & (trajectoryType == "Parabole")
        if hurricaneCategory == 5
           catCol=1;
        end;
        if hurricaneCategory == 4
           catCol=2;
        end;
        if hurricaneCategory == 3
           catCol=3;
        end;
        %IsInOnshore = inpolygon(Lai(i),Loi(i),coast.lat,coast.long);
        if  Lai(i) > 41.09 & Lai(i) < 50.35 & Loi(i) <-75.65 & Loi(i) > -93.36 % Great Lakes
          IsInOnshore =1;
        end
        if IsInOnshore == 1  & Lai(i) > 28.5      % if onshore
           Rmax = PR(5, catCol);
           Pc =  PR(4, catCol);
        end
        if IsInOnshore == 1  & Lai(i) < 28.501    % if onshore but small islands does not change Pc and Rmax
           Rmax = PR(3, catCol);
           Pc =  PR(2, catCol);
        end
        if IsInOnshore ==0                    % if offshore and Lai < 36.55
           Rmax = PR(3, catCol);
           Pc =  PR(2, catCol);
        end
        if Lai(i) > 36.55   &  IsInOnshore ==0    % if offshore but Lai > 36.55
           Rmax = PR(3, catCol);
           Pc =  PR(4, catCol);
        end
   end
    RmaxArray(i)= Rmax;     % Array of Radius of minimum Wind speed
    PcArray(i)=Pc;
     end
  RmWarrayFiltered=filter([1/3 1/3 1/3],1,RmWarray);
  RmaxArrayFiltered=filter([1/3 1/3 1/3],1,RmaxArray);

for i=1:hurricane_time        % PARA CADA PASSO DE TEMPO DE FURACAO
 ti = i*3600; %3600;    % originally 3600;       % hours = 3600[s] = 60 [min
 %IsInOnshore = inpolygon(Lai(i),Loi(i),coast.lat,coast.long);

 IsInOnshore = IsInOnshoreArray(i);
 RmW=RmWarrayFiltered(i);
 Rmax=RmaxArrayFiltered(i);
 Pc=PcArray(i);


   Pn=1008;   % Between 1000 and 1015 %944;    % Pn = 944 milibar for Andrew [44],
   %%%%%%%% Linear decaying above North Mississipi to Cleveland %%%%%%%%%%%
   if  Lai(i) > 35 & Lai(i) < 45 % & IsInOnshore == 1; % Decaying from North Mississipi to Cleveland
      Pc = Pc + (Pn-Pc)*(Lai(i) - 35)/(45-35);
   end
```

```
  if  Lai(i) > 44.9999 % & IsInOnshore == 1;              % Above Cleveland, no hurricane.
     Pc = Pn;
  end
  %%%%%%%% Linear decaying above North Mississipi to Cleveland %%%%%%%%%%%

 for k=1:mt                % COMPUTE A POTENCIA DE TODAS AS TURBINAS
  LakT=TurbTotal(k,1);
  LokT=TurbTotal(k,2);
if (alternative ==0) & (region == "USA") & (trajectoryType == "Parabole")
  % Calc of Hurricane speed in each turbine given the instantaneous distance
  hurricane_Model = 'Holland_and_Georgio';  % Holland and Georgio model



   %Pc=922;    % Pc = 922 milibar for Andrew [44],
   phi = Lai(i);    % Phi = Lai, latitude of hurricane eye or turbine ?
   phi2=phi*2*pi()/360;
   %Rmax = exp(2.636 - 0.00005086*(Pn - Pc)^2 + 0.0394899*phi2);  %[km]
  if  Rmaxmax < Rmax
     Rmaxmax = Rmax;
  end
  if  Rmaxmin > Rmax
     Rmaxmin = Rmax;
  end

  B = 1.38 + 0.00184*(Pn - Pc) - 0.00309*Rmax;
  %B = 1.6; % for Andrew [48]
   Omega = 2*pi()/(24*60*60); % [rad/s] - OK, Omega value is right.
   phi = Lai(i);  % supposing latitude 40 degree [degree]
   f = 2*Omega*sin((phi*2*pi())/360); % where
  LakT;       %=LaC+deltaLa_k;    %Latitude of turbine
  LokT;       %=LoC+deltaLo_k;    %Longitude of turbine
  Lai(i);       %=LaA+deltaLa_i;    %Latitude of hurricane after time ti
  Loi(i);       %=LoA+deltaLo_i;    %Longitude of hurricane after time ti
  u=size(Lai);
  u = length(Lai);
  %v=size(Loi);
  if i==u
  LaB=Lai(i)+2*(Lai(i)-Lai(i-1));        % Latitude of hurricane at destination
  LoB=Loi(i)+2*(Loi(i)-Loi(i-1));
  else
  LaB=1.5*Lai(i+1);        % Latitude of hurricane at destination (to avoid numerical error)
  LoB=1.5*Loi(i+1);        % Longitude of hurricane at destination
  end

  LaBs=LaB-Lai(i);
  LoBs=LoB-Loi(i);
  LakTs=LakT-Lai(i);
  LokTs=LokT-Loi(i);
  Lais=0;
  Lois=0;
  LokTs=LokTs-LoBs;
  LakTs=LakTs-LaBs;    %%%%
  LoBs=0;
  if LokTs == Lois
     LokTs = LokTs - 0.0000001
  end
  if (LakTs > 0)&(LokTs > 0)
     quadrant = 1;
  end
  if (LakTs > 0)&(LokTs < 0)
     quadrant = 4;
```

```
    end
    if (LakTs < 0)&(LokTs > 0)
       quadrant = 2;
    end
    if (LakTs < 0) & (LokTs < 0)
       quadrant = 3;
    end
    a = (distance(LakT, LokT, Lai(i), Loi(i)));  % [deg]
    b = (distance(LaB, LoB, Lai(i), Loi(i)));    % [deg]
    c = (distance(LakT, LokT, LaB, LoB));  % [deg]
    a = deg2km(a);     %[km]
    b = deg2km(b);     %[km]
    if b==0
       b=0.00000001;
    end
    c = deg2km(c);     %[km]
    angleUpto180 = acos((c*c - a*a - b*b)/(-2*a*b));
    if (quadrant==1) || (quadrant==2)
       alpha = angleUpto180;
    end
    if (quadrant==3) | (quadrant==4)
      alpha = 2*pi() - angleUpto180; % [radians]
    end

    alphaM(k,i)= alpha;
    alphadegree = 0;
    alphadegree = alpha*360/(2* pi());
    % alpha = pi()/4;
    %%% page 109 Giorgio, wrong equation Vg=((B/p)*((Rmax/r_h)^B)*(Pn-Pc)*exp(-(Rmax/r_h)^B) +
0.25*(Vtr*sin(theta_tr)-r_h*fc)^2)^0.5 + 0.5*(Vtr*sin(theta_tr)-r_h*fc)
    deltaP = (Pn - Pc);
    rho = 1.225;   % [kg/m^3]  density of dry air at 20oC
    rho = 1.096;   % [kg/m^3]  density of humid air and hot air
    % at 70 °F and 14.696 psi, dry air has a density of 0.074887 lb/ft³.
    %%% Georgio´s Hurricane speed equation (Vg)
    a=a;     % instantaneous distance between eye and turbine kT [km]
    Vg1 = 0.5*(Vtr*sin(alpha) - f*a);
    Vg2 = 0.25*(Vtr*sin(alpha) - f*a)^2 + (100*B*deltaP/rho)*((Rmax/a)^B)*exp(-(Rmax/a)^B);
    % Obs: Cui´s equation is right! [] (It is 100*B*deltaP/rho, not B*delta/rho);
    Vg = Vg1 + sqrt(Vg2);
    Vw = 0.923*Vg;  % Speed Vw at 90m wind turbine height
    Vwm(k,i)=Vw;


   % if (TurbineIsInOnshore==0) & (Vw < TurbTotal(k,4))   %VminOffshore)

    if (a > 491) & (a <= RmW) & (hurricaneCategory == 5) & IsInOnshore==0  %VminOffshore)
       VwForma = -0.087620055*a+92.99;
       Vw = min(VwForma, Vw);
    end
    if (a > 133) & (a <= RmW) & (hurricaneCategory == 4) & IsInOnshore==0  %VminOffshore)
       VwForma = -0.24747395*a+72.99;
       Vw = min(VwForma, Vw);
    end
    if (a > 135) & (a <= RmW) & (hurricaneCategory == 3) & IsInOnshore==0  %VminOffshore)
       VwForma = -0.170792398*a+52.99;
       Vw = min(VwForma, Vw);
    end


    if (a > 704) & (a <= RmW) & (hurricaneCategory == 5) & IsInOnshore==1  %VminOnshore)
       VwForma = -0.020603615*a+34.5;
```

```
      Vw = min(VwForma, Vw);
    end
    if (a > 464) & (a <= RmW) & (hurricaneCategory == 4) & IsInOnshore==1  %VminOnshore)
      VwForma = -0.029112878*a+32.5;
      Vw = min(VwForma, Vw);
    end
    if (a > 292) & (a <= RmW) & (hurricaneCategory == 3) & IsInOnshore==1  %VminOnshore)
      VwForma = -0.04275676*a+30.5;
      Vw = min(VwForma, Vw);
    end

    if (Vw < TurbTotal(k,4)) | (a > RmW)  %VminOffshore)
        Vw = TurbTotal(k,4);
    end
    Vwm(k,i)=Vw;

  end

    % Calculation of turbine wind power based on wind speed
    clear xq1;
    clear power;
    xq1 = 0:.01:101;
    plot(x,y,'o',xq1,ppval(cs,xq1),'-');
    power=ppval(cs,Vw);    %[p.u. value]
    Power = power*Tpower;  % [MW], each turbine 10 MW
    power_Profile(k,i) = Power;  % where i = hurricane time step and k = number of turbines
    ik=size(power_Profile);


  end  % end of iteration on number of turbines


  %if i>2 | i<hurricane_time-2
  %  RmWarray(i)=(RmWarray(i-1)+RmW)/2;
  %RmWarrayFiltered(i)=3*filter([1/3 1/3 1/3],1,RmWarray(i));
  %RmWarrayFiltered(i)= movmean(RmWarray(i),3);
  %indice=i-1;  %mod((i-2)/1);
  %RmWarrayFiltered(i)=RmWarray(indice);

  %RmWarrayFiltered(i)=RmWarray(antecedente);
  %RmWarrayFiltered(i)=(RmWarray(i-2)+RmWarray(i-1)+RmWarray(i)+RmWarray(i+1)+RmWarray(i+2))/5;%
mean(RmWarray(round(i-2):round(i+2)));
  %end
 end  % end of iteration of hurricane trajectory time
          Vwm(:,hurricane_time)=Vwm(:,hurricane_time-1);
          power_Profile(:,hurricane_time)=power_Profile(:,hurricane_time-1);
end  % power profile for USA Parabole

 %RmWarray=RmWarray ;
 %RmWarrayFiltered=  RmWarrayFiltered;
 %Dif= RmWarrayFiltered -  RmWarray
%                                                          %
%         End of Calculation of power profile for USA Parabole          %
%%%%%%%%%%%%%%%%%%%%%%%%%%%%%%%%%%%%%%%%%%%%%%%%%%%%%%%%%%%%%%%%%%%%%%
%%%%%%%%%%%%%

%%%%%%%%%%%%%%%%%%%%%%%%%%%%%%%%%%%%%%%%%%%%%%%%%%%%%%%%%%%%%%%%%%%%%%
%%%%%%%%%%%%%
% Aggregate power profile of each turbine to Total power of all turbines  %

  ki=size(power_Profile)
  GEN_time=zeros(1,hurricane_time);
```

```
        for taux=1:hurricane_time
            GEN_time(taux)=sum(power_Profile(:,taux));
        end
  ki=size(GEN_time)
%      End of Total power profile of all turbines for all hurricane time  %
%%%%%%%%%%%%%%%%%%%%%%%%%%%%%%%%%%%%%%%%%%%%%%%%%%%%%%%%%%%%%
%%%%%%%%%%%%


%%%%%%%%%%%%%%%%%%%%%%%%%%%%%%%%%%%%%%%%%%%%%%%%%%%%%%%%%%%%%
%%%%%%%%%%%%%
%   Plot hurricane Circle for USA Straight, USA Parabole, and Japan       %
%                                                                      %
if region == "USA"  & (trajectoryType == "Straight")
      if alternative == 0
         Rmax3= 3*Rmaxmax*1000;       % 3*91 km in meters
      end
      if alternative == 1
         Rmax3 = 148000;              % 148km radius in [m]
      end
end

if region == "Japan"
    Rmaxmax=169;
    Rmax3 = 3*Rmaxmax*1000;
end
if region == "USA" & (trajectoryType == "Straight")
    Rmaxmax=169; % Assuming normal speed 7 m/s is 450 km from Andrew´s eye
       if hurricaneCategory == 5;
          Rmax3 = 1408000;
       end
       if hurricaneCategory == 4;
          Rmax3 = 927000;
       end
       if hurricaneCategory == 3;
          Rmax3 = 585000;
       end
       if hurricaneCategory ~= 5 | hurricaneCategory ~= 4 | hurricaneCategory ~= 3;
          Rmax3 = 585000*0.85;
       end

end

if region == "Japan" | (region == "USA" & trajectoryType == "Straight")

       if hurricaneCategory == 5;
          Rmax3 = 1408000;
       end
       if hurricaneCategory == 4;
          Rmax3 = 927000;
       end
       if hurricaneCategory == 3;
          Rmax3 = 585000;
       end
       if hurricaneCategory ~= 5 | hurricaneCategory ~= 4 | hurricaneCategory ~= 3;
          Rmax3 = 585000*0.85;
       end
       if region == "Japan";
          Rmax3 = 625000;  % Typhon Marakot
       end

   RmaxAngle=Rmax3/(2*pi()*r);
```

```
  RmaxAngle=RmaxAngle*360;
  for i=1:360
     La=LaA+RmaxAngle*sin(i);                          %LaA just initialCircle
     Lo=LoA-sqrt(RmaxAngle*RmaxAngle-(La-LaA)*(La-LaA));
     Lopositive=LoA+sqrt(RmaxAngle*RmaxAngle-(La-LaA)*(La-LaA));   %LoA just initialCircle
     textm(La, Lo, '.');           %,'Color',trajectColor);
     textm(La,Lopositive,'.');       %,'Color',trajectColor);
  end
end

  %      Plot hurricane Circle for Parabole                         %
  if region == "USA"  & (trajectoryType == "Parabole")
     Rmaxmax=169;
     if hurricaneCategory == 5;
        Rmax3 = 428000*3;
     end
     if hurricaneCategory == 4;
        Rmax3 = 189000*3;
     end
     if hurricaneCategory == 3;
        Rmax3 = 160000*3;
     end
     if hurricaneCategory ~= 5 | hurricaneCategory ~= 4 | hurricaneCategory ~= 3;
        Rmax3 = 150000*3;
     end

     RmaxAngle=Rmax3/(2*pi()*r);
     RmaxAngle=RmaxAngle*360;
     LaACircle=Lat1(jp);
     LoACircle=Long1(jp);

      for iCircle=1:360
         La=LaACircle+RmaxAngle*sin(iCircle);
         Lo=LoACircle-sqrt(RmaxAngle*RmaxAngle-(La-LaACircle)*(La-LaACircle));
         Lopositive=LoACircle+sqrt(RmaxAngle*RmaxAngle-(La-LaACircle)*(La-LaACircle));   %LoA just initialCircle
         textm(La, Lo, '.','Color',trajectColor); %,'Color',trajectColor);
         textm(La,Lopositive,'.','Color',trajectColor); %,'Color',trajectColor);
      end
  end
  %      End of plot of hurricane circle for parabole                  %


% End of plot hurricane Circle for USA Straight, USA Parabole and Japan %
%%%%%%%%%%%%%%%%%%%%%%%%%%%%%%%%%%%%%%%%%%%%%%%%%%%%%%%%%%%%%%%%%%%%%%%%%%%%%%%%%%%%%%%%%%
%%%%%%%%%%%%%%%%%%%%%%%%%%


%%%%%%%%%%%%%%%%%%%%%%%%%%%%%%%%%%%%%%%%%%%%%%%%%%%%%%%%%%%%%%%%%%%%%%%%%%%%%%%%%%%%%%%%%%
%%%%%%%%%%%%%%%%%%%%%%%%%%
%                                                   %
%      Plot legend in the map of USA Straight, USA Parabole and Japan    %
%                                                   %
if region == "USA" & (trajectoryType == "Straigth")
  textm(27.734257, -123.823609,'Legend','FontWeight','bold','FontSize',11);
  textm(26.30451, -
123.89390,'...','HorizontalAlignment','left','VerticalAlignment','middle','FontWeight','bold','FontSize',14,'Color', 'r');
  textm(26.34451, -121.999390,'Turbines','FontWeight','bold','VerticalAlignment','middle','FontSize',10);
  textm(24.157481, -123.107281,'ooo','HorizontalAlignment','left','VerticalAlignment','middle','FontWeight','bold','FontSize',4);
  textm(24.557481, -121.5,'Trajectory per','FontWeight','bold','VerticalAlignment','middle','FontSize',10);
  textm(23.557481, -121.0,'hour','FontWeight','bold','VerticalAlignment','middle','FontSize',10);
end
```

```
if region == "USA"  & (trajectoryType == "Parabole")
   textm(32.763707, -67.081642,'LEGEND:','HorizontalAlignment','left','VerticalAlignment','middle','FontSize',12);
   textm(30.753707, -69.1642,'oooooooo','HorizontalAlignment','left','VerticalAlignment','middle','FontSize',2);
   textm(30.853707, -67.1642,'Trajectory of the eye','HorizontalAlignment','left','VerticalAlignment','middle','FontSize',12);
   textm(29., -67.401642,'of the hurricane per hour','HorizontalAlignment','left','VerticalAlignment','middle','FontSize',12);
   textm(27.943707, -69.1642,'.','HorizontalAlignment','left','VerticalAlignment','middle','FontWeight','bold','FontSize',28,'Color',
'r');
   textm(27.043707, -67.351642,'Wind turbine','HorizontalAlignment','left', 'VerticalAlignment','middle','FontSize',12);
   latLegend=[ 34  26  26  24  32  34 ]; % Interconnector
   lonLegend=[-69.9 -70 -70 -48  -46.3 -70 ] ;
   plotm(latLegend,lonLegend, 'Color','k','LineWidth',0.5);

end

if region == "Japan"
   textm(11,140.5,'Legend','FontWeight','bold','FontSize',11);
   textm(9.5,140.5,'...','HorizontalAlignment','left','VerticalAlignment','middle','FontWeight','bold','FontSize',14,'Color', 'r');
   textm(9,142,'Turbines','FontWeight','bold','VerticalAlignment','middle','FontSize',10);
   textm(7.5,140.3,'oooooo','HorizontalAlignment','left','VerticalAlignment','middle','FontWeight','bold','FontSize',4);
   textm(7.5,142,'Trajectory per','FontWeight','bold','VerticalAlignment','middle','FontSize',10);
   textm(6.3,142,'hour','FontWeight','bold','VerticalAlignment','middle','FontSize',10);
end
%                                                       %
% End of Plot legend in the map of USA Straight, USA Parabole and Japan   %
%%%%%%%%%%%%%%%%%%%%%%%%%%%%%%%%%%%%%%%%%%%%%%%%%%%%%%%%%%%%
%%%%%%%%%%%%

%%%%%%%%%%%%%%%%%%%%%%%%%%%%%%%%%%%%%%%%%%%%%%%%%%%%%%%%%%%%
%%%%%%%%%%%%
%                                                       %
%             Plot Figures with sobplots of                          %
%             (a) Power profile,                              %
%             (b) Average airspeed in all turbines,                     %
%             (c) Maximum speed profile in a turbine                    %
%                                                       %
%
%figure('Name','Power profile [MW]');
[mt,nt]=size(GEN_time);
figure();
   strCat = num2str(hurricaneCategory);
   strTrack = num2str(jp);
   strPowerProfile = strcat("Cat-",strCat," Track ",strTrack," (a) PowerProfile.txt");
   title(strPowerProfile)
subplot(3,1,1)
plot([1:nt],GEN_time,'LineWidth',1.5);
grid on
% ax.XMinorTick = 'on'
axh=gca;
set (axh, 'GridLineStyle','-','FontSize',13);
grid minor;
%title('(a)')
%xlabel('                                              time [hour]')
xlabel('                              (a)                               time [hour]','fontweight','bold','FontName','Times New
Roman','FontSize',14);
ylabel('Power [MW]','fontweight','bold','FontName','Times New Roman','FontSize',14); %,'FontType','Times New Roman')

%pause('on')
%pause(30)

WindAvg=zeros(1,hurricane_time);
    for taux8=1:hurricane_time
        WindAvg(taux8)=sum(Vwm(:,taux8))/mt_global;
```

```
    end
    clear taux8;

%pause(30)


subplot(3,1,2)
plot([1:nt],WindAvg,'LineWidth',1.5);
grid on
axh=gca;
set (axh, 'GridLineStyle','-','FontSize',13);
grid minor;
xlabel('                                   (b)                                   time [hour]','fontweight','bold','FontName','Times New
Roman','FontSize',14);
ylabel('Mean speed [m/s]','fontweight','bold','FontName','Times New Roman','FontSize',14); %,'FontType','Times New Roman')


%pause(30)


maximum = max(max(Vwm));
[x1,y1]=find(Vwm==maximum)
WindT3=zeros(1,hurricane_time);
x1=x1(1);
    for taux=1:hurricane_time
     WindT3(taux)=Vwm(x1,taux);
    end

subplot(3,1,3)
plot([1:nt],WindT3,'LineWidth',1.5);
grid on
axh=gca;
set (axh, 'GridLineStyle','-','FontSize',13);
grid minor;
%title('(c)')
%xlabel('                                                    time [hour]')
xlabel('                                   (c)                                   time [hour]','fontweight','bold','FontName','Times New
Roman','FontSize',14);
ylabel('Max speed [m/s]','fontweight','bold','FontName','Times New Roman','FontSize',14); %,'FontType','Times New Roman')

fprintf("Turbine maximum speed at 90m from sea level [m/s]:");
MaxspeedOnTurbineAt90m=max(Vwm(:))
fprintf("Hurricane maximum gradient speed  [m/s]:");
HurricaneMaxGradientspeed=max(Vwm(:)/0.923)

clear Turb_array;
clear Turb_rect;
clear Vwm;
clear alphaM;
clear WindT3;
clear WindSum;
%                                                          %
%      End of Plot power, mean airspeed and max speed profile curves      %
%%%%%%%%%%%%%%%%%%%%%%%%%%%%%%%%%%%%%%%%%%%%%%%%%%%%%%%%%%%%%%%%%%%%%%
%%%%%%%%%%%%%

%%%%%%%%%%%%%%%%%%%%%%%%%%%%%%%%%%%%%%%%%%%%%%%%%%%%%%%%%%%%%%%%%%%%%%
%%%%%%%%%%%%%
%       Plot characteristic curve of the turbine (power vs airspeed      %
%                                                          %
 figure();
 xq1 = 0:0.01:70;
```

```
 plot(x_global,y_global,'ks',xq1,ppval(cs,xq1),'-k','linewidth',2);   % plot once outside iteration x,y,'o', -k
 xlim([0 50])
 ylim([0 1.1])
 %title(' Wind turbine characteristic curve [10 MW]')
 xlabel('Wind speed [m/s]','fontweight','bold','FontName','Times New Roman','FontSize',18)
 ylabel('Power [p.u.]','fontweight','bold','FontName','Times New Roman','FontSize',18)
 grid on
 axh=gca;
 set (axh, 'GridLineStyle','-','fontweight','bold','FontSize',14);
 grid minor
 TurbTotal=TurbTotal;
 clear x_global;
 clear y_global;
 clear xq1;
%                                                    %
%    End of Plot characteristic curve of the turbine (power vs aispeed    %
%%%%%%%%%%%%%%%%%%%%%%%%%%%%%%%%%%%%%%%%%%%%%%%%%%%%%%%%%%%%%%%%%%%%%%%%%%%%%%%%%%%%

%%%%%%%%%%%%%%%%%%%%%%%%%%%%%%%%%%%%%%%%%%%%%%%%%%%%%%%%%%%%%%%%%%%%%%%%%%%%%%%%%%%%
%     Export to txt file the power and mean speed profile curves          %
%                                                    %
if region == "USA"
  strCat = num2str(hurricaneCategory);
  strTrack = num2str(jp);
  strPowerProfile = strcat("Cat-",strCat," Track ",strTrack," (a) PowerProfile.txt");
  csvwrite(strPowerProfile,GEN_time.')
  strTime = strcat("Cat-",strCat," Time",".txt");
  csvwrite(strTime,[1:nt].')
  strMeanSpeed = strcat("Cat-",strCat," Track ",strTrack," (b) MeanSpeed.txt");
  csvwrite(strMeanSpeed,WindAvg.')
  %clear WindAvg
else        %Japan"
  csvwrite('PowerProfile.txt',GEN_time.')
  csvwrite('time.txt',[1:nt].')
end
%%%%%%%%%%%%%%%%%%%%%%%%%%%%%%%%%%%%%%%%%%%%%%%%%%%%%%%%%%%%%%%%%%%%%%%%%%%%%%%%%%%%
clear GEN_time;


%close all  % close all figures
%pause(10)
% end    % end do jp

clear all
```
